PRECLINICAL AND CLINICAL DEVELOPMENT OF INTRATUMORALLY ADMINISTERED HU14.18-IL2 AS TREATMENT FOR NEUROBLASTOMA AND MELANOMA: THE IMPORTANCE OF TUMOR INFILTRATING LEUKOCYTES IN TUMORS TREATED WITH HU14.18-IL2

by

Richard Yang

A dissertation submitted in partial fulfillment of

the requirements for the degree of

Doctor of Philosophy

(Clinical Investigation)

at the

UNIVERSITY OF WISCONSIN-MADISON

2012

Date of final oral examination: 6/25/12

The dissertation is approved by the following members of the Final Oral Committee:

Paul M. Sondel, Professor, Pediatrics, Hematology/Oncology
David L. DeMets, Professor, Biostatistics and Medical Informatics
KyungMann Kim, Professor, Biostatistics and Medical Informatics
Deane F. Mosher, Professor, Biomolecular Chemistry
Mark R. Albertini, Associate Professor, Medicine, Hematology-Oncology
Erik A. Ranheim, Associate Professor, Pathology & Laboratory Medicine

To my father, Dr. Kwang-Ping Yang,

Who has been a constant strength for me.

You have never let me give up on myself.

Thanks, Dad.

Acknowledgements

I would like to express my gratitude to many people without whom I would never have made it this far. I am extremely grateful for the opportunities I've had to learn, develop, and work as a scientist under Paul Sondel's guidance and direction. Paul – thank you for the chance to pursue interesting scientific ideas from the initials questions and development of methods, to the presentation and publication of results. I have appreciated the trust and independence you have given to me, as well as the opportunity to be part of an outstanding scientific team.

The fresh viewpoints, input, and advocacy on my behalf of my committee, Drs. Mark Albertini, David DeMets, Michael Fleming, KyungMann Kim, Deane Mosher, and Erik Ranheim, have been essential for my success. I have been extremely well-supported and encouraged by Drs. Sasha Rakhmilevich, Jacek Gan, Jacquelyn Hank. Their scientific insights, breath of immunologic knowledge, and technical expertise have been critical. The members of the Sondel lab have been essential to my success as a graduate student. I've enjoyed the opportunities to collaborate scientifically and engage in many interesting conversations about research, medicine, and life over the years with laboratory members including post-doctoral fellows (Kory Alderson, Margaret Boyden, Ilia Buhtoiarov, David Delgado, Amy Erbe, Brian Gadbaw, Bartosz Grzywacz, Erik Johnson, Zane Neal, Brett Yamane), graduate students (Tony Koehn, Kim McDowell, Zulmarie Perez-Horta, Lori Scardino, Brenda Soto, Wei Wang), technicians (Mildred Felder, Lauren Nettenstrom, Stacy Ryu, Barry Wagner), and undergraduates (Mark Baldeshwiler, Megan Elsenheimer, Jacob Goldberg, Lizzie Guenther, Dustin Hess, Mitchell Luangrath, Emily Phillips, Lily Qu, Tyler Van De Voort, Julie Waisbren, Marcus Zuo).

Finally, many of the studies I've done were with the assistance of an undergraduate student, Nicholas Kalogriopoulos, with whom I've had the opportunity to train and learn. I would like to acknowledge all of the members of the University of Wisconsin-Madison Histopathology Core Laborary, especially Joseph Hardin, who taught me how to stain slide, Jane Weeks, who taught me to cut frozen sections on a cryostat, and Ella Ward. Thank you much, Songwon Seo, for all of you expertise and patience regarding statistical methods.

My time in graduate school, developing as a researcher and future physician, has been aided by the support of the Medical Scientist Training Program, especially Drs. Deane Mosher, Robert Blank, Anna Huttenlocher, and Mark Bukard, our steadfast administrator Paul Cook, as well as friends and colleagues in the program (Eric Bultman, Mike Devinney, John Floberg, Rene Roy, Chloe McCoy, Ariela Karasov, and Philip Mudd). I am grateful for the time and training of my physician-scientist mentors, Drs. Albertini, Ranheim, and Sondel. They have given me unique opportunities to learn and develop clinically, as well as to see other examples of excellent medical research.

I cannot imagine being better supported outside of my graduate research career than I have been. The friends and relationships I've had through Pres House have been a constant source of support, perspective and life outside of the lab. I am especially thankful for the friendship of Mark Elsdon, Eric Liu, Jonathan Reid, Eric Mischo, Miles McConnell, Connor Hanson, Haley Christensen, and Cody Hanson.

Finally, I am grateful for my wonderful family: Mom, Dad, and Carolyn. All of your constant support and unconditional love have been terrific.

Abstract

PRECLINICAL AND CLINICAL DEVELOPMENT OF INTRATUMORALLY ADMINISTERED HU14.18-IL2 AS TREATMENT FOR NEUROBLASTOMA AND MELANOMA: THE IMPORTANCE OF TUMOR INFILTRATING LEUKOCYTES IN TUMORS TREATED WITH HU14.18-IL2

Richard Yang

Under the supervision of Professor Paul M. Sondel

At the University of Wisconsin-Madison

Hu14.18-IL2, an immunocytokine (IC), consists of the humanized 14.18 (hu14.18) monoclonal antibody (mAb) genetically linked to human recombinant interleukin-2 (IL2). This mAb recognizes GD2, a disialoganglioside over-expressed on neuroblastoma and melanoma. Ch14.18, the chimeric form of hu14.18, has been tested as an investigational therapeutic agent, alone and combined with IL-2, in Phase I-III clinical trials. Recently, clinical benefit was proven in a published Phase III trial. Testing directly in tumor-bearing mice, intratumoral (IT) administration of ICs has shown an advantage compared to intravenous (IV) administration. In an A/J mouse model bearing subcutaneous GD2+ NXS2 neuroblastoma, IT hu14.18-IL2 treatment resulted in a greater antitumor response compared to IV hu14.18-IL2. This response was antigen-specific and dose-dependent. These studies indicate that clinical testing of IT hu14.18-IL2 in melanoma patients with measureable disease appears warranted.

To evaluate the antitumor mechanisms of IT-IC, and focus on the degree of tumor-infiltrating leukocytes (TILs), we examined the effects of IT hu14.18-IL2 in A/J mice bearing established GD2+ NXS2 neuroblastoma. We hypothesize that IT-IC administration results in increased and sustained levels of IC within the tumor, augmenting infiltration of immune effector cells into the tumor thereby enhancing antitumor response. We developed methods to evaluate these hypotheses in tumor-bearing mice and demonstrate prolonged IC retention and augmented numbers of activated T and NK cells within tumors. To model patterns of TILs in patients receiving IC in clinical trials, we developed a histological method in mice to identify and quantify TILs. Additionally, we used multicolor flow cytometry to quantify TILs and NKG2D expression on natural killer cells and cytotoxic T cells. We analyzed the profile of hu14.18-IL2 and TILs at the tumor site following IT versus IV delivery of hu14.18-IL2.

Finally, we present a retrospective analysis of parameters predictive of successful immunotherapy in mice. We evaluated levels and distributions of TILs in individual NXS2-bearing mice involved in hu14.18-IL2 administration studies. While differences are seen between treatment groups, substantial heterogeneity is observed within each treatment group. We analyze the immune infiltrate profile of TILs seen shortly after treatment, and demonstrate that there is a correlation between immune infiltration and clinical outcome.

Table of Contents

List of Figures

List of Tables

Chapter 1

Introduction and Background

1.1 Overview

The research presented in this thesis is focused on preclinical data obtained in studies directed towards clarifying mechanisms underlying the antitumor efficacy of intratumoral administration of an anti-GD2 immunocytokine. These preclinical studies were also designed to help inform the subsequent clinical monitoring, and analyses of biopsy samples, from patients that would be participating in a future clinical trial of this same form of intratumoral immunotherapy. The purpose of this introductory-background chapter is to summarize: a) the clinical setting and significance of anti-GD2 immunotherapy, b) the preclinical data leading to our interest in intratumoral administration of anti-GD2 immunocytokine, and c) the model system that we have used to test our hypothesis regarding some of the mechanisms of antitumor response.

1.2 Neuroblastoma – Clinical Strategies

Neuroblastoma is the most common malignancy in infants, the most common extracranial solid tumor of childhood, and the third most common cancer in children (Park et al., 2008; Ishola et al., 2007; Brodeur et al., 2002a; Matthay et al., 1999; Brodeur et al., 2002b). The average age at diagnosis is 17 months with 50–60% of patients having metastatic disease when diagnosed (Cheung et al., 2001; Cheung et al., 1997; Ater, 2004). Overall treatment has improved in children under 15 years of age with 5-year overall survival rates for newly diagnosed patients increasing from 52% in the 1970s to 69% in the last decade (Jemal et al., 2007; Ries et al., 2007).

Despite advances in the treatment of low- to intermediate-risk neuroblastoma, outcomes for patients with advanced disease have been historically poor, but recent data incorporating immunotherapy have shown significant improvement. Standard treatment for high-risk patients

includes multi-agent cytotoxic chemotherapy, surgery, radiation, and/or myeloablative chemotherapy with autologous stem cell transplantation, followed by cis-retinoic acid (CRA). CRA, an anti-proliferative agent, when given following completion of chemotherapy has been shown to have an increased survival effect in patients with stage 4 disease (Matthay et al., 1999; Schmidt et al., 2000; Kushner et al., 1994). With current standard therapy, most high risk patients achieve remission with no clinically evident disease (NED) status. However, complete eradication of tumor cells has remained elusive. Microscopic residual tumor cells (minimal residual disease) survive treatment and cause recurrent refractory disease. The 3-year event-free survival of these high risk patients remains as low as ~30% (Matthay et al., 1999; Cheung et al., 2001; Berthold et al., 2005; Franks et al., 1997). Fortunately, a recent COG randomized trial has shown that a combination of anti-GD2 antibody and cytokines in this setting can help prevent recurrence (Yu et al., 2001; Yu et al., 2010).

1.3 Melanoma – Clinical Strategies

The incidence of melanoma continues to rise, with >70,000 new cases in the USA estimated for 2010 (ACS, 2011). There will be ~8800 deaths from melanoma in the USA this year. Complete response (CR) can be achieved surgically for most newly diagnosed high risk melanoma patients. Even so, most patients who achieve CR after resection of metastatic disease eventually progress and die, with a median overall survival of ~15 months (Balch et al., 2001a; Balch et al., 2001b; Feun et al., 1982; Hsueh et al., 2002). Interferon alpha (IFN-α) is the only treatment that has been consistently shown to help prevent recurrence following surgery for high risk patients with resected stage III melanoma (Kirkwood et al., 2001). Many other immunotherapeutic strategies have been tested. Ipilimumab (anti-CTLA4) and IL-2 have shown

some anti-tumor effect (Hodi et al., 2010; Smith et al., 2008; Rosenberg et al., 1994). Vemurafenib (a BRAF V600E mutation kinase inhibitor) induces clinical responses in a majority of patients with previously treated BRAF V600–mutant metastatic melanoma (Sosman et al, 2012). In this study, the median overall survival was approximately 16 months. In spite of this, there is still a lack of effective systemic therapy for metastatic melanoma.

1.4 The Importance of GD2 Disialoganglioside

Surface antigens expressed on neuroblastoma that have been used as targets for mAbs include the gangliosides GD2, GD3 and GM3, and the glycoproteins CD56 (NCAM), L1-CAM, GP58 and GP95 (Cheung and Sondel, 2005). GD2 is a disialoganglioside antigen that is expressed on tumors of neuroectodermal origin including neuroblastoma and melanoma (Mujoo et al., 1987; Cheung et al., 1985). These tumors express GD2 with relatively little heterogeneity between cells (Schulz et al., 1984; Kramer et al., 1998). Patients with neuroblastoma were found to have significantly elevated free GD2 levels in serum compared with normal children and children with other tumors (Schulz et al., 1984). Also, GD2 expression is not lost from the cell surface of neuroblastoma cells even when bound to antibody, unlike other tumor antigens, described previously, that may be shed or internalized (Kramer et al., 1998).

In normal tissues, GD2 expression is largely limited to neurons, skin melanocytes, and peripheral pain fibers (Svennerholm et al., 1994), making it well suited for targeted antitumor therapy. Recently, GD2 has been "ranked" 12th in priority for clinical importance of all described human cancer antigens by an NCI workshop (Cheever et al., 2009). In addition to neuroblastoma and melanoma, GD2 is expressed on some soft tissue sarcomas, osteosarcomas,

and small cell lung cancers (Sondel and Hank, 2001; Mujoo et al., 1987). In all, GD2+ diseases account for ~8% of all cancer deaths in the US (ACS, 2004).

GD2 has been used extensively as a target in mAb therapy and has been the primary target of antibody recognition in neuroblastoma. In 1984, a murine mAb (mAb126) was produced against cultured human neuroblastoma cells (LAN1). The original murine anti-GD2 mAbs described were 3F8, 14.18 and 14.G2a (Mujoo et al., 1987; Cheung et al., 1985). Clinical testing has been performed with 3F8, 14.G2a, and ch14.18 (the human-mouse chimeric variant of 14.18) in neuroblastoma and melanoma (Cheung et al., 1987, Cheung et al., 1998, Handgretinger et al., 1992; Yu et al., 1998; Handgretinger et al., 1995; Murray et al., 1994; Saleh et al., 1992a; Saleh et al., 1992b).

Clinical Strategies of Anti-GD2 Therapy in Treatment of Neuroblastoma and Melanoma

The following section reviews recent and ongoing strategies using 14.18 derived anti-GD2 antibodies either as monotherapy or as part of a larger and more complex clinical treatment approach for neuroblastoma and melanoma. This approach using anti-GD2 antibodies and their combination with other treatments or strategies have shown enhanced and promising clinical effects.

1.5 Anti-GD2 Single Agent Antibody Therapy

1.5.1 ADCC and CDC

An ideal anticancer agent would specifically target tumor cells and minimize injury to healthy cells (Sondel and Hank, 2001). Monoclonal antibody (mAb) therapy creates specificity to tumor cells through its recognition of cell surface antigens found exclusively on tumor cells or

that are found in much greater amounts on tumor cells compared to normal cells (Stephenson et al., 1995; Sondel et al., 2003). Currently, mAbs are in use in the detection, diagnosis, and treatment of neuroblastoma (Franks et al., 1997; Jurcic et al., 1997; Moss et al., 1991; Seeger et al., 2000). Antibodies can mediate destruction of tumor cells through several mechanisms including antibody-dependent cell-mediated cytotoxicity (ADCC). After the variable region of the antibody binds to antigen on the tumor cell, the Fc portion of the antibody can bind to the Fc receptors on monocytes, macrophages, neutrophils and/or natural killer (NK) cells and stimulate tumor cell lysis via ADCC (Colucci et al., 2003; Lammie et al., 1993).

In addition, complement-dependent cytotoxicity (CDC) may be induced after an antibody binds to the tumor cell surface (Sondel and Hank, 2001). However, dose limiting toxicities (DLT) caused by anti-GD2 mAb do occur and include fever, chills, anaphylactoid reactions most likely from cytokine and complement activation, and transient neuropathic pain, which are controllable with analgesics. These toxicities are mostly likely the result of mAb recognition of GD2 on peripheral pain fibers and complement deposition (Lammie et al., 1993; Xiao et al., 1997; Yuki et al., 1997; Svennerholm et al., 1994; Yu et al., 1998).

1.5.2 Ch14.18 Clinical Testing

A human-mouse chimeric form of the 14.18 murine anti-GD2 mAb, designated ch14.18, was subsequently created to reduce the immunogenicity associated with the murine antibody (**Figure 1-1**). The chimeric antibody is less immunogenic and is more effective than 14.G2a in mediating lysis of neuroblastoma cells with human NK cells (Barker et al., 1991). The ch14.18 antibody has undergone clinical testing as a single-agent therapy. Simon et al. have published their results using standard induction treatment (chemotherapy with autologous stem cell rescue)

for children and infants with stage 4 neuroblastoma followed by consolidation with chimeric 14.18 antibody for 5 days every 2 months, versus 12 months of oral maintenance chemotherapy or no further therapy (Simon et al., 2004). In patients <1 year old, there was no significant difference in event-free survival or overall survival in the three consolidation groups, with an overall survival of >90%. In patients >1 year old, the 3-year overall survival of ch14.18 treatment was superior to maintenance therapy or no additional therapy (P = 0.018) (Simon et al., 2005), although there was no difference in event free survival.

1.6 Anti-GD2 Antibodies Combined with other Agents

1.6.1 Antibody plus ADCC-Augmenting Cytokines

As the mechanisms of mAb-based tumor cell lysis via ADCC and CDC were discovered, it was evident that the antibody must accomplish three separate jobs to kill a tumor cell. First, the antibody must recognize and bind to the tumor cell. Second, it must bind long enough and avoid internalization to adequately signal immune effector mechanisms. Third, the activated immune effector cells or effector proteins must be able to create a destructive signal (Sondel and Hank, 2001). Since mAb-mediated tumor cell destruction relies on ADCC and/or CDC to kill tumor cells, strong effector functions are required. However, effector function, particularly ADCC, is often compromised in cancer patients due to immune suppression from metastatic cancer and/or chemotherapy (Yuki et al., 1997; Hank et al., 1990; Kushner et al., 1989). It is thought that the addition of cytokines that activate cells to mediate enhanced ADCC to mAb therapy will augment effector cell function and improve the overall antibody therapy efficacy (Sondel and Hank, 2001).

1.6.2 14.G2a + IL-2 Trial

Interleukin 2 (IL-2) is a strong pro-inflammatory cytokine with effects on both innate immunity, increasing the number and activation state of NK cells, and adaptive immunity, stimulating antigen-specific T cells (Mulé et al., 1987; Sondel and Hank, 1997). A Phase I trial through the Children's Cancer Group involved 33 patients. IL-2 was administered by three 96 hr infusions on days 1, 8, and 15 over consecutive weeks and 14.G2a was given as a daily 2 h infusion between days 9-13 (Frost et al., 1997). The treatment timing sought to take advantage of IL-2 induced lymphocytosis and maximal NK cell cytotoxic activity seen in several previously conducted *in vitro* analyses (Hank et al., 1999). One patient had a partial response with a 70% size decrease in an abdominal tumor facilitating complete resection. Three additional patients had a transient reduction in microscopic bone marrow disease but no overall reduction in tumor burden. Serum samples from these patients were found to have sufficient levels of 14.G2a to result in ADCC of GD2-positive tumor cells in *in vitro* assays (Hank et al., 1994). Human anti-mouse antibody reactions (HAMA) were also noted.

1.6.3 Ch14.18 + GM-CSF + IL-2 + CRA Pilot Trial

Testing of ch14.18 in refractory neuroblastoma included co-administration of GM-CSF in studies done by the Pediatric Oncology Group (Yu et al., 1997; Yu et al., 1995). Also, the Children's Cancer Group conducted a Phase I clinical trial of ch14.18 with GM-CSF in children with neuroblastoma immediately after hematopoietic stem cell transplant (Ozkaynak et al., 2000). Results of this trial determined the MTD of ch14.18 in combination with GM-CSF to be 40 mg/m^2/day for 4 days in the early post-transplant period. A subsequent Phase I study found the MTD of ch14.18 to be 25 mg/m^2/d for 4 days given concurrently with 4.5 x 10^6 U/m^2/d of

IL-2 for 4 days with alternating cycles of IL-2 and GM-CSF. Though two patients experienced DLTs from ch14.18 and IL-2, this combination was deemed tolerable in the early post-transplant period. This study also found that cis-RA can be safely administered between courses of ch14.18 and cytokines (Gilman et al., 2009).

1.6.4 Phase III Neuroblastoma Ch14.18 + GM-CSF + IL-2 + CRA Trial

Preliminary data led to the design of the Children's Oncology Group (COG) Phase III trial, ANBL0032, which prospectively examined this ch14.18 + GM-CSF + IL-2 + CRA combination therapy in patients after myeloablative chemotherapy and autologous stem cell rescue. CRA was added to the regimen because it was shown previously in a Phase III clinical trial to improve overall survival in patients with stage 4 neuroblastoma (4). Following autologous transplant, patients were randomized to receive CRA alone or CRA in combination with ch14.18 and GM-CSF (in courses 1, 3 and 5) and IL-2 (in courses 2 and 4) (Yu et al., 2010).

From 226 patients with high-risk neuroblastoma, the results showed a two-year event-free survival of 66% in the immunotherapy group versus 46% in the standard treatment group ($p=0.0115$). Overall survival at two years was 86% for the immunotherapy group versus 75% for the standard treatment group ($p= 0.016$). The results from this phase III trial have been recently reported (Yu et al., 2010).

This study shows a substantive increase in survival for high risk neuroblastoma. It is the first clinical trial to document that a combination of an anti-cancer mAb with ADCC-augmenting cytokines is an effective anticancer therapy. Also, it is the first time an antibody targeting a non-protein antigen (as GD2 is a glycolipid) has proven to be effective for immunotherapy of cancer. The 20% improvement in 2-year prevention of relapse for children with neuroblastoma receiving

the experimental immunotherapy represents an advance in treatment that is being regarded now as the treatment of choice for high risk patients that achieve remission, in order to decrease the chance of relapse (Yu et al., 2010).

This study also shows the use of a monoclonal antibody combined with cytokines (GM-CSF and IL-2) to enhance antibody dependent cell-mediated cytotoxicity (ADCC) having made an impact on increasing survival in neuroblastoma in a minimal residual disease setting. Other monoclonal antibodies also mediate ADCC (Rituxan, Erbitux, Herceptin), but have yet to be tested with cytokines in a minimal residual disease setting. This trial may portend future clinical trials testing cytokine combinations in more common malignancies that are currently treated with monoclonal antibodies (Yu et al., 2010).

1.7 Immunocytokines (ICs) - Antibodies Linked to Cytokines

Immunocytokines (IC) are synthetic fusion proteins that consist of tumor-specific monoclonal antibodies (mAb) linked to an immune-stimulating cytokine.

1.7.1 Ch14.18-IL2

The ch14.18-IL2 is an immunocytokine (IC) formed by linking IL-2 to the carboxyl end of the constant region of the chimeric mouse–human IgG1 ch14.18 mAb (Johnson et al., 2007; Gillies et al., 1993; Gillies et al., 1992). Preclinical data in mice show that treatment with ch14.18-IL2 is far superior to comparable doses of ch14.18 mAb combined with IL-2 in mediating antitumor effects. In general, ADCC depends on the number and function of Fc receptors (FcR) on effector cells including activated NK cells (Sondel and Hank, 2001; Hank et al., 1990; Sondel et al., 2008; Weng et al., 2003). However, activated NK cells also have

augmented IL-2 receptor (IL-2R) expression (Voss et al., 1990) leading to a dramatic *in vitro* response to IL-2 (Sondel et al., 1988). In mouse models, the IL-2 component of this IC can activate NK cells without FcR, through their IL-2R (Weil-Hillman et al., 1989). Thus, it is thought that IC-facilitated T-cell binding to tumor cells is mediated via IL-2Rs and IC-facilitated binding of NK cells to tumor cells is mediated via FcRs and IL-2Rs (Gillies et al., 1992; Hank et al., 1996). Data suggest that ch14.18-IL-2 could function as both a T-cell inducing vaccine as well as an activator of NK mediated ADCC. These data provided the basis for initiating clinical testing of this 14.18 based IC molecule as therapy for neuroblastoma and melanoma (Sondel et al., 2008) using an immunocytokine based on the humanized, rather than chimeric, form of the mAb; this IC is hu14.18-IL2.

1.7.2 Hu14.18-IL2

1.7.2.1 Structure and Preclinical Development

Hu14.18-IL2 (**Figure 1-2**) is a n immunocytokine (IC) consisting of a human recombinant human interleukin-2 (IL2) molecule genetically linked to each IgG heavy chain of the hu14.18 monoclonal antibody (mAb) (Gillies et al., 1992). Hu14.18 monoclonal antibody recognizes the GD2 disialoganglioside that is over expressed on tumors of neuro-ectodermal origin such as neuroblastoma and melanoma (Cheung et al., 1987; Ribas et al., 2009). When murine (14.G2a) or chimeric (ch14.18) anti-GD2 IgG mAbs are injected intravenously (IV) in mice, half-life is 2–5 days (Yu et al., 1998; Mulé et al., 1987). In contrast, the half-life of the ch14.18-IL-2 and hu14.18-IL2 is only ~4hrs (Kendra et al., 1999) when injected intravenously into mice. These data led to hu14.18-IL2 being given frequently (daily) to maintain both IL-2 and hu14.18 *in vivo* activity (Sondel et al., 2008).

1.7.2.2 Phase I Testing in Neuroblastoma and Melanoma

Initial trial results of hu14.18-IL2 in subjects with GD2+ tumors documented that the hu14.18-IL2 immunocytokine (IC) is clinically safe and well-tolerated at doses that induce immunologic activation.

1.7.2.2.1 Melanoma

A phase I study performed at the UWCCC (King et al., 2004) treated 33 adults with refractory MEL. Patients received 2 monthly courses of IC, consisting of 3 consecutive daily infusions (over 4 hours) each course. This was a standard dose escalation (0.8, 1.6, 3.2, 4.8, 6.0 and 7.5 mg/M^2/d) phase I study. Hu14.18-IL2 was tolerated acceptably at the 3.2 and 4.8 mg/m^2 dose levels. At 6.0 mg/m^2, 1 pt developed hypoxia, requiring entry of 3 more patients at that dose level. At 7.5 mg/m^2, one pt developed hypoxia and hypotension, and one developed a transiently elevated ALT/AST; both qualified as DLT. Thus, with 2 of 6 patients developing DLT at 7.5 mg/m^2, this dose level met study criteria for MTD, and the phase-2 dose was selected to be 6.0 mg/M^2/d.

1.7.2.2.1 Neuroblastoma

The Children's Oncology Group has completed a Phase I trial using hu14.18-IL2 in 27 pediatric patients with recurrent neuroblastoma using four courses of hu14.18-IL2 for patients with stable disease (Osenga et al., 2006). The MTD was 12 mg/m^2/day with dose limiting toxicities (DLTs) of hypotension, allergic reaction, blurred vision, neutropenia, thrombocytopenia, and leukopenia. No CR or PR was noted, but three patients had clinical

changes suggestive of antitumor activity with radiographic and bone marrow response. Immune activation was noted with elevated sIL-2Rα and lymphocytosis. All toxicities were reversible, and there were no treatment-related deaths.

1.7.2.3 Phase II Studies

1.7.2.3.1 Melanoma

A Phase II protocol evaluated the antitumor activity of hu14.18-IL2 in advanced MEL. Fourteen patients received 3 daily IV doses of 6.0 mg/M^2/d IC in each of 2 monthly courses. Nine had PD after 2 cycles. Four patients had stable disease (SD) following 2 cycles and went on to complete 4 cycles. The duration of SD in these pts was from 3 to 4 months. One patient had a PR (shrinkage of a hepatic metastasis) and completed 4 cycles. The duration of the PR was < 4 months before progressive disease (PD) was noted. Grade 3 toxicities were noted in 5 patients and reversed in <24h. Only 3 patients required a dose reduction in IC (2 for transient hypotension and 1 for grade 2 elevated Cr with oliguria).

These data suggested that this agent had limited activity at this dose and schedule in patients with measurable recurrent melanoma (Albertini et al, Submitted). This observation was consistent with preclinical data suggesting immunocytokine was less effective in the setting of macroscopic disease (see section 1.7.3, below). For melanoma, we wanted to instead focus our testing of IV-IC on patients we felt more likely to benefit; namely those with melanoma at very high risk for recurrence who are currently NED, and those patients with tumor that might be amenable to treatment with intratumoral immunocytokine.

1.7.2.3.2 Neuroblastoma

A Phase II study (COG-ANBL0322) of hu14.18-IL2 in children with recurrent or refractory neuroblastoma was designed to evaluate the clinical antitumor activity and *in vivo* immunological effects of hu14.18-IL2. Also, this study sought to differentiate between patients with bulky disease and patients with minimal evaluable neuroblastoma. Patients received 3 daily IV doses of 12.0 mg/M^2/d hu14.18-IL2 in each of 4 monthly courses (Shusterman et al., 2010). Fifteen patients had disease measurable by standard radiographical criteria (stratum-1) and 24 patients had disease evaluable only by meta-iodobenzylguanidine (MIBG) scanning and/or bone marrow (BM) histology (stratum-2). Responses were confirmed by independent radiological review and immunocytochemical (ICC) evaluation of the bone marrow.

No responses were seen in the 15 stratum-1 patients. In the 24 stratum-2 patients, 5 showed CR (MIBG and BM/ICC resolution). These response data support the conclusion that this agent and regimen have clinical activity in stratum-2 but not in stratum-1 patients (Shusterman et al., 2010). As all patients in this study had recurrent/refractory disease to prior multi-modality therapy, these responses are of interest to pediatric oncologists (Sondel et al., 2010).

1.8. Influential Factors in Hu14.18-IL2 Immunotherapy

1.8.1 Intratumoral (IT) Administration of Immunotherapy

Localized versus systemic administration of immunocytokines has been tested directly in tumor-bearing mice and has shown an advantage of IT administration of ICs compared to IV. In a SCID mouse model using human melanoma xenografts and infused human peripheral blood lymphocytes, therapeutic effects of ICs consisting of an anti-EGFR mAb linked to IL2 fusion

protein (IL2-FuP) or TNF (TNF-FuP) showed improved antitumor effects when administered IT compared to IV (Christ et al., 2001). IT injection of intact IC resulted in a survival advantage compared to IT injection of the mAb and IL2 as separate IT injections. Survival time was prolonged by the intratumoral application of FuP. In mice bearing subcutaneous Lewis lung carcinomas transfected with EpCAM, IT injection of huKS-IL12/IL2 (huKS1/4 mAb linked to a cytokine combination of IL2 and IL-12) resulted in complete resolution of tumor (Gillies et al., 2002). In addition, recent preclinical data have shown that intratumoral injection of hu14.18-IL2 (IT-IC) into the GD2+ NXS2 neuroblastoma in A/J mice has a greater ability to slow the growth of measureable tumors compared to intravenously injected hu14.18-IL2 (IV-IC) (Johnson et al., 2008). This response was antigen-specific, dose-dependent, and greater than IT injection of IL2 alone. The increased activity of IT compared to IV hu14.18-IL2 in NXS2 tumors was seen even in the absence of T cells.

Clinical testing of intratumoral IL-2 in melanoma has shown improvement in intratumorally treated lesions (Weide et al., 2010). A complete response that lasted ≥6 months was documented in 70% of all injected metastases. A complete local response of all treated metastases was achieved in 33 patients (69%), including 11 patients who had between 20 and 100 metastases. Response rates were higher for patients who had stage III disease compared with patients who had stage IV disease. Intratumoral IL-2 treatment elicited complete local responses in a high percentage of patients. Patients with cutaneous metastasis without lymph node involvement in stage III and with soft-tissue metastasis without visceral involvement in stage IV showed unexpected favorable survival rates after intratumoral treatment with IL-2 (Weide et al., 2011). As these clinical studies show local benefit of IT IL2 in melanoma patients, and preclinical data show intratumoral IC treatment is more effective that intratumoral IL2, clinical

testing of IT hu14.18-IL2 in melanoma patients with measureable disease appears warranted. Together with our lab's preclinical data with IT-IC, these clinical data with IT-IL2 suggest that melanoma patients with measurable disease may benefit from a localized treatment regimen of IT-hu14.18-IL2.

1.8.2 Influence of Systemic and Tumor Infiltrating Leukocytes

Immunocytokines (ICs) are capable of augmenting significant antitumor effects in murine models by targeting the therapy to the tumor and stimulating the immune system to selectively destroy the cancer cells. Preclinical data have also shown that these immunocytokine mediated antitumor effects are largely mediated by Natural Killer (NK) cells as well as T cells. In a syngeneic A/J murine model of neuroblastoma, the IV administration of the anti-GD2 ch14.18–IL2 fusion protein induced a cell-mediated antitumor response that eradicated established bone marrow and liver metastases more efficiently than equivalent mixtures of antibody and recombinant human IL2 (Lode et al., 1997). The effector mechanism involved was shown to be exclusively dependent on natural killer (NK cells) (Lode et al., 1998). In a syngeneic BALB/c model, the huKS1/4-IL2 IC, a humanized antibody against epithelial cell adhesion molecule (EpCAM) linked to IL2, was used to elicit a T cell-mediated eradication of established pulmonary and hepatic CT26-KSA murine colon carcinoma metastases (Xiang et al., 1997).

A recent trial of hu14.18-IL2 in children with relapsed neuroblastoma showed antitumor activity that was associated with genotypes indicating a clinical role for NK cells (Shusterman et al., 2010, Delgado et al., 2010). Patients were genotyped for KIR, HLA, and FcR alleles to determine whether KIR receptor–ligand mismatch or specific FcγR alleles were associated with antitumor response. Of 38 patient DNA samples, 24 were found to have autologous KIR/KIR-

ligand mismatch and 14 were matched. Of the 24 mismatched patients, 7 experienced either complete response or improvement of their disease after IC therapy. There was no response or comparable improvement of disease in patients who were matched. Therefore, KIR/KIR-ligand mismatch was associated with response/improvement to IC ($P = 0.03$). There was a trend toward patients with the FcγR2A 131-H/H genotype showing a higher response rate than other FcγR2A genotypes ($P = 0.06$). This report indicated that response or improvement of relapsed/refractory neuroblastoma patients after hu14.18-IL2 treatment is associated with autologous KIR/KIR-ligand mismatch, consistent with a role for natural killer cells in this clinical response.

A formal analysis via Pubmed and Embase investigated the prognostic influence of TILs in clinical studies (Gooden et al., 2011). Studies were included in which the prognostic significance of intratumoral CD3+, CD4+, CD8+, and FoxP3+ lymphocytes were determined (Gooden et al., 2011). In this pooled analysis, CD3+ TILs had a positive effect on survival with a hazard ratio (HR) of 0.58 for death, as did CD8+ TILs with a HR of 0.71. FoxP3+ regulatory TILs were not linked to overall survival, with a HR of 1.19. A separate meta-analysis of studies found that intraepithelial TILs are a robust predictor of outcome in ovarian cancer and define a specific class of patients, whose distinct tumor biology should be taken into account in devising appropriate therapeutic strategies (Hwang et al., 2012). Lack of intraepithelial TILs is significantly associated with a worse survival among patients (Hwang et al., 2012). The absence of TILs, together with increasing Breslow thickness, presence of ulceration and male sex, also predicts sentinel lymph node (SLN) metastasis in patients undergoing SLN biopsy for primary cutaneous melanoma (Taylor et al., 2007). In melanomas with a brisk TIL infiltrate, the probability of a positive SLN was 3.9% as compared with 26.2% for melanomas in which TILs were absent (Taylor et al., 2007). High levels of intratumoral TILs are associated with improved

recurrence-free survival in stage 1A non-small-cell lung cancer patients as well as a reduced likelihood of systemic recurrence (Horne et al., 2011). Also, when angiolymphatic invasion is not present, the beneficial effects of TILs become even more profound (Horne et al., 2011).

1.8.3 Influence of Initial Tumor Load

Results in tumor bearing mice treated with the hu14.18-IL2 molecule and other similarly configured molecules document that the most striking antitumor effects are obtained when the tumor burden is quite low (Neal et al., 2004). Mice treated with 5 days of hu14.18-IL2 IC beginning on days 3, 5, 7, or 9 after IV injection of NXS2 tumor cells displayed a range of antitumor effects. Mice treated with hu14.18-IL2 beginning on day 9 after tumor inoculation showed 50–80 metastatic foci, whereas mice beginning treatment on days 3 or 5 had relatively few (<10) detectable metastases. This indicated that hu14.18-IL2 is more effective when initiated early after induction of metastases when there is a smaller tumor burden.

Many clinical studies have found that staging is important for the efficacy of a variety of treatments. Lung cancer is broadly subclassified on the basis of histological features into squamous cell carcinoma, adenocarcinoma, large cell carcinoma and small cell carcinoma, and the histopathological type of lung cancer correlates with tumor behavior and prognosis (Beadsmoore and Screaton, 2003). Moreover, heterogeneity in clinical biology of localized gastric cancer (LGC) is best reflected after chemoradiation in presurgical and postsurgical pathologic stages, and correlation of outcome with presurgical staging may facilitate strategies to individualize therapy for LGC (Patel et al., 2007).

A stage IV neuroblastoma study found that metastatic patterns in neuroblastoma correlate with tumor biological features and event-free survival (EFS) (DuBois et al., 1999). EFS was

decreased in patients with bone, bone marrow, CNS, intracranial/ orbital, lung, and pleural metastases, and improved in those with liver and skin metastases. MYCN amplification and unfavorable Shimada histopathology correlated with increased frequencies of bone and intracranial or orbital metastases in infants and with increased frequencies of intracranial or orbital, liver, and lung metastases in older patients.

Since precise anatomic staging is important for prognosis in neuroblastoma patients, several systems have been used and are being designed for accurate staging. For example, the International Neuroblastoma Staging System (INSS) was formulated to incorporate the basic elements of several systems and to define the significance of tumor resectability, anatomic "midline", and lymph node involvement (Haase et al., 1995).

1.9 Hypothesis Experimental Approach

Our lab has previously shown the IT hu14.18-IL2 route of administration provides better local antitumor effects than IV hu14.18-IL2 in tumor-bearing mice. The mechanisms involved in improved antitumor effects seen with IT-IC administration are not clear. In order to evaluate the antitumor mechanisms of IT-IC, and focus on the degree of leukocyte infiltration, we will evaluate the effects of IT hu14.18-IL2 in A/J mice bearing established GD2+ NXS2 neuroblastoma.

Currently, there have not been any studies examining the intratumoral use of hu14.18-IL2 therapy for GD2+ tumor in patients. The clinical and pre-clinical mouse data mentioned above suggest that future clinical trials testing the potential toxicity and antitumor effects of localized (intratumoral) hu14.18-IL2 in melanoma patients with measurable disease may lead to a strategy with both enhanced antitumor effects and less systemic toxicity. In order to model such an

immunotherapy regimen, and investigate leukocyte infiltration, we will use a preclinical mouse model of the GD2+ NXS2 murine neuroblatoma and intratumoral injection of hu14.18-IL2. In order to evaluate potential mechanism, and clarify what mechanistic parameters to evaluate in future patients that receive intratumoral hu14.18-IL2, we have developed a novel quantitative method of histology to identify and quantify leukocyte infiltration patterns in murine tumors injected intratumorally with hu14.18-IL2. In this way, we can investigate the anti-tumor effect of localized hu14.18-IL2 treatment on a cellular level.

Our overriding hypothesis is that the targeting of activated leukocytes, and especially NK cells, to tumors via anti-GD2 mAb will enable IC to induce clinically meaningful *in vivo* anti-tumor activity in patients with $GD2^{+}$ tumors. In addition, we hypothesize that IT-IC administration results in increased and sustained levels of the IC in the tumor, augmenting infiltration of immune effector cells into the tumor thereby enhancing the antitumor response. This project presents histologic and flow cytometry studies to test this hypothesis.

Figure 1-1. Monoclonal Antibodies and Immunocytokines.

(A) A chimeric monoclonal antibody (mAb) combines the constant region of a human antibody with the variable domain of a murine antibody. The antigen specificity is conferred by the murine variable domain. **(B)** In the humanized mAb, the murine framework determinants of both the heavy and light chains are replaced with human framework determinants, but the antigen specificity of the original murine mAb is retained. **(C, D)** Fusion proteins or immunocytokines combine the mAb with covalently linked cytokines, such as molecules of interleukin 2 (IL-2), to the end of each of the heavy chains at the C-terminus.

Figure 1-1.

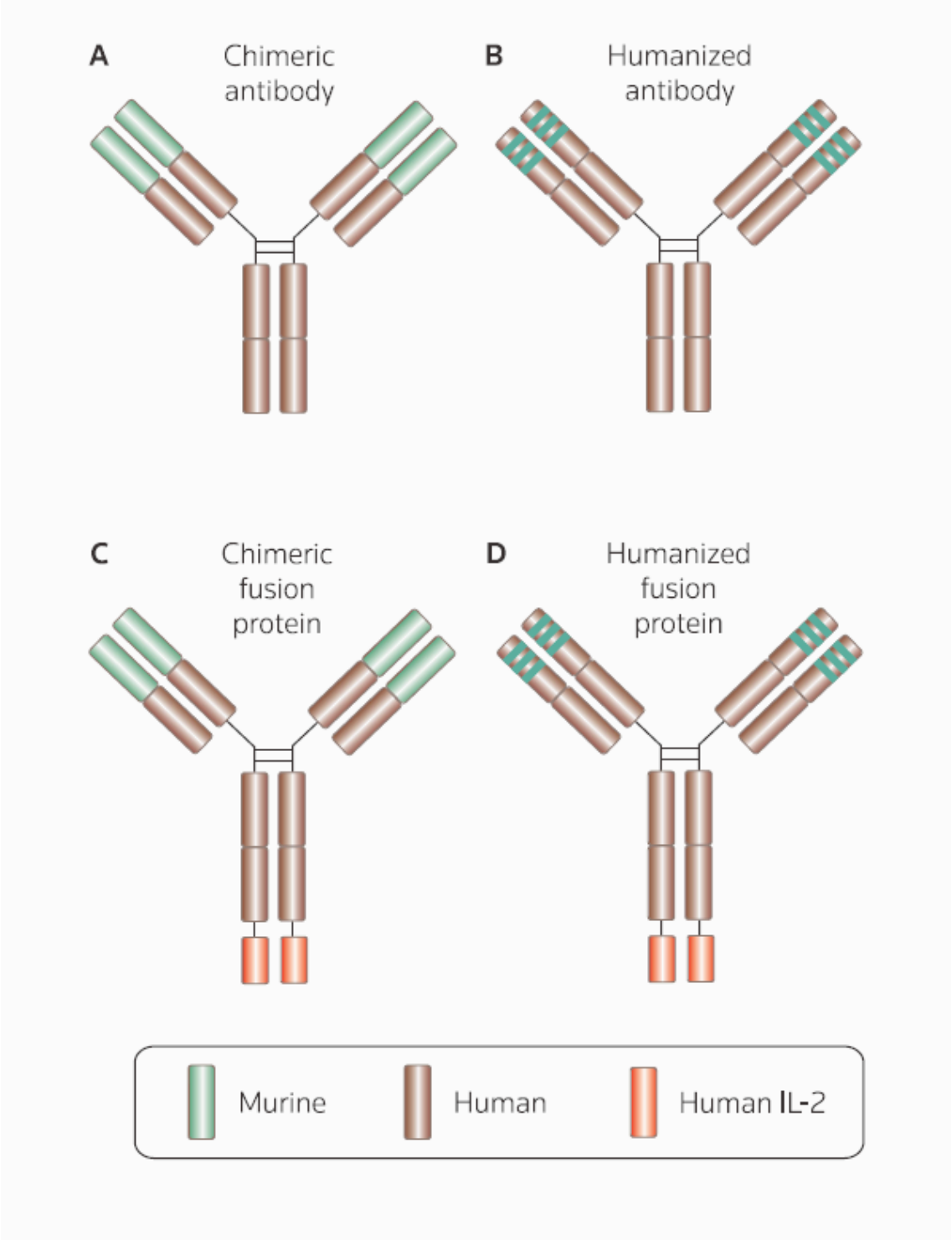
A
Chimeric antibody
B
Humanized antibody
C
Chimeric fusion protein
D
Humanized fusion protein
Murine
Human
Human IL-2

Figure 1-2. Hu14.18-IL2 Structure.

Hu14.18-IL2, an immunocytokine (IC), consists of the humanized 14.18 (hu14.18) monoclonal antibody (mAb) genetically linked to 2 molecules of human recombinant interleukin-2 (IL-2). The hu14.18 monoclonal antibody recognizes the GD2 disialoganglioside that is over expressed on tumors of neuro-ectodermal origin such as neuroblastoma and melanoma.

Figure 1-2.

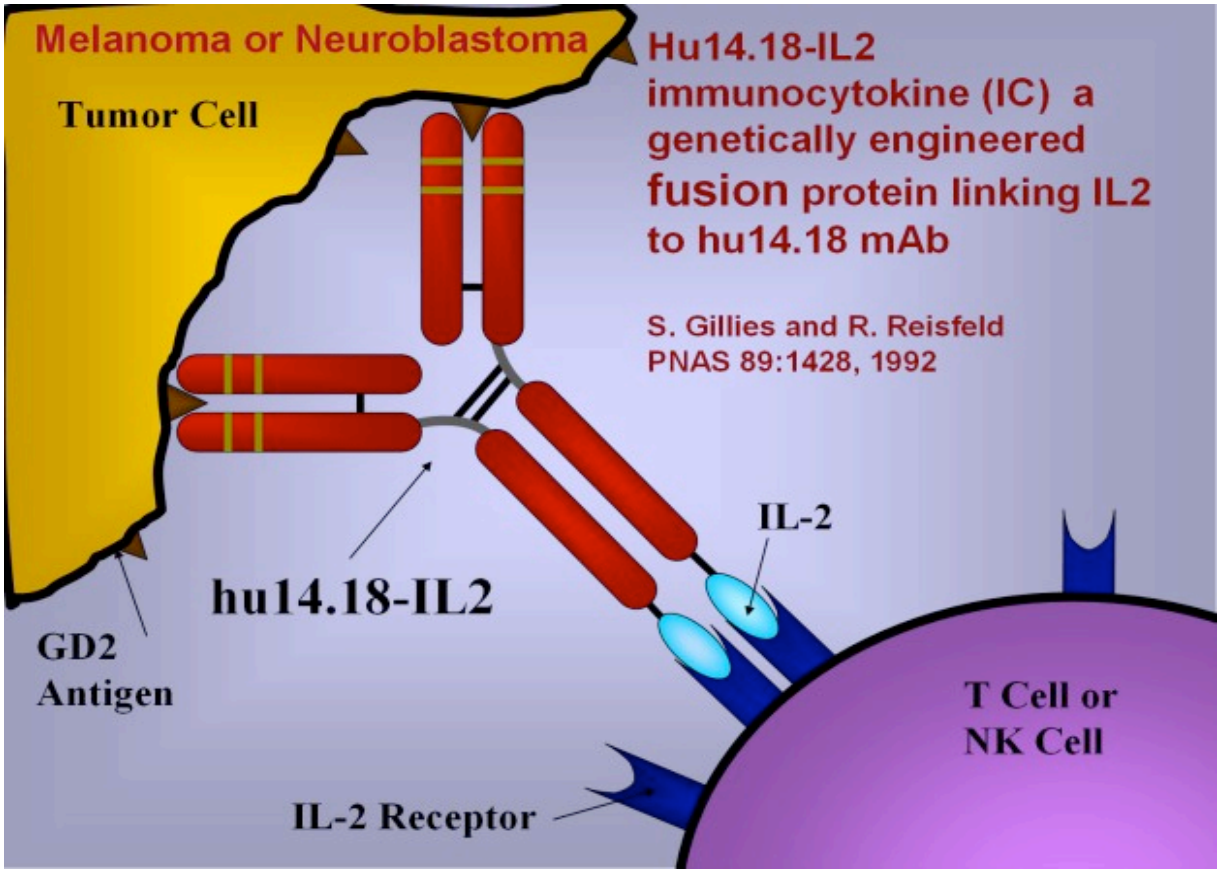
Melanoma or Neuroblastoma
Tumor Cell
Hu14.18-IL2
immunocytokine (IC) a
genetically engineered
fusion protein linking IL2
to hu14.18 mAb
S. Gillies and R. Reisfeld
PNAS 89:1428, 1992
IL-2
hu14.18-IL2
GD2
Antigen
T Cell or
NK Cell
IL-2 Receptor

Chapter 2

Material and Methods

2.1 Introduction

The general methods and reagents used for the experiments presented in this thesis are described below. They include many experimental techniques which have been used routinely by our laboratory team for many years as well as some modifications of these, and some newer techniques, that have been incorporated into the studies presented in this thesis. Specific details for a given experiment are noted in the individual figures.

2.2 Mice

We obtained 7-8 week old female A/J mice from Jackson Laboratories (Bar Harbor, Maine). All mice were housed in university-approved facilities and were handled according to National Institutes of Health and University of Wisconsin-Madison Research Animal Resource Center (RARC) guidelines. All experimentation was performed in accordance to protocols approved by the National Institutes of Health and by the Animal Care and Use Committees of UW-Madison.

2.3 Cell lines

2.3.1 NXS2 Murine Neuroblastoma

NXS2 is a moderately immunogenic, highly metastatic, murine neuroblastoma hybrid cell line that was created as previously described (Lode et al., 1997). Briefly, hybridization of the GD2-negative C1300 murine neuroblastoma cell line (A/J background) with murine dorsal root ganglional cells from C57BL/6J mice was used to create the murine NX31T28 cell line. The NXS2 subline was generated by the selection of NX31T28 cells with high GD2 expression.

NXS2 cells are of A/J background, that is, $H2K^k$ positive/$H2K^b$ negative (Lode et al., 1997). The murine NXS2 cell line was grown in Dulbecco's modified Eagle's medium (DMEM, Mediatech, Herndon, VA) with high glucose (4.5g/L) supplemented with penicillin (100U/ml), streptomycin (100μg/ml), L-glutamine (2mM) (Life Technologies, Inc., Grand Island, NY) and 10% heat-inactivated fetal calf serum (FCS, Sigma Chemicals, St. Louis, MO). Cells were maintained at 37°C in a humidified 5% CO_2 atmosphere.

2.3.1.1 Assessment of GD2 on NXS2 Neuroblastoma

GD2 expression on NXS2 was assessed by flow cytometry. Cells were trypsinized for 5 minutes to release the cells from the bottom of a tissue culture flask. After blocking out the trypsin with FCS in DMEM media, cells were centrifuged 900 rpm for 5 minutes and the supernatant removed. After resuspension in DMEM media, the NXS2 cells were stained with 0.5μg of hu14.18-IL2 FITC or a no antibody control. After staining 30 minutes at 4ºC, stained cells were washed with flow buffer (PBS supplemented with 2% FCS), centrifuged 900 rpm for 5 minutes, and the supernatant removed. Stained cells were resuspended in 250μL flow buffer and propidium iodide (PI). Cells were analyzed using the Becton Dickinson (BD) FACS Calibur. Analyses of data were performed using FlowJo software, version 6.4.7. We found that NXS2 expresses a moderate level of GD2 (**Figure 2-1**).

2.3.2 B16-RAE-1gamma Murine Melanoma

B16-RAE-1gamma melanoma (a gift from Dr. Lewis Lanier of UCSF) was grown in Dulbecco's modified Eagle's medium (DMEM, Mediatech) with 1.0g/L glucose supplemented with penicillin (100U/ml), streptomycin (100μg/ml), L-glutamine (2mM) (Life Technologies),

10% heat-inactivated fetal calf serum (FCS, Sigma), 2mg/mL G418 (Mediatech), and 1 μg/mL puromycin (Sigma). Cells were maintained at 37°C in a humidified 5% CO_2 atmosphere.

2.4 Immunocytokines (ICs) and Immunotherapy

The humanized hu14.18-IL2 (APN301, Apeiron Biologics, Vienna, Austria) was supplied by the NCI Biologics Resources Branch (Frederick, MD) via a collaborative relationship with Merck KGaA (Darmstadt, Germany). Hu14.18-IL2 is an immunocytokine consisting of an intact human interleukin-2 (IL2) genetically linked to the carboxyl-termini of each human IgG1 heavy chain of the hu14.18 mAb (Gillies et al., 1992). The humanized huKS-IL2 IC (EMD273066) is a similarly structured immunocytokine, but with IL2 linked to a humanized mAb that recognizes the Epithelial Cell Adhesion Molecule (EpCAM); it was generated and provided by EMD-Lexigen Research Center (Billerica, MA).

2.5 Well-Established Tumor Model

A/J mice were injected subcutaneously with 2 x 10^6 cells of NXS2 murine neuroblastoma in 100μl PBS in the lower right quadrant of the abdomen. Tumors were allowed to grow until the average volume was 30-150 mm^3 (Volume measured with mechanical calipers = width x width x length / 2), normally this required 14-18 days. Mice were then randomized into appropriate treatment groups and received 50μg of IC treatment daily for 3 consecutive days (either IV or IT). Mice were given IV IC by tail vein injection in 100μl PBS. IT injections consisted of IC in 100μl PBS, delivered into the subcutaneous tumor with a 30 gauge needle. Control treatments consisted of an equivalent volume of PBS administered by IT injection.

2.6 Early-Established Two Tumor Model

Figure 2-2 shows the schematic of the early-established tumor model including the cell depletion reigmens. This treatment model was used in a previous report from our lab (Johnson et al., 2008) that examined intratumorally injected immunocytokines in different mouse models. A/J mice were injected subcutaneously with 2 x 10^6 cells of NXS2 murine neuroblastoma in 100µl on Day 0 in the lower right quadrant of the abdomen to establish an initial (primary) tumor. After 4 days mice were injected again subcutaneously with 2 x 10^6 cells of NXS2 murine neuroblastoma in 100µl in the lower left quadrant of the abdomen to establish a second (distant) tumor. Mice were randomized on day 4 (immediately prior to antibody injections to deplete T or NK cells and to the second tumor implantation) into appropriate treatment groups and received 15µg of IC treatment daily for 5 consecutive days (Days 7-11). Mice were given IV IC by tail vein injection in 100µl PBS. IT injections consisted of IC in 100µl PBS, placed into the primary tumor with a needle. IT treatment was only done to the primary (local) tumor. Control treatments consisted of an equivalent volume of PBS administered by IV or IT injection. Tumor volumes of the initial (local) and secondary (distant) tumors were measured using mechanical calipers (Volume = width x width x length / 2).

2.7 Cell Depletion Regimens

Local and distant tumors were induced according to the early-established tumor model. To deplete NK cells, mice were injected intraperitoneally (I.P.) with 1.6 mg anti-asialo GM1 antibody (Wako Chemicals Richmond, VA) or 1.6 mg Rabbit IgG isotype control (Sigma) in a total volume of 200µL PBS on days 4, 9, and 16. To deplete T cells, mice were injected I.P. with mixtures of anti-CD4 and anti-CD8 mAbs (250 µg of each) or 500 µg Rat IgG (Sigma) isotype

control in a total volume of 200μL PBS on days 4, 9, and 16. Mice received 5 daily IT injections (Days 7-11) of 15μg hu14.18-IL2 (IC) to the primary tumor in a volume of 50μL PBS or 50μL control PBS. Tumor volumes were measured using mechanical calipers.

2.8 Endpoints for Progressive Tumor Growth

The endpoint of all tumor growth and survival studies was death of the animal or excessive tumor burden as determined by both tumor size (15mm in any direction) and the condition and behavior of the animal. These criteria are established by the RARC guidelines. The decision to euthanize an animal was made by an independent observer without regard for treatment group.

2.9 Hu14.18-IL2 IC Retention Experiments

Tumors were induced according to the well-established tumor model and then randomized to receive a single treatment of IT-IC (intratumoral injection of 50μg hu14.18-IL2 in 100μL PBS), IV-IC (intravenous injection of 50 μg hu14.18-IL2 in 100μL PBS), or IT-KS (intratumoral injection of 50μg huKS-IL2 in 100μL PBS). Mice were sacrificed at various times after treatment and their tumors were taken for flow cytometry.

2.10 Histology Experiments and Immunohistochemistry (IHC)

Mice treated according to the well-established tumor model were sacrificed 48 hours after treatment completion and their tumors resected for histology. The tumors were embedded in OCT, flash frozen in liquid nitrogen, and stained. Briefly, frozen sections were cut onto slides using a cryostat, fixed in cold acetone and dried. After rehydration, sections were blocked with

5% Rabbit serum (Sigma) for 25 min, washed and incubated with optimally titered mAb [rat anti-mouse CD45(clone 30-F11, eBioscience), CD3 (clone 17A2, eBioscience), CD4(clone GK1.5, eBioscience) , CD8 (clone 53-6.7, eBioscience) , F4/80 (clone BM8, eBioscience) , NKG2A/C/E (clone 20d5, eBioscience)] overnight in 1% Rabbit Serum. Following a wash, a biotinylated rabbit anti-rat secondary antibody was applied for 90 min and followed by ABC avidin-biotin complex (Vector Labs, Burlingame, CA). Slides were developed with DAB (Vector Labs, Burlingame, CA) for 4.5 min, counterstained with Mayer's hematoxylin (Sigma) for 90 sec and washed in running tap water for 5 min and mounted.

2.11 Quantitation of Immunohistochemistry (IHC)

A histological method to identify and quantify leukocyte infiltration patterns in these IT-IC treated tumors was developed. Digital pictures of these stained sections were taken at low magnification (10x) and quantitative analysis was performed using ImageJ software (NIH). The visual fields were placed on reproducible grids, and five representative areas of the same size within each frozen section were chosen. These 5 "subsamples" were inspected visually so that positive and negative cells could be manually counted within each subsample (**Figure 2-3**). Analogous grids and subsamples of the same size were obtained for each individual frozen section specimen being analyzed. This manual counting was done using a blinded system, by 2 separate individuals. These results were confirmed by a boarded hematopathologist who assessed the methods and analyses (Dr. Erik Ranheim). Percentages of subsamples were averaged within a sample and significance tests were performed using the Prism 5, Version 5.0.4, software (GraphPad).

2.12 Flow Cytometry

2.12.1 Preparation of Cells

Tumors were established and mice treated according to the well-established tumor model. Forty eight hours after treatment completion, mice were sacrificed and their tumors and spleens resected for flow cytometry. Single cell suspensions were made by disassociating the tissues through brass mesh (30 openings per inch) and then 50 micron nylon filters. Cell counts were determined using a Beckman Coulter cell counter or hemacytometer.

2.12.2 Staining of Cells

About 1 million cells were stained with the following antibodies at 4°C for 30 min: FITC conjugated anti-mouse NKG2A/C/E (clone 20d5, eBioscience), PE conjugated anti-mouse NKG2D (clone CX7, eBioscience), PE-Cy5 conjugated anti-mouse F4/80 (clone BM8, Biolegend), PerCP-eFluor710 conjugated anti-mouse F4/80 (clone BM8, eBioscience), PE-Cy7 conjugated anti-mouse CD4 (clone GK1.5, eBioscience), APC conjugated anti-mouse CD3e (clone 145-2C11, Biolegend), AlexaFluor700 conjugated anti-mouse CD45 (clone 30-F11, Biolegend), APC-eFluor780 conjugated anti-mouse CD8a (clone 53-6.7, eBioscience), CD16/32 Fc Block (clone 93, Biolegend), PE conjugated goat anti-human IL2 (clone MQ1-17H12, eBioscience) and PE conjugated goat anti-human IgG Fc Gamma (cat 12-4998-82, eBioscience). Cells were washed with flow buffer (PBS supplemented with 2% FCS) and centrifuged 900rpm for 5 minutes. After removal of the supernatant, cells were resuspended in 0.25mL of flow buffer and 0.6µg of DAPI (30 µL at 20 µg/mL in flow buffer).

2.12.3 Surface Phenotypic Analysis of Cells

Cells were analyzed using the Becton Dickinson (BD) LSRII. Compensation beads were used as positive color standards to subtract out overlapping emission spectra on adjacent color channels. Analyses of data were performed using FlowJo software. Fluorochromes Minus Ones (FMOs) were used to distinguish positively stained populations. Erythrocytes were subtracted from the denominator to allow analyses to focus only on nucleated cells. Our gating strategy for these flow studies are presented in **Figure 2-4**. Results are reported as % positive cells, or as mean fluorescence intensity (MFI) units.

2.12.4 Assessment of NKG2D ligands on NXS2

Although NXS2 cells cultured *in vitro* do not express RAE-1gamma (a primary ligand for murine NKG2D), NXS2 cells, when taken from a subcutaneous tumor and disaggregated, do demonstrate strong expression of RAE-1gamma. This is shown in **Figure 2-5**. These tumor/stromal cells were disaggregated from a mouse that died due to progressive disease from subcutaneous NXS2. These cells were then stained with Rat anti-mouse RAE-1 gamma PE (Red line, clone CX1, eBioscience) or with Rat IgG2b Isotype control PE (Blue line, clone eB149/10H5, eBioscience). The data demonstrate strong and relatively homogeneous staining for RAE-1gamma.

2.13 Wright-Giemsa Staining

PEC (10^4-10^5 cells in 100 µl media with FCS) were centrifuged at 800 rpm for 3 minutes using a Shandon Cytospin 2. After air drying for 5 minutes, slides were fixed in 100% methanol 2 minutes, allowed to dry, and stained horizontally with Wright Giemsa Stain (Sigma) for 45

seconds. An equal volume of glass filtered water was immediately added to the Wright Giemsa stain solution, and staining with this mixture was performed for 10 minutes, after which the slides were washed off with glass filtered water and destained horizontally with glass filtered water for 5 minutes. Slides were allowed to dry and mounted with glass coverslips using cytoseal 60. Pictures of cells were taken under 40x magnifications with attached computer software (Magnafire 2.1).

2.14 Statistical Methods

In all figures, p-values are represented with asterisks (*) as follows: <0.05 = (*), <0.01= (**), <0.001 = (***), <0.0001 = (****). Graphs were generated and significance tests were performed using the GraphPad Prism 5, Version 5.04, software. Contingency tables and graphs were analyzed using a Chi-squared statistic test or the Fisher's exact test (for small samples) to generate p-values. Survival curves were generated using the method described by Kaplan and Meier and statistically compared using the log rank (Mantel-Haenszel) test.

In all figures with bar graphs, one-tailed or two-tailed (if there was no *a priori* hypothesis) Student's t-tests under the normality assumption were used to determine significance of differences in antitumor responses (tumor volume, tumor infiltration, tumor growth inhibition, and delivery and retention of IC) between experimental and relevant control groups. Data are presented as mean ± standard error of the mean (SEM) and considered statistically significant for p values less than 0.05. Due to the exploratory nature of these analyses, multiplicity adjustments were not made.

In all scatter plot figures testing for correlation, asterisks after treatment groups in the legend represent a statistically significant different slope of each group's regression line model

compared to 0. For comparisons between treatment groups, “s” or “x” indications are used in place of asterisks, to test whether the slopes or elevations, respectively, of each group’s regression line are statistically significantly different from each other. Slope comparisons between regression analyses are tested and similarly indicated with “s” values (^{s}) as follows: <0.05 is represented with one s (^{s}), <0.01 = (^{ss}), <0.001 = (^{sss}) and <0.0001 = (^{ssss}). Regression lines with significantly different slopes cannot be tested for differences in elevation because they will intersect at some point in space. In cases when slopes are not significantly different, elevation comparisons between regression analyses are tested and similarly indicated with “x” values (^{x}) as follows: <0.05 is represented with one x (^{x}), <0.01 = (^{xx}), <0.001 = (^{xxx}) and <0.0001 = (^{xxxx}).

Figure 2-1. Assessment of GD2 on NXS2 mouse neuroblastoma

GD2 expression on NXS2 was assessed by flow cytometry. NXS2 murine neuroblastoma cells were stained with 0.5µg hu14.18-IL2 FITC (blue). Hu14.18-IL2 is known to bind specifically to GD2 disialogangioside (Gillies et al., 1992). A no antibody control (red line) was also made for comparison. Cells were analyzed using the Becton Dickinson (BD) FACS Calibur. Analyses of data were performed using FlowJo software, version 6.4.7. Dead cells were excluded from analysis (gated out by propidium iodide positivity). We found that NXS2 expresses a moderate level of GD2.

Figure 2-1.

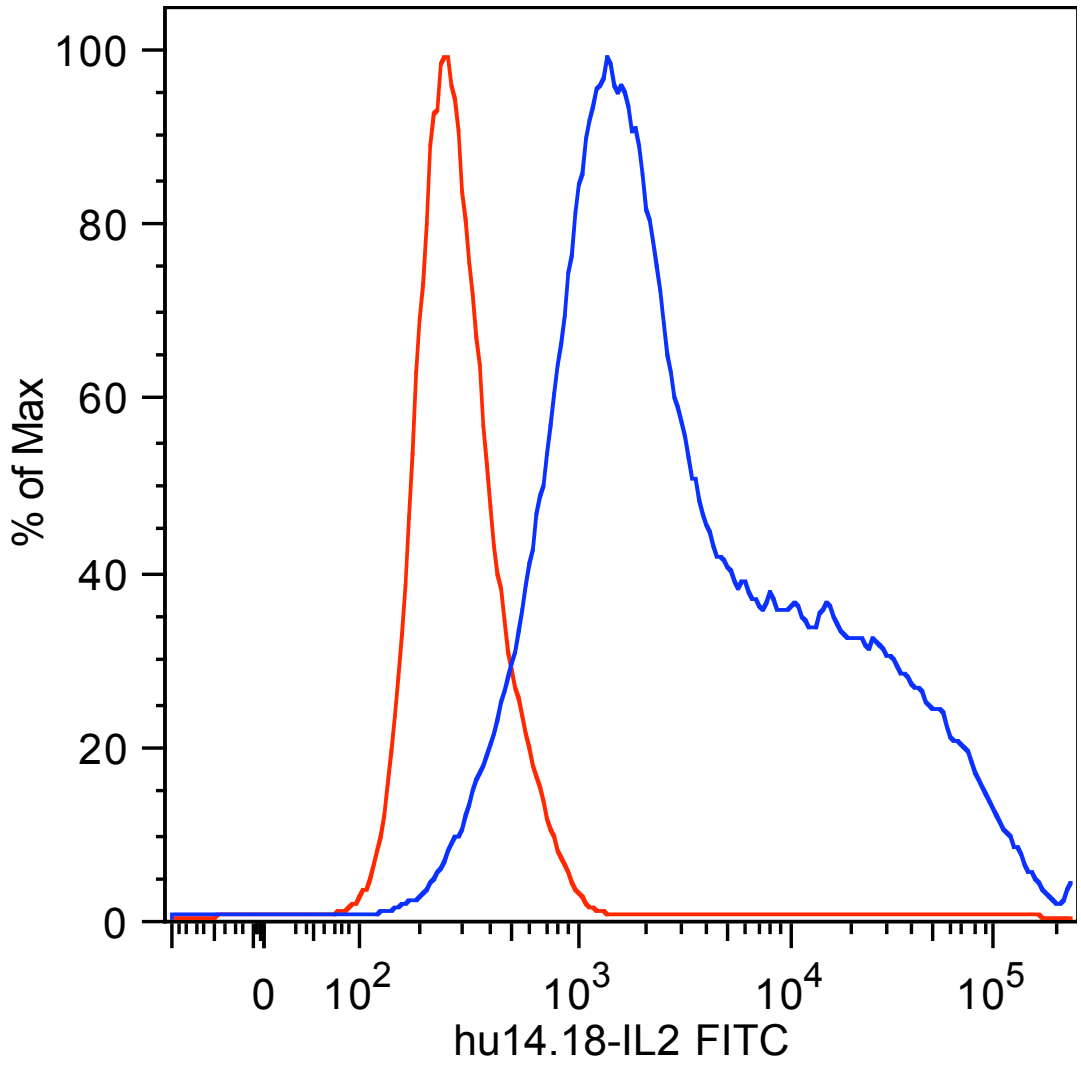

Figure 2-2. Early Established Tumor Model Dosing Schedule

The early-established tumor model was used to examine the role of NK cell or T cell depletion in intratumorally hu14.18-IL2 treated mice. A/J mice were injected subcutaneously with 2 x 10^6 cells of NXS2 murine neuroblastoma in 100µl on Day 0 in the lower right quadrant of the abdomen to establish an initial (primary) tumor. After 4 days mice were injected again subcutaneously with 2 x 10^6 cells of NXS2 murine neuroblastoma in 100µl in the lower left quadrant of the abdomen to establish a second (distant) tumor. Mice were randomized on day 4 (immediately prior to depletion antibody injections and second tumor implantation) into appropriate treatment groups and received 15µg of IC treatment daily for 5 consecutive days (Days 7-11). Mice were given IV IC by tail vein injection in 100µl PBS. IT injections consisted of IC in 100µl PBS, placed into the primary tumor with a needle. IT treatment was only done to the primary (local) tumor. Control treatments consisted of an equivalent volume of PBS administered by IV or IT injection. Tumor volumes of the initial (local) and secondary (distant) tumors were measured using mechanical calipers (Volume = width x width x length / 2).

Figure 2-2.

	Week	Week 1							Week 2								Week 3	
	Day	0	1	2	3	4	5	6	7	8	9	10	11	12	13	14	15	16
NXS2 Cell Line	Primary Engraftment	X																
	Secondary Engraftment					X												
	Randomization					X												
Intra-peritoneal Depletion Injections	Anti-asialo GM1					X					X							X
	Rabbit IgG					X					X							X
	Anti-CD4					X					X							X
	Anti-CD8					X					X							X
	Rat IgG					X					X							X
Therapy	Intratumoral PBS								X	X	X	X	X					
	IT hu14.18-IL2								X	X	X	X	X					

Figure 2-3. Quantification of Immunohistochemistry.

In order to quantify the average percent of certain infiltrating leukocytes in these visually striking stained tissue sections, we developed a histological and statistical method using the freely available software imaging and statistical programs ImageJ and R, respectively. Digital pictures of stained sections were taken at low magnification (10x) and quantitative analysis was performed using ImageJ software. Each section was counted using 5 subsamples per section. For each subsample, the number of positively staining cells was counted to get a numerator. The cell density of the tissue section (the denominator) was obtained by extrapolation from count data from a smaller region within each subsection. Percent positivity was obtained from these data by dividing positively stained cells by overall cell density and multiplying by 100. A comprehensive data table was then created with a percent positivity for each subsample. These data were imported into the statistical program "R" and Mixed-Effect regression models were created for each leukocyte marker, accounting for between-mouse and within-mouse variability. Treatment groups were compared to percent positivity for each of these leukocyte markers and histograms were made using these comprehensive statistical models.

Figure 2-3.

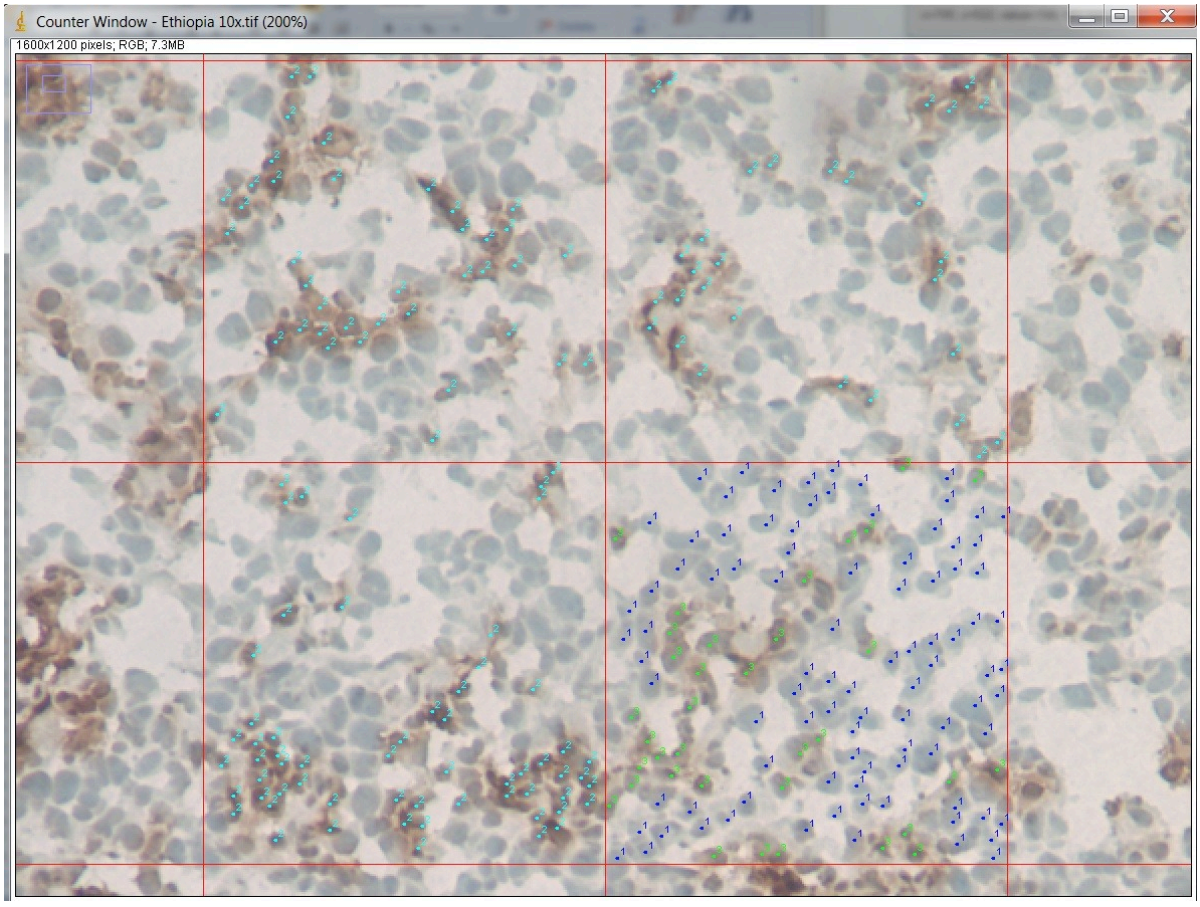
Counter Window - Ethiopia 10x.tif (200%)
1600x1200 pixels; RGB; 7.3MB

Figure 2-4. Gating Strategy.

This was our gating strategy to obtain Total Live Nucleated Cells (TLNCs) or CD45+ cells. We first gated on "Cells" using forward and side scatter (upper left figure), then on single cells ("Singlets") using forward scatter width (upper right figure), then on live cells using DAPI (lower left figure), and then (lower right figure) on CD45(+) cells to get tumor infiltrating leukocytes and on CD45(-) cells to get tumor and stromal cells. Total Live Nucleated Cells (TLNCs) were obtained from the figure in the lower right by the addition of DAPI-negative CD45(-) cells and CD45(+) cells.

Figure 2-4.

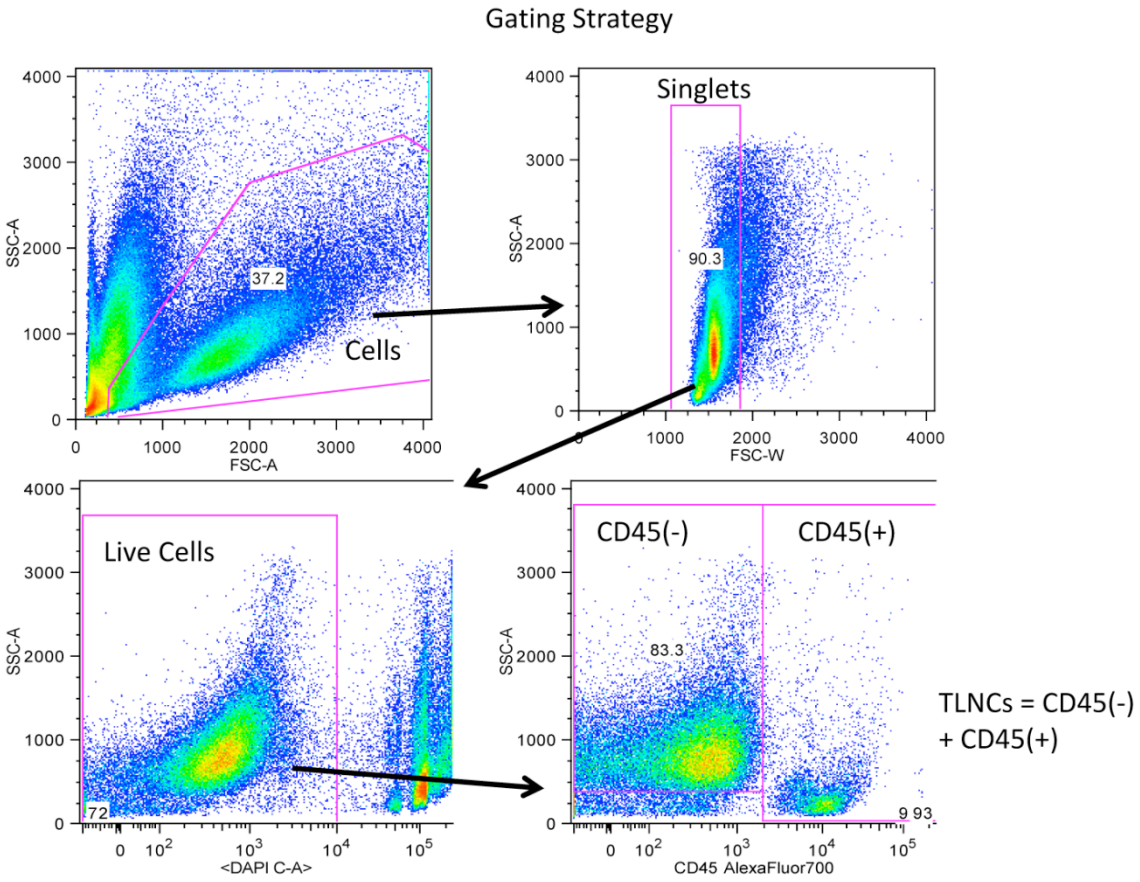
Gating Strategy
SSC-A
FSC-A
37.2
Cells
Singlets
90.3
FSC-W
Live Cells
72
<DAPI C-A>
CD45(-)
CD45(+)
83.3
9.93
CD45 AlexaFluor700
TLNCs = CD45(-)
+ CD45(+)

Figure 2-5. RAE-1gamma Expression on NXS2 ex-vivo.

To assess whether NXS2 murine neuroblastoma expresses NKG2D ligands, we stained a NXS2 tumor *ex vivo* with a rat anti-mouse RAE-1gamma-PE antibody (clone CX1, eBioscience). These tumor and stromal cells were disaggregated from a mouse that died due to progressive disease from subcutaneous NXS2. These cells were then stained with Rat anti-mouse RAE-1 gamma PE (Red line, clone CX1, eBioscience) or with Rat IgG2b Isotype control PE (Blue line, clone eB149/10H5, eBioscience). The data demonstrate strong, and relatively homogeneous staining for RAE-1gamma. The gating strategy was similar to the method mentioned above (F**igure 2-4**). We first gated on "Cells" using forward and side scatter, then on single cells ("Singlets") using forward scatter width, then on live cells using DAPI, and then on CD45(-) cells to get tumor and stromal cells.

Figure 2-5.

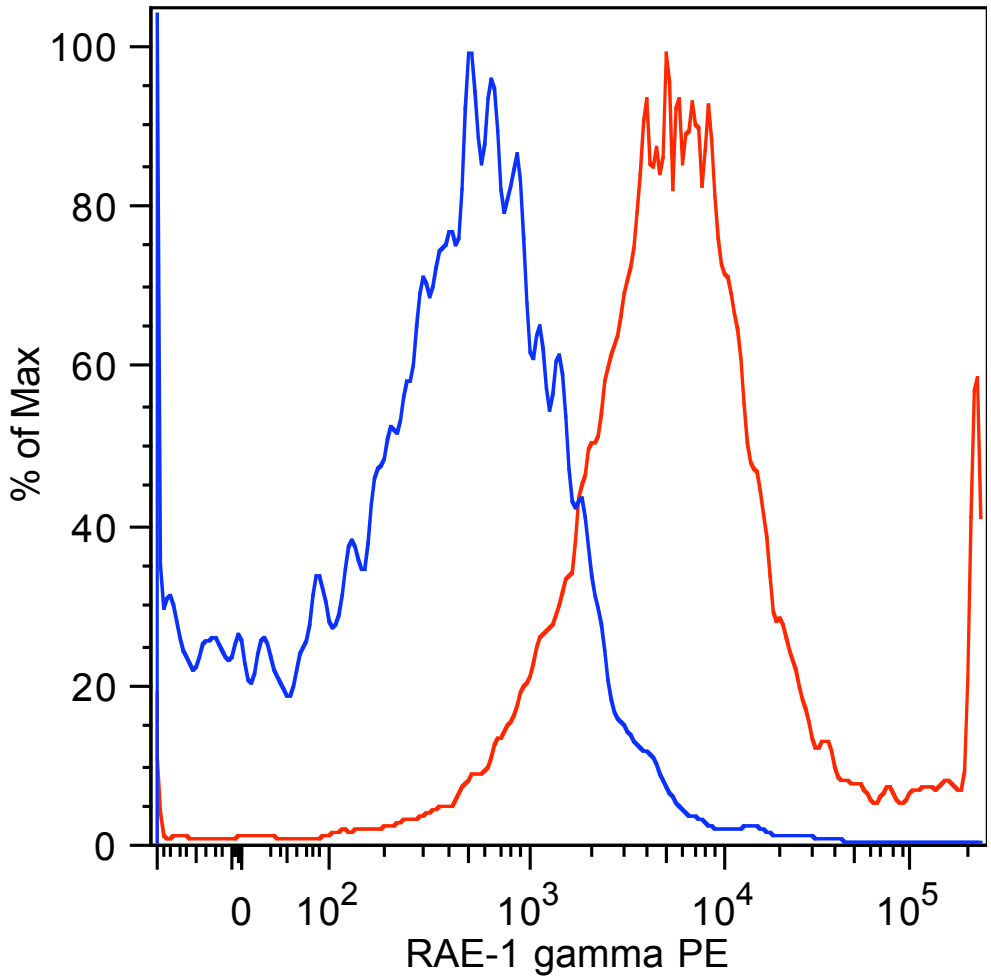

Chapter 3

Intratumoral hu14.18-IL2 (IC) Induces Local and Systemic Antitumor Effects that Involve Both Activated T- and NK cells as well as Enhanced IC Retention

3.1 Abstract

Hu14.18-IL2 is an immunocytokine (IC) consisting of human IL2 linked to hu14.18 mAb, which recognizes the GD2 disialoganglioside. Phase 2 clinical trials of intravenous hu14.18-IL2 (IV-IC) in neuroblastoma and melanoma are underway, and have already demonstrated activity in neuroblastoma. We have previously shown that intratumoral hu14.18-IL2 (IT-IC) compared to IV-IC results in enhanced antitumor activity in mouse models. Studies presented here were designed to determine the mechanisms involved in this enhanced activity and to support the future clinical testing of IT administration of immunocytokines. Improved survival and inhibition of growth of both local and distant tumors were observed in A/J mice bearing subcutaneous NXS2 neuroblastomas treated with IT-IC versus IV-IC or control mice. The local and systemic antitumor effects of IT-IC were inhibited by depletion of NK cells or T cells. IT-IC resulted in increased NKG2D receptors on intratumoral NKG2A/C/E+ NKp46+ NK cells and NKG2A/C/E+ CD8+ T cells when compared to control or IV-IC mice. NKG2D levels were augmented more in tumor-infiltrating lymphocytes (TILs) compared to splenocytes, supporting the localized nature of the intratumoral changes induced by IT-IC treatment. Prolonged retention of IC at the tumor site was seen with IT-IC compared to IV-IC. Overall, IT-IC compared to IV-IC resulted in increased numbers of activated T- and NK cells within tumors, better IC retention in the tumor, enhanced inhibition of tumor growth, and improved survival.

3.2 Introduction

Immunocytokines (IC) are synthetic fusion proteins that consist of tumor-specific monoclonal antibodies (mAb) linked to an immune-stimulating cytokine. Hu14.18-IL2, originally created and described by Steve Gillies (Gillies et al., 1992), is an IC consisting of human interleukin-2 (IL2) linked to each IgG heavy chain of the hu14.18 mAb, which recognizes the GD2 disialoganglioside present on tumors of neuro-ectodermal origin (i.e. neuroblastoma, melanoma) (Gillies et al., 1992). ICs are capable of augmenting significant antitumor effects in murine models by targeting the therapy to the tumor and stimulating the immune system to selectively destroy the cancer cells. In a syngeneic A/J murine model of neuroblastoma, the IV administration of the anti-GD2 ch14.18–IL2 fusion protein induced a cell-mediated antitumor response that eradicated established bone marrow and liver metastases more efficiently than equivalent mixtures of antibody and recombinant human IL2 (Lode et al., 1997). The effector mechanism involved was shown to be exclusively dependent on natural killer (NK cells) (Lode et al., 1998). In a syngeneic BALB/c model, the huKS1/4-IL2 IC, a humanized antibody against epithelial cell adhesion molecule (EpCAM) linked to IL2, was used to elicit a T cell-mediated eradication of established pulmonary and hepatic CT26-KSA murine colon carcinoma metastases (Xiang et al., 1997). Again, mixtures of monoclonal antibody huKS1/4 with recombinant human IL2 were less effective and only partially reduced tumor load (Xiang et al., 1997). In a human melanoma (A375GFP) xenograft murine model, the immunocytokine scFvMEL/TNF, a fusion of human tumor necrosis factor (TNF) and an antibody single chain variant fragment (scFv) against the melanoma gp240 antigen (scFvMEL), targets melanoma cells *in vivo* and results in pronounced antitumor effects after systemic administration (Liu et al., 2006).

Clinical trials involving predecessors to the immunocytokine hu14.18-IL2 to treat GD2+ tumors such as neuroblastoma have shown progress in recent years. A recent Phase 3 trial using a chimeric anti-GD2 mAb (ch14.18) in combination with IL2, GM-CSF and 13-cisretinoic acid (CRA) showed an increase (66% vs 46%) in event free survival (EFS) in pediatric neuroblastoma patients over the previous standard of care maintenance therapy, CRA (Yu et al., 2010). The hu14.18-IL2 itself has also shown clinical activity in children with recurrent, refractory neuroblastoma. A phase I clinical trial sponsored by the Children's Oncology Group (COG) and using the hu14.18-IL2 as a treatment for children with refractory or recurrent neuroblastoma showed immune activation as evidenced by elevated serum levels of soluble IL2 receptor alpha and lymphocytosis (Osenga et al., 2006). The maximal tolerated dose was determined to be 12 $mg/m^2/d$ when administered i.v. over 4 hours for three consecutive days. This study showed that hu14.18-IL2 could be administered safely in pediatric patients at doses that induce immune activation. Subsequently, a phase II study through Children's Oncology Group (COG) showed that recurrent neuroblastoma patients with non-bulky disease (evaluable only by sensitive ^{123}I-MIBG scintigraphy or bone marrow histology) treated with hu14.8-IL2 intravenously at 12 $mg/m^2/d$ for 3 days every 4 weeks had a 21.7% (5 out of 23) complete response (CR) rate (Shusterman et al., 2010). These 5 patients had complete response (CR) status lasting 9, 13, 20, 30 and 35+ months, respectively, in duration. In contrast, patients with bulky disease (measurable by standard radiographic criteria) showed 0 out of 13 responses. This study showed that hu14.18-IL2 warrants further testing in children with nonbulky high-risk neuroblastoma.

Hu14.18-IL2 has also been tested in adult melanoma patients. A phase I clinical trial of hu14.18-IL2 in patients with metastatic melanoma showed immune activation as measured by lymphocytosis, increased peripheral-blood natural killer activity, and increased serum levels of

the soluble IL2 receptor alpha with reversible clinical toxicities at an MTD of 7.5 mg/m^2/d (King et al., 2004). In addition, eight of 33 (24%) patients had stable disease after two courses of therapy. A separate phase I/II study of hu14.18-IL2 in patients with stage IV unresectable, cutaneous metastatic melanoma and showed systemic immune activation as demonstrated by increases in serum levels of sIL2R, IL10, and neopterin as well as increased tumor infiltration by T cells in post-dosing biopsies (Ribas et al., 2009). Stable disease was seen in 2 out of 9 (22%) patients treated with 4 mg/m^2/d of hu14.18-IL2 given as a 4-h IV infusion on 3 consecutive days every four weeks. These two patients had stable disease status determined after courses 2 or 4, but progressing 4 months later in each.

Localized versus systemic administration of immunocytokines has been tested directly in tumor-bearing mice and has shown an advantage of IT administration of ICs compared to IV. In a SCID mouse model using human melanoma xenografts and infused human peripheral blood lymphocytes, therapeutic effects of ICs consisting of an anti-EGFR mAb linked to IL2 fusion protein (IL2-FuP) or TNF (TNF-FuP) showed improved antitumor effects when administered IT compared to IV (Christ et al., 2001). IT injection of intact IC resulted in a survival advantage compared to IT injection of the mAb and IL2 as separate IT injections. Survival time was prolonged by the intratumoral application of FuP. In mice bearing subcutaneous Lewis lung carcinomas transfected with EpCAM, IT injection of huKS-IL12/IL2 (huKS1/4 mAb linked to a cytokine combination of IL2 and IL-12) resulted in complete resolution of tumor (Gillies et al., 2002). In a subcutaneous GD2+ NXS2 neuroblastoma mouse model, IT hu14.18-IL2 treatment resulted in a greater antitumor response, compared to IV hu14.18-IL2 injection. This response was antigen-specific, dose-dependent, and greater than IT injection of IL2 alone (Johnson et al., 2008). The increased activity of IT compared to IV hu14.18-IL2 in NXS2 tumors was seen even

in the absence of T cells (Johnson et al., 2008). Clinical administration of intratumoral IL2 in melanoma patients has shown local antitumor effects (Weide et al., 2010; Weide et al., 2011). As these clinical studies show local benefit of IT IL2 in melanoma patients, and these preclinical studies show IT-IC is more effective than IT IL2 in tumor bearing mice, clinical testing of IT hu14.18-IL2 in melanoma patients with measureable disease appears warranted.

The mechanisms involved in improved antitumor effects seen with IT-IC administration are not clear. In order to evaluate the antitumor mechanisms of IT-IC, and focus on the degree of leukocyte infiltration, we have evaluated the effects of IT hu14.18-IL2 in A/J mice bearing established GD2+ NXS2 neuroblastoma. We hypothesize that IT-IC administration results in increased and sustained levels of the IC in the tumor, augmenting infiltration of immune effector cells into the tumor thereby enhancing the antitumor response. We have developed methods to evaluate these hypotheses in tumor-bearing mice and demonstrate prolonged IC retention at tumor and augmented numbers of activated T and NK cells in TILs. In order to model patterns of infiltrating leukocytes in tumors in patients receiving IC in clinical trials, we have developed a histological method in a preclinical mouse model to identify and quantify these infiltrating immune cells. Additionally, we have used multicolor flow cytometry to quantify the expression of the killing ligand NKG2D on NK cells and cytotoxic T cells (CTLs) as well as analyze the profile of hu14.18-IL2 and TILs at the tumor site following IT vs. IV delivery of hu14.18-IL2.

3.3 Material and Methods

3.3.1 Mice

We obtained 7-8 week old female A/J mice from Jackson Laboratories (Bar Harbor, Maine). All mice were housed in university-approved facilities and were handled according to National Institutes of Health and University of Wisconsin-Madison Research Animal Resource Center (RARC) guidelines.

3.3.2 Cell lines

NXS2 is a moderately immunogenic, highly metastatic, murine neuroblastoma hybrid cell line that was created as previously described (Lode et al., 1997). Briefly, hybridization of the GD2-negative C1300 murine neuroblastoma cell line (A/J background) with murine dorsal root ganglional cells from C57BL/6J mice was used to create the murine NX31T28 cell line. The NXS2 subline was generated by the selection of NX31T28 cells with high GD2 expression. NXS2 cells are of A/J background, that is, $H2K^k$ positive/$H2K^b$ negative (Lode et al., 1997). The murine NXS2 cell line was grown in Dulbecco's modified Eagle's medium (DMEM, Mediatech, Herndon, VA) supplemented with penicillin (100U/ml), streptomycin (100µg/ml), L-glutamine (2mM) (Life Technologies, Inc., Grand Island, NY) and 10% heat-inactivated fetal calf serum (FCS, Sigma Chemicals, St. Louis, MO). Cells were maintained at 37°C in a humidified 5% CO_2 atmosphere.

3.3.3 ICs and immunotherapy

The humanized hu14.18-IL2 (APN301, Apeiron Biologics, Vienna, Austria) was supplied by the NCI Biologics Resources Branch (Frederick, MD) via a collaborative

relationship with Merck KGaA (Darmstadt, Germany). Hu14.18-IL2 is an immunocytokine consisting of an intact human interleukin-2 (IL2) genetically linked to the carboxyl-termini of each human IgG1 heavy chain of the hu14.18 mAb (Gillies et al., 1992). The humanized huKS-IL2 IC (EMD273066) was generated and provided by EMD-Lexigen Research Center (Billerica, MA).

3.3.4 Tumor Models

3.3.4.1 Well-Established Tumor Model

A/J mice were injected subcutaneously with 2 x 10^6 cells of NXS2 murine neuroblastoma in 100µl PBS in the lower right quadrant of the abdomen. Tumors were allowed to grow until the average volume was 30-150 mm^3 (Volume measured with mechanical calipers = width x width x length / 2), normally this required 14-18 days. Mice were then randomized into appropriate treatment groups and received 50µg of IC treatment daily for 3 consecutive days (either IV or IT). Mice were given IV IC by tail vein injection in 100µl PBS. IT injections consisted of IC in 100µl PBS, delivered into the subcutaneous tumor with a 30 gauge needle. Control treatments consisted of an equivalent volume of PBS administered by IT injection.

3.3.4.2 Early-Established Two Tumor Model

A/J mice were injected subcutaneously with 2 x 10^6 cells of NXS2 murine neuroblastoma in 100µl on Day 0 in the lower right quadrant of the abdomen to establish an initial (primary) tumor. After 4 days mice were injected again subcutaneously with 2 x 10^6 cells of NXS2 murine neuroblastoma in 100µl in the lower left quadrant of the abdomen to establish a second (distant) tumor. Mice were randomized on day 4 (immediately prior to depletion antibody injections and

second tumor implantation) into appropriate treatment groups and received 15µg of IC treatment daily for 5 consecutive days (Days 7-11). Mice were given IV IC by tail vein injection in 100µl PBS. IT injections consisted of IC in 100µl PBS, placed into the primary tumor with a needle. IT treatment was only done to the primary (local) tumor. Control treatments consisted of an equivalent volume of PBS administered by IV or IT injection. Tumor volumes of the initial (local) and secondary (distant) tumors were measured using mechanical calipers (Volume = width x width x length / 2).

3.3.5 Endpoints for Progressive Tumor Growth

The endpoint of all tumor growth and survival studies was death of the animal or excessive tumor burden as determined by both tumor size (15mm in any direction) and the condition and behavior of the animal. These criteria are established by the RARC guidelines. The decision to euthanize an animal was made by an independent observer without regard for treatment group.

3.3.6 Cell Depletion Regimens

Local and distant tumors were induced according to the early-established tumor model. To deplete NK cells, mice were injected intraperitoneally (I.P.) with 1.6 mg anti-asialo GM1 antibody (Wako Chemicals Richmond, VA) or 1.6 mg Rabbit IgG isotype control (Sigma) in a total volume of 200µL PBS on days 4, 9, and 16. To deplete T cells, mice were injected I.P. with mixtures of anti-CD4 and anti-CD8 mAbs (250 µg of each) or 500 µg Rat IgG (Sigma) isotype control in a total volume of 200µL PBS on days 4, 9, and 16. Mice received 5 daily IT injections

(Days 7-11) of 15μg hu14.18-IL2 (IC) to the primary tumor in a volume of 50μL PBS or 50μL control PBS. Tumor volumes were measured using mechanical calipers.

3.3.7 IC Retention Experiments

Tumors were induced according to the well-established tumor model and then randomized to receive a single treatment of IT-IC (intratumoral injection of 50μg hu14.18-IL2 in 100μL PBS), IV-IC (intravenous injection of 50 μg hu14.18-IL2 in 100μL PBS), or IT-KS (intratumoral injection of 50μg huKS-IL2 in 100μL PBS). Mice were sacrificed at various times after treatment and their tumors were taken for flow cytometry.

3.3.8 Histology Experiments and Immunohistochemistry (IHC)

Mice treated according to the well-established tumor model were sacrificed 48 hours after treatment completion and their tumors resected for histology. The tumors were embedded in OCT, flash frozen in liquid nitrogen, and stained. Briefly, frozen sections were cut onto slides using a cryostat, fixed in cold acetone and dried. After rehydration, sections were blocked with 5% Rabbit serum (Sigma) for 25 min, washed and incubated with optimally titered mAb [rat anti-mouse CD45(clone 30-F11, eBioscience), CD3 (clone 17A2, eBioscience), CD4(clone GK1.5, eBioscience) , CD8 (clone 53-6.7, eBioscience) , F4/80 (clone BM8, eBioscience) , NKG2A/C/E (clone 20d5, eBioscience)] overnight in 1% Rabbit Serum. Following a wash, a biotinylated rabbit anti-rat secondary antibody was applied for 90 min and followed by ABC avidin-biotin complex (Vector Labs, Burlingame, CA). Slides were developed with DAB (Vector Labs, Burlingame, CA) for 4.5 min, counterstained with Mayer's hematoxylin (Sigma) for 90 sec and washed in running tap water for 5 min and mounted.

3.3.9 Quantitation of IHC

A histological method to identify and quantify leukocyte infiltration patterns in these IT-IC treated tumors was developed. Digital pictures of these stained sections were taken at low magnification (10x) and quantitative analysis was performed using ImageJ software (NIH). The visual fields were placed on reproducible grids, and five representative areas of the same size within each frozen section were chosen. These 5 "subsamples" were inspected visually so that positive and negative cells could be manually counted within each subsample. Analogous grids and subsamples of the same size were obtained for each individual frozen section specimen being analyzed. This manual counting was done using a blinded system, by 2 separate individuals. These results were confirmed by a boarded hematopathologist who assessed the methods and analyses (author EAR). Percentages of subsamples were averaged within a sample and significance tests were performed using the Prism 5, Version 5.0.4, software (GraphPad).

3.3.10 Flow Cytometry

Tumors were established and mice treated according to the well-established tumor model. Forty eight hours after treatment completion, mice were sacrificed and their tumors and spleens resected for flow cytometry. Single cell suspensions were made by disassociating the tissues through brass mesh (30 openings per inch) and then 50 micron nylon filters. Cell counts were determined using a Beckman Coulter cell counter or hemacytometer. About 1 million cells were stained with the following antibodies at 4°C for 30 min: FITC conjugated anti-mouse NKG2A/C/E (clone 20d5, eBioscience), PE conjugated anti-mouse NKG2D (clone CX7, eBioscience), PE-Cy5 conjugated anti-mouse F4/80 (clone BM8, Biolegend), PerCP-eFluor710

conjugated anti-mouse F4/80 (clone BM8, eBioscience), PE-Cy7 conjugated anti-mouse CD4 (clone GK1.5, eBioscience), APC conjugated anti-mouse CD3e (clone 145-2C11, Biolegend), AlexaFluor700 conjugated anti-mouse CD45 (clone 30-F11, Biolegend), APC-eFluor780 conjugated anti-mouse CD8a (clone 53-6.7, eBioscience), CD16/32 Fc Block (clone 93, Biolegend), PE conjugated goat anti-human IL2 (clone MQ1-17H12, eBioscience) and PE conjugated goat anti-human IgG Fc Gamma (cat 12-4998-82, eBioscience). Cells were washed and analyzed using the Becton Dickinson (BD) LSRII. Analyses of data were performed using FlowJo software. Fluorochromes Minus Ones (FMOs) were used to distinguish positively stained populations. Erythrocytes were subtracted from the denominator to allow analyses to focus only on nucleated cells. Results are reported as % positive cells, or as mean fluorescence intensity (MFI) units. In order to obtain Total Live Nucleated Cells (TLNCs) or CD45+ cells. We first gated on "Cells" using forward and side scatter, then on single cells ("Singlets") using forward scatter width, then on live cells using DAPI, and then on CD45(+) cells to get tumor infiltrating leukocytes and on CD45(-) cells to get tumor and stromal cells. Total Live Nucleated Cells (TLNCs) were obtained by the addition of DAPI-negative CD45(-) cells and CD45(+) cells.

3.3.11 Statistical Methods

One-tailed or two-tailed (if there was no *a priori* hypothesis) Student's t-tests under the normality assumption were used to determine significance of differences in antitumor responses (tumor volume, tumor infiltration, tumor growth inhibition, and delivery and retention of IC) between experimental and relevant control groups. Survival curves were generated using the Kaplan - Meier method and statistically compared using the Log Rank (Mantel-Cox) proportional hazard test. Data are presented as mean ± SEM (Standard Error of the Mean) and

considered significant for p values less than 0.05. Due to the exploratory nature of these analyses, multiplicity adjustments were not made. In all figures, p-values are represented with asterisks (*) as follows: <0.05 = (*), <0.01= (**), <0.001 = (***), <0.0001 = (****). Graphs were generated and significance tests were performed using the GraphPad Prism 5, Version 5.04, software.

3.4 Results

3.4.1 IT-IC treatment results in enhanced inhibition of tumor growth and augmented survival compared to controls

Using the well-established tumor model, we established the antitumor effects of IT-IC compared to no treatment (NT) and intratumoral PBS (IT-PBS) control groups. IT-IC treatment induced greater inhibition of tumor growth than NT or IT-PBS (Figure 3-1A). IT-IC also resulted in improved survival compared to the controls (Figure 3-1B). Even though the change in growth induced by IT-IC is seen quickly (48 hours after the last IT-IC treatment) in Figure 3-1A, histological evaluation confirms an immunotherapeutic effect. Hematoxylin and eosin stains of IT-IC treated tumors showed increased lymphocyte infiltration, greater cell death, and increased necrosis compared to no treatment controls (Figures 3-1C,D) and IT-PBS controls (not shown).

3.4.2 Tumors treated with IT-IC are characterized by increased NK and T cells

Frozen sections of tumors were stained for various cell-specific surface markers. Figure 3-2 shows representative samples of an NXS2 tumor treated with localized hu14.18-IL2 and stained with an antibody specific for the CTL marker CD8a. There was a visually striking increase in the amount of infiltrating CTLs compared to the control tumor treated with IT-PBS (Fig. 3-2A vs. Fig. 3-2B). Representative samples of an NXS2 tumor treated with localized hu14.18-IL2 and stained with an antibody specific for NKG2A/C/E, a marker of mouse NK cells, also showed a striking increase in the amount of infiltrating NK cells compared to IT-PBS (Fig. 3-2C vs. 3-2D). We developed a histological method to quantify and characterize the augmented TILs seen in these IT-IC treated tumors.

Digital pictures of these stained sections were taken at low magnification (10x) and quantitative analysis was performed using ImageJ software. The visual fields were placed on reproducible grids, and five representative areas of the same size within each frozen section were used to manually count positive and negative cells within each subsample. Percentages of subsamples were averaged within a sample and significance tests were performed using the GraphPad Prism 5 software.

By this method, IT-IC treated tumors showed higher tumor leukocyte infiltration compared to the controls. An overall increase in leukocyte infiltration was demonstrated by an increase in CD45+ cells in the IT-IC treated tumors (Figure 3-2E). These treated tumors also had increased numbers of T cells and macrophages as shown by increases in CD3+,CD4+, CD8a+ cells and F4/80+ cells, respectively (Figure 3-2E). An increased frequency of cells bearing the NKG2A receptor was also seen in the IT-IC treated tumors; these NKG2A+ cells are presumably licensed NK cells and/or activated cytotoxic T cells (Figure 3-2E) (Vance et al., 2002; McMahon et al., 2002). These data were later confirmed by flow cytometry (see below).

3.4.3 T cells and NK cells are involved in the antitumor effects of IT-IC against local and distant tumors

We wanted to determine whether these TILs were involved in the observed antitumor effects of IT-IC. In this series of experiments, tumor-bearing mice were depleted of CD4+/CD8a+ T cells, NK cells (asialo GM1+), or double depleted of CD4+/CD8a+ T cells and NK cells. The early-established two-tumor mouse model was used for these depletion studies in order to evaluate the antitumor effects of IT-IC on the local-primary (injected) and distant-secondary (non-injected) tumor. The early-established model, enables IC treatment to begin

when tumors are smaller, enabling this immunotherapy to have greater measurable anti-tumor effects; this is in contrast to the well established tumor model (as used in Fig. 3-1), where larger tumors are needed in order to be able to collect tumor 48 hours after treatment for flow cytometry and histology studies. IT hu14.18-IL2 treatment was given only to the local (primary) tumor and tumor sizes of both the local and distant tumors were measured.

Figure 3-3A shows that IT-IC induced marked inhibition of growth of the local tumor compared to IT-PBS. The antitumor effect of IT-IC on the local tumor was nearly abrogated by the T cell depletion. In addition, NK cell depletion caused substantial inhibition of the antitumor effects of IT-IC on the local tumor. Thus both T and NK cells are involved in the antitumor effects of IT-IC against the local tumor in this model. Figure 3-3B shows that, in the absence of T or NK depletion, administration of IT-IC to the local tumor dramatically inhibits the growth of the distant (non-injected) tumor (compared to the growth of the distant tumor in mice that received IT-PBS). Figure 3-3B shows that NK cell depletion as well as T cell depletion causes virtual abrogation of the IT-IC antitumor effect on the distant tumor, suggesting that local IT-IC treatment of the primary tumor results in systemic immune activation, causing anti-tumor effects at the distant tumor site.

Survival data show reduced survival of IT-IC treated mice when either NK or T cells are depleted (Figure 3-3C) in this early-established tumor model. Depletion of T cells or NK cells in IT-IC treated mice resulted in no long-term survivors compared to IT-IC treated mice without depletion, which had 62.5% (10 out of 16) long-term, tumor-free survivors. These 10 tumor-free mice were rechallenged by subcutaneous injection of two million NXS2 cells approximately 110 days after implantation of their initial local primary tumor. Ninety percent of the rechallenged mice (9 out of 10) rejected the tumor rechallenge and remained tumor-free. This result suggests

that mice rendered tumor-free by IT-IC treatment developed long-term memory T cell immunity to NXS2, as shown previously for mice with early tumors made tumor free by the combination of IV-IC and IL2 treatment (Neal et al., 2004).

3.4.4 IT-IC treatment causes better inhibition of tumor growth and enhancement of survival than IV-IC treatment

We hypothesized that local injection of IC will induce better antitumor effects than systemic injection. Therefore, the antitumor effects of IT-IC were compared to those of IV-IC. Mice bearing a single established subcutaneous NXS2 tumor were treated with IT-IC or IV-IC beginning on Day 0. Inhibition of tumor growth was more striking in IT-IC treated mice compared to IV-IC treated mice (Figure 3-4A). IT-IC treated mice also demonstrated improved survival compared to IV-IC treated mice (Figure 3-4B).

3.4.5 IT-IC treatment is characterized by higher percentage of NKG2A/C/E+ cells and a lower percentage of living tumor cells in the tumor than seen following IV-IC treatment

IT-IC treatment induced greater inhibition of tumor growth compared to IV-IC treatment (Figure 3-4A). IT-IC also resulted in improved survival compared to IV-IC (Figure 3-4B). As a result, we wanted to compare the TILs of IT-IC treated mice to those of IV-IC treated mice. Tumors of treated mice (and untreated control mice) were harvested 48 hours after the last IC treatment, frozen, sectioned, and histologically stained for various cell-specific surface markers (Figure 3-4C) or taken, disaggregated, filtered, and stained with fluorescent antibodies for analysis by flow cytometry (Figure 3-4D). The IHC analyses showed that IT-IC and IV-IC caused significant increases in NK cells, CD3 cells and CD8 cells (Figure 3-4C). In the flow

cytometry analyses, these increases in NK cells and CD8 cells after IC treatment were confirmed (Figure 3-4D). In addition, the flow cytometry analyses showed tumors taken from IT-IC treated mice had a higher percentage (%) of NKG2A/C/E+ cells and CD8a+ cells (measured as a % of total viable nucleated cells) compared to tumors taken from IV-IC treated mice (Figure 3-4D). Tumors taken from IT-IC treated mice also had a higher % of F4/80 macrophages compared to untreated mice (Figure 3-4D). This "increase" in % macrophages is relative to all other cells in the tumor; since the IT-IC treated tumors are actually smaller than the untreated tumors, the increased % of macrophages (relative to total live nucleated cells remaining in the tumor) likely corresponds to an actual decrease in actual numbers of macrophages. This is even more clear when macrophages are evaluated as a % of tumor infiltrating leukocytes (CD45+ cells) as shown in Figure 3-4E. For these calculations in Figure 3-4D, erythrocytes were subtracted from the total viable cells to account for recovered viable nucleated cells. We then analyzed (Figure 3-4E) the presence of these leukocyte populations as a percentage of TILs (CD45+ cells), rather than as a percentage of total viable nucleated cells including tumor cells. IT-IC resulted in a significant decrease in the % of CD4+ T cells in the TIL population compared to IV-IC and no treatment. Both IV-IC and IT-IC caused increases in the % of NK cells (as detected by NKp46 and NKG2A/C/E) and CTL (CD8a+). Both IV-IC and IT-IC treatments resulted in some detectable decreases in the % of macrophages (F4/80+) (Figure 3-4E) in these tumors compared to the % of macrophages in the untreated tumors. This "decrease" in % macrophages is relative to all leukocytes and reflects the fact that the tumors have decreased in size with IT-IC treatment and have an increase in % of CD45+ cells (per total live cells, as seen in Figure 3-4D). The fact that the % macrophages have increased less prominently than CD8 cells or NK cells relative to TLNC (in Fig. 3-4D), explains why the macrophages (as a % of CD45+ cells) go down in

Figure 3-4E, while the CD8 and NK cells go up (in Figure 3-4D) with IT-IC treatment. The % of NKG2A/C/E+ cells was significantly higher for IT-IC than IV-IC (Figure 3-4E). These flow cytometry studies also showed that IT-IC treated tumors have lower percentages of living tumor cells than IV-IC treated tumors (Figure 3-4F), consistent with the tumor growth and survival data summarized above (Figs. 3-4A and B).

3.4.6 IT-IC treatment induces a greater increase of NKG2A/C/E+ and NKG2D+ T- and NK cells locally than systemically

Our depletion studies showed that both NK cells and T cells are involved in the antitumor effects of IT-IC (Figure 3-3). Similarly, the IHC and flow cytometry studies show increases in NK and CD8 cells in IT-IC treated tumors (Fig. 3-4C-E). We evaluated the phenotypes of these NK and CD8 cells in TILs and compared them to NK and CD8 cells found in the spleen. We characterized the presence of NKG2A/C/E+ cells, shown to be necessary for self recognition (Vance et al., 1998), within the separate populations of NK cells (NKp46+, Fig. 3-5A) and cytotoxic T cells (CD8a+, Fig. 3-5B). The level of NKp46+ cells that co-express NKG2A/C/E in untreated mice was similar in the tumor and in the spleen (Fig. 3-5A). Tumors treated with IT-IC or IV-IC had an increase in the proportion of NKp46+ cells that co-express NKG2A/C/E (Fig. 3-5A). Statistical significance was not found in the difference of the augmented co-expression of NKG2A/C/E with IT-IC vs. IV-IC. A similar effect was also seen in the spleen. Namely, the IT-IC and IV-IC treatment both induced similar augmented co-expression (over that seen in untreated mice) of NKG2A/C/E on NKp46+ spleen cells (Fig 3-5A); the frequencies of the NKG2A/C/E phenotype on NKp46+ cells in spleens are comparable to those seen in the TILs. In contrast, when examining CD8+ cells for co-expression of NKG2A/C/E the data in Figure 3-5B

demonstrate that even without treatment, the % of CD8 cells that co-express NKG2A/C/E is far higher in the TIL population than in the spleen. In the TILs and spleens, both IT-IC and IV-IC treatment induced significant increases in the percentages of CD8 cells that co-express NKG2A/C/E over that seen in untreated mice. However, the percentages seen in the TILs are 10-15 fold greater than those seen in the spleen. We further examined these NK and CD8 cells that co-express NKG2A/C/E for the level of their surface expression of the NKG2D effector receptor (Fig. 3-5C and D). We found that tumors treated with IV-IC or IT-IC had significantly higher expression levels (MFI) of NKG2D+ on NKp46+ NKG2A/C/E+ co-expressing NK cells than found in control mice (Fig. 3-5C). In contrast, these increases in NKG2D MFI were not seen in the comparable populations in the spleen (Fig. 3-5C). Similar analyses were done for NKG2D expression on the cells co-expressing CD8 and NKG2A/C/E (Fig. 3-5D). As in Figure 3-5C, the MFI of NKG2D in the CD8+ TIL population was augmented by IT-IC and by IV-IC. The level of NKG2D augmentation on these CD8+ TIL after IC treatment was not statistically significant for IT vs. IV delivery ($p = 0.107$). These MFI levels of NKG2D in the CD8+/NKG2A/C/E+ TIL populations were significantly higher than the MFI levels of NKG2D seen in the comparable splenic populations (Fig. 3-5D). We have examined expressivity of NKG2D ligands on NXS2 and have found a large increase in RAE-1γ expression on tumor cells obtained from NXS2 cells harvested from tumors growing in vivo (data not shown).

3.4.7 IT-IC treatment results in augmented delivery and retention of IC in the tumor compared to IV-IC

We next compared the delivery and retention of IC in tumor tissue following IT-IC and IV-IC treatment. Tumors of IV-IC and IT-IC treated mice were taken at various time points post

treatment, disaggregated, filtered, and stained with fluorescently labeled anti-human FcGamma (FcG) chain or anti-human IL2 (as two separate ways to detect IC still bound to the NXS2) for analysis by flow cytometry. In order to compare the effect of the GD2-specific hu14.18-IL2 IC in these studies to the delivery and retention of a non-specific IC that could not bind specifically to the GD2+ NXS2 tumor, we also evaluated animals that received IT administration of the KS-IL2 IC, which consists of IL2 linked to an mAb that recognizes the EpCAM, and does not recognize GD2 (and thus is not able to specifically recognize the EpCAM-negative NXS2 tumor). Because absolute MFI values are not consistent from day to day, data collected in these experiments were normalized to the MFI values for our negative control, the IT-KS-IL2 group. By doing this, the graphs in Figure 3-6 show the fold change of hu14.18-IL2 IC present on tumor cells after IT or IV treatment compared to IT-KS-IL2. IT-IC and IV-IC both had fold changes greater than 1, indicating that the GD2-specific hu14.18-IL2 IC better localizes to the NXS2+ tumor compared to the non-specific IC, KS-IL2; furthermore, since the NXS2 tumor is GD2+ but does not have IL2 receptors, the specific IC (hu14.18-IL2) would be expected to localize better to NXS2 than would the non-specific IC (KS-IL2) or unconjugated free IL-2.

There was a ~65-fold (Figure 3-6A) and a ~150-fold (Figure 3-6B) increase in the amount of IC detected on tumor cells after treatment with IT-IC compared to treatment with IV-IC when detecting IC with the anti-Fcγ antibody and anti-IL2 antibody (Fig. 3-6A and 3-6B), respectively, 15 minutes post treatment. This indicates that initially after treatment, local IC administration results in far more IC being present at the tumor site than systemic IV administration. Figures 3-6A and 3-6B show that over the 75 hours after IT or IV injection, the IC level detected in the tumor (after IT-IC treatment) plateaus between 4 and 6 hours, with lower levels detected at 27 and 75 hours. There is substantially more area under the curve when IC is

given IT compared to IV. At 27 and 75 hours post treatment, there was no difference in tumor IC concentration between IT and IV treated mice.

Interestingly, Figure 3-6A (FcG) and 3-6B (IL2) show that IC administered systemically (IV) seems to take some time to reach the tumor site. At 15 minutes and 1 hour post IV-IC treatment, there is the same amount of IC present on tumor cells as there was after the control IT-KS-IL2 treatment (MFI Ratio = 1). However, there is ~5-fold increase and 2-fold increase in IC at the 3.5 hour time point (Figure 3-6A-B), using anti-FcG antibody or anti-IL2 antibody, respectively. This is followed by an eventual decrease in IC at 75 hours.

3.5 Discussion

Data presented in this report help elucidate possible mechanisms of enhanced antitumor effects of localized hu14.18-IL2 therapy and assist in distinguishing the IT-IC antitumor effect from the IV-IC antitumor effect. In this study, we show that IT-IC treatment induces improved inhibition of tumor growth and augmented survival compared to no treatment or treatment with IT-PBS. Immunohistochemical and flow cytometric analyses show an increased percentage of NK and T cells in IT-IC treated tumors. Depletion studies show that T cells and NK cells are involved in the antitumor effects of IT-IC on directly injected local tumors and on non-injected distant tumors in those same animals. Depletion of either immune cell population substantially attenuates the observed antitumor effects on both the local and distant tumors. These data suggest that both T cells and NK cells are necessary for the local and distant antitumor effects observed under these conditions. While NK cells may be playing a more direct and immediate effect (through ADCC), and T cells may be having a more delayed effect, through an adaptive immune response, we are not able to clarify these mechanisms from the data presented here. Furthermore, other possible mechanisms (direct induction of tumor apoptosis, or disruption of the tumor micro-environment or tumor vascular system) also may be possible.

We also show that IT-IC treatment causes better tumor growth inhibition and survival than IV-IC treatment, which is consistent with flow cytometry analyses demonstrating that IT-IC results in a lower percentage of living tumors cells than IV-IC treatment. Furthermore, flow cytometry analyses show that IT-IC treatment is characterized by a higher percentage of NKG2A/C/E+ cells. IT and IV treatment with hu14.18-IL2 increases the fraction of NK cells and CD8 cells that express NKG2A/C/E, while IT-IC increases expression levels of the NKG2D

effector receptor on NK and CD8 cells to a greater degree than does IV-IC. Finally, flow cytometry analyses were used to show that IT-IC treatment results in augmented delivery and retention of IC to tumor compared to IV-IC treatment.

While ICs allow the targeting of immune-stimulating cytokines directly to the tumor microenvironment, systemic administration is still limited by dose-limiting toxicities (Osenga et al., 2006; King et al., 2004). These dose-limiting toxicities are due to the systemic effects of the IL2 component of the IC (ie: fever, capillary leakage, and secondary effects of capillary leakage, such as hypotension) and effects from the mAb component of the IC; for this hu14.18-IL2 IC, these include neuropathic pain due to mAb recognition of selective GD2-expressing peripheral nerves. Finding a strategy of IC administration that would maximize the direct delivery of IC to the tumor site and potentially decrease dose-limiting systemic toxicities would be clinically beneficial. Using the NXS2 model, we demonstrate a greater antitumor response with localized IC administration compared to an equivalent systemic IC dose in the treatment of established subcutaneous tumors. Importantly, IT-hu14.18-IL2 treatment increased delivery of IC to the tumor site; substantially higher levels of IC were found for several hours at the tumor site following IT-IC vs. IV-IC.

IT-IC resulted in complete resolution of both the directly treated local and non-injected distant tumors in several mice. There are several mechanisms that may be resulting in the antitumor effects of both local and distant tumors. IT-IC may be circulating and having a systemic effect; IT-IC may be inducing a systemic immune response by the host's immune system, or a combination of both. We acknowledge that our experimental design may play some role in our observation that NK depletion (which begins on day 4, 4 days after implantation of the primary tumor and just prior to the implantation of the secondary tumor) more potently

interferes with the IC effects against the distant tumor than the primary one. We also know from previous studies that T cells from treated mice can respond to NXS2 in an antigen-dependent manner (18). Our results indicate that IT-IC induces a systemic immune response. T cells and NK cells were required for rejection of both primary and distant tumors and 90% of mice that became tumor-free following IT-IC treatment were able to subsequently reject rechallenge with 2 x 10^6 NXS2 cells.

The IL2 component of the IC augments the effects of the mAb, and has been shown to increase the number and activation state of NK cells, as well as to stimulate tumor cell killing by antigen-specific T-cells (Sondel and Hank, 1997). The IL2 component can stimulate both NK and T-cells via the IL2 receptor, independent of Fc or T-cell receptor binding, respectively (Gillies et al., 1992, Mule et al., 1987; Voss et al., 1990; Weil-Hillman et al., 1989). Using a metastatic model of NXS2 neuroblastoma metastasizing to bone marrow in A/J mice, IV hu14.18-IL2 therapy has been previously shown to be exclusively NK cell mediated (Lode et al., 1997; Lode et al., 1998). In contrast, our model investigates possible immune effector cells within well-established subcutaneous tumors and shows a necessary role of both NK and T cells in response to localized IT hu14.18-IL2 therapy. There is an increased percentage of NKG2A+ on CD8a+ T cells as well as an increased NKG2D expression on CD8a+/NKG2A+ T cells in tumors versus spleens within similarly treated mice (Figure 3-5B-D). This may suggest at least some inherent importance of T cells in combating tumor cells in this model since NKG2A/C/E+ cells has been shown to be necessary for self recognition (Vance et al., 1998). Furthermore, the statistically significant increase in NKG2D expression on NK cells after IT-IC vs. IV-IC treatment (Fig. 3-5C), may reflect a mechanism that plays some part in the enhanced antitumor effect of IT vs. IV IC treatment. In addition, the increased expression of NKG2D might also be

considered a marker of activation, and suggest that other pathways (not assayed for in this study) might also be further activated by IT-IC than IV-IC.

Depletion data from a two-tumor model showed that T cells, as well as NK cells, play a large role in the IT-IC antitumor effect compared to the previously shown NK-predominant cell-mediated IV-IC antitumor effect (Lode et al., 1998). Perhaps having substantial IL2 bound to the surface of tumor cells after IT-IC treatment (Fig. 3-6B) is directly or indirectly responsible for increasing these specific lymphocytes (NKG2A/C/E+ TIL) or altering their phenotype (increasing expression of NKG2D effector receptor) and enhancing the antitumor effect compared to IV-IC treatment. *In vitro* data suggest that IC on tumor cells enables cells with IL2 receptors to form more activated immune synapses with the tumor cells than they would using mAb in combination with IL2 (Gubbels et al., 2011; Buhtoiarov et al., 2011). When treating IT-IC vs. IV-IC, there is a small but significant increase in NKG2D expression on NKp46+/NKG2A+ double positive cells as well as a small, but not significant increase in NKG2D expression on CD8a+/NKG2A+ cells (Figure 3-5C-D). This may indicate a phenotypic advantage of resulting TILs when treating with IT-IC. Expression of NKG2D on activated CD8+ T cells has been shown to account for TCR independent cytotoxicity against malignant cells *in vitro* (Verneris et al., 2004). Its enhanced expression on CD8+ TILs, but not spleen cells, following IV or IT treatment with IC in our study, demonstrates the localized activation of T cells, at the tumor site, induced by IC treatment. We have examined expressivity of NKG2D ligands on NXS2 and have found a large increase in RAE-1γ expression ex-vivo (data not shown). Therefore, NKG2D may be playing a direct role in the enhanced antitumor effects in addition to being a marker of activation.

Previous data have shown therapeutic and safety benefits of localized versus systemic IC therapy in preclinical models (Christ et al., 2001; Gillies et al., 2002; Johnson et al., 2008) as well as localized versus systemic immune therapy in melanoma patients (Weide et al., 2010; Weide et al., 2011). Our studies confirm and extend this previous work by evaluating possible underlying mechanisms of IT administration of IC, as well as showing antitumor efficacy in an established measureable disease setting in a pre-clinical model. IHC infiltration data collected using the quantitative method we developed is consistent with infiltration data collected by flow cytometry. Even though the experimental design intended for each animal within a treatment group to be identical to one another, there is substantial heterogeneity within treatment groups, which is the topic of a separate manuscript (Yang RK et al, in preparation). The preclinical data presented in this report demonstrate several unique antitumor effects of IT-IC compared to equivalent doses of systemic IC. Flow cytometry analyses of IC delivery and retention show a substantial difference in the amount of IC present at initial time points at the tumor site between IT and IV administration. This direct exposure to greater concentrations of IT-IC at the tumor site between IT-IC and IV-IC may be at least partially responsible for the different tumor response rates and the different infiltration and expression patterns of TIL between the two treatment groups. These mechanisms of enhanced activity by localized IT treatment provide further justification for proceeding with clinical testing of IT-IC, potentially testing IT delivery of hu14.18-IL2 in patients with GD2+ tumors, such as melanoma patients with metastatic disease having cutaneous, subcutaneous or readily injectable involved lymph nodes. Furthermore, the type of analyses presented in this preclinical report might also be conducted on biopsies of patient samples following IT-IC administration. Such immune monitoring by IHC and flow cytometry may become a potential means to assess immunologic effects of IC treatment; if these

parameters show correlation with antitumor effect, they may be considered as indicators for prognosis of patients' response to IT-IC.

Figure 3-1. Intratumoral hu14.18-IL2 Shows Enhanced Antitumor Effects Compared to Control Treatments

Tumors were established according to the well-established tumor model. (A) Tumor growth curves of IT-IC treated (n=12), IT-PBS treated (n=12), and untreated (n=8) subcutaneous NXS2 in A/J mice. Data presented were obtained from two independent experiments. (B) Kaplan-Meier survival curves of IT-IC treated (n=13), IT-PBS treated (n=6), and untreated (n=5) mice. Data represent three independent experiments. (C) H&E stain of IT-IC treated NXS2 4 days post treatment initiation. (D) H&E stain of untreated NXS2.

Figure 3-1.

(A)

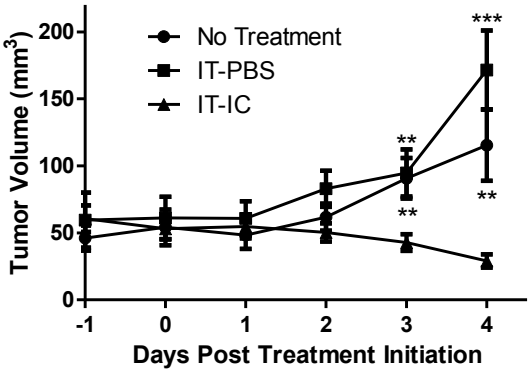

(B)

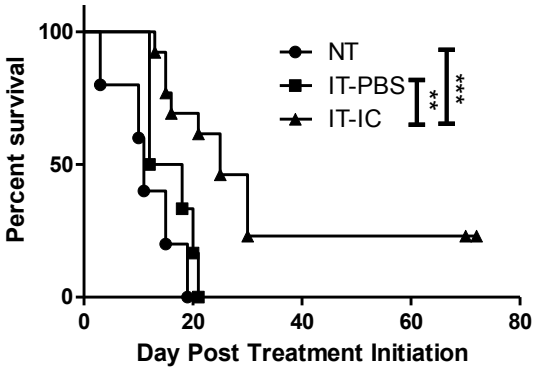

(C)

(D)

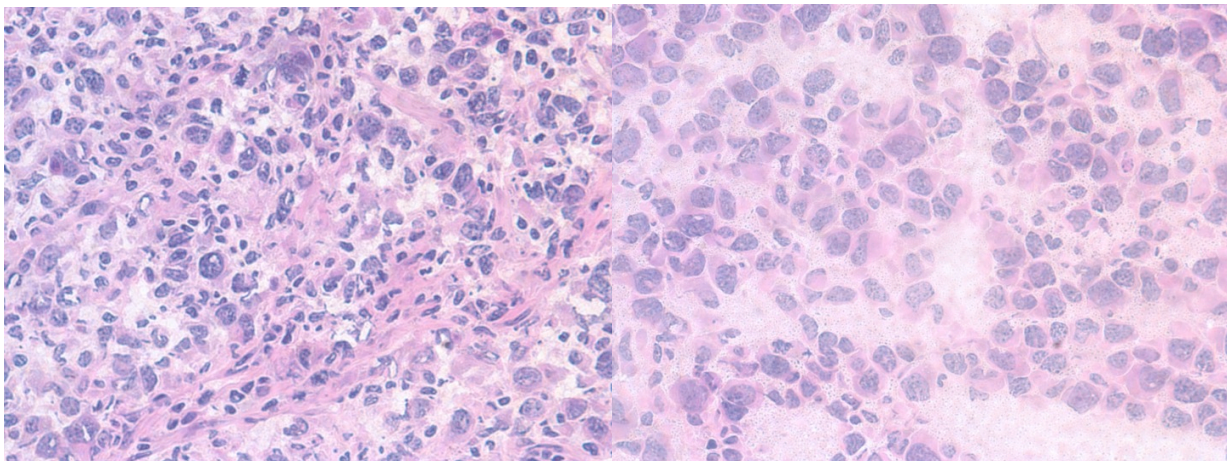

Figure 3-2. Intratumoral hu14.18-IL2 is Distinguished by Increased TILs

Representative immunohistochemical (IHC) stains of subcutaneous NXS2 tumor frozen sections were digitally photographed. Sections were stained with either anti-CD8a (A, B) or anti-NKG2A/C/E (C, D) antibodies. Sections from either IT-IC treated tumors (A, C) or untreated tumors (B, D) are shown. (E) Quantification of IHC pictures using the manual counting method. IT-IC treated (n=20) tumors are characterized by higher tumor leukocyte infiltration percentages (CD45+, CD3+, CD8a+, NKG2A+, F4/80+) than IT-PBS treated (n=10) and untreated (n=15) tumors. Data presented were obtained from three independent experiments.

Figure 3-2.

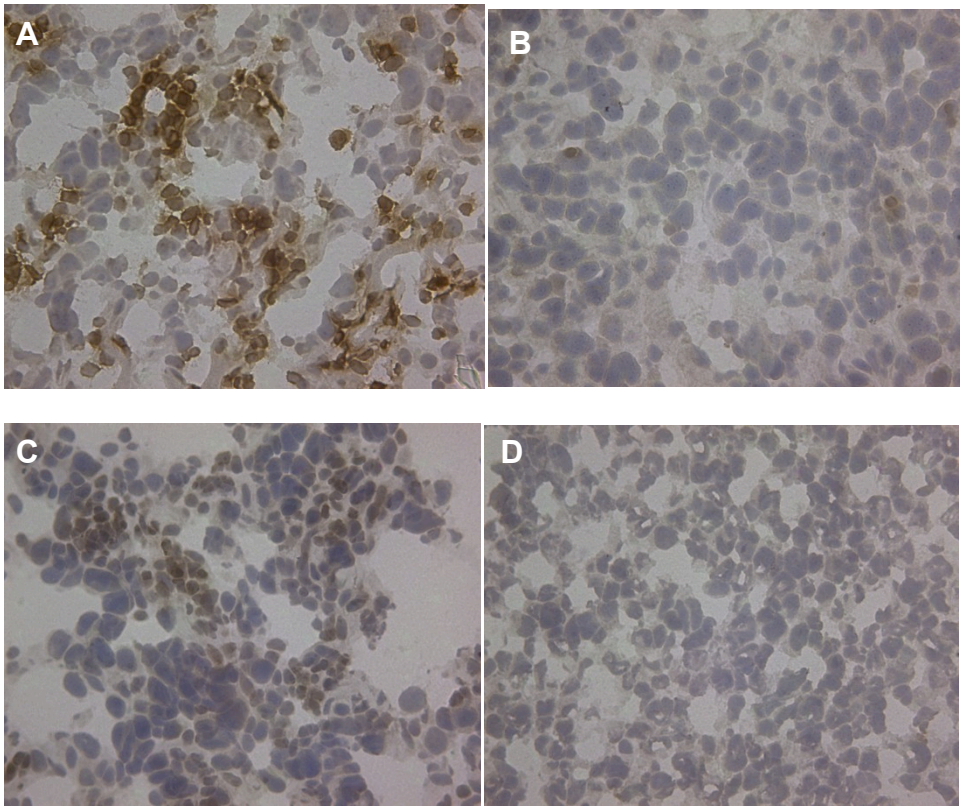
A
B
C
D

(E)

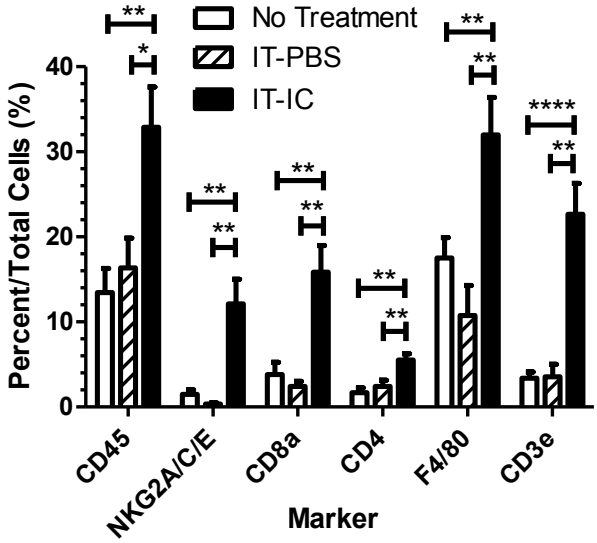
No Treatment
IT-PBS
IT-IC
Percent/Total Cells (%)
0
10
20
30
40
CD45
NKG2A/C/E
CD8a
CD4
F4/80
CD3e
Marker

Figure 3-3. T cell and NK Cell Depletion Reduces IT-IC Induced Antitumor Effects

Tumors were established according to the early-established tumor model. Local tumor (A) and distant tumor (B) growth curves of IT-IC treated T cell depleted (n=8), IT-IC treated NK cell depleted (n=16), IT-IC treated without depletion (n=16), and IT-PBS treated (n=16) mice bearing subcutaneous NXS2 tumors. (C) Kaplan-Meier survival curves of mice with the early established 2-tumor NXS2 model, shown in Fig. 3-3A and 3-3B for groups receiving IT-IC treatment, with and without NK or T cell depletion. Data presented were obtained from two independent experiments.

Figure 3-3.

(A)

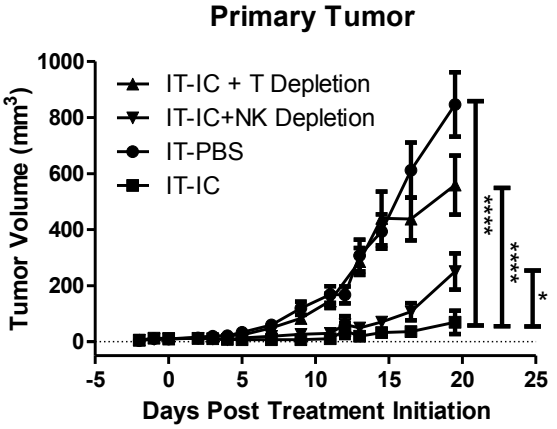

(B)

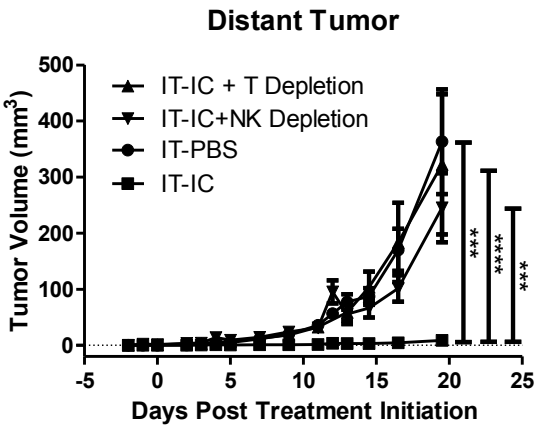

(C)

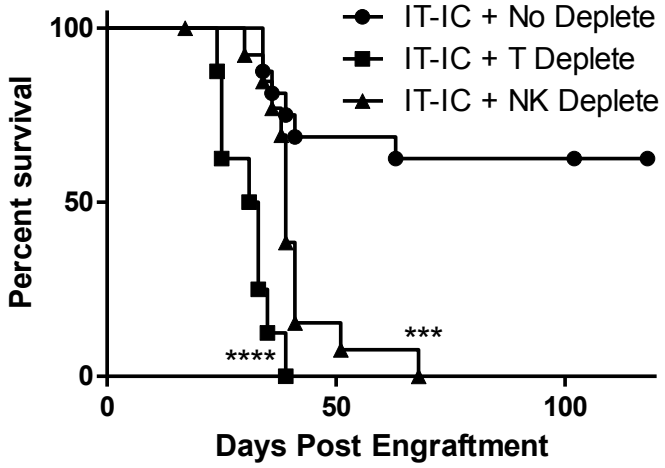

Figure 3-4. IT-IC is More Effective than IV-IC in Slowing Tumor Growth and Prolonging Survival

Tumors were established according to the well-established tumor model. Mice given IT-IC, IV-IC, and no treatment were followed. Tumor growth curves (n=30 per group, four independent experiments) (A) and Kaplan-Meier survival curves (n=13 per group, three independent experiments) (B) are plotted. Mice in these treatment groups were also sacrificed for characterization of the TILs, using both manual blinded counting of immunohisotochemistry pictures (n=15 per group, three independent experiments) (C) as well as flow cytometric analyses (TLNCs = Total Live Nucleated Cells) (D). (E) Populations of TILs as a percentage of total leukocytes within a tumor (CD45+) are also plotted. (F) Populations of live NXS2 tumor cells as a percentage of TLNCs within a tumor are also plotted. (D-F: n=11 per group, three independent experiments)

Figure 3-4.

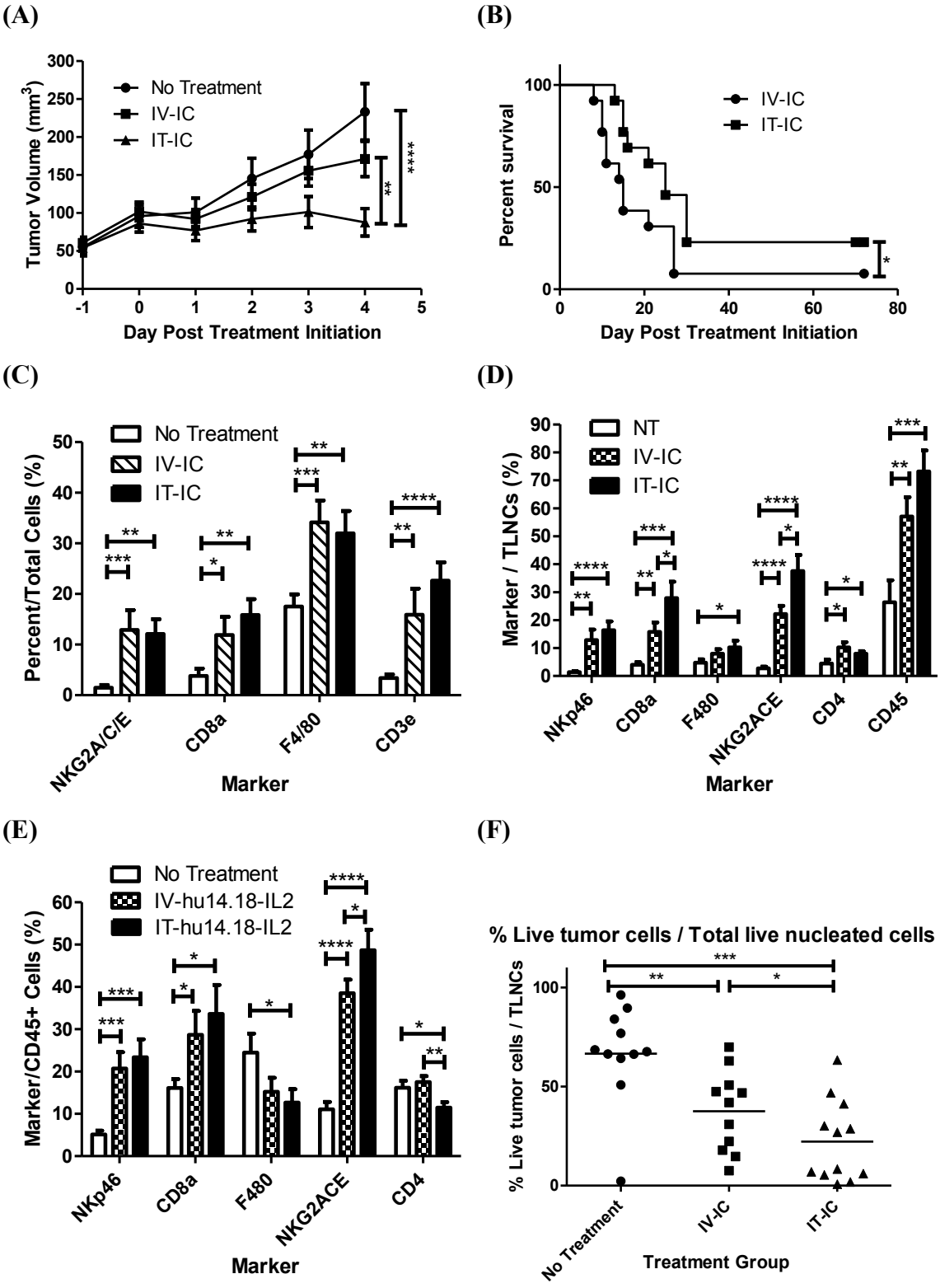
(A)
Tumor Volume (mm3)
No Treatment
IV-IC
IT-IC
Day Post Treatment Initiation
(B)
Percent survival
IV-IC
IT-IC
Day Post Treatment Initiation
(C)
Percent/Total Cells (%)
No Treatment
IV-IC
IT-IC
NKG2A/C/E
CD8a
F4/80
CD3e
Marker
(D)
Marker / TLNCs (%)
NT
IV-IC
IT-IC
NKp46
CD8a
F480
NKG2ACE
CD4
CD45
Marker
(E)
Marker/CD45+ Cells (%)
No Treatment
IV-hu14.18-IL2
IT-hu14.18-IL2
NKp46
CD8a
F480
NKG2ACE
CD4
Marker
(F)
% Live tumor cells / Total live nucleated cells
% Live tumor cells / TLNCs
No Treatment
IV-IC
IT-IC
Treatment Group

Figure 3-5. Treatment with hu14.18-IL2 Increases NKG2A/C/E+ NK and T cells in tumor and spleen and Increases NKG2D Expression within Tumors

Flow cytometric analyses show percentages of NKG2A/C/E+ cells within the NKp46+ natural killer cell populations (A) and the CD8a+ cytotoxic T cell populations (B) within tumors and spleens. Flow cytometric analyses of NKG2D expression on NKp46+/NKG2A/C/E+ natural killer cell populations (C) and the CD8a+/NKG2A/C/E+ cytotoxic T cell populations (D) within tumors and spleens. All data represent three independent experiments with n=11 mice per group.

Figure 3-5.

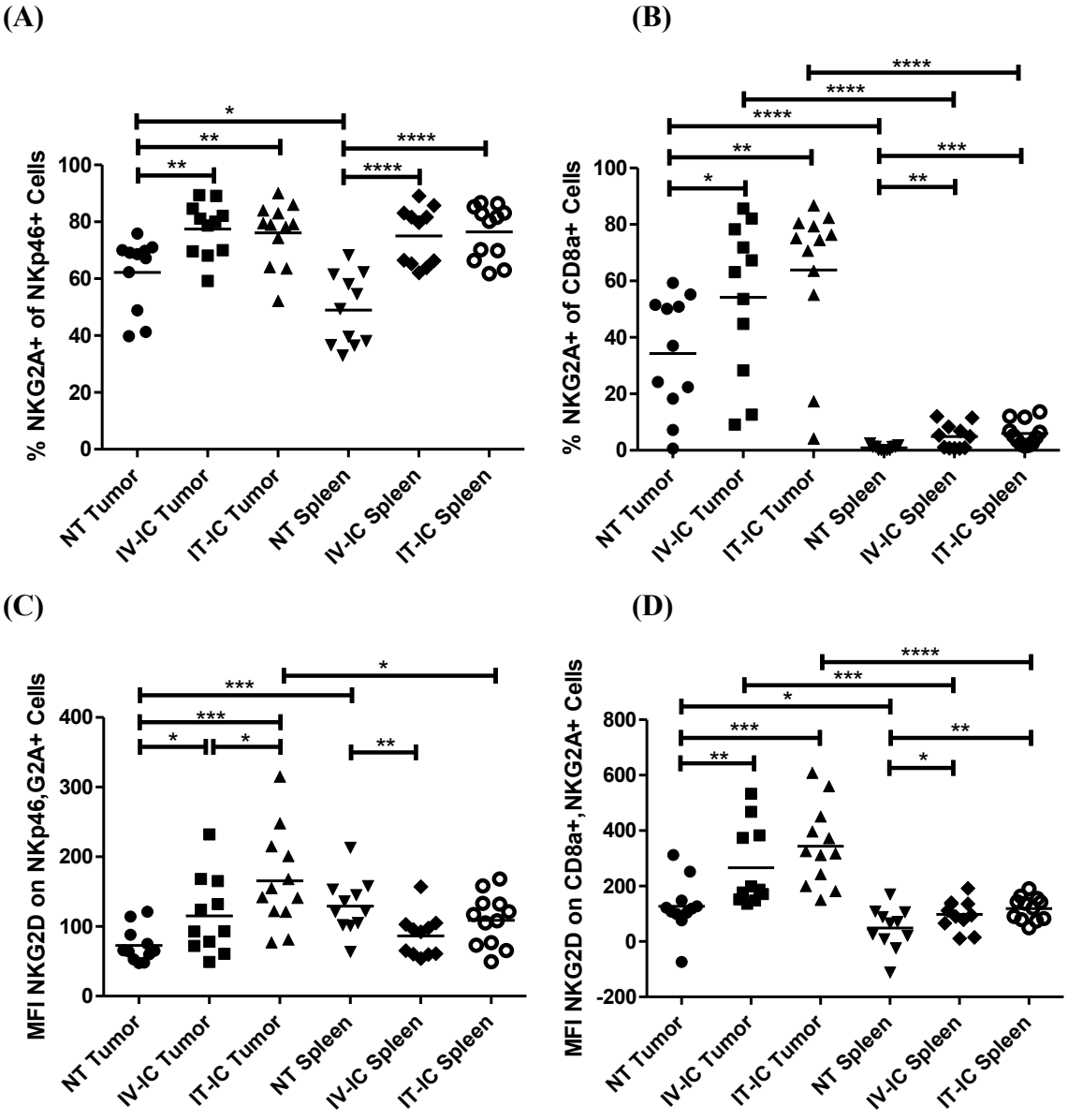
(A)
% NKG2A+ of NKp46+ Cells
NT Tumor
IV-IC Tumor
IT-IC Tumor
NT Spleen
IV-IC Spleen
IT-IC Spleen
(B)
% NKG2A+ of CD8a+ Cells
(C)
MFI NKG2D on NKp46,G2A+ Cells
(D)
MFI NKG2D on CD8a+,NKG2A+ Cells

Figure 3-6. IT-IC Treatment Results in Augmented IC Localization and Increased IC Retention Compared to IV-IC

Tumor-bearing mice given hu14.18-IL2 IT or IV were sacrificed at varying times and their tumors disaggregated. (A) Flow cytometric measurements of levels of human IgG FcG antibody fragment on NXS2 tumor cells ex-vivo at various times post treatment. (B) Flow cytometric measurements of levels of human IL-2 on NXS2 tumor cells ex-vivo at various times post treatment. All values of MFI are normalized to an intratumoral non-specific control immunocytokine (IT-KS-IL-2). Data represent three independent experiments with ~6 mice per group per timepoint.

Figure 3-6.

(A)

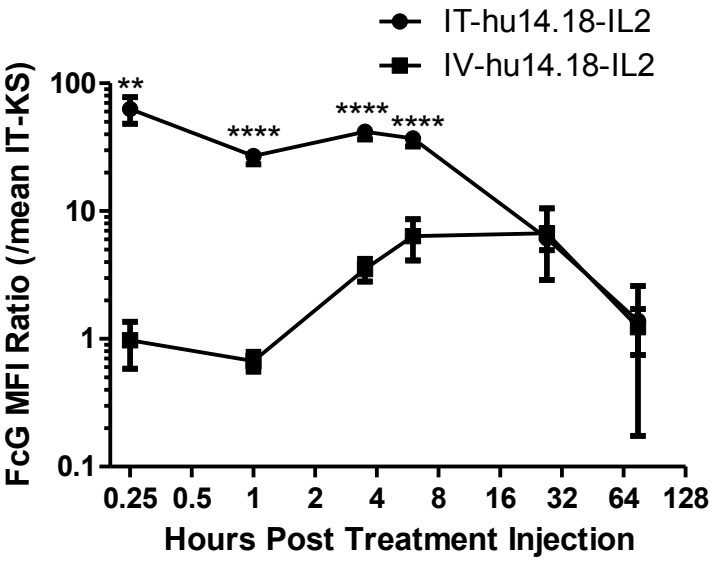
IT-hu14.18-IL2
IV-hu14.18-IL2
FcG MFI Ratio (/mean IT-KS)
100
10
1
0.1
**
****
****
****
0.25 0.5 1 2 4 8 16 32 64 128
Hours Post Treatment Injection

(B)

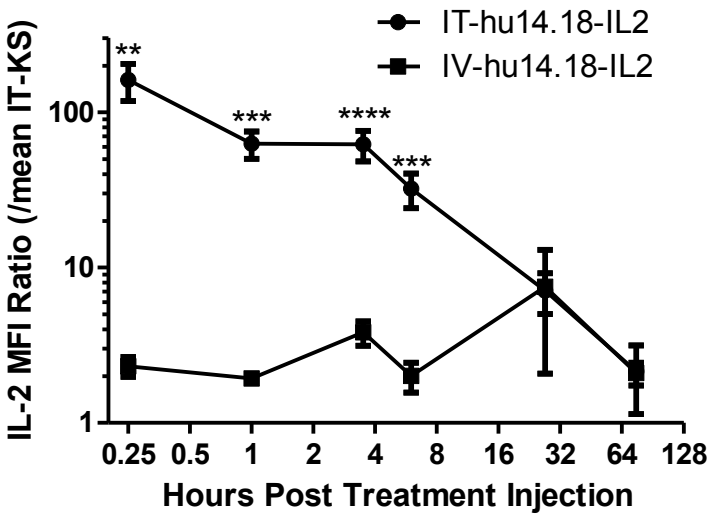
IT-hu14.18-IL2
IV-hu14.18-IL2
IL-2 MFI Ratio (/mean IT-KS)
100
10
1
**
***
****
***
0.25 0.5 1 2 4 8 16 32 64 128
Hours Post Treatment Injection

Chapter 4

Small Tumor Burden at Treatment Initiation Correlates with Higher Density of Tumor Infiltrating Lymphocytes and Better Antitumor Efficacy of hu14.18-IL2 in Mice

4.1 Abstract

Hu14.18-IL2 is an immunocytokine (IC) consisting of human IL-2 linked to hu14.18 mAb, which recognizes the GD2 disialoganglioside. Phase II clinical trials of intravenous hu14.18-IL2 (IV-IC) in neuroblastoma and melanoma are underway, and have already demonstrated activity in neuroblastoma. In our Phase II trial, lower neuroblastoma burden at the time of treatment was associated with a greater likelihood of clinical response to IV-IC. We have previously shown that intratumoral hu14.18-IL2 (IT-IC) compared to IV-IC results in enhanced local and systemic antitumor activity in tumor-bearing mice. We sought to investigate the impact of tumor burden on the efficacy of hu14.18-IL2 as treatment for GD2+ neuroblastoma in a mouse model. Studies presented here describe analyses of initial tumor burden at treatment and its effects on treatment efficacy of hu14.18-IL2, tumor-infiltrating leukocytes, tumor progression, and survival outcome in A/J mice bearing subcutaneous NXS2 neuroblastoma. Our data show that smaller tumor burden at treatment initiation is an important factor leading to increased tumor-infiltrating leukocytes, decreased cancer progression, and increased overall survival. We also show that increased tumor-infiltrating lymphocytes shortly after treatment initiation correlate with inhibition of cancer growth and improvement in overall survival. Furthermore, NXS2 tumor shrinkage shortly after treatment initiation is necessary for long-term survival. These data demonstrate that, in this model system, initial tumor size is a strong predictor of 14.18-IL2-induced lymphocyte infiltration and treatment outcome.

4.2 Introduction

Immunocytokines (IC) are synthetic fusion proteins that consist of tumor-specific monoclonal antibodies (mAb) linked to an immune-stimulating cytokine. Hu14.18-IL2 is an IC consisting of human interleukin-2 (IL2) linked to each IgG heavy chain of the hu14.18 mAb, which recognizes the GD2 disialoganglioside present on tumors of neuro-ectodermal origin (i.e. neuroblastoma, melanoma) (Gillies et al., 1992). ICs are capable of augmenting significant antitumor effects in murine models by targeting the therapy to the tumor and stimulating the immune system to selectively destroy the cancer cells (Lode et al., 1997; Lode et al., 1998; Neal et al., 2004).

The hu14.18-IL2 IC has been tested in adults with melanoma and in children with neuroblastoma (Osenga et al., 2006; Shusterman et al., 2010; King et al., 2004; Ribas et al., 2009) and has shown clinical activity in children with neuroblastoma (Shusterman et al., 2010). A recent phase II study through the Children's Oncology Group (COG) showed that recurrent or refractory neuroblastoma patients with non-bulky disease (evaluable only by sensitive ^{123}I-MIBG scintigraphy or bone marrow histology) treated with hu14.8-IL2 intravenously at 12 mg/m^2/d for 3 days every 4 weeks had a 21.7% (5 out of 23) complete response (CR) rate (Shusterman et al., 2010). In contrast, of 13 patients with bulky disease (measurable by standard radiographic criteria) none showed measurable response ($p = 0.03$ for response in the non-bulky vs. bulky disease groups) (Shusterman et al., 2010). Genotyping analyses from these patients showed that responses were also associated with favorable Killer Immunoglobulin-like receptor (KIR) – KIR ligand relationships, suggesting an in vivo role for NK mediated antitumor effects (Delgado et al., 2010). These clinical data suggest that the immune antitumor activity of hu14.18-IL2 warrants further testing in children with non-bulky high-risk neuroblastoma.

Prior studies in A/J mice bearing the metastatic NXS2 neuroblastoma have shown that IV treatment with hu14.18-IL2 can effectively eliminate very small subcutaneous tumors, and small disseminated metastases, with greater efficacy observed if systemic treatment was initiated early after IV seeding of experimental metastases (Neal et al., 2004). In order to enhance local IC delivery, our lab has shown that intratumoral administration of immunocytokine (IT-IC) induces greater local antitumor effects than IV administration (Johnson et al., 2008). We have recently shown that IT-IC compared to IV-IC results in increased numbers of activated T- and NK cells within tumors, better IC retention in the tumor, enhanced inhibition of tumor growth, and improved survival (Yang et al., In Revision). These analyses also showed that IC treatment was associated with activation of NK cells as well as T cells, selectively within tumors, as measured by augmented expression of the NKG2D activation receptor on these cells.

In our immunotherapy studies of hu14.18-IL2 treatment of NXS2-bearing mice, different groups of mice receive different treatments depending on the experimental goals of the study. For example, one distinct group might receive IV-IC, one may receive IT-IC and a third may receive no treatment. All mice in all groups are from the same strain, of the same age, and received identical tumor cell doses. The observed distinct outcomes between groups are used to make conclusions regarding the different treatments that distinguish the groups (Neal et al., 2004; Johnson et al., 2008; Yang et al., In Revision). However, for virtually every outcome parameter (tumor growth, survival time, lymphocyte subset infiltrate, etc.) there is substantial heterogeneity within treatment groups, even though the experimental design intended for each animal within a treatment group to be identical to one another. We sought to identify biologic differences within treatment groups to help account for the heterogeneous outcomes observed. As we have shown that the level and type of tumor infiltrating lymphocytes (TILs) can

distinguish between treatment groups, we chose to focus on the number and phenotype of TILs as well as the initial tumor burden, as parameters to evaluate within treatment groups to potentially account for tumor growth heterogeneity.

This choice of TIL number and phenotype was also influenced by substantial clinical data indicating that such correlations have clinical significance.A formal analysis via Pubmed and Embase investigated the prognostic influence of TILs in clinical studies (Gooden et al., 2011). Studies were included in which the prognostic significance of intratumoral CD3+, CD4+, CD8+, and FoxP3+ lymphocytes were determined (Gooden et al., 2011). In this pooled analysis, CD3+ TILs had a positive effect on survival with a hazard ratio (HR) of 0.58 [95% confidence interval (CI) 0.43-0.78] for death, as did CD8+ TILs with a HR of 0.71 (95% CI 0.62-0.82). FoxP3+ regulatory TILs were not linked to overall survival, with a HR of 1.19 (95% CI 0.84-1.67). A separate meta-analysis of studies found that intraepithelial TILs are a robust predictor of outcome in ovarian cancer and define a specific class of patients, whose distinct tumor biology should be taken into account in devising appropriate therapeutic strategies (Hwang et al., 2012). Lack of intraepithelial TILs is significantly associated with a worse survival among patients (Hwang et al., 2012). The absence of TILs, together with increasing Breslow thickness, presence of ulceration and male sex, also predicts sentinel lymph node (SLN) metastasis in patients undergoing SLN biopsy for primary cutaneous melanoma (Taylor et al., 2007). In melanomas with a brisk TIL infiltrate, the probability of a positive SLN was 0.039 as compared with 0.262 for melanomas in which TILs were absent ($p<0.001$) (Taylor et al., 2007). High levels of intratumoral TILs are associated with improved recurrence-free survival in stage 1A non-small-cell lung cancer patients as well as a reduced likelihood of systemic recurrence (Horne et al.,

2011). Also, when angiolymphatic invasion is not present, the beneficial effects of TILs become even more profound (Horne et al., 2011).

Staging is a well known predictor of prognosis as well as of treatment efficacy. For example, heterogeneity in clinical biology of localized gastric cancer (LGC) is best reflected after chemoradiation in presurgical and postsurgical pathologic stages, and correlation of outcome with presurgical staging may facilitate strategies to individualize therapy for LGC (Patel et al., 2007). A stage IV neuroblastoma study found that metastatic patterns in neuroblastoma correlate with tumor biological features and event-free survival (EFS) (DuBois et al., 1999). Neuroblastoma EFS was decreased in patients with bone, bone marrow, CNS, intracranial/ orbital, lung, and pleural metastases.

This current study represents an evaluation of the parameters predictive of successful immunotherapy in a mouse model; we have focused these analyses at the individual mouse level. We have evaluated, by histology and flow cytometry, the level and distribution of TILs in individual NXS2-bearing mice involved in studies of hu14.18-IL2 administration (IT-IC, IV-IC and control treatment). While differences are seen between these treatment groups, substantial heterogeneity is observed within each treatment group. We here analyze the immune infiltrate profile of TILs seen shortly after hu14.18-IL2 treatment. Our analyses demonstrate that even within the same treatment group, there is a correlation between initial tumor burden and immune infiltration, between immune infiltration and clinical outcome, and thus also between initial tumor burden and clinical outcome.

4.3 Material and Methods

4.3.1 Mice

We obtained 7-8 week old female A/J mice from Jackson Laboratories (Bar Harbor, Maine). All mice were housed in university-approved facilities and were handled according to National Institutes of Health and University of Wisconsin-Madison Research Animal Resource Center (RARC) guidelines.

4.3.2 Cell lines

NXS2 is a moderately immunogenic, highly metastatic, GD2+ murine neuroblastoma hybrid cell line that was created as previously described (Lode et al., 1997). The murine NXS2 cell line was grown in Dulbecco's modified Eagle's medium (DMEM, Mediatech, Herndon, VA) supplemented with penicillin (100U/ml), streptomycin (100µg/ml), L-glutamine (2mM) (Life Technologies, Inc., Grand Island, NY) and 10% heat-inactivated fetal calf serum (FCS, Sigma Chemicals, St. Louis, MO). Cells were maintained at 37°C in a humidified 5% CO_2 atmosphere.

4.3.3 ICs and immunotherapy

The humanized hu14.18-IL2 (APN301, Apeiron Biologics, Vienna, Austria) was supplied by the NCI Biologics Resources Branch (Frederick, MD) via a collaborative relationship with Merck KGaA (Darmstadt, Germany) and Apeiron Biologics.

4.3.4 Tumor Model

A/J mice were engrafted subcutaneously with 2 x 10^6 cells of NXS2 murine neuroblastoma in 100µl PBS in the lower right quadrant of the abdomen. Developed tumors were

measured with mechanical calipers and allowed to grow until the average volume was 30-150 mm^3 (Volume = width x width x length / 2). Mice were then randomized into three treatment groups and received 50μg of IC treatment daily for 3 consecutive days (either IV or IT), or control treatment. Mice were given IV-IC by tail vein injection in 100μl PBS. IT-IC injections consisted of IC in 100μl PBS, delivered into the subcutaneous tumor with a 30 gauge needle. Control mice were untreated or treated with an equivalent volume of PBS administered by IT injection.

4.3.5 Endpoints for Progressive Tumor Growth

The endpoint of all tumor growth and survival studies was death of the animal or excessive tumor burden as determined by both tumor size (15mm in any direction) and the condition and behavior of the animal. These criteria are established by the RARC guidelines. The decision to euthanize an animal was made by an independent observer without regard for treatment group. Time to death/euthanasia was measured from treatment initiation.

4.3.6 Histology Experiments and Immunohistochemistry (IHC)

Mice treated according to the well-established tumor model were sacrificed 48 hours after treatment completion and their tumors resected for histology. The tumors were embedded in OCT, flash frozen in liquid nitrogen, and stained with rat anti-mouse CD45 (clone 30-F11, eBioscience), CD3 (clone 17A2, eBioscience), CD4 (clone GK1.5, eBioscience), CD8 (clone 53-6.7, eBioscience), F4/80 (clone BM8, eBioscience), NKG2A/C/E (clone 20d5, eBioscience). Briefly, frozen sections were cut onto slides using a cryostat, fixed in cold acetone and dried. After rehydration, sections were blocked with 5% Rabbit serum (Sigma) for 25 min, washed and

incubated with optimally titered primary antibody overnight in 1% Rabbit Serum. Following a wash, a biotinylated rabbit anti-rat secondary antibody was applied for 90 min and followed by ABC avidin-biotin complex (Vector Labs, Burlingame, CA). Slides were developed with DAB (Vector Labs, Burlingame, CA) for 4.5 min, counterstained with Mayer's hematoxylin (Sigma) for 90 sec and washed in running tap water for 5 min and mounted.

4.3.7 Quantitation of IHC

A novel quantitative method of histology to identify and quantify leukocyte infiltration patterns in these IT-IC treated tumors was developed (Yang et al., In Revision). Digital pictures of these stained sections were taken at low magnification (10x) and quantitative analysis was performed using ImageJ software (NIH). The visual fields were placed on reproducible grids, and five representative areas of the same size within each frozen section were chosen and these "subsamples" were inspected visually so that positive and negative cells could be manually counted within each subsample. Analogous grids and subsamples of the same size were obtained for each individual frozen section specimen being analyzed. This manual counting was done using a blinded system, by 2 separate individuals (authors RKY& NAK). These were confirmed by a board certified hematopathologist who regularly assessed their methods and results (author EAR). Percentages of subsamples were averaged within a sample and significance tests were performed on the averages using the Prism 5, Version 5.0.4, software (GraphPad).

4.3.8 Flow Cytometry

Tumors were established and mice were treated as described in the Methods section under "Tumor Model". Forty eight hours after treatment completion, mice were sacrificed and

their tumors and spleens resected for flow cytometry. Single cell suspensions were made by disassociating the tissues through brass mesh (30 openings per inch) and then 50 micron nylon filters. Cell counts were determined using a Beckman Coulter cell counter or hemacytometer. About 1 million cells were stained with the following antibodies at 4°C for 30 min: FITC conjugated anti-mouse NKG2A/C/E (clone 20d5, eBioscience), PE conjugated anti-mouse NKG2D (clone CX5, eBioscience), PE-Cy5 conjugated anti-mouse F4/80 (clone BM8, Biolegend), PerCP-eFluor710 conjugated anti-mouse F4/80 (clone BM8, eBioscience), PE-Cy7 conjugated anti-mouse CD4 (clone GK1.5, eBioscience), APC conjugated anti-mouse CD3e (clone 145-2C11, Biolegend), AlexaFluor700 conjugated anti-mouse CD45 (clone 30-F11, Biolegend), APC-eFluor780 conjugated anti-mouse CD8a (clone 53-6.7, eBioscience), CD16/32 Fc Block (clone 93, Biolegend), PE conjugated goat anti-human IL-2 (clone MQ1-17H12, eBioscience) and PE conjugated goat anti-human IgG Fc Gamma (cat 12-4998-82, eBioscience). Cells were washed and analyzed using the Becton Dickinson (BD) LSRII. Analysis of data was performed using FlowJo software. Fluorochromes Minus Ones (FMOs) were used to distinguish positively stained populations. Erythrocytes were subtracted from the denominator to account for differences in angiogenesis between tumors. Results are reported as % positive cells, or as mean fluorescence intensity (MFI) units.

4.3.9 Statistical Methods

In all figures, p-values are represented with asterisks (*) as follows: <0.05 is represented with one asterisk (*), <0.01 = (**), <0.001 = (***) and <0.0001 = (****). Slope comparisons between regression analyses are tested and similarly indicated with “s” values (^{s}) as follows: <0.05 is represented with one s (^{s}), <0.01 = (^{ss}), <0.001 = (^{sss}) and <0.0001 = (^{ssss}). Regression

lines with significantly different slopes cannot be tested for differences elevations because they will intersect at some point in space. In cases when slopes are not significantly different, elevation (covariate-adjusted means) comparisons between regression analyses are tested (Zar JH, 1984) and similarly indicated with "x" values (^{x}) as follows: <0.05 is represented with one x (^{x}), <0.01 = (^{xx}), <0.001 = (^{xxx}) and <0.0001 = (^{xxxx}). Contingency tables and graphs were analyzed using a Chi-squared statistic test or the Fisher's exact test (for small samples) to generate p-values. Survival curves were generated using the method described by Kaplan and Meier and statistically compared using the log rank (Mantel-Haenszel) test. In figures with bar graphs, one-tailed or two-tailed (if there was no a priori hypothesis) Student's t-tests were used to determine statistical significance of observed differences between experimental and relevant control values. Data are presented as mean ± standard error of the mean (SEM) and considered statistically significant for p values less than 0.05. In all scatter plot figures testing for correlation, asterisks after treatment groups in the legend represent a statistically significant different slope of each group's regression line model compared to 0. For comparisons between treatment groups, "s" or "x" indications are used in place of asterisks, to test whether the slopes or elevations, respectively, of each group's regression line are statistically significantly different from each other. Graphs were generated and significance tests were performed using Prism 5, Version 5.04, software (GraphPad). Due to the exploratory nature of the reported statistical inference, no adjustments were made for multiple testing throughout.

4.4 Results

4.4.1 Initial Tumor Volume Inversely Correlates with Survival in hu14.18-IL2 Treated Mice

We first sought to determine whether the initial tumor volume (measured in each mouse, in each treatment or control group, on the day treatment was initiated) is prognostic or predictive for survival outcome in tumor-bearing mice after treatment with IC (either IV or IT). Tumors were induced and tumor-bearing mice were distributed to 3 different groups in a way that the initial tumor volumes were distributed evenly amongst all three groups. The median initial tumor volume for all animals was 34 mm^3 in all three groups together. These three groups were then randomly assigned to 3 days of IT-IC, IV-IC or control treatment. These animals were then evaluated for survival and for tumor growth. After completion of the experiment and collection of all data, mice were analyzed for survival outcome stratified by initial (Day 0 = Day of treatment initiation) tumor volume (either < $34mm^3$ or > $34mm^3$) (**Fig. 4-1**). Data in Figure 4-1 compare control mice to the combined data for IT-IC and IV-IC treated groups. Hu14.18-IL2 treated mice initially bearing tumors smaller than $34mm^3$ showed an increased long-term survival percentage (30.8% survival) compared to mice bearing tumors larger than $34mm^3$ (0% survival) as well as to control mice (0% survival) (**Fig. 4-1A**). Hu14.18-IL2 treated mice initially bearing tumors smaller than $34mm^3$ also showed improved survival time compared to control mice initially bearing tumors smaller than $34mm^3$ (**Fig. 4-1B**). However, hu14.18-IL2 treated mice bearing tumors larger than $34mm^3$ did not survive significantly longer than control treated mice initially bearing tumors larger than $34mm^3$ (**Fig. 4-1B**). This indicates that smaller initial tumor volume is predictive for improved overall survival induced by hu14.18-IL2 treatment.

Conversely, IC treatment did not provide any survival advantage for the mice with larger initial tumor volume.

4.4.2 Hu14.18-IL2 Treatment of Mice with Smaller Initial Tumor Volume Leads to Increased Tumor NK Infiltration and NKG2D Expression on Tumor NK cells and CD8+ T cells

We hypothesized that smaller initial tumor volume at the time of hu14.18-IL2 treatment may affect the immune profile of that tumor, which may influence growth of that animal's tumor as well as survival. To examine the effect of initial tumor load on tumor infiltrating leukocytes (TILs) found 4 days later in the IT-IC, IV-IC, and no treatment groups, treated and untreated NXS2 tumors from tumor-bearing mice were harvested from mice euthanized 4 days following the initiation of treatment; tumors were dissected, disaggregated, and characterized for TIL populations by flow cytometry. Unlike the experimental model used in Fig. 4-1, where the endpoint was survival, this study intentionally sacrificed all mice 4 days after treatment in order to evaluate the tumors by flow cytometry. In order to make certain that adequate tumor mass was available (4 days after initiating treatment) in all mice to enable sufficient cells for flow cytometry analyses, the treatment in this experiment was begun later after implanting the subcutaneous tumors in these mice, so that the tumor volumes at the time of treatment initiation was larger than that in the study shown in Fig. 4-1. Thus the median initial tumor volume for all mice whose tumors were taken for flow cytometry in this study (Fig. 4-2) was 101.6 mm^3. Supplementary figure 4-1 contains the analogous continuous data for all mice in this study. The amount of CD45+ leukocytes in IT-IC treated tumors, as a percentage of Total Nucleated Cells (TNCs), is significantly higher when the initial volume is less than 101.6 mm^3 compared to

tumors initially larger than 101.6 mm^3 in volume (**Fig. 4-2A**). This trend was also seen in the no treatment group and in the IV-IC treated group (**Fig. 4-2A**), but was not significant for the IV-IC group. Interestingly, we did observe significant increases in leukocyte density after treatment with both IT and IV hu14.18-IL2 compared to control treatment for the tumors that were initially > 101.6 mm^3. However, we only observed significant increases in leukocyte density after treatment with IT hu14.18-IL2 compared to control treatment for the tumors < 101.6 mm^3 (**Fig. 4-2A**). For all panels in figure 4-2, we have included more detailed correlation comparisons in the online supplementary data (Supplementary Figure 4-1A-F).

We sought to further characterize this CD45+ population. The amount of F4/80+ macrophages in the tumor as a percentage of CD45+ leukocytes is significantly higher for each treatment group in tumors that are initially larger than 101.6 mm^3 compared to tumors smaller than 101.6 mm^3 (**Fig. 4-2B**). Treatment also had little effect on the amount of F4/80+ macrophages in the tumor, as seen by similar percentages of macrophages in treated and untreated tumors in the cohort with large initial tumors (**Fig. 4-2B**), as well as similar (but smaller) percentages of macrophages in the 3 treatment groups for the animals starting with a smaller tumor volume. The amount of NKp46+ NK cells as a percentage of CD45+ leukocytes is significantly higher in IC treated tumors compared to untreated tumors in the animals starting with small tumors (Fig. 4-2C); this same increase in NK cells in IC treated tumors vs. control tumors was also seen in the animals starting with larger tumors (**Fig. 4-2C**). In addition, the amounts of NKp46+ NK cells in IT-IC treated tumors as a percentage of CD45+ leukocytes are significantly higher in smaller initial tumors compared to larger initial tumors (**Fig. 4-2C**). This trend is not observed in the IV-IC treated or untreated tumors (**Fig. 4-2C**), indicating that IT-IC treatment was required for this augmented induction of NKp46+ NK cells in the tumors that start

smaller. The amount of CD8+ T cells in IT-IC and IV-IC treated tumors, as a percentage of CD45+ leukocytes, is similar in initially smaller tumors compared to initially larger tumors (**Fig. 4-2D**). The percentage of CD8+ T cells in IC treated tumors, appears higher than the percentage of CD8+ T cells in the untreated tumors, independent of initial tumor volume (**Fig. 4-2D**), although this increase is non-significant when comparing the IV treated smaller tumors to untreated smaller tumors. These results suggest that IC treatment (IV or IT) induces somewhat similar percentage of CD8+ T cell infiltration regardless of initial tumor burden.

The activation status of these infiltrating NKp46+ NK and CD8+ CTL populations is potentially important for antitumor activity. We tested for the expression of the effector receptor NKG2D on NKG2A/C/E+ NKp46+ NK cells (considered "licensed" NK cells), and NKG2A/C/E+ CD8+ cells (considered activated CTL) (Vance et al., 2002; McMahon et al., 2002), hypothesizing that the activating NKG2D receptor may be expressed on these cells. NKp46+ NKG2A/C/E+ co-expressing NK cells in initially small, IT-IC treated tumors had increased expression levels (augmented MFI) of the NKG2D effector receptor compared to initially large, IT-IC treated tumors (**Fig. 4-2E**). NKG2D levels on NKp46+ NKG2A/C/E+ NK cells are higher in IV or IT treated larger tumors compared to untreated larger tumors, and much higher in IT treated smaller tumors than in the untreated and IV-IC treated smaller tumors (**Fig. 4-2E**). The pattern of augmented NKG2D expression on CD8+ NKG2A/C/E+ co-expressing CTLs (**Fig. 4-2F**) on IT-IC treated and on smaller initial tumors is similar to that seen on NKp46+ NKG2A/C/E+ NK cells (**Fig. 4-2E**).

4.4.3 Increased Tumor Leukocyte Infiltration Results from Higher CD8+ T cell Density, but not NK Density, in Mice receiving IT-IC and Correlates with Higher NKG2D Expression on NK cells and CD8+ T cells

Next, we evaluated which kinds of infiltrating leukocytes (CD45+ cells) are responsible in the accounting of overall increases in tumor leukocyte density. For ease of biologic interpretation, a cutoff at the median percent CD45+/TNC (41.2% for all mouse tumors taken for flow cytometry) was used to distinguish tumors with high (>41.2%) or low (<41.2%) tumor leukocytes. We compared mice that showed >41.2% CD45+/TNCs cells with those showing < 41.2% CD45+/TNCs cells. These same data as continuous scatter plots are shown in Supplementary Figure 4-2. The amount of NKp46+ NK cells in the tumor as a percentage of CD45+ leukocytes rises with IC treatment in animals with CD45 > 41.2% and also rises in those with CD45 < 41.2% (**Fig. 4-3A**). The amount of NKp46+ NK cells in the tumor as a percentage of CD45+ cells is similar within these 2 treatment groups [i.e.: between tumors with low (<41.2%) and high (>41.2%) CD45+ leukocyte densities (**Fig. 4-3A**)]. These data suggest that NK cell infiltration increases with IC treatment, but that differential increases of NK cells does not account for the substantial increase in the overall % of CD45+ leukocytes seen after IC treatment in the tumors with >41.2% CD45+ cells. In contrast, the amount of CD8+ T cells in the tumor (as a percentage of CD45+ leukocytes) is higher in IT-IC treated tumors with high CD45+ densities compared to the amount of CD8+ T cells in the tumor (as a percentage of CD45+ leukocytes) in IT-IC treated tumors with low CD45+ densities (39.7% vs. 21.3%) (**Fig. 4-3B**). These data suggest that a preferential increase in CD8+ CTLs are in part responsible for the increases in overall CD45+ leukocytes in those IT-IC treated tumors that show > 41.2% CD45+ leukocyte densities. Moreover, we found that IT-IC treated tumors that have high leukocyte

(>41.2% CD45+) densities also have higher levels of NKG2D on NKp46+ NK cells (**Fig. 4-3C**) and on CD8+ T cells (**Fig. 4-3D**) compared to the NKG2D MFI values seen on these same NK cell and CD8 cell subsets in tumors with low leukocyte densities (<41.2% CD45). These data suggest that IT-IC treatment that is capable of inducing high CD45+ leukocyte infiltration is also associated with the presence of activated infiltrating NK cells and CD8+ T lymphocytes, as evidenced by augmented NKG2D expression.

4.4.4 Tumor NK Cell and CD8+ T cell Infiltration Inversely Correlate with Tumor Growth following IC Treatment

We wished to identify types of infiltrating leukocytes that may be involved in the observed antitumor activity. We developed a histological method (detailed in the Methods Section) to identify and quantify leukocyte infiltration patterns in tumors. We sought to examine if the presence of any types of leukocytes correlate with percent tumor growth, as this could indicate which cells were most prevalent in shrinking tumors. We plotted the percent infiltrate of different leukocyte subsets within each tumor against the change in tumor size (from the time of treatment initiation to 4 days later when the animals were euthanized and tumors harvested for histological analyses) for that same animal, expressed as a percentage of its original tumor volume [Percent (%) Tumor Growth = 100 x (Tumor Volume at Day 4 – Initial Tumor Volume) / Initial Tumor Volume]. Within each treatment group (IT-IC, IV-IC, or Control), we used linear regression analysis to test whether tumor growth was correlated with infiltrate.

We observed a negative correlation (significantly negative slope compared to 0) between NKG2A/C/E+ cells and percent tumor growth in IV-IC and IT-IC treated tumors but not in PBS treated tumors (**Fig. 4-4A**). These negative slopes indicates that more NK cells correlate with

less tumor growth in the IV-IC and IT-IC groups. These same negative correlations were also seen with CD8+ T cells in hu14.18-IL2 treated mice, but not in control mice (**Fig. 4-4B**). Furthermore, the elevations of the IV-IC lines are higher than that of the IT-IC lines for NK cell (**Fig. 4-4A**) and CTL (**Fig. 4-4B**) [specific p values for these comparisons are indicated as (^{x}), (^{xx}), etc. (see statistical methods section and figure legend)]. The different elevations of these lines for IT-IC and IV-IC indicate that, even at similar percentages of NK and T cell infiltration, IV-IC treated tumors grew more than IT-IC treated tumors [ie: in **Figs. 4-4A** and **4-4B**, at any value of % NK cells or % CTLs along the x-axis, the value for the blue (control) and red (IV-IC) line is higher than the value for the black (IT-IC) line]. Interestingly, control treated mice (IT-PBS, NT) did not show a significant negative correlation; namely the blue lines in **Figs. 4-4A** and **4-4B** do not have a slope that is significantly different than 0, indicating no significant relationship between these tumor lymphocytes and tumor growth (although there is a non-significant trend towards more tumor growth with smaller percentages of NK cells and CD8 cells). Overall, tumors that shrank in size (values below the dashed line at 0% change in volume on the y-axis) tended to have more tumor lymphocyte infiltrate than tumors that grew (**Figs. 4-4A and 4-4B**). Furthermore, this was an incremental relationship; the greater the lymphocyte infiltrate, the more shrinkage (or less growth) observed for the IT-IC group as well as for the IV-IC group.

We confirmed these histological results in separate experiments with separate animals, using flow cytometry. Flow cytometric analyses showed the same negative correlation between percent tumor leukocytes and percent tumor growth in the IT-IC treated mice (**Fig. 4-4C**). The elevations of the IV-IC and IT-PBS lines are again higher than that of the IT-IC lines, suggesting that IV-IC and IT-PBS treated tumors grew more than IT-IC treated tumors, even when

comparing similar values for leukocyte infiltration (**Fig. 4-4C**) [as in **Figs. 4-4A** and **4-4B**, here in **4-4C** at any value of % CD45 cells along the x-axis, the value for the blue (control) and red (IV-IC) line is higher than the value for the black (IT-IC) line]. We then evaluated the immune profile of treated and untreated tumors, stratified by whether the tumors grew or shrank (**Fig. 4-4D**). **Supplementary Fig. 4-3** shows the raw data for these comparisons from **Fig. 4-4D**. IT-IC was the only treatment group that had a significant number of tumors shrink and is thus why IV-IC and untreated shrinking tumors are not included in the analysis shown in **Fig. 4-4D**. IT-IC treated tumors that grew and IV-IC treated tumors that grew have similar infiltration profiles (**Fig. 4-4D**). IT-IC treated tumors that shrank have a different TIL pattern than seen in IT-IC treated tumor that grew, with significantly higher amounts of CD8+ T cells and NKp46+ NK cells, but significantly lower amounts of F4/80+ macrophages in tumors as percentages of CD45+ leukocytes (**Fig. 4-4D**). These data suggest that CD8+ T cells and NKp46+ NK cells play important roles in the IC-induced antitumor effect. In contrast, these data suggest that F4/80+ macrophage infiltration may be associated with tumor growth and potentially antagonistic to the antitumor activity of IT-IC (at least in the IT-IC treated tumors that grew). Unlike NK cells and CD8 cells, the amount of CD4+ T cells in the tumor as a percentage of CD45+ leukocytes is not significantly different between IT-IC treated tumors that grew and IT-IC treated tumors that shrank.

4.4.5 NKG2D Expression on NK cells and CD8+ T cells Correlates with Tumor Volume Reduction Following Hu14.18-IL2 Treatment

Since relatively similar amounts of Leukocyte (CD45+), NK and CD8 cell infiltration between IT-IC and IV-IC treated tumors were observed (**Figs. 4-2A, C, D**, and **4-3A, B**), but the

IT-IC group showed much better tumor shrinkage than IV-IC group (**Figs. 4-4A, B, C**), we were interested in other immune mechanisms to potentially account for this enhanced antitumor effect of IT-IC over IV-IC. The activation status of infiltrating lymphocytes may be important for the observed antitumor effect. We tested for the expression of the effector receptor NKG2D (a known activation marker) on NKG2A/C/E+ NKp46+ NK cells and NKG2A/C/E+ CD8+ CTL cells to evaluate whether NKG2D expression correlates with tumor growth or shrinkage. NKG2D expression on NKp46+ NKG2A/C/E+ NK cells in IT-IC treated tumors (**Fig. 4-5A**) and NKG2D expression on CD8+ NKG2A/C/E+ T cells in IT-IC treated tumors (**Fig. 4-5B**) correlates with reduction in tumor volume (the higher the NKG2D expression, the smaller the tumor). There is an incremental relationship between the increase in NKG2D MFI and tumor shrinkage seen for the IT-IC groups (black lines) in **Figs. 4-5A** and **4-5B**. This correlation is not statistically significant in the IV-IC treatment group (red lines in **Figs. 4-5A** and **4-5B)**, suggesting that NKG2D expression may contribute to the enhanced tumor shrinkage in the IT-IC treatment group compared to IV-IC. Untreated mice show a similar relationship between NKG2D on NK cells and CTLs with percent tumor growth (**Fig. 4-5A and 4-5B**). Thus, even in the absence of treatment, tumors with the greatest spontaneous growth are the ones with the lowest density of NKG2D on their infiltrating lymphocytes. The elevation of the IV-IC line is significantly higher than that of the IT-IC line, suggesting that IV-IC treated tumors grew more than IT-IC treated tumors, even when comparing similar levels of NKG2D expression [as in **Figs. 4-4A**, **4-4B**, and **4-4C** at any value of NKG2D MFI along the x-axis, the value for the red (IV-IC) line is higher than the value for the black (IT-IC) line]. Other factors in conjunction with NKG2D expression levels are likely contributing to the observed antitumor effect. **Fig. 4-5C** shows the same data as in **Figs. 4-5A** and **4-5B** in bar graph form with t-test comparisons.

We examined the level of NKp46+ NKG2A/C/E+ NK cell activation through NKG2D expression against the level of CD8+ NKG2A/C/E+ T cell activation through NKG2D activation, to see if augmentation of NKG2D on NK cells and CTLs occurs in parallel in individual mice. We found that, in all treatment groups, augmented NKG2D expression on NK cells positively correlated with augmented NKG2D expression on activated CTLs (**Fig. 4-5D**); namely the mice with the greatest NKG2D on NK cells also showed the greatest NKG2D on their CTLs. These data suggest that the stimulation and activation of these NK and T cells is not independent, and that the hu14.18-IL2 IC treatment has the ability to activate both NK and T cells when given IT or IV.

4.4.6 Initial Tumor Load Shows an Inhibitory Interaction Effect on Hu14.18-IL2 Treatment and Correlates with Tumor Growth

Next we examined whether tumor load at the time of treatment initiation influenced the antitumor activity of hu14.18-IL2 therapy. **Fig. 4-6A** shows significant direct incremental relationships between initial tumor volume and Day 4 (after treatment initiation) Tumor Volume in all mice. IT-IC treated mice (black line) had a significantly steeper slope compared to control mice (blue line) ($p=0.013$), indicating an interaction effect of initial tumor volume on IT-IC treatment relative to control mice. As initial tumor volume increases, the IT-IC antitumor treatment effect gradually disappears. This is demonstrated by all three lines "meeting" at the far right of the graph, as there is no difference in Day 4 tumor volumes between treatment groups at these large initial tumor volumes.

Fig. 4-6B represents the same data as in **Fig. 4-6A**; however, in order to illustrate decreasing efficacy of treating tumors with increasing initial volumes, mice were separated into

quartiles based on their initial tumor volumes (cutoffs at 33.86 mm^3, 76.28 mm^3, and 130.93 mm^3). **Fig. 4-6B** shows that in the three lowest quartiles (0-130.9 mm^3), IT-IC treated mice had significantly less tumor at Day 4 compared to control mice, whereas there is no difference in the highest quartile (>130.93 mm^3). These data indicate that large initial tumor burden negated the antitumor effects of hu14.18-IL2 therapy.

Fig. 4-6C shows a significant inverse incremental relationship between initial tumor volume and reduction in tumor volume in the IT-IC treated mice, indicating that the smaller the initial tumor volume the less tumor growth observed with IT-IC treatment. Note that the line for the control mice has a significant negative slope. This is consistent with known sigmoidal growth patterns for tumors; a number of physiological factors slow the growth rate of untreated tumors as they get larger. Thus, in **Fig. 4-6C**, the untreated tumors (blue line) that have the smallest initial tumor volume actually show the greatest growth (measured as percent change in volume) over the next 4 days. The slopes of the lines for the IT-IC and IV-IC treated mice are significantly positive compared to the very negative slope of the line for the control mice. This translates to the IV-IC and IT-IC lines "meeting" the control line at the far right of the graph, such that there is no effect of IC treatment, vs. control, for the tumors that are largest at the time of treatment initiation. In contrast, as one moves farther to the left on the x-axis (smaller initial tumor size), the IV-IC and IT-IC lines move farther away (less tumor growth) from the control group (blue) line, indicating that smaller initial tumor volume has an incremental effect on the ability of IC treatment to modify the growth of tumors, compared to control tumors. The regression line (black) for the IT-IC treated mice is significantly lower than that of the IV-IC treated mice (red line), indicating greater amounts of tumor shrinkage are induced by IT vs. IV IC at all levels of initial tumor volume.

Fig. 4-6D, which represents the same data as in **Fig. 4-6C**, shows that when initial tumor volume was less that 130.93 mm^3 (lowest three quartiles), IT-IC treated mice showed significantly less tumor growth compared to control mice as well as significantly less tumor growth compared to IV-IC treated mice. However, when initial tumor burdens were greater than 130.93 mm^3, there seemed to be no significant effect of hu14.18-IL2 therapy (either IV or IT) on tumor growth compared to control mice. Again, these data indicate that large initial tumor burden negated the antitumor growth effects of hu14.18-IL2 therapy.

4.4.7 Tumor Shrinkage at 4 Days Post Treatment Initiation is Necessary for Long-Term Survival in hu14.18-IL2 Treated Mice

We next wanted to determine if we could identify the particular subset of mice that would be long-term, tumor-free survivors based on the initial response to treatment observed 4 days post treatment initiation. For ease of biologic interpretation, a cutoff at 0% Tumor Growth was used to distinguish growing tumors (>0% Tumor Growth) from shrinking tumors (<0% Tumor Growth). We observed that all control (IT-PBS, untreated) mice showed tumor growth by 4 days post treatment initiation and that all of these mice eventually died of tumor-related death (**Figs. 4-7A,B**). Also, we observed that all hu14.18-IL2 treated mice that did not show any tumor shrinkage by 4 days post treatment initiation eventually died of tumor-related death (**Figs. 4-7A,B**). However, IC treated mice that did show any tumor shrinkage by 4 days post treatment initiation had an increased chance (44%) of long-term, tumor-free survival (determined 70 days following treatment initiation) up (compared to mice that did not show tumor shrinkage by day 4 (0% survival) (**Fig. 4-7A**). These data demonstrate the immediate antitumor effect of the hu14.18-IL2 immunocytokine and the long-term significance for overall survival of this

immediate effect. These data indicate that tumor shrinkage soon after administration of the IC could potentially be used as a prognostic factor for long-term survival following this IC immunotherapy.

4.5 Discussion

Initial small tumor load (DuBois et al., 1999) and enhanced TIL infiltration (Gooden et al., 2011; Hwang et al., 2012; Taylor et al., 2007; Horne et al., 2011) have been noted as two independent prognostic factors for therapeutic benefit of immunotherapy and cancer host survival. The results presented here show, for the first time to our knowledge, that initial small tumor volume correlates with increased rapid TIL infiltration in response to monoclonal-antibody-based immunotherapy (in this case, hu14.18-IL2). This indicates that, in this model system, small tumor burden and increased TIL infiltration are two linked, rather than independent, factors that are predicative of a favorable *in vivo* antitumor response to immunotherapy.

We examined whether tumor volume at treatment initiation was an important factor in overall survival. Our data show that smaller initial tumor volume correlated with increased survival in hu14.18-IL2 treated mice, indicating that tumor volume at treatment initiation is prognostic for survival after IT-IC treatment. Next, we examined whether tumor volume at treatment initiation was an important factor affecting the change in tumor infiltrating leukocytes associated with hu14.18-IL2 treatment. Our data show that hu14.18-IL2 treatment of mice with lower initial tumor volume leads to increased tumor leukocyte and NK infiltration and increased NKG2D expression on tumor infiltrating NK cells and CD8+ T cells. These data indicate that smaller initial tumor volume when treatment begins is predictive of the level of increased tumor infiltrating lymphocytes. We examined which immune cells correlated with the increase in tumor leukocytes seen in small tumors treated with IT-IC. Our data show that increased tumor leukocyte infiltration seen in IT-IC treated tumors correlated with CD8+ cytotoxic T cells as well

as higher NKG2D expression on CTLs and NK cells. This indicates that much of the increase in tumor leukocytes seen in small tumors treated with IT-IC was due to CD8+ CTLs.

Next, we examined whether increases in tumor infiltrating leukocytes, such as CD8+ CTLs or NKp46+ NK cells, resulted in better treatment outcomes such as tumor shrinkage. Using quantitative histological analyses, our data show that increased NKG2A/C/E+ and CD8+ cells inversely correlated with tumor growth (as measured by percent tumor growth). When comparing IT-IC treated mice whose tumors shrank against those whose tumors grew, our flow cytometry data showed a statistically significant increase in CTLs and NK cells as well as a statistically significant decrease in tumor macrophages in the tumors that shrank. These data suggest that CTLs and NK cells were involved in the process of tumor shrinkage, while the presence of macrophages appeared to be associated with tumor growth rather than shrinkage.

We also found that NKG2D expression on CD8+ cells and on NK cells inversely correlated with tumor growth (measured by Percent Tumor Growth), which suggested a role of NKG2D expression on NK cells and on CD8 cells in tumor shrinkage. Interestingly, in individual mice, the level of augmented NKG2D expression on activated NK cells was found to correlate directly with the level of augmented NKG2D on CTLs. This suggests a shared relationship for the level of augmented NKG2D on NK and on CD8+ TILs, which also is involved in helping to inhibit tumor growth. Studies by Verneris et al show that ligation of NKG2D on NK cells directly induces cytotoxicity (Verneris et al., 2004). They also showed that NKG2D expression is up-regulated upon IL-2 activation and expansion of CD8+ T cells. T cells activated and expanded in low and high concentrations of IL-2 both showed comparable up-regulation of NKG2D, but only cells cultured in high-dose IL-2 were cytotoxic. Verneris et al also showed that the activated CD8+ T cells demonstrated cytotoxicity against malignant target

cells, which occurs through NKG2D-mediated recognition and signaling and not through the TCR (Vance et al., 2002). NKG2D triggering accounts for the majority of MHC-unrestricted cytotoxicity of activated and expanded CD8+ T cells (Karimi et al., 2005). In this report, we show how NKG2D up-regulation in the tumor infiltrating leukocytes (specifically on NK cells and on CD8+ T cells) correlates with slower tumor growth, in treated as well as in untreated animals. In our prior work (Yang et al., In Revision), we found that NKG2D upregulation in IT-IC and IV-IC treated animals (but not in control animals) was seen on NK and CD8+ TILs in the tumors, but not seen on NK and CD8+ cells in the spleens, suggesting that the NK and T activation induced by the IC treatment was occurring in the tumor microenvironment, potentially due to tumor-specific localization of the IC in the GD2+ tumors.

We also examined whether tumor burden at treatment initiation played a role in hu14.18-IL2 induced tumor shrinkage. Our data showed that smaller tumor load at treatment initiation increased the likelihood of tumor shrinkage in IT-IC treated mice. The opposite was true in control mice; namely control tumors that were smaller at the time of "treatment initiation" actually showed greater % change in size than the tumors that were larger at the time of treatment initiation. These data are consistent with our findings that hu14.18-IL2 treatment of smaller tumors leads to higher tumor infiltrating leukocytes and that increased tumor leukocytes correlate with shrinkage of tumors.

We also examined whether initial tumor growth or shrinkage influenced overall survival outcome. Our data showed that tumor shrinkage detected 4 days after starting treatment was predictive of increased long term survival in hu14.18-IL2 treated mice. Conversely, tumor progression detected 4 days after starting treatment in control and in hu14.18-IL2 treated mice was predictive of continued tumor progression and ultimate death due to progressive disease.

These data are consistent with our previous findings that hu14.18-IL2 treatment of smaller tumors leads to increased anti-metastatic effect against NXS2 neuroblastoma (Neal et al., 2004). Our data in NK and T cell depleted mice indicate that both NK and T cells are involved in the overall antitumor effect of IC in this system (Yang et al, In Revision). Even so, as adaptive T cells responses normally take >5 days to develop, it seems unlikely that an adaptive T cell response can account for this shrinkage seen on day 4. It may be that a combination of innate immune responses, antibody-dependent cell mediated cytotoxicity, and NKG2D induced antitumor effects (by NK cells and CD8+ T cells) may account for the initial tumor shrinkage, which is essential (in this model) for resultant long-term tumor-free survival. This requirement for early tumor shrinkage after one course of therapy to develop long term benefit is different from that of recently described for clinical immune benefit obtained with ipilimumab. As immune benefit with ipilimumab is mediated by an adaptive T cell response (which takes time to develop), occasional patients show tumor growth during and shortly after treatment, followed by late detection of antitumor effects (tumor shrinkage) (Hodi et al., 2010; Saenger and Wolchok, 2008).

Interestingly, **Fig. 4-6B**, which shows the relationship between tumor volume at treatment initiation and percent tumor growth, indicates that the relationship seen between the 3 different treatment groups is highly dependent upon initial tumor volume. Above 130.9 mm^3 of tumor volume, there seems to be little to no effect of hu14.18-IL2 therapy, injected either intratumorally or intravenously. This is shown by the finding that the regression lines of the three treatment groups seem to intersect at this initial tumor volume. However, when tumor burden is less that 130.9 mm^3, there are significant effects of both IT and IV hu14.18-IL2 therapy in slowing tumor growth compared to control treated tumors.

CD8+ T cells likely play a role in the hu14.18-IL2 mediated tumor shrinkage effect. **Fig. 4-4D** shows that CD8+ T cells are the cell type that is most increased when IT-IC treated tumors are shrinking compared to those that are growing. Also, natural killer cells (NKp46+ cells) very likely have some role in tumor shrinkage because they are also significantly increased in IT-IC treated shrinking tumors compared to IT-IC treated growing tumors. These results are consistent with our prior results that show IT-IC treatment can be dramatically inhibited in this model by either NK or T cell depletion (Yang et al, In Revision). Conversely, macrophages (F4/80+ cells) are significantly decreased (when measured as a percentage of the CD45+ cells) in IT-IC treated shrinking tumors compared to IT-IC treated growing tumors (**Fig. 4-4D**); their relative decrease in shrinking tumors may reflect the disproportionate increase of NK and CD8+ cells, but may also indicate an inhibitory role for macrophages in the IT-IC mediated tumor shrinkage process.

It may be useful to determine signatures that could be distinguished in patients, either prior to IC treatment or soon after treatment initiation, which are predictive of beneficial antitumor effect. Such predictive signatures could be then used in clinical decision making regarding treatment continuation or changing to alternate therapies. We have identified several parameters (measured before and shortly after treatment initiation) in this animal model that appear to be indicators of prognosis. Some of these are already being used in clinical decision-making. Clinical stage of disease is a primary factor used to predict prognosis and help with treatment assignation. Based on these preclinical data, as well as our clinical phase II data showing greater likelihood of response for patients with less “bulky disease” (6), we hypothesize that patients should be treated with IC (either IT-IC or IV-IC) when tumor volume is at a minimum, as larger tumor size interferes with the ability of IC treatment to mediate beneficial antitumor effects. Tumor growth patterns soon after IC treatment initiation may also be studied

as a potential predictor of long term benefit. If these murine studies translate to the clinical setting, patients with tumors that have a reduction in size within the first few days post treatment initiation may have a greater possibility for long-term benefit. Our preclinical data suggest that patients with tumors that continue to grow soon after treatment initiation are much less likely to benefit from IC treatment.

Analyses of TILs, determined by histologic evaluation or by flow cytometry, might also be used as an important prognostic determinant. Soon after IC treatment initiation, tumor infiltration might be used as an indicator of treatment efficacy. If extensive clinical testing demonstrates that the murine data we have obtained actually translate to the clinical setting, then several parameters may be of clinical utility. Patients with high CD8+ T cell, high NKp46+ NK cell, and low M2 macrophage tumor infiltrating populations after initial treatment may have a higher likelihood of experiencing a more potent antitumor effect. The NKG2D expression of NK cells and activated CTLs may also be indicative of the potential for a more potent IC-induced antitumor effect. This immune profile could be investigated as a potential predictive parameter of beneficial IC treatment. Lack of this signature may indicate that treatment adjustments need to be made.

Our data suggest that the stimulation and activation of NK and T cells are not independent (**Fig. 4-5C**) and that the activation of these infiltrating lymphocytes is important for antitumor activity and survival in this mouse model. Furthermore, the data presented here demonstrate that even in groups of genetically identical mice, receiving identical doses of tumor implants and identical antitumor treatments, quantitative measures of initial tumor size and of TIL patterns are clearly predictive of response to treatment. These data indicate that the ultimate response to tumor immunotherapy, either beneficial or ineffective, is determined (at least in part)

by quantitative factors that might be manipulated to enhance antitumor efficacy, or measured for prognostic purposes. Translating these observations into clinical evaluations will require large clinical analyses with standardizable parameters for immune measurements, in order to determine if the principles identified in this mouse model may also pertain to clinical treatments with analogous immunotherapies.

Figure 4-1. Initial Tumor Volume Inversely Correlates with Survival in hu14.18-IL2 Treated Mice

A/J mice bearing subcutaneous NXS2 tumors were treated with 3 daily doses of hu14.18-IL2 (either IV or IT), received control treatment (IT-PBS or no treatment). After the experiment was completed, mice were stratified by initial tumor volume around the median initial treatment volume of $34mm^3$ and analyzed for survival outcome. (A) Contingency table showing the long term outcomes of mice treated with IC (hu14.18-IL2 IV or IT) stratified by median initial tumor volume of $34mm^3$ or control mice (IT-PBS or untreated). (B) Kaplan Meier curves showing number of survival days post-treatment initiation in IC treated or control groups stratified by median initial tumor volume of $34mm^3$. Experiments represent data from 3 independent experiments with a total of 37 mice.

Figure 4-1.

(A)

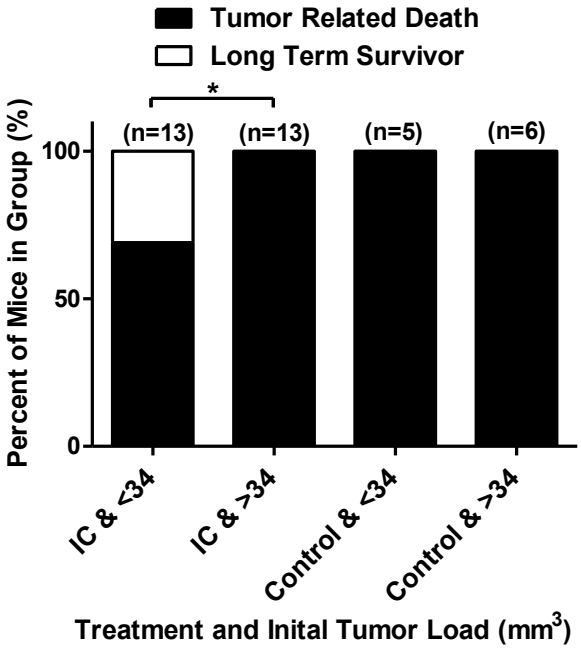
Tumor Related Death
Long Term Survivor
*
(n=13)
(n=13)
(n=5)
(n=6)
Percent of Mice in Group (%)
100
50
0
IC & <34
IC & >34
Control & <34
Control & >34
Treatment and Inital Tumor Load (mm3)

(B)

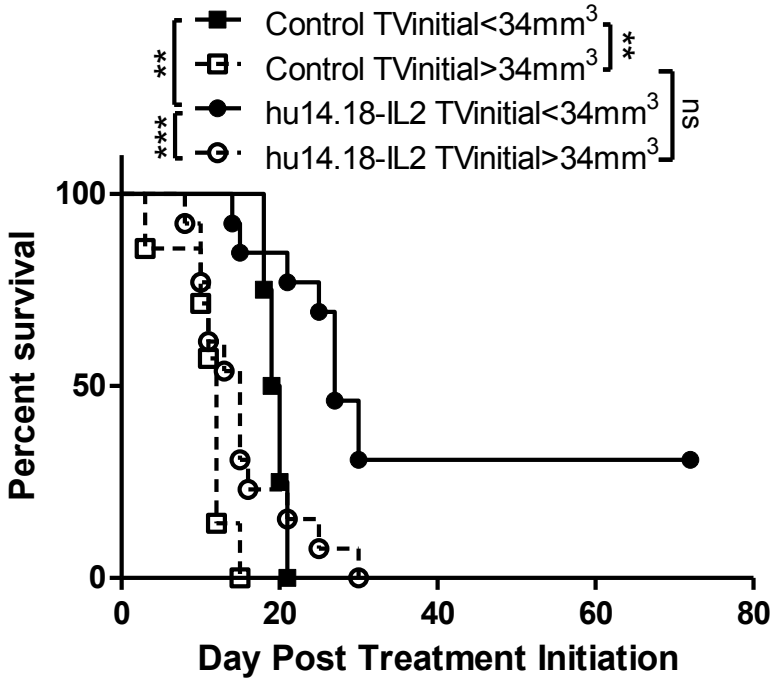
Control TVinitial<34mm3
Control TVinitial>34mm3
hu14.18-IL2 TVinitial<34mm3
hu14.18-IL2 TVinitial>34mm3
**
**
***
ns
Percent survival
100
50
0
0
20
40
60
80
Day Post Treatment Initiation

Figure 4-2. Hu14.18-IL2 Treatment of Mice with Smaller Initial Tumor Volume Leads to Increased Tumor NK Infiltration and NKG2D Expression on Tumor NK and CD8+ T cells

A/J mice bearing subcutaneous NXS2 tumors were treated with IT-IC, IV-IC or Untreated. Mice were sacrificed 4 days post-treatment initiation and tumors underwent flow cytometric analysis. Initial tumor volumes of all mice are stratified into groups greater or less than the median value of 101.6 mm^3 and these groups are compared to each other for the post-treatment parameters, detected by flow cytometry, shown. **(A):** post-treatment tumor leukocytes (CD45+ cells) are presented as a percentage of Total Live Nucleated Cells (TNCs) within the tumor; **(B):** macrophages (F4/80+) are presented as a percentage of leukocytes (CD45+) within the tumor; **(C):** natural killer cells (NKp46+) are presented as a percent of mouse leukocytes (CD45+); **(D):** cytotoxic T cells (CD8+) are presented as a percent of mouse leukocytes (CD45+); **(E):** NKG2D expression levels are presented as MFI on NKp46+, NKG2A+ activated natural killer cells; and **(F):** NKG2D expression levels are presented as MFI on CD8+, NKG2A+ activated CTLs. Asterisks in comparison bars represent the level of statistical significance for differences in the graphed values between the 2 indicated groups. Results represent data from 6 independent experiments with an average of 19 mice within each treatment group.

Figure 4-2.

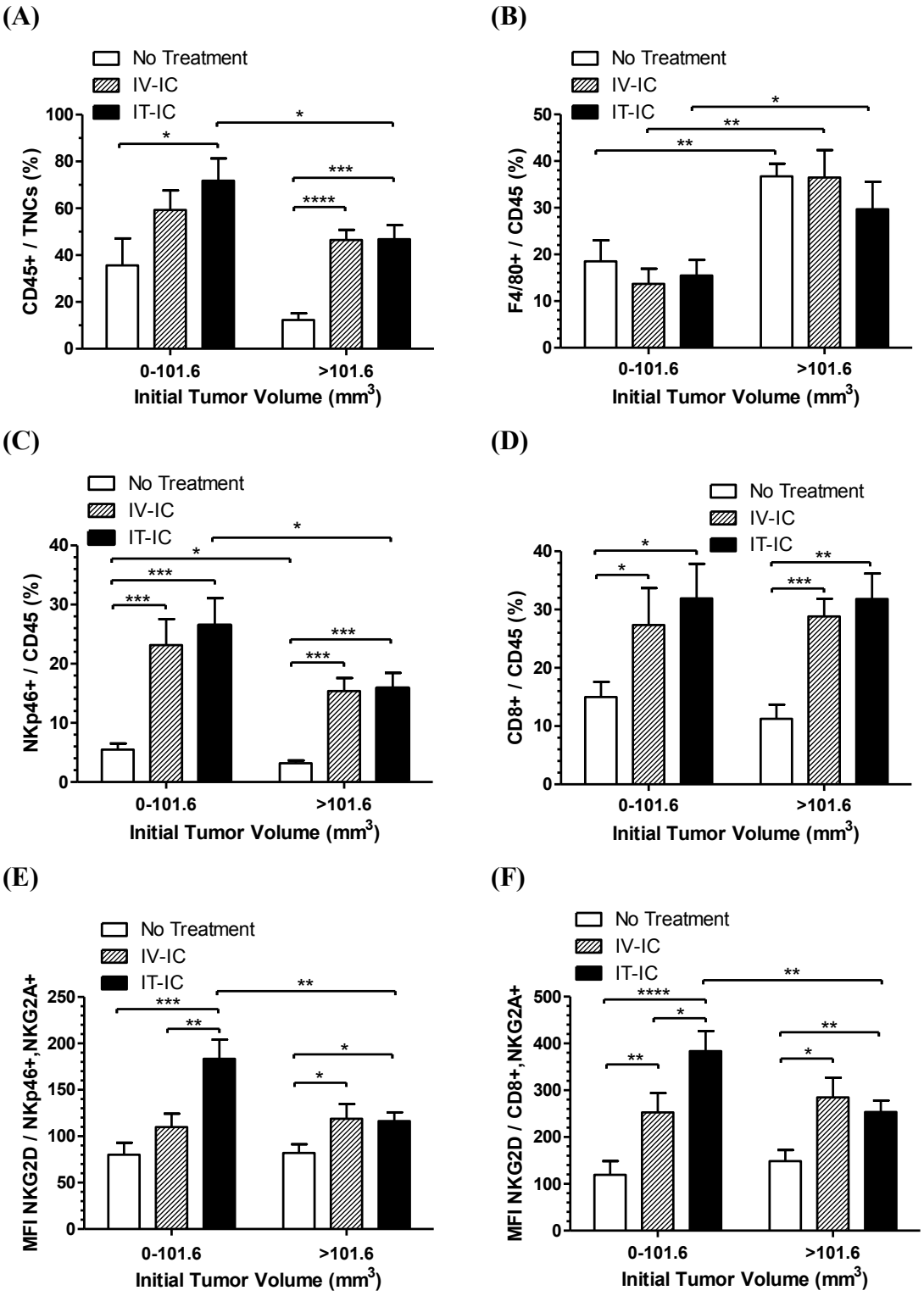
(A)
No Treatment
IV-IC
IT-IC
CD45+ / TNCs (%)
0-101.6
>101.6
Initial Tumor Volume (mm3)
(B)
F4/80+ / CD45 (%)
(C)
NKp46+ / CD45 (%)
(D)
CD8+ / CD45 (%)
(E)
MFI NKG2D / NKp46+,NKG2A+
(F)
MFI NKG2D / CD8+,NKG2A+

Figure 4-3. Increased Tumor Leukocyte Infiltration Results from Higher CD8+ T cell but not NK Density, in Mice receiving IT-IC and Correlates with Higher NKG2D Expression on NK cells and CD8+ T cells

A/J mice bearing subcutaneous NXS2 tumors were treated with IT-IC, IV-IC or Untreated. Mice were sacrificed 4 days post-treatment initiation and tumors underwent flow cytometric analysis. Post-treatment tumor leukocytes (CD45+ cells) as a percentage of Total Live Nucleated Cells (TNCs) within the tumor are stratified at 41.6% CD45+/TNCs. These two groups are compared to each other for the indicated parameters: **(A):** natural killer cells (NKp46+) as a percent of mouse leukocytes (CD45+); **(B):** cytotoxic T cells (CD8+) as a percent of mouse leukocytes (CD45+); **(C):** NKG2D expression levels as MFI on NKp46+, NKG2A+ activated natural killer cells; and **(D):** NKG2D expression levels as MFI on CD8+, NKG2A+ activated CTLs. Asterisks in comparison bars represent statistical significance in values of each group. Results represent data from 6 independent experiments with an average of 19 mice within each treatment group.

Figure 4-3.

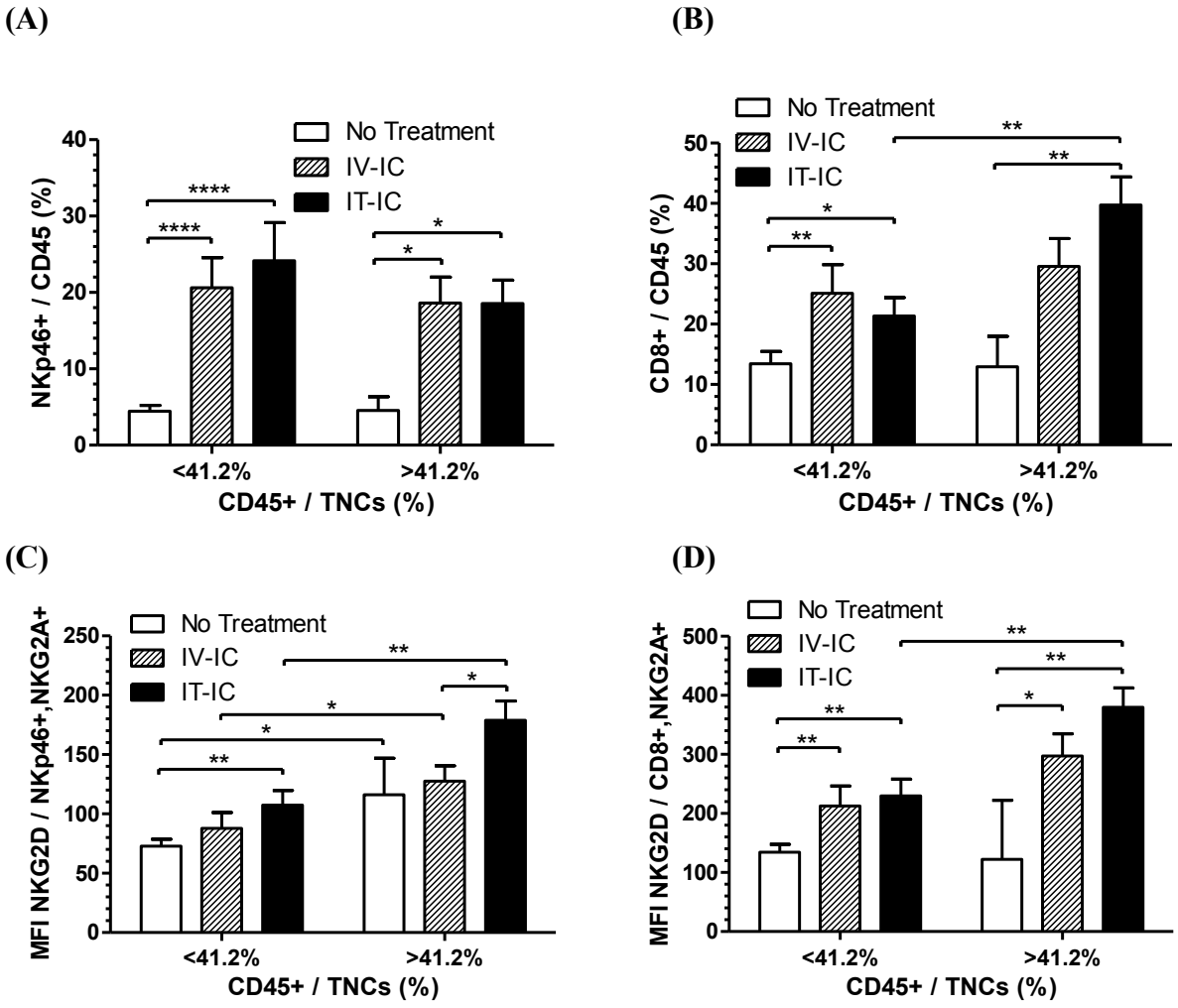
(A)
(B)
(C)
(D)
No Treatment
IV-IC
IT-IC
NKp46+ / CD45 (%)
CD8+ / CD45 (%)
MFI NKG2D / NKp46+,NKG2A+
MFI NKG2D / CD8+,NKG2A+
<41.2%
>41.2%
CD45+ / TNCs (%)

Figure 4-4. Tumor NK Cell and CD8+ T cell Infiltration Inversely Correlates with Tumor Growth Following IC Treatment

A/J mice bearing subcutaneous NXS2 tumors were treated with IT-IC, IV-IC or Control treatment. Mice were sacrificed 4 days post-treatment initiation and tumors underwent quantitative histological (A-B) or flow cytometric analyses (C-D). (A-B) After immunohistochemistry, 5 distinct microscopic fields were counted in a blinded fashion within each mouse's tumor. NKG2A/C/E+ cells (A) and CD8a+ cytotoxic T cells (B) as a percentage of Total Nucleated Cells (TNCs) within the each mouse's tumor are plotted against each mouse's percent tumor growth. (A-B) represent data from 3 independent experiments, with an average of 18 mice total within each treatment group. Horizontal error bars represent standard error of the mean for subsamples within an individual mouse. (C) Post-treatment tumor leukocytes (CD45+ cells) as a percentage of Total Live Nucleated Cells (TNCs) are plotted against each mouse's percent tumor growth. (D) Mice are stratified by treatment group and by tumor growth or shrinkage. Within each group, tumor immune cells (CD8+, NKp46+, F4/80+, CD4+) are shown as a percentage of tumor leukocytes (CD45+ cells). Asterisks in (D) compare tumor immune cell populations between IT-IC treated mice whose tumor grew vs. IT-IC treated mice whose tumor shrank. (C-D) represent data from 6 independent experiments with an average of 19 mice total within each treatment group. Note, the IT-IC treatment group consists of 6 mice that had tumors shrink and 15 mice that had tumors grow.

Figure 4-4.

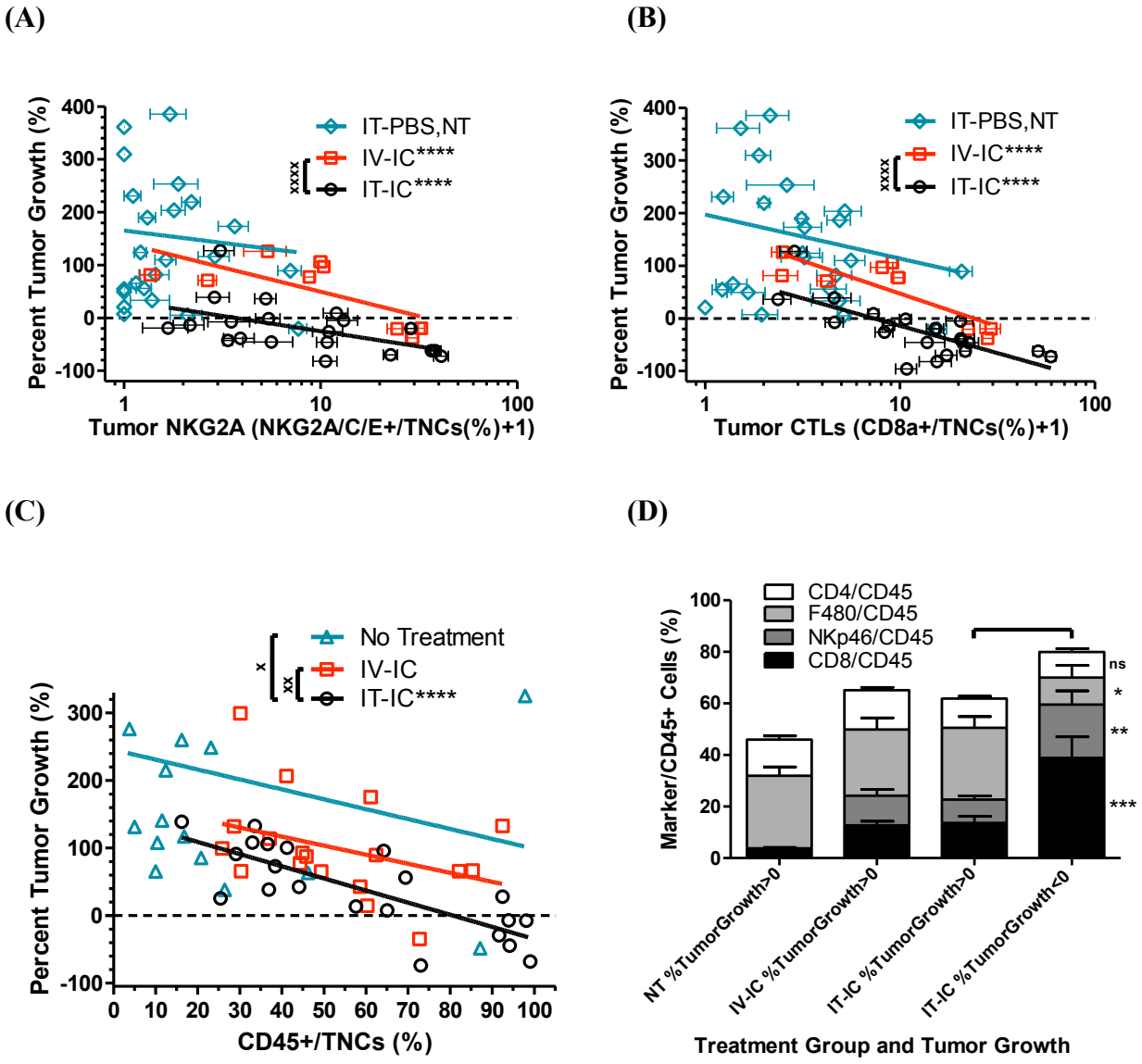
(A)
(B)
Percent Tumor Growth (%)
IT-PBS,NT
IV-IC****
IT-IC****
xxxx
Tumor NKG2A (NKG2A/C/E+/TNCs(%)+1)
Tumor CTLs (CD8a+/TNCs(%)+1)
(C)
(D)
No Treatment
IV-IC
IT-IC****
x
xx
CD45+/TNCs (%)
CD4/CD45
F480/CD45
NKp46/CD45
CD8/CD45
Marker/CD45+ Cells (%)
ns
*
**
***
NT %TumorGrowth>0
IV-IC %TumorGrowth>0
IT-IC %TumorGrowth>0
IT-IC %TumorGrowth<0
Treatment Group and Tumor Growth

Figure 4-5. NKG2D Expression on NK and CD8+ T cells Correlates with Tumor Volume Reduction following Hu14.18-IL2 Treatment

A/J mice bearing subcutaneous NXS2 tumors were treated with IT-IC or IV-IC or received no treatment. Mice were sacrificed 4 days post-treatment initiation and tumors underwent flow cytometric analysis. Using flow cytometry, post-treatment tumor NKG2D expression (MFI) on activated natural killer cells (**A**) and cytotoxic T cells (**B**) are plotted against each mouse's percent tumor growth. **Figure 4-5C** shows bar graphs of the same data in **Figures 4-5A** and **4-5B**. In **Figure 4-5D**, within each mouse's tumor, NKG2D expression (MFI) on activated NKp46+, NKG2A/C/E+ natural killer cells (y-axis) is plotted against that same animal's NKG2D MFI on CD8+, NKG2A/C/E+ cytotoxic T cells (x-axis). In all scatter plot figures testing for correlations (**A, B, D**), asterisks in the legend represent a statistically significant different slope of each groups' regression line model compared to 0. Comparisons between treatment groups are indicated by the "x" designation in place of asterisks, as described in the statistical methods section, to test whether the elevations of each groups' regressions line are significantly different from each other. All panels represent data from 6 independent experiments with an average of 19 mice total within each treatment group.

Figure 4-5.

(A)

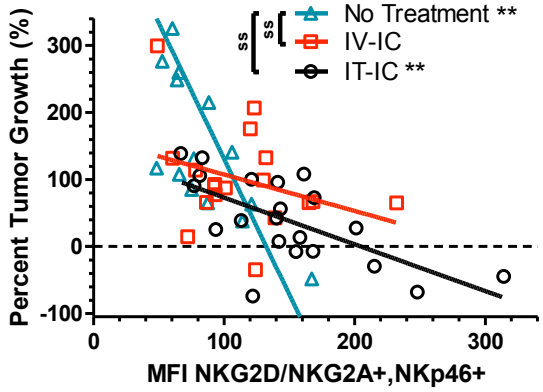

(B)

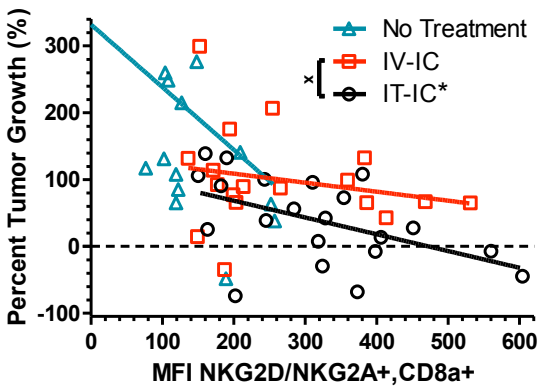

(C)

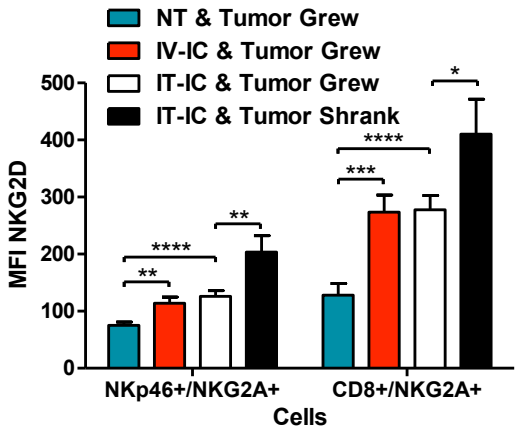

(D)

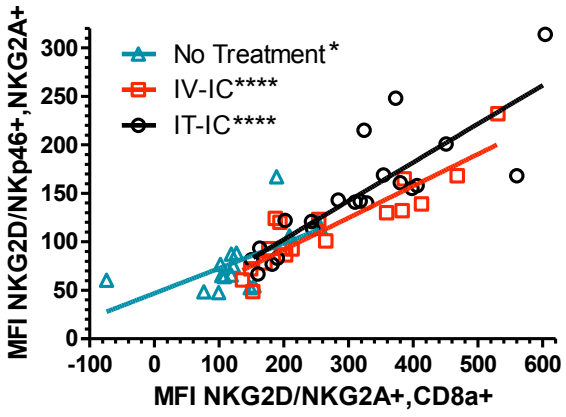

Figure 4-6. Initial Tumor Load Shows an Inhibitory Interaction Effect on Hu14.18-IL2 Treatment and Correlates with Tumor Growth

Four days after randomization and treatment initiation, A/J mice bearing subcutaneous NXS2 were sacrificed for flow cytometric analysis of their tumors. **Figure 4-6A** shows individual mouse tumor volumes at the day of randomization (Initial Tumor Volume (mm^3)) plotted against Day 4 Tumor Volume. Linear regression models for each treatment group are shown. Asterisks marking individual treatment groups within the legend represent a statistically significant different slope of each group's regression line compared to 0. Comparisons between treatment groups, using "s" or "x" indications in place of asterisks, test whether the slopes or elevations, respectively, of each group's regression line are significantly different from each other. Regression lines with significantly different slopes cannot be tested for differences in elevations because they will intersect at some point in space. **Figure 4-6B** shows Day 4 Tumor Volume data stratified into four quartiles based on initial tumor volume (separated by 33.9, 76.3, 130.9) as well as three treatment groups. **Figures 4-6C** and **4-6D** show analogous graphs as **Figure 4-6A** and **4-6B**, using Percent Tumor Growth instead of Day 4 Tumor Volume. Percent Tumor Growth = [100 x (Tumor Volume at Day 4 – Initial Tumor Volume) / Initial Tumor Volume]. All panels represent data from 11 independent experiments with an average of 48 mice total within each treatment group.

Figure 4-6.

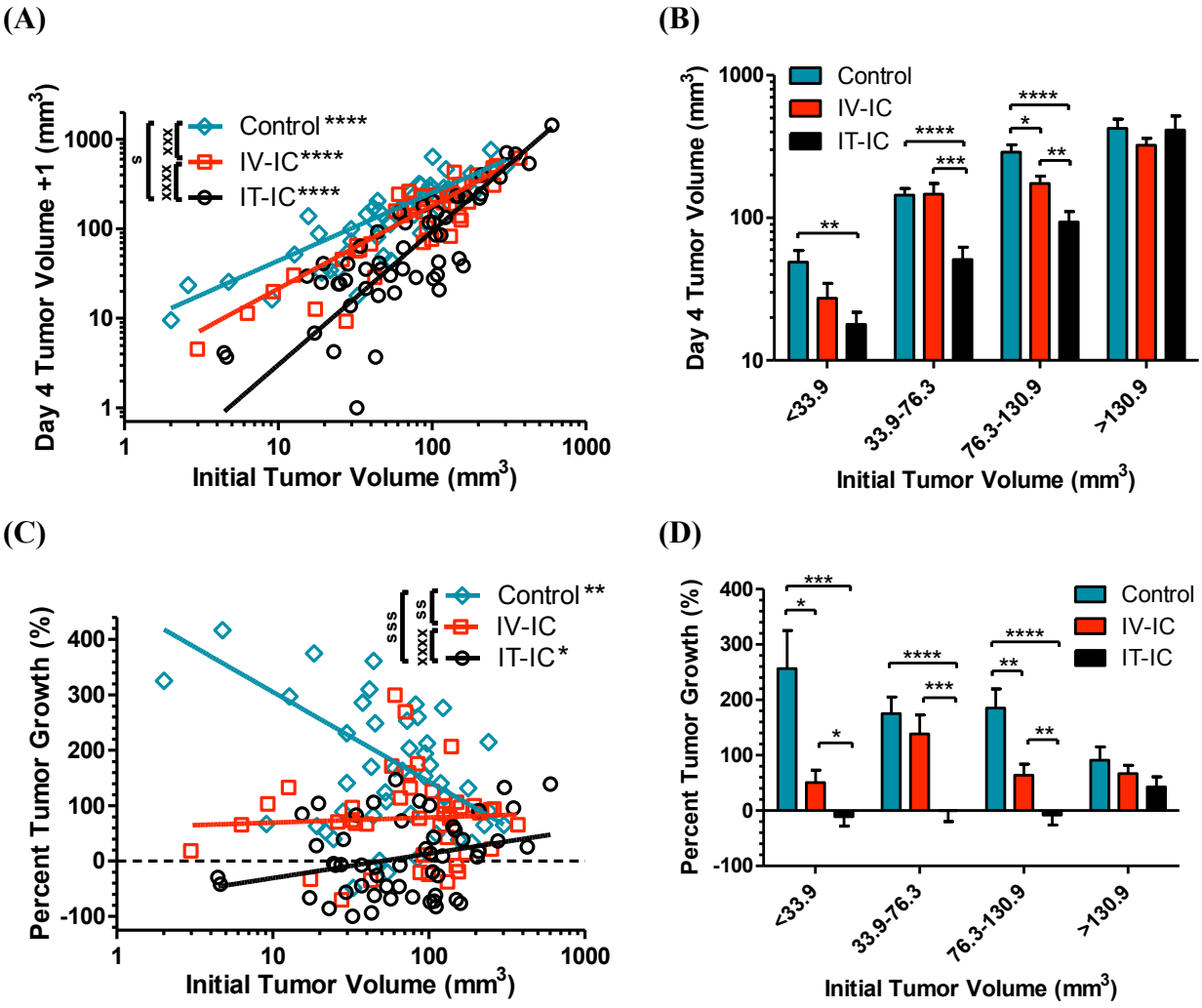
(A)
Day 4 Tumor Volume +1 (mm3)
Initial Tumor Volume (mm3)
Control****
IV-IC****
IT-IC****
(B)
Day 4 Tumor Volume (mm3)
Control
IV-IC
IT-IC
<33.9
33.9-76.3
76.3-130.9
>130.9
Initial Tumor Volume (mm3)
(C)
Percent Tumor Growth (%)
Initial Tumor Volume (mm3)
Control**
IV-IC
IT-IC*
(D)
Percent Tumor Growth (%)
Control
IV-IC
IT-IC
<33.9
33.9-76.3
76.3-130.9
>130.9
Initial Tumor Volume (mm3)

Figure 4-7. Tumor Shrinkage Detected 4 days after Initiating Treatment with IC is Predictive of Increased Long Term Survival in hu14.18-IL2 Treated Mice

A/J mice bearing subcutaneous NXS2 tumors were treated with 3 daily doses of hu14.18-IL2 (either IV or IT) or control treated (IT-PBS or Untreated). After the experiment was completed, mice were stratified by Percent Tumor Growth around 0%, which indicated whether each individual mouse's tumor grew (Percent Tumor Growth > 0%) or shrank (Percent Tumor Growth < 0%) in size over 4 days. Survival outcome data were analyzed on control mice (IT-PBS and untreated) and hu14.18-IL2 treated mice, with each treatment group stratified by percent tumor growth. (**A**) Contingency graph showing the long term outcomes of mice treated with hu14.18-IL2 (IC) or control mice, stratified by percent tumor growth measure 4 days after starting treatment. None of the control mice showed tumor shrinkage. (**B**) Kaplan Meier curves showing number of survival days post-treatment initiation in IC treated or control groups stratified by Percent Tumor Growth. All panels represent data from 3 independent experiments with a total of 36 mice in all 3 experiments.

Figure 4-7.

(A)

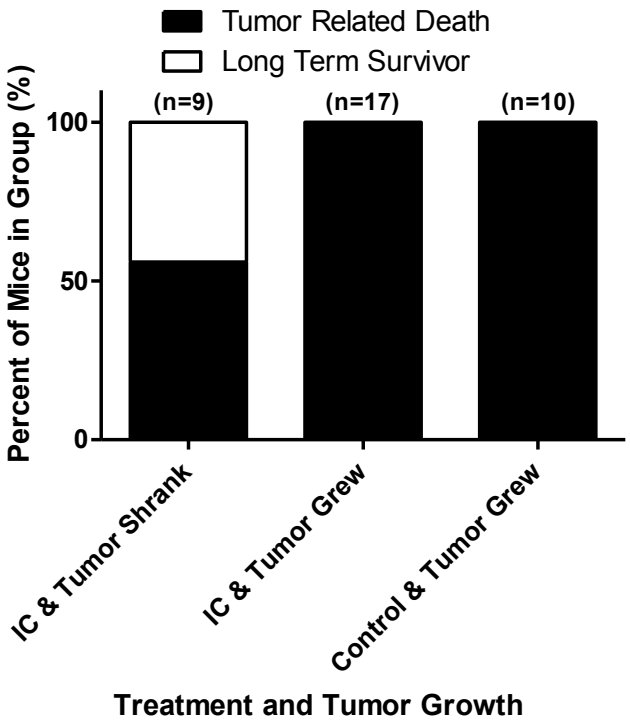
Tumor Related Death
Long Term Survivor
(n=9)
(n=17)
(n=10)
Percent of Mice in Group (%)
100
50
0
IC & Tumor Shrank
IC & Tumor Grew
Control & Tumor Grew
Treatment and Tumor Growth

(B)

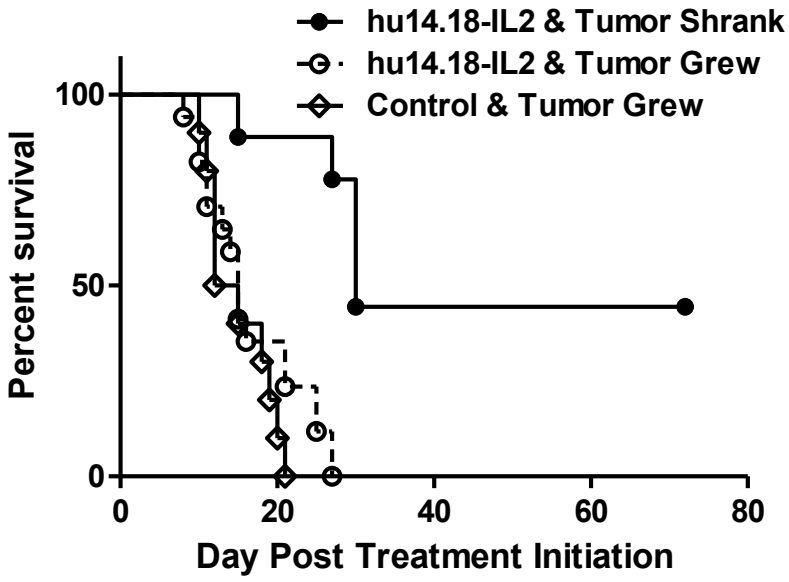
hu14.18-IL2 & Tumor Shrank
hu14.18-IL2 & Tumor Grew
Control & Tumor Grew
Percent survival
100
50
0
0
20
40
60
80
Day Post Treatment Initiation

Supplementary Figure 4-1. Hu14.18-IL2 Treatment of Mice with Smaller Initial Tumor Volume Leads to Increased Tumor NK Infiltration and augmented NKG2D expression on Tumor NK and CTL cells

This figure presents the same data as is presented in **Figure 4-2**. A/J mice bearing subcutaneous NXS2 tumors were treated with IT-IC, IV-IC or Untreated. Mice were sacrificed 4 days post-treatment initiation and tumors underwent flow cytometric analysis. Initial tumor volumes of all mice are plotted against each mouse's post-treatment parameters, detected by flow cytometry. **(A):** post-treatment tumor leukocytes (CD45+ cells) are presented as a percentage of Total Live Nucleated Cells (TNCs) within the tumor; **(B):** macrophages (F4/80+) are presented as a percentage of TNCs within the tumor; **(C):** natural killer cells (NKp46+) are presented as a percent of mouse leukocytes (CD45+); **(D):** cytotoxic T cells (CD8+) are presented as a percent of mouse leukocytes (CD45+); **(E):** NKG2D expression levels are presented as MFI on NKp46+, NKG2A+ activated natural killer cells; and **(F):** NKG2D expression levels are presented as MFI on CD8+, NKG2A+ activated CTLs. Linear regression models for each treatment group are shown. Asterisks marking individual treatment groups within the legend represent a statistically significant different slope of each group's regression line compared to 0. Comparisons between treatment groups, using "s" or "x" indications in place of asterisks, test whether the slopes or elevations, respectively, of each group's regression line are significantly different from each other. Regression lines with significantly different slopes cannot be tested for differences in elevations because they will intersect at some point in space. All panels represent data from 6 independent experiments with an average of 19 mice within each treatment group.

Supplementary Figure 4-1.

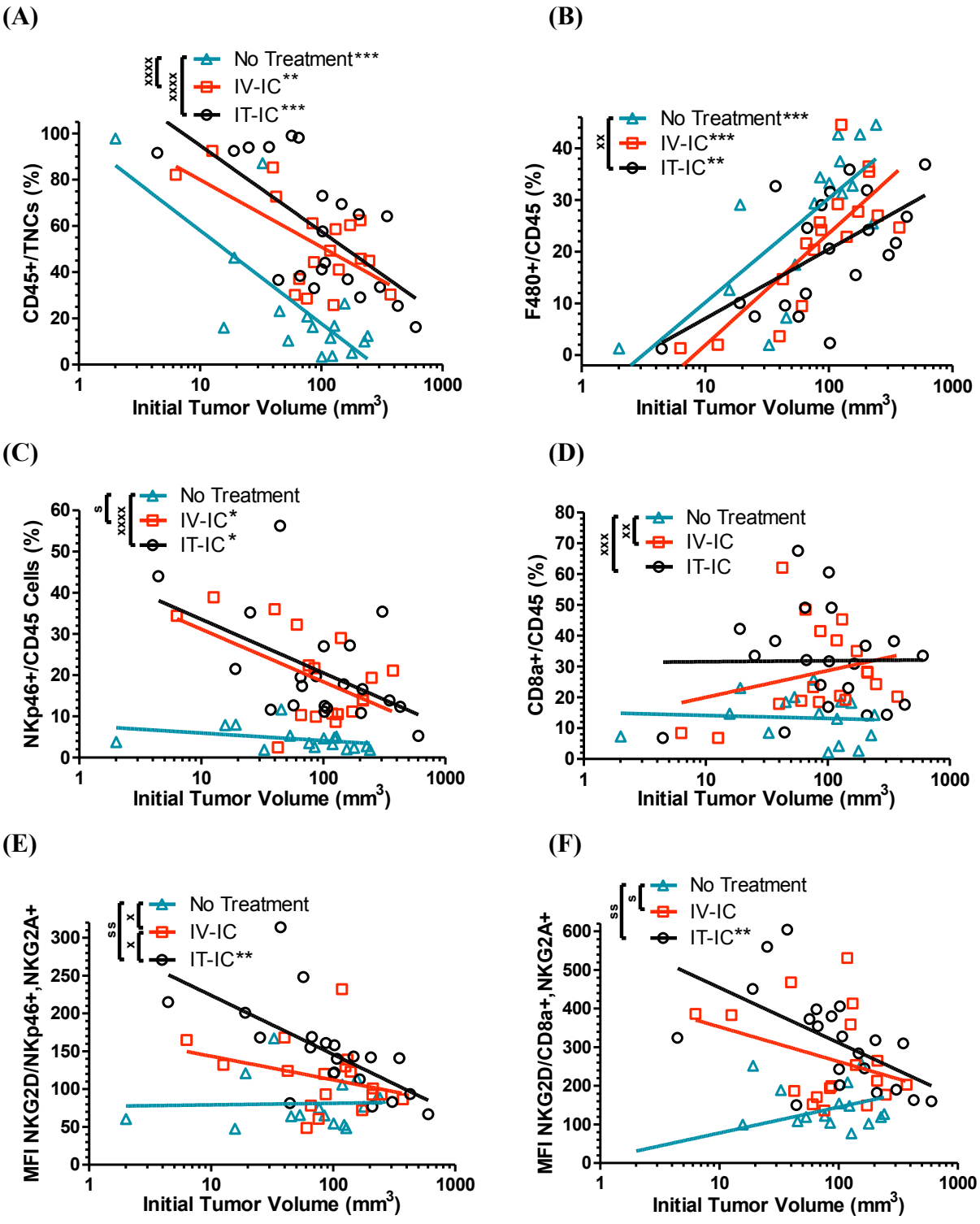

Supplementary Figure 4-2. Increased Tumor Leukocyte Infiltration after IT-IC Treatment is Associated with Higher CTL Density and Higher NKG2D Expression on NK cells and CTLs

This figure presents the same data as is presented in **Figure 4-3**. A/J mice bearing subcutaneous NXS2 tumors were treated with IT-IC, IV-IC or Untreated. Mice were sacrificed 4 days post-treatment initiation and tumors underwent flow cytometric analysis. Post-treatment tumor leukocytes (CD45+ cells) as a percentage of Total Live Nucleated Cells (TNCs) within the tumor are plotted against **(A):** natural killer cells (NKp46+) as a percent of mouse leukocytes (CD45+); **(B):** cytotoxic T cells (CD8+) as a percent of mouse leukocytes (CD45+); **(C):** NKG2D expression levels as MFI on NKp46+, NKG2A+ activated natural killer cells; and **(D):** NKG2D expression levels as MFI on CD8+, NKG2A+ activated CTLs. Linear regression models for each treatment group are shown. Asterisks marking individual treatment groups within the legend represent a statistically significant different slope of each group's regression line compared to 0. Data represent results from 6 independent experiments with an average of 19 mice within each group.

Supplementary Figure 4-2.

(A)

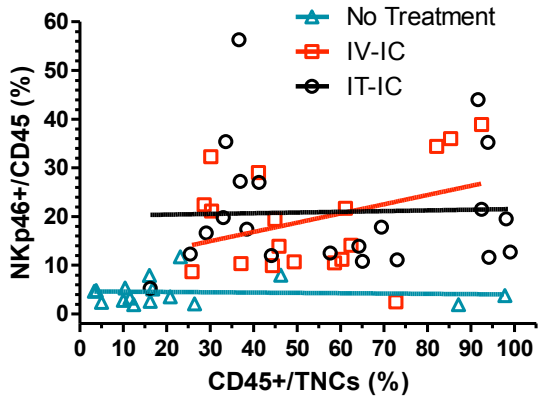

(B)

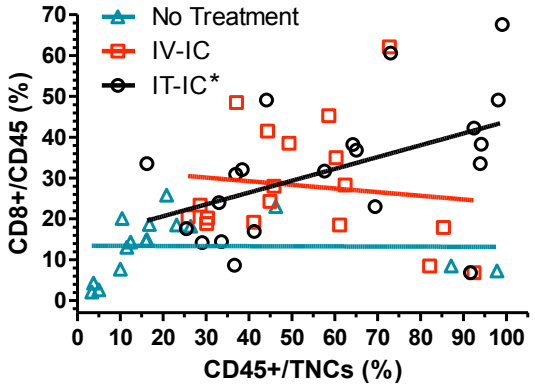

(C)

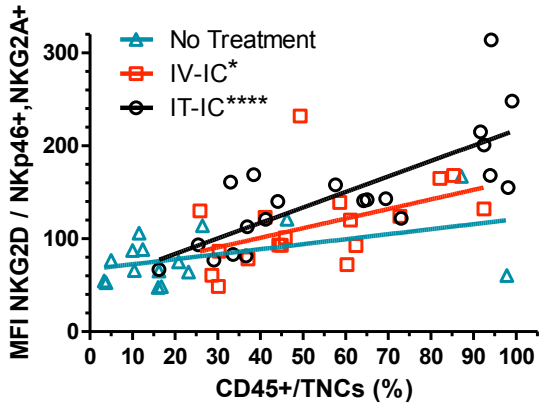

(D)

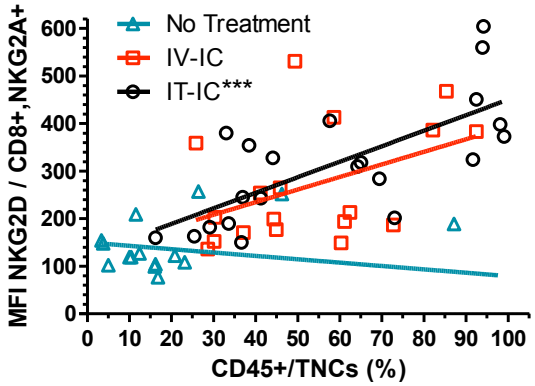

Supplementary Figure 4-3. Tumor NK Cell and CD8+ T cell Infiltration Inversely Correlates with Tumor Growth Following IC Treatment

This figure presents the same data as is presented in Figure 4-4D. A/J mice bearing subcutaneous NXS2 tumors were treated with IT-IC, IV-IC or Control treatment (No Treatment or IT-PBS). Mice were sacrificed 4 days post-treatment initiation and tumors underwent flow cytometric analyses. Mice are stratified by treatment group (IT-IC, IV-IC, No Treatment) and tumor growth (% Tumor Growth >0%) or shrinkage (% Tumor growth <0%). Within each group, tumor infiltrating leukocyte subtypes (A: CD8+, B: NKp46+, C: F4/80+, D: CD4+) are shown as a percentage of tumor leukocytes (CD45+ cells) using flow cytometric analysis. Asterisks provide p values for comparisons between immune cell populations. All panels represent data from 6 independent experiments with an average of 19 mice total within each treatment group.

Supplementary Figure 4-3.

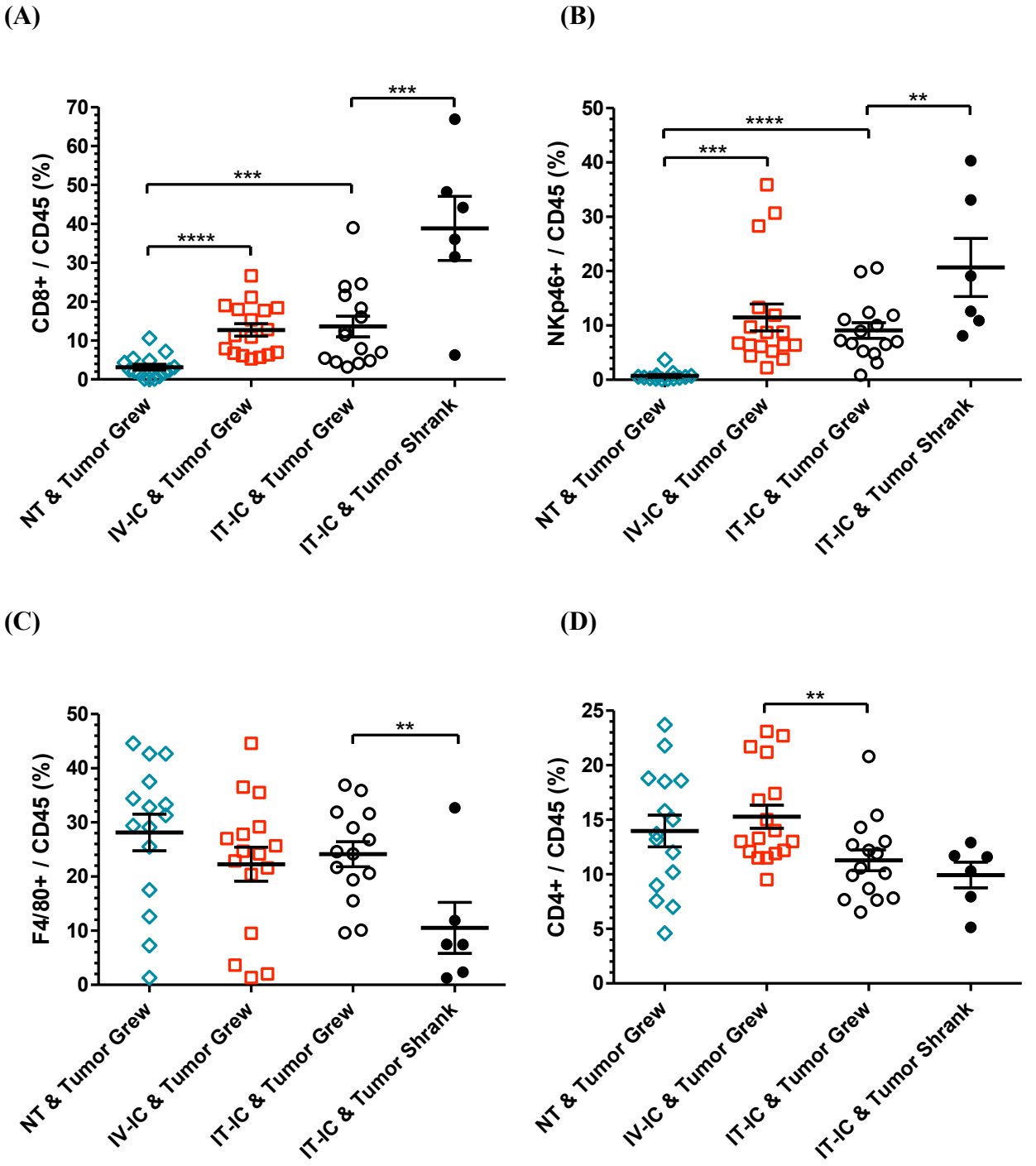

Chapter 5

Additional Projects in Clinical Research

5.1 Overview

This chapter of this PhD thesis provides an overview of additional work that I have been fortunate enough in which to participate. It begins with a project examining GD2 status of melanoma patients in a pilot clinical trial (CO-05601) which sought to treat patients with late stage but resectable melanoma with systemic hu14.18-IL2 before or after surgery. This study seeks to determine whether GD2 status of patients' melanoma is prognostic for time to recurrence after hu14.18-IL2 therapy. Many of the other additional works emphasize histological or cellular morphologic data, as many of the members of the Sondel laboratory would seek my assistance with these techniques. I present these works in reverse order of their publication date or completion.

5.2 Characterization of GD2 Tumor Antigen in Melanoma Patients from CO-05601

5.2.1 Introduction

GD2 has been used extensively as a target in mAb therapy and has been the primary target of antibody recognition in neuroblastoma. Clinical testing has been performed with the GD2 specific mAbs 3F8, 14.G2a, and ch14.18 (the human-mouse chimeric variant of 14.18) in neuroblastoma and melanoma (Cheung et al., 1998, Yu et al., 1998; Handgretinger et al., 1995; Murray et al., 1994; Saleh et al., 1992a).

A pilot trial (CO-05601) of intravenous hu14.18-IL2 in subjects with completely resectable recurrent stage III or stage IV melanoma is currently underway at the University of Wisconsin-Madison. The goals of this trial are to look at effects of intravenous hu14.18-IL2 on melanoma and to look at time to progression in this population. This trial sought to evaluate 16 patients, beginning IV-IC in half of the patients before surgery and half of patients after surgery,

with all patients scheduled to receive 3 monthly treatment courses (either 2 or 3 courses after surgical attainment of complete clinical remission).

We examined the level of GD2 expression in these patients' melanomas in this study treating with hu14.18-IL2. More specifically, we are interested in investigating whether there is a correlation between the GD2 positivity of a patient's melanoma and time to progression or overall survival time subsequent to receiving hu14.18-IL2. Since the hu14.18-IL2 immunocytokine is specific for GD2, we hypothesized that patients with melanoma highly expressing GD2 will have increased time to recurrence compared to patients whose melanoma does not express GD2.

5.2.2 Methods

We developed and utilized a robust and specific method for evaluating the level of GD2 positivity in melanoma tissue. OCT embedded and flash frozen patient melanoma tissue blocks from this clinical trial were obtained from Dr. Erik Ranheim, the protocol pathologist. These samples were sectioned 5 microns thick onto slides, fixed in acetone, and stained with 14.G2a (a mouse antibody specific for human GD2) or a mouse IgG2a isotype control. A biotinylated goat anti-mouse polyclonal secondary antibody (#BA-9200, Vector, Burlingame, CA) and an avidin-biotin complex were used to amplify the primary antibody signal. Tissue sections were developed with the DAB or NovaRed dye (Vector, Burlingame, CA) and counterstained with Mayer's hematoxylin (Sigma). GD2 expression in tumors was evaluated in 13 melanoma patients and these GD2 expression data were semi-quantified using a 0 - 100% grading scale, read by two blinded observers (RKY and NAK).

5.2.3 Results

Figure 5-1 shows an immunohistochemical stain done to validate a histological methology to gauge GD2 levels in patient melanoma tissue. Melanoma tissue from a patient in the currently open study of hu14.18-IL2 in patients with resectable melanoma (CO-05601) was stained with 14.G2a, which is shown in **Figure 5-1A**. **Figure 5-1B** shows a closely overlapping section stained with a mouse isotype control antibody. **Figure 5-1** clearly shows that we have a robust and specific method for evaluating GD2 expression in patients' melanoma, which will be used in correlation studies of GD2 level with outcome data for patients who received the hu14.18-IL immunocytokine.

Results are shown as a data table in **Table 5-1**. Results were blinded assessments of GD2 positive staining under a high powered microscope. Out of 13 evaluated patients' tissue, 5 patients (#7, 9, 10, 12, 13) (~38.4%) had at least one tissue section with a strong positive GD2 signal. In addition, there were 5 more patients (#11, 14, 16, 17, 18) (~38.4%) who had at least one tissue section with a weak positive GD2 signal. Only 3 patients (#2, 4, 6) out of the 13 patients evaluated (23.1%) had only negatively staining melanoma tissue sections. Therefore, 10 out of 13 evaluated patients (72.1%) showed some amount of detectable GD2 expression in their frozen tissue sections.

Figure 5-2 shows a Kaplan-Meier survival curve of patients stratified by GD2 expression on their melanoma as determined by immunohistochemical (IHC) staining with 14.G2a. Patients with negative GD2 expression in their melanoma had a median time to recurrence of 5.75 months compared to patients with strong (5.375 months) or weak (13.5 months) GD2 expression. Patients with negative GD2 expression in their melanoma tended to have shorter post on-study

time to recurrence compared to patients with weak or strong GD2 expression, though the trend is not significant.

5.2.4 Discussion

Our percentage of (72.1%) within the melanoma population (10 out of 13 positive for GD2) is close to that found by others. Since there were very few patients with undectable GD2 in their melanona tissue (n=3), there is a lack of power to determine a significant relationship between GD2 expression in melanoma and time to recurrence after hu14.18-IL2 therapy in this small study. Though we are not able to show a significant increase in the time to recurrence for hu14.18-IL2 treated patients with GD2+ melanoma compared to those with GD2(-) melanoma, we believe this trend is interesting and deserves further investigation. Furthermore, as the number of patients in this study was small and the GD2 expression and immune infiltrate patterns (not shown) were quite heterogeneous, it has not been possible to identify any clear difference in the histology for those samples obtaind before the hu14.18-IL2 treatment vs. those biopsies obtained after 1 course of hu14.18-IL2 treatment. In addition, we note that even within patients, different lesions can show different phenotype (i.e.: patient 9 had 3 lesions evaluated; 2 were strongly positive for GD2 and 1 was negative). For this reason, we would recommend that future analyses of the potential effect of immunotherapy on clinical lesions be evaluated by comparing pretreatment biopsies with post-treatment biopsies from the same lesion (whenever possible).

5.3 Genotypes of NK cell KIR Receptors, Their Ligands, and Fcγ Receptors in the Response of Neuroblastoma Patients to Hu14.18-IL2 Immunotherapy

I was fortunate enough to be included in this study examining associations comparing individual cellular phenotype with outcome to autologous stem cell transplant and hu14.18-IL2 immunotherapy for neuroblastoma. I was involved in the editing and revision process for this study. This study found an association between the mismatch status of a patient's killer immunoglobulin-like receptor (KIR)/KIR-ligands with patients' improved outcome (showing complete response or improvement of their disease) after IC therapy ($P = 0.03$). DNA from 38 patients were evaluated: 24 were found to have autologous KIR/KIR-ligand mismatch; 14 were matched. Of the 24 mismatched patients, 7 experienced either complete response or improvement of their disease after IC therapy. There was no response or comparable improvement of disease in patients who were matched. Therefore, KIR/KIR-ligand mismatch was associated with response/improvement to hu14.18-IL2. This report indicated that response or improvement of relapsed/refractory NBL patients after IC treatment is associated with autologous KIR/KIR-ligand mismatch, consistent with a role for natural killer cells in this clinical response.

Delgado DC, Hank JA, Kolesar JM, Lorentzen DF, Gan J, Seo S, Kim KM, Shusterman S, Gillies SD, Reisfeld RA, Yang RK, Gadbaw BC, DeSantes KD, London WB, Seeger RC, Maris JM, and Sondel PM. Genotypes of NK cell KIR Receptors, Their Ligands, and Fcγ Receptors in the Response of Neuroblastoma Patients to Hu14.18-IL2 Immunotherapy. Cancer Research. 2010 Dec 1;70(23):9554-61. [PMID: 20935224]

5.4 The anti-tumor effect of resveratrol alone or in combination with immunotherapy in a neuroblastoma model

I was fortunate enough to be included in this study examining hu14.18-IL2 in combination with peritumoral resveratrol as anti-tumor immunotherapy in subcutaneous GD2+ neuroblastoma bearing mice. I was involved in the consultation, execution, and photography of the immunohistochemistry portion of this report.

5.4.1 Immunohistochemistry

Twenty four hours after the last injection of RV, tumors were excised and embedded in tissue freezing medium (OCT). Frozen tissue sections were cut at 5 μm on the cryostat and fixed in cold acetone for 10 minutes. Nonspecific binding was blocked with 10% goat serum in PBS for one hour. The slides were incubated with CD45 (Ly-5) rat monoclonal primary antibody (eBioscience, San Diego, CA, 14-0451-85,clone 30F11) at a 1:160 dilution in PBS with 1% goat serum for one hour at 37° C. Sections were incubated with a biotinylated goat anti-rat (Vector Laboratories, Burlingame, CA) at 1:200 for one hour. Slides were incubated 30 minutes with Vectastain ABC Elite (Vector Laboratories, Burlingame CA). Slides were developed with DAB (3,3-diaminobenzidine) (Vector Laboratories, Burlingame CA), counterstained with Mayer's hematoxylin, dehydrated and cover slipped with permount. For Hematoxylin and Eosin (H&E) staining a modified version of the routine Mayer's staining protocol was used. Slides containing dried frozen sections were fixed in 100% EtOH for 2 minutes. Sections were stained with Mayer's Hematoxylin, for 15 minutes, and washed in running tap water for 20 minutes. Sections were counterstained with Eosin (Surgipath, Richmond, IL) for 30 seconds. The slides were the

dehydrated and mounted. Slides were blindly photographed by one of the authors using an AxioPhot microscope (Zeiss, Thornwood, New York).

5.4.2 Influence of RV on leukocyte counts and tumor infiltration

We examined the effects of RV treatment on immune cells. Peritumoral treatment with RV alone did not reduce, but seemed to increase the infiltration of leukocytes into the tumor microenvironment. This was seen in the CD45 staining for infiltrating leukocytes (**Fig. 5-3a,b**). The H&E staining revealed that tumors obtained from mice treated with RV alone or in combination with IC, showed areas of significant tumor necrosis (**Fig. 5-3f, h**) when compared to tissue from tumors treated with DMSO or IC alone (**Fig. 5-3e,g**). The tumor tissue destruction was more prominent in tumors from mice receiving combination therapy (**Fig. 5-3h**) than RV alone (**Fig. 5-3f**). These combined results of the blood counts and histology suggest that the peritumoral injections of RV caused tumor tissue damage without interfering with leukocyte infiltration into the tumor or changing the leukocytes in the circulation. Furthermore the combination of RV and IC appeared to induce more tumor damage than RV alone.

Soto BL, Hank JA, Van De Voort TJ, Subramanian L, Polans AS, Rakhmilevich AL, Yang RK, Seo S, Kim K, Reisfeld RA, Gillies SD, Sondel PM. The anti-tumor effect of resveratrol alone or in combination with immunotherapy in a neuroblastoma model. Cancer Immunology, Immunotherapy. 2011 May;60(5):731-8. [PMID: 21340652]

5.5 Soluble interleukin-2 receptor α activation in a Children's Oncology Group randomized trial of interleukin-2 Therapy for Pediatric Acute Myeloid Leukemia.

I was fortunate enough to be included in this study examining the immune activation of pediatric AML patients undergoing IL-2 immunotherapy. For this report, I was involved in the serum sample preparation, writing, editing, and revision processes. CCG-2961, opened in August 1996 and closed in December 2002, was a phase 3 trial for previously untreated AML. Eligible patients were age 1 day to less than 21 years with French-American and -British (FAB) AML subtypes M0-M2 and M4-M7. Patient received standard aggressive multi-agent chemotherapy for their AML. After completing all chemotherapy, patients still in remission were randomized to observation or to a ~2 week regimen of IV IL2. CCG-B972 was a correlative biology study that provided for acquisition and banking of serum specimens for sIL-2Ra assessment from these same patients.

5.5.1 Methods

Specimens stripped of identifiers were shipped overnight to the COG Immunology Reference Laboratory at the University of Wisconsin. Clinical data were sent to the COG Operations office. Samples were frozen at -20ºC. For analysis, all samples were thawed and spun down. One milliliter of supernatant was preserved with 1 ml 1% thimerosal at 48C. Samples designated as ‘‘on study,’’ ‘‘pre IL-2 day 0,’’ ‘‘no IL-2 day 0’’, and ‘‘no IL-2 day 28’’ were diluted 1/5; samples labeled ‘‘IL-2 day 4,’’ and ‘‘IL-2 day 18’’ were diluted 1/20 to fit in the optimal assay range (0–2,000 pg/ml) according to manufacturer’s specifications for the sIL-2ra enzyme-linked immunosorbent assay (ELISA; DuoSet ELISA Development Kit; R&D Systems).

5.5.2. Results

The CCG-2961 is the first study to evaluate serial concentrations of sIL-2Ra in the context of a large randomized controlled clinical trial of IL-2 in a relatively homogeneous population. The trial shows sIL-2Ra concentrations are elevated in untreated pediatric AML patients compared to those of healthy controls and some other cancer patients. sIL-2Ra concentrations decline during chemotherapy and show consistent and significant dose-dependent increases during IL-2 treatment but not during observation in control patients. These findings provide clear evidence of biologic activity of IL-2. However, the clinical results indicated that the IL2 treatment did not provide any benefit in overall or event free survival. Based on this study, the COG is no longer studying the use of IL2 in this clinical setting.

Lange BJ, Yang RK, Gan J, Hank JA, Sievers EL, Alonzo TA, Gerbing RB, Sondel PM. Soluble interleukin-2 receptor α activation in a Children's Oncology Group randomized trial of interleukin-2 Therapy for Pediatric Acute Myeloid Leukemia. Pediatric Blood and Cancer. 2011 Sep;57(3):398-405. [PMID: 21681921]

5.6 Tumor-associated myeloid cells can be activated in vitro and in vivo to mediate antitumor effects

I was fortunate enough to be included in this study examining the immune activation of tumor associated myeloid cells. For this report, I was involved in the histological assessment of immune cells, as well as editing and revision. This study tested the possibility of activating tumor-associated myeloid cells to mediate antitumor effects using anti-CD40 monoclonal antibody and CpG1826. Treatment of mice bearing established peritoneal B16 tumors with anti-CD40 and CpG resulted in activation of tumor-associated PEC, reduction in local tumor burden and prolongation of mouse survival. This report indicated that in tumor-bearing hosts, tumor-associated myeloid cells can be activated to mediate antitumor effects with anti-CD40 and CpG.

5.6.1 Methods - Wright-Giemsa Staining

Peritoneal cells (10^4-10^5 cells in 100 µl media with FCS) were centrifuged at 800 rpm for 3 minutes using a Shandon Cytospin 2. After air drying for 5 minutes, slides were fixed in 100% methanol 2 minutes, allowed to dry, and stained horizontally with Wright Giemsa Stain (Sigma) for 45 seconds. An equal volume of glass filtered water was immediately added to the Wright Giemsa stain solution, and staining with this mixture was performed for 10 minutes, after which the slides were washed off with glass filtered water and destained horizontally with glass filtered water for 5 minutes. Slides were allowed to dry and mounted with glass coverslips using cytoseal 60. Pictures of cells were taken under 40x magnifications with attached computer software (Magnafire 2.1).

5.6.2 Results - Characterization of Sorted Peritoneal Cells from Tumor-Bearing Mice

Histological evaluation showed that $CD11b^{+}Gr\text{-}1^{high}$ cells (**Fig. 5-4b**) and $CD11b^{+}Gr\text{-}1^{high}F4/80^{-}$ cells (**Fig. 5-4f**) consisted mostly of granulocytes with a smaller percentage of Mϕ/monocytic cells, while a reverse relationship between granulocytes and Mϕ/monocytes was observed in $CD11b^{+}Gr\text{-}1^{int/-}$ cells (**Fig. 5-4b**) and $CD11b^{+}Gr\text{-}1^{high}F4/80^{+}$ cells (**Fig. 5-4f**). In an attempt to obtain more pure cell populations, $CD11b^{+}$ PEC were sorted according to their Gr-1 expression and side/forward scatter characteristics (using the gates for granulocytes and monocytes) as shown in **Fig. 5-4i**. As a result, relatively pure populations of granulocytes and Mϕ/monocytes, respectively, were obtained (**Fig. 5-4j**).

Rakhmilevich AL, Baldeshwiler MJ, Van De Voort TJ, Felder MA, Yang RK, Kalogriopoulos NA, Koslov DS, Van Rooijen N, Sondel PM. Tumor-associated myeloid cells can be activated in vitro and in vivo to mediate antitumor effects. Cancer Immunology, Immunotherapy. 2012 Mar 6. [PMID: 22392192]

5.7 Intratumoral Delivery of Low Doses of Anti-CD40 mAb Combined with Monophosphoryl Lipid A induces T Cell-Independent, Local and Systemic Antitumor Effects in Mice

I was fortunate enough to be included in this study examining the immune activation of tumor associated myeloid cells. For this report, I was involved in the histological assessment of immune cells, as well as editing and revision. This study utilized anti-CD40 monoclonal antibody (anti-CD40) combined with monophosphoryl lipid A (MPL) to assess the antitumor synergy between the two agents in tumor-bearing mice. Results showed that the antitumor effects of anti-CD40 are enhanced by subsequent treatment with MPL, even in T cell-deficient hosts. These preclinical data suggest that the anti-CD40+MPL combined regimen is appropriate for clinical testing in human patients, including cancer patients that may be immunosuppressed from prior chemotherapy.

5.7.1 Methods - Wright-Giemsa Staining

Peritoneal cells (10^4-10^5 cells in 100 µl media with FCS) were centrifuged at 800 rpm for 3 minutes using a Shandon Cytospin 2. After air drying for 5 minutes, slides were fixed in 100% methanol 2 minutes, allowed to dry, and stained horizontally with Wright Giemsa Stain (Sigma) for 45 seconds. An equal volume of glass filtered water was immediately added to the Wright Giemsa stain solution, and staining with this mixture was performed for 10 minutes, after which the slides were washed off with glass filtered water and destained horizontally with glass filtered water for 5 minutes. Slides were allowed to dry and mounted with glass coverslips using cytoseal 60. Pictures of cells were taken under 40x magnifications with attached computer software (Magnafire 2.1, Optronics, Goleta, California).

5.7.2 Results - CD11b^{+} F4/80^{+} Gr-1^{low} macrophages and CD11b^{+} F4/80^{-} Gr-1^{high} monocytes are activated by anti-CD40 and MPL

In order to identify the specific subset of effector cells that can be activated by MPL on day 3 after anti-CD40 priming, PECs were collected from mice that had been injected with anti-CD40 3 days earlier, stained, gated on CD11b^{high} cells, sorted into 4 sub-populations based on their expression of immunophenotypic surface markers (Fig. 5-5*A*), and were further characterized by histological staining (Fig. 5-5*B*). Subpopulation 1 consisted of monocytes and naïve macrophages. Subpopulation 2 expressed slightly less F4/80 and slightly more Gr-1, and was shown by histological staining (Fig 2*B*) to be a distinct population from subpopulation 1. Subpopulation 2 consisted of a relatively pure population of activated macrophages. In order to identify more precisely which cells were activated in the experiment shown in Fig.5-5, this population of CD11b^{+} Gr-1^{+} cells was further purified by forward scatter and side scatter qualities into two distinct populations, one predominantly consisting of granulocytes (Fig. *5-5B,* 3) and the other, monocytes (Fig. 5-5*B,* 4).

Tyler J. Van De Voort, Mildred A.R. Felder, Richard K. Yang, Paul M. Sondel, and Alexander L. Rakhmilevich. Intratumoral delivery of low doses of anti-CD40 mAb combined with monophosphoryl lipid A induces T cell-independent, local and systemic antitumor effects in mice. (Submitted, Journal of Immunology, 2012)

Table 5-1. Expression of GD2 Antigen in Melanoma Patients from CO-05601

Patient frozen tissue blocks of the NED (IV-IC) melanoma trial were obtained from Dr. Erik Ranheim. These samples were sectioned 5 microns thick onto slides, fixed in acetone, and stained with 14.G2a, a mouse anti-GD2 antibody, along with a mouse IgG2a isotype control. Melanoma issue from 13 patients were obtained, stained, and evaluated for GD2 expression. Results are blinded readings (by authors RKY and NAK) of GD2 positivity staining under a high powered microscope.

Table 5-1.

Trial Patient Number	Arm	Surgery Date	Block	GD2 Reviewer 1 (RKY)	GD2 Reviewer 2 (NAK)	Interpretation
2	B	4/17/08	A	0-5%	~0%	**Negative**
4	C	5/29/08	A	0%	~0%	**Negative**
6	B	9/15/09	A	0-1%	~0%	**Negative**
7	B	10/6/09	A	**5-25%**	**~60%**	**Strong Positive**
7	B	10/6/09	B	**50-75%**	**~60%**	**Strong Positive**
9	A	2/9/10	A	**50-75%**	**~70%**	**Strong Positive**
9	A	2/9/10	A	**25-50%**	**~25%**	**Strong Positive**
9	A	2/9/10	B	0-1%	~0%	**Negative**
10	A	5/13/10	A	0-1%	~0%	**Negative**
10	A	5/13/10	B	**75-100%**	**~90%**	**Strong Positive**
11	A	11/18/10	A	0-1%	**~25%**	**Weak Positive**
11	A	11/18/10	B	**5-25%**	~0%	**Weak Positive**
12	B	8/20/10	A	**25-50%**	**~65%**	**Strong Positive**
12	B	8/20/10	B	**25-50%**	**~40%**	**Strong Positive**
13	A	9/9/10	A	**25-50%**	**~20%**	**Strong Positive**
13	A	9/9/10	B	**5-25%**	**~10%**	**Weak Positive**
14	B	9/13/10	A	0-1%	~0%	**Negative**
14	B	9/28/10	B	**5-25%**	**~40%**	**Weak Positive**
16	B	11/9/10	A	0-1%	**~5%**	**Weak Positive**
17	B	1/6/11	A	**1-5%**	**~25%**	**Weak Positive**
18	A	3/16/11	A	**25-50%**	**~35%**	**Weak Positive**
18	A	3/16/11	B	0-1%	**~5%**	**Weak Positive**

Figure 5-1. GD2 Postivity in Patient Melanoma is Clearly Distinguishable

The resected melanoma of a human patient in this trial shows a visually striking amount of GD2 positivity. Melanoma tissue from a patient (#12) in the currently open study of hu14.18-IL2 in patients with resectable melanoma (CO-05601) was embed in OCT, flash frozen in liquid nitrogen, cut into sections on a cryostat, fixed in cold acetone, and stained with a mouse antibody specific for human GD2. In panel **(A),** a section of melanoma is stained with a mouse 14.G2a antibody. Panel **(B)** shows a closely overlapping section stained with a mouse IgG2a isotype control. (10x magnification)

Figure 5-1.

(A)

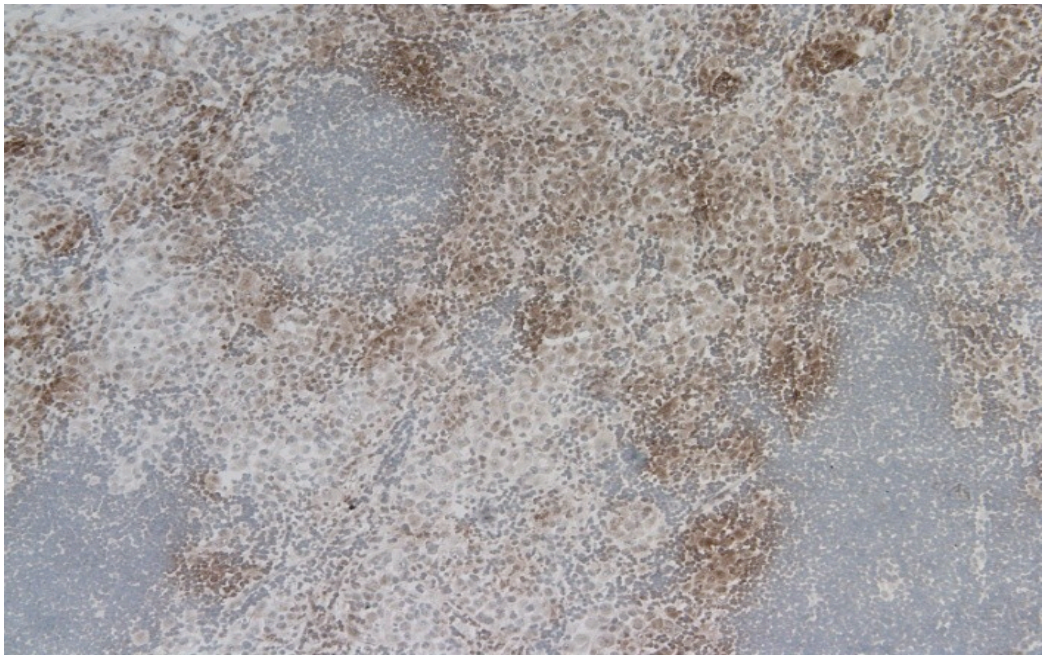

(B)

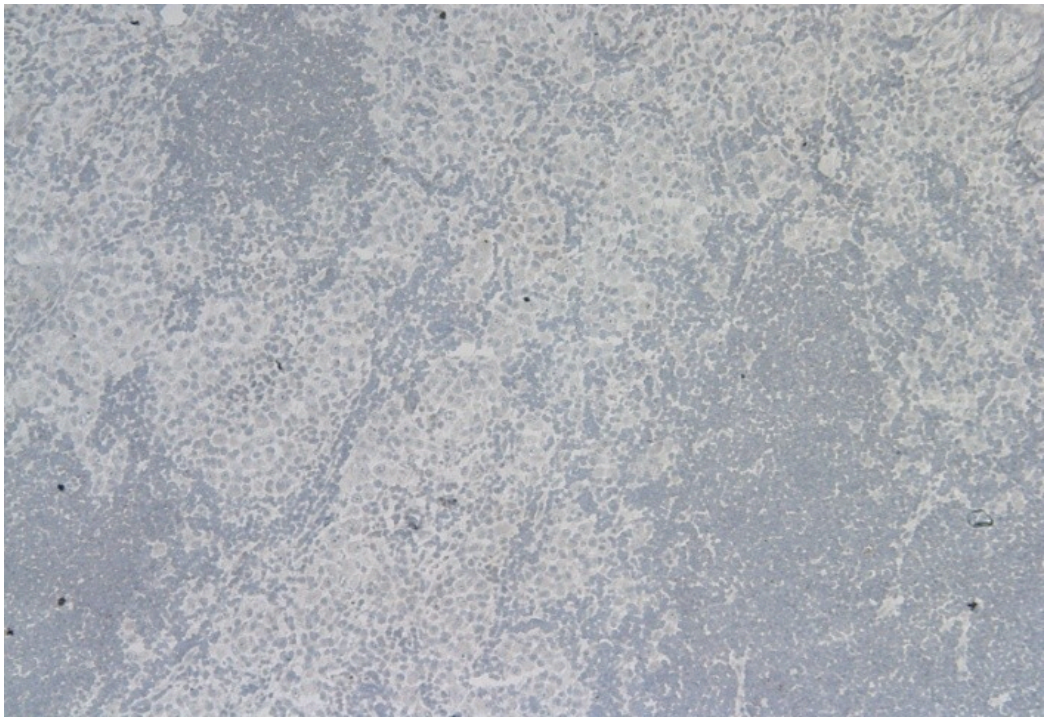

Figure 5-2. Patients with GD2(+) Melanoma Show a Non-Significant Trend for Longer Post On-Study Time to Recurrence After Hu14.18-IL2 Treatment Compared to Patients with GD2(-) Melanoma

Kaplan-Meier survival curve of patients stratified by GD2 expression on their melanoma as determined by immunohistochemical (IHC) staining with 14.G2a. Patients with negative GD2 expression in their melanoma had a median time to recurrence of 5.75 months compared to patients with strong (5.375 months) or weak (13.5 months) GD2 expression.

Figure 5-2.

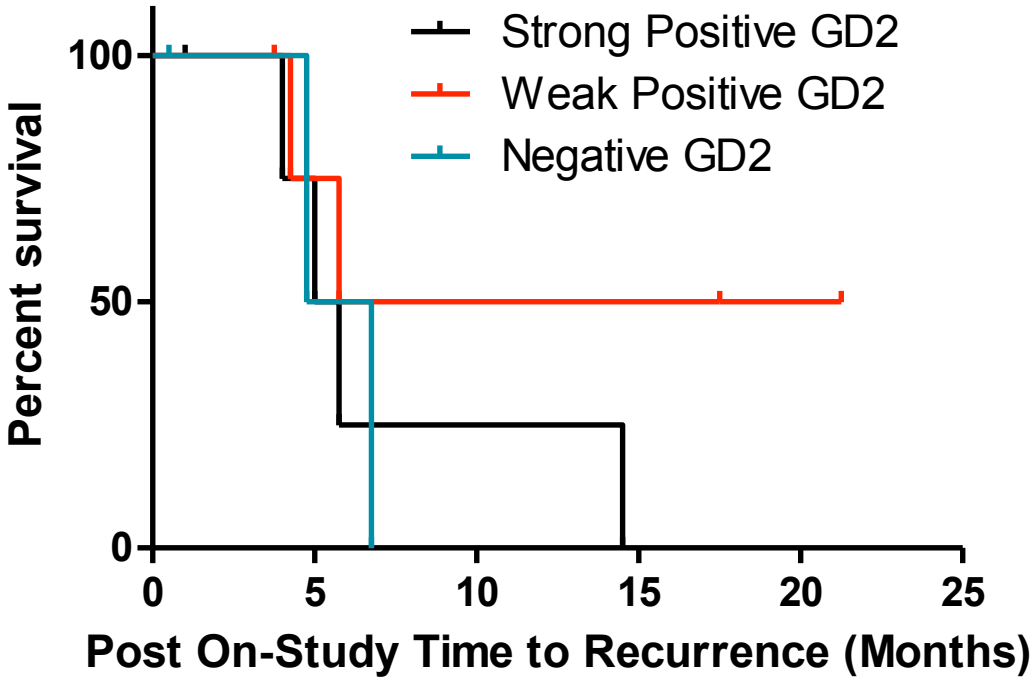
Strong Positive GD2
Weak Positive GD2
Negative GD2
100
50
0
Percent survival
0
5
10
15
20
25
Post On-Study Time to Recurrence (Months)

Figure 5-3. Immunohistochemistry of tumors from the IC/RV combination study

Tumor tissue was obtained on day 20 from mice treated with peritumoral (p.t.) DMSO (a,e), p.t. 20mg RV (b,f), IC i.v. (c,g) or IC + RV in combination (d,h). Tissue was stained with anti-CD45 (a–d) and, H & E (e–h). Pictures were taken on a bright field at 10X, the inserts on each picture are at 40X. Representative fields are show.

Figure 5-3.

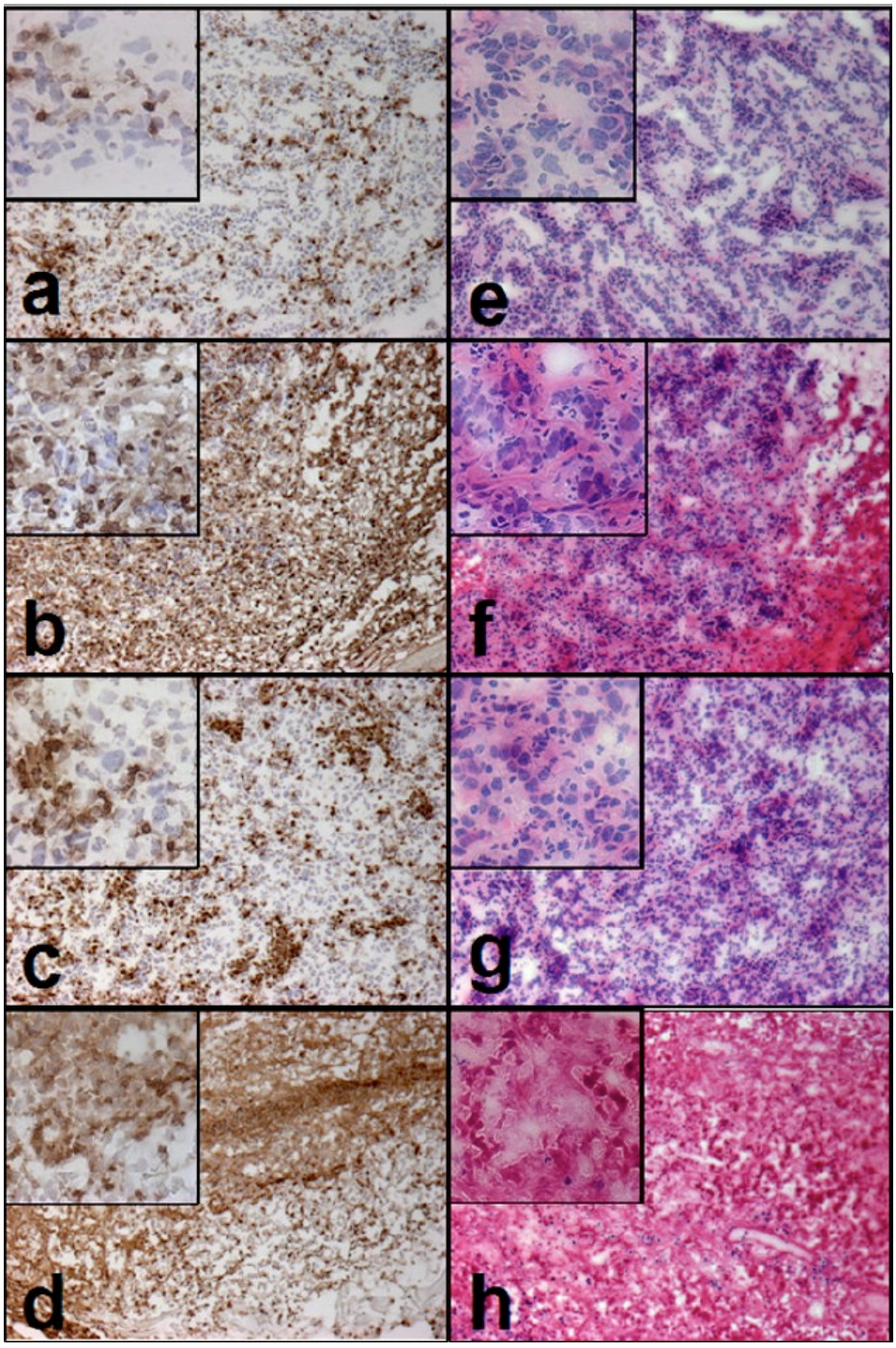

Figure 5-4. Morphology of Sorted Peritoneal Cells (PECs) from Tumor-Bearing Mice

PECs were obtained 14–15 days after injecting C57BL/6 mice i.p. with 1 x 105 B16 cells. PEC were sorted based on their phenotype (A, E, I) and also forward-side scatter characteristics (I). The sorting strategy of PEC from TBM is depicted in A, E and I. The morphology of sorted cell fractions from naive and TBM is presented in B, F and J. The numbers designate the sorted cell fraction for that experiment; namely in A, the designations 2, 3 and 4 correspond to the populations shown in B, where ‘‘1’’ depicts sorted CD11b+ PEC from naive mice. Similarly, in E, the designations 5 and 6 correspond to those same designated populations in F. In I, the designations 7, 8 and 9 correspond to those designations in J.

Figure 5-4.

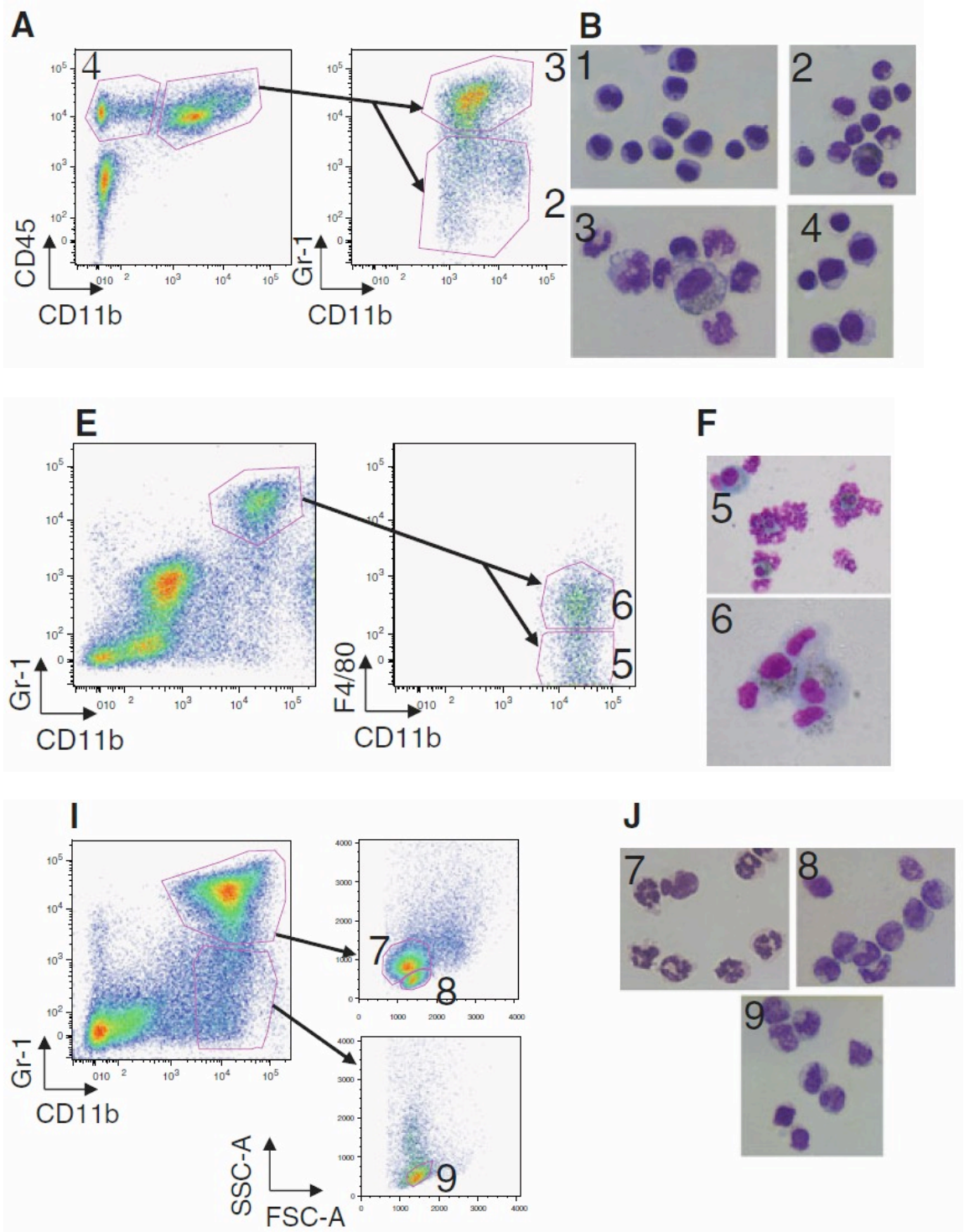
A
B
4
3
2
1
2
3
4
CD45
CD11b
Gr-1
CD11b
E
F
6
5
5
6
Gr-1
CD11b
F4/80
CD11b
I
J
7
8
9
7
8
9
Gr-1
CD11b
SSC-A
FSC-A

Figure 5-5. $CD11b^{+}$ $F4/80^{+}$ $Gr\text{-}1^{low}$ macrophages and $CD11b^{+}$ $F4/80^{-}$ $Gr\text{-}1^{high}$ monocytes are activated by anti-CD40 and MPL.

C57BL/6 mice were injected i.p. with 500 μg anti-CD40 on day 0. **(A)** On day 3, mice were euthanized and their PEC were collected, stained, gated on $CD11b^{high}$ cells and sorted into 4 sub-populations by a FACSAria cell sorter. The cells were divided as follows: (1) $CD11b^{+}$ $F4/80^{++}$ $Gr\text{-}1^{low}$ (monocytes), (2) $CD11b^{+}$ $F4/80^{+}$ $Gr\text{-}1^{dim}$ (activated macrophages). A separate group of cells showed a $CD11b^{+}$ $F4/80^{-}$ $Gr\text{-}1^{high}$ phenotype; these were further divided by forward and side scatter into populations (3) (granulocytes), and (4) (monocytes). **(B)** Each cell population was stained with a Wright-Giemsa stain to identify cell types based on morphology. The relative sizes of each sorted cell population have been maintained, and these 4 micrographs all show 40x magnification.

Figure 5-5.

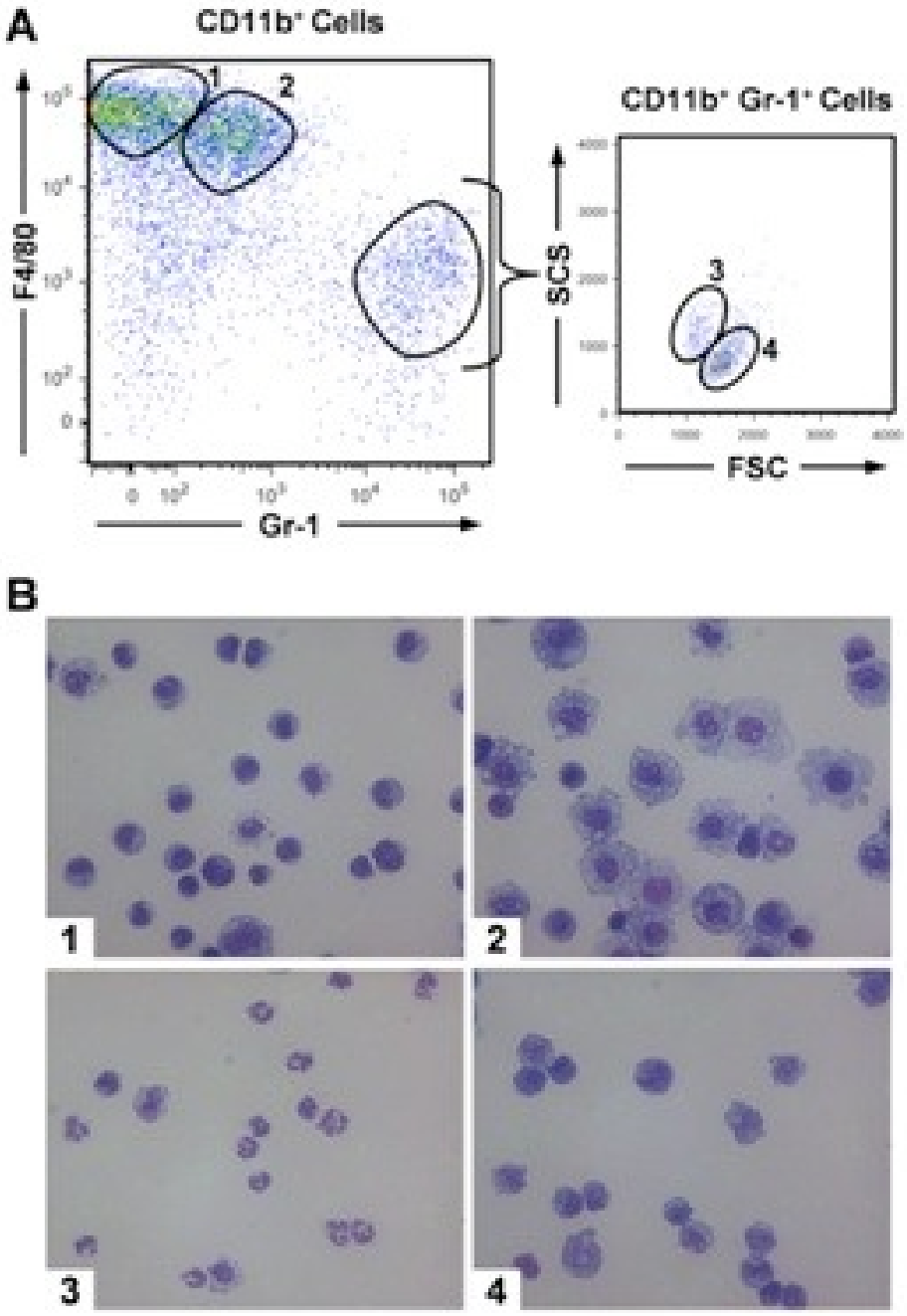

Chapter 6

Discussion

6.1 Overview

This final chapter of this PhD thesis provides an overview of the conclusions made from the work presented in the prior 5 chapters. It emphasizes the data presented in the preclinical model system, included in chapters 2, 3 and 4. I then turn to some of the potential biological and clinical implications of this work for future study and for possible translation into clinical research and treatment.

6.2 Summary of Data

6.2.1 Role of Intratumoral (IT) hu14.18-IL2 Efficacy in GD2+ Neuroblastoma Mouse Model

Data presented in this thesis help elucidate possible mechanisms of enhanced antitumor effects of localized hu14.18-IL2 therapy and assist in distinguishing the IT-IC antitumor effect from the IV-IC antitumor effect. In chapter 3, we show that IT-IC treatment induces improved inhibition of tumor growth and augmented survival compared to no treatment or treatment with IT-PBS. Immunohistochemical and flow cytometric analyses show an increased percentage of NK and T cells in IT-IC treated tumors. Depletion studies show that T cells and NK cells are involved in the antitumor effects of IT-IC on directly injected local tumors and on non-injected distant tumors in those same animals. Depletion of either immune cell population (NK cells or T cells) substantially attenuates the observed antitumor effects on both the local and distant tumors. These data suggest that both T cells and NK cells are necessary for the local and distant antitumor effects observed under these conditions. While NK cells may be playing a more direct and immediate effect (through ADCC), and T cells may be having a more delayed effect, through an adaptive immune response, we are not able to clarify these mechanisms from the data

presented here. Furthermore, other possible mechanisms (direct induction of tumor apoptosis, or disruption of the tumor micro-environment or tumor vascular system) also may be possible.

We also show that IT-IC treatment causes better tumor growth inhibition and survival than IV-IC treatment. This improved in vivo antitumor efficacy of IT-IC vs. IV-IC is consistent with several mechanistic observations that we made in the studies presented in this thesis. Our flow cytometry analyses demonstrate that IT-IC results in a lower percentage of living tumors cells than IV-IC treatment. Furthermore, flow cytometry analyses show that IT-IC treatment is characterized by a higher percentage of NKG2A/C/E+ cells. IT and IV treatment with hu14.18-IL2 increases the fraction of NK cells and CD8 cells that express NKG2A/C/E, while IT-IC increases expression levels of the NKG2D effector receptor on NK and CD8 cells to a greater degree than does IV-IC. Finally, flow cytometry analyses were used to show that IT-IC treatment results in augmented delivery and retention of IC to tumor compared to IV-IC treatment.

6.2.2 Role of Tumor Infiltrating Leukocytes in IT hu14.18-IL2 (IC) Immunotherapy

We examined whether increases in tumor infiltrating leukocytes, such as CD8+ CTLs or NKp46+ NK cells, resulted in better treatment outcomes such as tumor shrinkage. Using quantitative histological analyses, our data show that increased NKG2A/C/E+ and CD8+ cells inversely correlated with tumor growth (as measured by percent tumor growth). When comparing IT-IC treated mice whose tumors shrank against those whose tumors grew, our flow cytometry data showed a statistically significant increase in CTLs and NK cells as well as a statistically significant decrease in tumor macrophages in the tumors that shrank. These data suggest that CTLs and NK cells were involved in the process of tumor shrinkage, while macrophages appeared to be associated with tumor growth rather than shrinkage.

We also found that NKG2D expression on CD8+ cells and on NK cells inversely correlated with tumor growth (measured by Percent Tumor Growth), which suggested a role of NKG2D expression on NK cells and CD8 cells in tumor shrinkage. Interestingly augmented NKG2D expression on activated NK cells was found in the same mice that had augmented NKG2D on CTLs, suggesting a shared relationship of augmented NKG2D on TILs in helping to mediate tumor shrinkage. In this thesis, we show how NKG2D up-regulation in the tumor infiltrating leukocytes correlates with slower tumor growth, in treated as well as in untreated animals (Chapter 4). In Chapter 3 we found that NKG2D upregulation in IT-IC and IV-IC treated animals was seen in the tumors, but not in the spleens, suggesting that the NK and T activation induced by the IC treatment was occurring in the IC-treated tumor microenvironment. We also showed that the NXS2 tumors growing in mice have strong expression of ligands that enable them to be recognized by the NKG2D receptors on the NK and CD8 T cells.

6.2.3 Role of Initial Tumor Load in Intratumoral hu14.18-IL2 (IC) Immunotherapy

We examined whether tumor volume at treatment initiation was an important factor in overall survival (Chapter 4). Our data show that smaller initial tumor volume correlated with increased survival in hu14.18-IL2 treated mice, indicating that tumor volume at treatment initiation is prognostic for survival after IT-IC treatment. Next, we examined whether tumor volume at treatment initiation was an important factor affecting the change in tumor infiltrating leukocytes associated with hu14.18-IL2 treatment. Our data show that hu14.18-IL2 treatment of mice with lower initial tumor volume leads to increased tumor leukocyte and NK infiltration and increased NKG2D expression on tumor NK cells and CD8+ T cells. These data indicate that smaller initial tumor volume when treatment begins is predictive of the level of increased tumor

infiltrating lymphocytes. We examined which immune cells correlated with the increase in tumor leukocytes seen in small tumors treated with IT-IC. Our data show that increased tumor leukocyte infiltration seen in IT-IC treated tumors correlated with CD8+ cytotoxic T cells as well as higher NKG2D expression on CTLs and NK cells. This indicates that much of the increase in tumor leukocytes seen in small tumors treated with IT-IC was due to CD8+ CTLs.

We also examined whether tumor burden at treatment initiation played a role in hu14.18-IL2 induced tumor shrinkage. Our data showed that smaller tumor load at treatment initiation increased the likelihood of tumor shrinkage in IT-IC treated mice. The opposite was true in control mice; namely control tumors that were smaller at the time of "treatment initiation" actually showed greater % change in size than the tumors that were larger at the time of treatment initiation. These data are consistent with our findings that hu14.18-IL2 treatment of smaller tumors leads to higher tumor infiltrating leukocytes and that increased tumor leukocytes correlate with shrinkage of tumors. Finally, we examined whether initial tumor growth or shrinkage influenced overall survival outcome. Our data showed that tumor shrinkage detected 4 days after starting treatment led to increased long term survival in hu14.18-IL2 treated mice. Conversely, tumor progression detected 4 days after starting treatment in control and hu14.18-IL2 treated mice led to decreased overall survival. These data are consistent with our previous findings that hu14.18-IL2 treatment of smaller tumors leads to an increased anti-metastatic effect against NXS2 neuroblastoma (Neal et al., 2004).

Interestingly, **Figure 4-6B**, which shows the relationship between tumor volume at treatment initiation and day 4 tumor volume, indicates that the relationship between treatment groups is highly dependent upon initial tumor volume. When tumors are over 130.9 mm^3 in volume (highest quartile), there seems to be little to no effect of hu14.18-IL2 therapy, injected

either intratumorally or intravenously. This is shown by the finding that the regression lines of the three treatment groups seem to intersect at this initial tumor volume. However, when tumor burden is less that 130.9mm^3 (lowest three quartiles), there are significant effects of both IT and IV hu14.18-IL2 therapy in slowing tumor growth compared to control treated tumors.

6.3 Biological Implications of Work

The IL2 component of the hu14.18-IL2 augments the effects of the mAb, and has been shown to increase the number and activation state of NK cells, as well as to stimulate tumor cell killing by antigen-specific T-cells (Sondel and Hank, 1997). The IL2 component can stimulate both NK and T-cells via the IL2 receptor, independent of Fc or T-cell receptor binding, respectively (Gillies et al., 1992; Mule et al., 1987; Voss et al., 1990; Weil-Hillman et al., 1989). Using a metastatic model of NXS2 neuroblastoma metastasizing to bone marrow in A/J mice, IV hu14.18-IL2 therapy in mice with early microscopic metastases has been previously shown to be exclusively NK cell mediated (Lode et al., 1997; Lode et al., 1998). In contrast, our model investigates possible immune effector cells within well-established subcutaneous tumors and shows a necessary role of both NK and T cells in response to localized IT hu14.18-IL2 therapy.

IT-IC resulted in complete resolution of both the directly treated local and non-injected distant tumors in several mice. There are several mechanisms that may be resulting in the antitumor effects of both local and distant tumors. IT-IC may be circulating and having a systemic effect; IT-IC may be inducing a systemic adaptive immune response by the host's immune system, or a combination of both. We know from previous studies that T cells from treated mice can respond to NXS2 in an antigen-dependent manner (Neal et al., 2004). Our results indicate that IT-IC induces a systemic immune response. T cells and NK cells were

required for rejection of both primary and distant tumors. Some role exists for antigen specific T cell memory, as 90% of mice that became tumor-free following IT-IC treatment were able to subsequently reject rechallenge with 2 x 10^6 NXS2 cells.

6.3.1 Role NK Cells

Natural killer cells (NKp46+ cells) very likely have some role in tumor shrinkage because they are significantly increased in IT-IC treated shrinking tumors compared to IT-IC treated growing tumors (**Fig. 4-4D**). These results are consistent with our prior results that show IT-IC treatment can be dramatically inhibited in this model by either NK or T cell depletion (**Fig 3-3C**). Also, the statistically significant increase in NKG2D expression on NK cells after IT-IC vs. IV-IC treatment (**Fig. 3-5C**), may reflect a mechanism that plays some part in the enhanced antitumor effect of IT vs. IV IC treatment. In addition, the increased expression of NKG2D might also be considered a marker of activation, and suggest that other pathways (not assayed for in this study) might also be further activated by IT-IC than IV-IC.

6.3.2 Role of CD8+ T cells

CD8+ T cells likely play a large role in the hu14.18-IL2 mediated tumor shrinkage effect. **Figure 4-4D** shows that CD8+ T cells are the cell type that is most increased in frequency when IT-IC treated tumors are shrinking compared to those that are growing. Also, there is an increased percentage of cells co-expressing NKG2A+ and CD8a+ as well as an increased NKG2D expression on CD8a+/NKG2A+ T cells in tumors versus spleens within similarly treated mice (**Fig. 3-5B,D**). This may suggest at least some inherent importance of T cells in

combating tumor cells in this model since NKG2A/C/E+ cells have been shown to be necessary for self recognition (Vance et al., 1998).

Depletion data from a two-tumor model showed that T cells, as well as NK cells, play a large role in the IT-IC antitumor effect compared to the previously shown NK-predominant cell-mediated IV-IC antitumor effect (Lode et al., 1998). Perhaps having substantial IL2 bound to the surface of tumor cells after IT-IC treatment (**Fig. 3-6B**) is directly or indirectly responsible for increasing these specific lymphocytes (NKG2A/C/E+ TIL) or altering their phenotype (increasing expression of NKG2D effector receptor) and enhancing the antitumor effect compared to IV-IC treatment. *In vitro* data suggest that IC on tumor cells enables cells with IL2 receptors to form more activated immune synapses with the tumor cells than they would using mAb in combination with IL2 (Gubbels et al., 2011; Buhtoiarov et al., 2011).

6.3.3 Role of NKG2D

Studies by Verneris et al show that ligation of NKG2D on NK cells directly induces cytotoxicity (Verneris et al., 2004). They showed that NKG2D expression is up-regulated upon IL-2 activation and expansion of CD8+ T cells. T cells activated and expanded in low and high concentrations of IL-2 both up-regulated NKG2D expression equally, but only cells cultured in high-dose IL-2 were cytotoxic. Verneris et al also showed that the activated CD8+ T cells demonstrated cytotoxicity against malignant target cells, which occurs through NKG2D-mediated recognition and signaling and not through the TCR (Vance et al., 2002). NKG2D triggering accounts for the majority of MHC-unrestricted cytotoxicity of activated and expanded CD8+ T cells (Karimi et al., 2005).

When treating IT-IC vs. IV-IC, there is a small but significant increase in NKG2D expression on NKp46+/NKG2A+ double positive cells as well as a small, but not significant increase in NKG2D expression on CD8a+/NKG2A+ cells (**Fig. 3-5C,D**). This may indicate a phenotypic advantage of resulting TILs when treating with IT-IC. Expression of NKG2D on activated CD8+ T cells has been shown to account for TCR independent cytotoxicity against malignant cells *in vitro* (Verneris et al., 2004). Its enhanced expression on CD8+ TILs, but not spleen cells, following IV or IT treatment with IC in our study, demonstrates the localized activation of T cells, at the tumor site, induced by IC treatment. We have examined expressivity of NKG2D ligands on NXS2 and have found a large increase in RAE-1gamma expression ex-vivo (data not shown). Therefore, NKG2D may be playing a direct role in the enhanced antitumor effects in addition to being a marker of activation. Interestingly, our data suggest that the stimulation and activation of NK and T cells are not independent (**Fig. 4-5C**) and that the activation of these infiltrating lymphocytes is important for antitumor activity and survival in this mouse model.

6.3.4 Role of Macrophages

Conversely, macrophages (F4/80+ cells) are significantly decreased in IT-IC treated shrinking tumor compared to IT-IC treated growing tumors (**Fig. 4-4D**), which may indicate an inhibitory role of macrophages in the IT-IC mediated tumor shrinkage process.

6.3.5 Biological Variation

The data presented here demonstrate that even in groups of genetically identical mice, receiving identical doses of tumor implants and identical antitumor treatments, quantitative

measures of initial tumor size and of TIL patterns are clearly predictive of response to treatment. These data indicate that the ultimate response to tumor immunotherapy, either beneficial or ineffective, is determined (at least in part) by quantitative factors that might be manipulated to enhance antitumor efficacy, or measured for prognostic purposes. Translating these observations into clinical evaluations will require large clinical analyses with standardizable parameters for immune measurements, in order to determine if the principles identified in this mouse model may also pertain to clinical treatments with analogous immunotherapies.

6.4 Clinical Implications of Work

Using an A/J mouse NXS2 neuroblastoma model, our lab had previously demonstrated the enhanced local and systemic antitumor effects of intratumoral-IC (IT-IC) compared to IV-IC. IT-IC compared to IV-IC resulted in increased numbers of activated T- and NK cells within tumors, better IC retention in the tumor, enhanced inhibition of tumor growth, and improved survival (Chapter 3). Although we had shown that IC treatment can augment potent antitumor activity in mouse models and in clinical trials, IC administration can also have diverse effects in terms of overall outcome; in other words, not all treated mice or all treated patients show a beneficial effect. Therefore, we sought to find signatures that might be distinguished in patients, either prior to IC treatment or soon after treatment initiation, which might be predictive of tumor growth inhibition vs. tumor progression.

6.4.1 Potential Impact on Metastatic Melanoma Treatment

It may be useful to determine signatures that could be distinguished in patients, either prior to IC treatment or soon after treatment initiation, which are predictive of beneficial

antitumor effect. Such predictive signatures could be then used in clinical decision making regarding treatment continuation or changing to alternate therapies. We have identified several parameters (measured before and shortly after treatment initiation) in this animal model that appear to be indicators of prognosis in these treated mice. Some of these are already being used in clinical decision-making.

6.4.1.1 Potential Usefulness of Histology

Analyses of TILs, determined by histologic evaluation or by flow cytometry, might be used as an important prognostic determinant. Soon after IC treatment initiation, tumor infiltration might be used as an indicator of treatment efficacy. If the murine data we have obtained translate to the clinical setting, patients with high CD8+ T cell, high NKp46+ NK cell, and low F4/80+ macrophage tumor infiltrating populations after initial treatment may have a higher likelihood of experiencing a more potent antitumor effect. The NKG2D expression of NK cells and activated CTLs may also be indicative of the potential for a more potent IC-induced antitumor effect. This immune profile could be investigated as a potential predictive parameter of beneficial IC treatment. Lack of this signature may indicate that treatment adjustments need to be made.

6.4.1.1.2 Small Tumor Leads to Better Outcome

Clinical stage of disease is a primary factor used to predict prognosis and help with treatment assignation. Based on these preclinical data, as well as our clinical phase II data showing greater likelihood of response for patients with less “bulky disease” (Shusterman et al., 2010), we hypothesize that patients should be treated with IC (either IT-IC or IV-IC) when tumor volume is at a minimum, as larger tumor size interferes with the ability of IC treatment to

mediate beneficial antitumor effects. Tumor growth patterns soon after IC treatment initiation may also be studied as a potential predictor of long term benefit. If these murine studies translate to the clinical setting, patients with tumors that have a reduction in size within the first few days post treatment initiation may have a greater possibility for long-term benefit. Our preclinical data suggest that patients with tumors that continue to grow soon after treatment initiation are much less likely to benefit from IC treatment.

6.4.1.1.3 Small Tumor Leads to High TILs

Initial small tumor load (DuBois et al., 1999) and enhanced TIL infiltration (Gooden et al., 2011; Hwang et al., 2012; Taylor et al., 2007; Horne et al., 2011) serve as two independent prognostic factors for therapeutic benefit of immunotherapy and cancer host survival. The results presented in Chapter 4 show, for the first time to our knowledge, that the initial small tumor volume correlates with increased rapid TIL infiltration in response to 14.18-IL2, indicating that small tumor burden and increased TIL infiltration are two linked, rather than independent, factors which are predicative of the favorable clinical response to immunotherapy.

6.4.2 Potential Importance of GD2+ Status

GD2 has been used extensively as a target in mAb therapy and has been the primary target of antibody recognition in neuroblastoma. In normal tissues, GD2 expression is largely limited to neurons, skin melanocytes, and peripheral pain fibers (Svennerholm et al., 1994), making it reasonably well suited for targeted antitumor therapy. Recently, GD2 has been "ranked" 12th in priority for clinical importance of all described human cancer antigens by an NCI workshop (Cheever et al., 2009). In addition to neuroblastoma and melanoma, GD2 is

expressed on some soft tissue sarcomas, osteosarcomas, and small cell lung cancers (Sondel and Hank, 2001; Mujoo et al., 1987). In all, GD2+ diseases account for ~8% of all cancer deaths in the US (ACS, 2004).

Using histologic data from patients with melanoma, we examined whether there was a difference in time to recurrence for melanoma patients receiving hu14.18-IL2, stratified by GD2 expression level on each patient's tumor. All evaluable patients in this study received hu14.18-IL2 after surgical removal of all clinically evident melanoma. In this small pilot study of Stage III/IV recurrent, refractory melanoma (CO-05601), **Figure 5-2** suggests that there may be a small (but not significant with small sample size) difference in time to recurrence (measured from time of study entry) between patients with histologically confirmed GD2(+) melanoma compared to those with GD2(-) melanoma. These histologic data from patients in study CO-05601 suggest that GD2+ status may be a valuable assessment tool when deciding whether or not to put patients on study using an anti-GD2 mAb-based agent, given the antigen specific nature of the therapy.

6.5 Implications: Role of Intratumoral (IT) hu14.18-IL2 in Cancer Immunotherapy

6.5.1. Background

While ICs allow the targeting of immune-stimulating cytokines directly to the tumor microenvironment, systemic administration is still limited by dose-limiting toxicities (Osenga et al., 2006, King et al., 2004). These dose-limiting toxicities are due to the systemic effects of the IL2 component of the IC (ie: fever, capillary leakage, and secondary effects of capillary leakage, such as hypotension) and effects from the mAb component of the IC; for this hu14.18-IL2 IC, these include neuropathic pain due to mAb recognition of selective GD2-expressing peripheral

nerves. Finding a strategy of IC administration that would maximize the direct delivery of IC to the tumor site and potentially decrease dose-limiting systemic toxicities would be clinically beneficial. Using the NXS2 model, we demonstrate a greater antitumor response with localized IC administration compared to an equivalent systemic IC dose in the treatment of established subcutaneous tumors. Importantly, IT-hu14.18-IL2 treatment increased delivery of IC to the tumor site; substantially higher levels of IC were found for several hours at the tumor site following IT-IC vs. IV-IC.

Previous data have shown therapeutic and safety benefits of localized versus systemic IC therapy in preclinical models (Christ et al., 2001; Gillies et al., 2002; Johnson et al., 2008) as well as localized versus systemic immune therapy in melanoma patients (Weide et al., 2010; Weide et al., 2011). Our studies confirm and extend this previous work by evaluating possible underlying mechanisms of IT administration of IC, as well as showing antitumor efficacy in an established measureable disease setting in a pre-clinical model. IHC infiltration data collected using the quantitative method we developed is consistent with infiltration data collected by flow cytometry. Even though the experimental design intended for each animal within a treatment group to be identical to one another, there is substantial heterogeneity within treatment groups. The preclinical data presented in this thesis demonstrate several unique antitumor effects of IT-IC compared to equivalent doses of systemic IC. Flow cytometry analyses of IC delivery and retention show a substantial difference in the amount of IC present at initial time points at the tumor site between IT and IV administration. This direct exposure to greater concentrations of IT-IC at the tumor site between IT-IC and IV-IC may be at least partially responsible for the different tumor response rates and the different infiltration and expression patterns of TIL between the two treatment groups. These mechanisms of enhanced activity by localized IT

treatment provide further justification for proceeding with clinical testing of IT-IC, potentially testing IT delivery of hu14.18-IL2 in patients with GD2+ tumors, such as melanoma patients with metastatic disease having cutaneous, subcutaneous or readily injectable involved lymph nodes. Furthermore, the type of analyses presented in this thesis might also be conducted on biopsies of patient samples following IT-IC administration. Such immune monitoring by IHC and flow cytometry may become a potential means to assess immunologic effects of IC treatment; if these parameters show correlation with antitumor effect, they may be considered as indicators for prognosis of patients' response to IT-IC.

6.5.2 Phase I/II Trial of Intratumoral Administration of Hu14.18-IL2 in Subjects with Advanced Melanoma

Utilizing the rationale above, a combined phase I/II protocol has been designed to evaluate the effect of intratumoral administration hu14.18-IL2 for patients with Stage III or Stage IV melanoma thought to have completely resectable disease. This protocol has been approval as a part of an NIH R01 competitive renewal grant.

6.5.2.1 Objectives

6.5.2.1.1 Primary Objectives

The first primary objective in this first in human trial of IT-IC is to determine the localized and systemic toxicity and the maximum tolerated dose (MTD) of local administration of hu14.18-IL2. The second primary objective is to evaluate the clinical anti-tumor activity (both locally and systemically) of IT-IC in subjects with advanced melanoma.

6.5.2.1.2 Secondary Objectives

An important secondary objective is to evaluate for histological evidence of antitumor activity based on the presence of necrotic tumor cells, inflammatory infiltrate, cellular phenotype of infiltrate, and presence of IC within the tumor at selected post-treatment timepoints. Tumor histology will be evaluated in treated lesions and distant lesions.

Another secondary objective is to evaluate serial serum samples to determine the pharmacokinetics of IC administered intratumorally. In addition this study will evaluate adverse events associated with IT-IC for 3 consecutive days administered on an every 3-week basis. Also, this study will evaluate the immunologic activation induced *in vivo* by IT-IC as well as determine the induction of anti-idiotypic antibodies (anti-hu14.18) and antibody against the cytokine part of the compound (anti-Fc-IL2).

6.5.2.2 Hypotheses

The protocol hypothesizes that local IT IC will have antitumor effects against measurable tumors. In addition, we hypothesize that IT-IC will generate systemic levels of IC. Also, we hypothesize that IT-IC will activate systemic IL-2 response. Finally, we hypothesize that IT-IC will act as a vaccine and induce T-cell memory response.

6.5.2.3 Schema and Tumor Biopsy Times

6.5.5.3.1 Treatment Dose and Schedule

Phase I is the dose-escalation phase with (n = 3) patients at each dose level. Phase II is separated into two distinct stages. In stage 1, the protocol will treat a total of 15 patients at the

MTD, if activity is seen, and consider proceeding to stage 2. In stage 2, the protocol will enter 15 additional patients to a total of 30 patients entered at MTD.

The initial IC dose will be 1.0 mg/M2/injection. Six dose levels are scheduled for study: Level 1 (1.0 mg/M^2/day), Level II (2.0 mg/M^2/day), Level III (4.0 mg/M^2/day), Level IV (6.0 mg/M^2/day), Level V (8.0 mg/M^2/day), and Level VI (10.0 mg/M^2/day). Additional doses, if necessary, may be added by increasing the dose in 25% increments. Hu14.18-IL2 will be given on days 1, 2, and 3 of each course of therapy as an intratumoral and peritumoral injection. Treatment courses will be repeated every 21 days at the same dose, provided that there is no dose limiting toxicity. Subjects can receive a maximum of 5 courses of therapy.

Each treatment course will be 3 weeks in duration. Intratumoral administration of immunocytokine (IT-IC) will be performed on 3 consecutive days (i.e., d1-3) of each treatment course. Day 1 of Courses 2, 3, 4, and 5 (weeks 4, 7, 10, and 13) is Day 22 of the previous course (+/- 7 days leeway to facilitate clinical scheduling). Table 6-1 describes scheduling of treatments and biopsy times.

6.5.2.3.2 Tumor Biopsy Time Schema

Each eligible patient will have at least 2 cutaneous, subcutaneous or readily palpable lymph node lesions that are at least 1.0 cm but no greater than 5.0 cm in greatest dimension. The easiest lesion to repeatedly inject will be designated “lesion A” and it will be injected daily with hu14.18-IL2 for 3 consecutive days in each 3-week course of treatment. Preclinical studies suggest that biopsies soon after IT-IC (1-3 days) may reveal interesting biological changes within lesions by histologic assessment. Table 6-2 describes scheduling and locations of biopsies.

6.5.2.4 Histologic Assessment

This protocol seeks to monitor histologically patient biopsies and excised tumors before and after localized therapy of hu14.18-IL2. When possible, comparison between pre and post-Rx biopsies from the same tumor will be made due to patient-to-patient and lesion-to-lesion variability. To assess immunological response to therapy within lesions, this protocol seeks to examine tumor inflammatory infiltrate, cellular phenotype, persistent hu14.18-IL2 in tumor, GD2 expression as well as necrotic tumor cells

6.5.2.4.1 Biopsy and resection specimen handling and pathologic analysis

All biopsies and all freshly resected tumor specimens at UW will be taken immediately to the surgical pathology suite adjacent to the operating room. The specimen will then be serially sectioned with submission of the appropriate tissue for permanent, paraffin-embedded sections to ensure accurate pathologic analysis of resection margins, as well as high-quality hematoxylin and eosin stained sections for morphologic analysis of the tumor and for evaluation of necrosis, apoptosis, and any inflammatory infiltrate. These sections also will be assessed by immunohistochemical analysis for the presence of CD4 and CD8 positive T cells, NK cells (CD56 and CD16), and macrophages (CD68) (the antibodies for which all function well on formalin-fixed tissues).

6.5.2.4.2 Handling of fresh tissue samples.

The remaining unfixed tissue will be divided into specimens that will be sent to our research lab for derivation of autologous cultured tumor cell lines and bulk tumor lysate (for use

as pulsed antigen for in vitro immunologic assays), and tissue that will be frozen in OCT for frozen sections or cryopreserved for pilot molecular studies. The standard protocol for frozen section analysis will include assessment of activation markers on infiltrating T cells (NKG2D, CD69) and for evidence of regulatory T cells (CD25 and FoxP3) by double immunolabeling with CD3, CD4, or CD8, as appropriate. Finally, we will assess the expression of GD2 on tumor cells (the target antigen of hu14.18-IL2) before and after study treatment, as well as the presence of hu14.18-IL2 bound to tumor cells after study treatment.

6.5.2.5 Summary

This study was designed to assess the feasibility, toxicity, and efficacy of intratumorally injected hu14.18-IL2 in late stage melanoma patients. We have shown promising data in preclinical models using this approach. The timing of the biopsy specimens in this study (at least for biopsies obtained in course 1) corresponds, somewhat, to the timing found in this thesis (particularly the studies presented in Chapters 3 and 4) investigating this IT-IC approach in tumor bearing mice. In addition, we are considering including flow-cytometry analyses of disaggregated tumor in this clinical study (as done for the murine tumors in Chapters 3 and 4). However we need to obtain pilot data on this flow methodology before incorporating such flow evaluations of these clinical biopsies into the clinical protocol.

While this protocol, in DRAFT form was submitted to the NCI as a major objective of an R01 grant, that has been funded, the protocol still remains in DRAFT form. Its submission to the FDA for an Investigational New Drug (IND) approval, and its submission to the IRB for clinical approval and activation are pending. Before these submissions, the newly formulated clinical material needed for this first in human IT-IC trial needs to be approved for clinical use by The

FDA. Apeiron Biologicals Inc. of Austria is preparing this submission to go to the FDA (with input from our laboratory). We are hopeful that this trial will be approved and activated sometime in 2013. If so, I would plan to be involved in the histological and flow cytometry analyses described in this protocol, during my 3rd and 4th years of medical school as an MD PhD student in the UW MSTP.

6.6 Thesis Summary

In summary, we feel the data presented in this thesis (and elsewhere) justify that this method of IT-IC immunotherapy deserves further investigation, including testing (and potential development) in patients with readily accessible GD2+ lesions.

TABLE 6-1. Immunological Assessment Schema

This table shows the schedule of tumor biopsies for treated and untreated lesions

		Week 1				Week 2	Week 3	Week 4
DAY	**Base Line**	**1**	**2**	**3**	**4**	**8**	**15**	**22(1)**
Treatment with Hu14.18-IL2		**X**	**X**	**X**				
Serum hu14.18-IL2 levels		**X/X**		**X/X**				
Anti-hu14.18-IL2 Ab		**X/**		**X/**	**X**	**X**		**X**
Biopsy or resection of Lesion A for histology[1]	**X**					**Day 6[1]**		**Day 6 of course 3**
Biopsy of Lesion B for histology[1]	**X**							**Day 6 of course 3**
Soluble IL2 receptor	**X**	**X/**		**X/**	**X**	**X**		**X**

X/ = pre-IC

/X = post-IC

[1] Biopsies/resections will be performed at baseline and day 6 (+/- 2 d to facilitate scheduling) of course 1 for Lesion A and, as detailed in the schema, following course 3 for Lesions A and B, on day 6 of course 3. In addition to pilot studies analyzing for hu14.18-IL2 *in vivo* binding, immunohistologic components, including viable tumor cells, necrotic tumor and lymphocyte infiltration and assessing for T cell responses (including $CD8^+$, $CD4^+$) and NK phenotypes and for macrophages, will be performed on the biopsy samples.

TABLE 6-2. Tumor Lesion Biopsy Schema

This table shows the schematic of tumor biopsies for treated and untreated lesions in each course.

A. For subjects with 2 biopsiable lesions (designated lesions A and B):

Lesion	Course 1	Course 2	Course 3
A*	IT-IC[2]	IT-IC	IT-IC—Resect d6
B	Observe	Observe	Resect d6

B. For subjects with 3 biopsiable lesions (designated lesions A, B, and C):

Lesion	Course 1	Course 2	Course 3
A*	IT-IC	IT-IC	IT-IC—Resect d6
B	Observe	Observe	Resect d6
C	Resect pre-Course 1 for Histology	n/a	n/a

C. For subjects with >3 biopsiable lesions (designated lesions A, B, C, D, etc.):

Lesion	Course 1	Course 2	Course 3
A*	IT-IC	IT-IC	IT-IC—Resect d6
B	Observe	Observe	Resect d6
C	Resect pre-Course 1 for Histology	n/a	n/a
D, etc.	Observe	Observe	Observe

* For all patients, “lesion A” is the Index Lesion, and must meet strict eligibility criteria, that will enable it to be biopsied prior to treatment, biopsied again 5 days after the initial treatment, and then resected (or biopsied) after course 3 of treatment.

Reference List

American Cancer Society. (2004). Cancer Facts and Figures. Atlanta, GA, ACS publications.

American Cancer Society. (2011). Cancer Facts and Figures. ACS publications, Atlanta GA.

Ater JL. Neuroblastoma. (2004). In Behrman: Nelson Textbook of Pediatrics (17th edn) (Behrman, R.E., Kliegman, R.M. and Jenson, H.A., eds), (2004) pp. 1709-1711, Saunders.

Balch CM, Buzaid AC, Soong SJ, Atkins MB, Cascinelli N, Coit DG, Fleming ID, Gerschenwald JE, Houghton Jr A, Kirkwood JM, McMasters KM, Mihm MF, Morton DL, Reintgen DS, Ross MI, Sober A, Thompson JA, and Thompson JF. (2001a). Final Version of the American Joint Committee on Cancer Staging System for Cutaneous Melanoma. J Clin Oncol, 2001, 19:3635-3648. [PMID: 11504745]

Balch CM, Soong SJ, Gershenwald JE, Thompson JF, Reintgen DS, Cascinelli N, Urist M, McMasters KM, Ross MI, Kirkwood JM, Atkins MB, Thompson JA, Coit DG, Byrd D, Desmond R, Zhang Y, Liu PY, Lyman GH, Morabito A. (2001b) Prognostic Factors Analysis of 17,600 Melanoma Patients: Validation of the American Joint Committee on Cancer Melanoma Staging System. J Clin Oncology, 2001 Aug, 9(16):3622-3634. [PMID: 11504744]

Barker E, Mueller BM, Handgretinger R, Herter M, Yu AL, Reisfeld RA. (1991). Effect of a chimeric anti-ganglioside GD2 antibody on cell-mediated lysis of human neuroblastoma cells. Cancer Res. 1991 Jan 1;51(1):144-9. [PMID: 1988079]

Beadsmoore CJ, Screaton NJ. (2003). Classification, staging and prognosis of lung cancer. Eur J Radiol. 2003 Jan;45(1):8-17. [PMID: 12499060]

Berthold F, Boos J, Burdach S, Erttmann R, Henze G, Hermann J, Klingebiel T, Kremens B, Schilling FH, Schrappe M, Simon T, Hero B. (2005). Myeloablative megatherapy with autologous stem-cell rescue versus oral maintenance chemotherapy as consolidation treatment in patients with high-risk neuroblastoma: a randomised controlled trial. Lancet Oncol. 2005 Sep;6(9):649-58. [PMID: 16129365]

Brodeur GM, Maris JM. (2002a). Neuroblastoma. In Principles and practice of pediatric Oncology. Eds. Pizzo PA and Poplack DG. Lippincott. Philadelphia. Pp 895-938.

Brodeur GM. (2002b). Significance of intratumoral genetic heterogeneity in neuroblastomas. Med Pediatr Oncol. 2002 Feb;38(2):112-3. [PMID: 11813176]

Buhtoiarov IN, Neal ZC, Gan J, Buhtoiarova TN, Patankar MS, Gubbels JA, Hank JA, Yamane B, Rakhmilevich AL, Reisfeld RA, Gillies SD, Sondel PM. (2011). Differential internalization of hu14.18-IL2 immunocytokine by NK and tumor cell: impact on conjugation, cytotoxicity, and targeting. J Leukoc Biol. 2011 Apr;89(4):625-638. [PMID: 21248148]

Cheever MA, Allison JP, Ferris AS, Finn OJ, Hastings BM, Hecht TT, Mellman I, Prindiville SA, Viner JL, Weiner LM, Matrisian LM. (2009). The prioritization of cancer antigens: a national cancer institute pilot project for the acceleration of translational research. Clin Cancer Res. 2009 Sep 1;15(17):5323-37. [PMID: 19723653]

Cheung NK, Saarinen UM, Neely JE, Landmeier B, Donovan D, Coccia PF. (1985). Monoclonal antibodies to a glycolipid antigen on human neuroblastoma cells. Cancer Res. 1985 Jun;45(6):2642-9. [PMID: 2580625]

Cheung NK, Lazarus H, Miraldi FD, Abramowsky CR, Kallick S, Saarinen UM, Spitzer T, Strandjord SE, Coccia PF, Berger NA. (1987). Ganglioside GD2 specific monoclonal antibody 3F8: a phase I study in patients with neuroblastoma and malignant melanoma. J Clin Oncol. 1987 Sep;5(9):1430-40. [PMID: 3625258]

Cheung, NK, et al. (1997). Treatment of advanced stage neuroblastoma. In Principles and Practice of Genitourinary Oncology (Reghavan, D., ed.), pp. 1101-1111, Lippincott, Williams, and Wilkins.

Cheung NK, Kushner BH, Cheung IY, Kramer K, Canete A, Gerald W, Bonilla MA, Finn R, Yeh SJ, Larson SM. (1998). Anti-G(D2) antibody treatment of minimal residual stage 4 neuroblastoma diagnosed at more than 1 year of age. J Clin Oncol. 1998 Sep;16(9):3053-60. [PMID: 9738575]

Cheung NK, Kushner BH, Kramer K. (2001). Monoclonal antibody-based therapy of neuroblastoma. Hematol Oncol Clin North Am. 2001 Oct;15(5):853-66. Review. [PMID: 11765377]

Cheung NK and Sondel PM. (2005). Neuroblastoma immunology and immunotherapy. In Neuroblastoma (Cohn, S. and Cheung, N.K., eds), pp. 223-242, Springer Press.

Christ O, Seiter S, Matzku S, Burger C, Zoller M. (2001). Efficacy of local versus systemic application of antibody-cytokine fusion proteins in tumor therapy. Clin Cancer Res. 2001;7(4):985–998. [PMID: 11309350]

Colucci F, Caligiuri MA, Di Santo JP. (2003). What does it take to make a natural killer? Nat Rev Immunol. 2003 May;3(5):413-25. [PMID: 12766763]

Delgado DC, Hank JA, Kolesar J, Lorentzen D, Gan J, Seo S, Kim KM, Shusterman S, Gillies SD, Reisfeld RA, Yang R, Gadbaw B, DeSantes KD, London WB, Seeger RC, Maris J, and Sondel PM. The Role for Genotypes of Killer Ig-Like Receptors (KIRs), Their Ligands, and Fcγ Receptors on Responses of Neuroblastoma Patients to Hu14.18-IL2: A Children's Oncology Group Report. Cancer Research, 70:9554-9661, 2010. [PMID: 20935224]

DuBois SG, Kalika Y, Lukens JN, Brodeur GM, Seeger RC, Atkinson JB, Haase GM, Black CT, Perez C, Shimada H, Gerbing R, Stram DO, Matthay KK. (1999). Metastatic sites in stage IV and IVS neuroblastoma correlate with age, tumor biology, and survival. J Pediatr Hematol Oncol. 1999 May-Jun;21(3):181-9. [PMID: 10363850]

Feun LG, Gutterman J, Burgess MA, Hersh EM, Mavligit G, McBride CM, Benjamin RS, Richman SP, Murphy WK, Bodey GP, Brown BW, Mountain CF, Leavens ME, Freireich EJ. (1982). The natural history of resectable metastatic melanoma (stage IVA melanoma). Cancer, 1982, 60:1656. [PMID: 7116298]

Franks LM, Bollen A, Seeger RC, Stram DO, Matthay KK. Neuroblastoma in adults and adolescents: an indolent course with poor survival. Cancer. 1997 May 15;79(10):2028-35. [PMID: 9149032]

Frost JD, Hank JA, Reaman GH, Frierdich S, Seeger RC, Gan J, Anderson PM, Ettinger LJ, Cairo MS, Blazar BR, Krailo MD, Matthay KK, Reisfeld RA, Sondel PM. (1997). A phase I/IB trial of murine monoclonal anti-GD2 antibody 14.G2a plus interleukin-2 in children with refractory neuroblastoma: a report of the Children's Cancer Group. Cancer. 1997 Jul 15;80(2):317-33. [PMID: 9217046]

Gillies SD, Reilly EB, Lo KM, Reisfeld RA. (1992). Antibody-targeted interleukin 2 stimulates T-cell killing of autologous tumor cells. Proc Natl Acad Sci U S A. 1992 Feb 15;89(4):1428-32. [PMID: 1741398]

Gillies SD, Young D, Lo KM, Roberts S. (1993). Biological activity and in vivo clearance of antitumor antibody/cytokine fusion proteins. Bioconjug Chem. 1993 May-Jun;4(3):230-5. [PMID: 8324014]

Gillies SD, Lan Y, Brunkhorst B, Wong WK, Li Y, Lo KM. (2002). Bi-functional cytokine fusion proteins for gene therapy and antibody-targeted treatment of cancer. Cancer Immunol Immunother. 2002;51(8):449–460. [PMID: 12202906]

Gilman AL, Ozkaynak MF, Matthay KK, Krailo M, Yu AL, Gan J, Sternberg A, Hank JA, Seeger R, Reaman GH, Sondel PM. (2009). Phase I study of ch14.18 with granulocyte-macrophage colony-stimulating factor and interleukin-2 in children with neuroblastoma after autologous bone marrow transplantation or stem-cell rescue: a report from the Children's Oncology Group. J Clin Oncol. 2009 Jan 1;27(1):85-91. Epub 2008 Dec 1. [PMID: 19047298]

Gooden MJ, de Bock GH, Leffers N, Daemen T, Nijman HW. (2011). The prognostic influence of tumour-infiltrating lymphocytes in cancer: a systematic review with meta-analysis. Br J Cancer. 2011 Jun 28;105(1):93-103. [PMID: 21629244]

Gubbels, JA, Gadbaw B, Buhtoiarov IN, Horibata S, Kapur AK, Patel D, Hank JA, Gillies SD, Sondel PM, Patankar MS, Connor J. (2011). Ab-IL2 fusion proteins mediate NK cell immune synapse formation by polarizing CD25 to the target cell-effector cell interface. Cancer Immunol Immunother. 2011 Dec;60(12):1789-1800. [PMID: 21792658]

Haase GM, Atkinson JB, Stram DO, Lukens JN, Matthay KK. (1995). Surgical management and outcome of locoregional neuroblastoma: comparison of the Childrens Cancer Group and the international staging systems. J Pediatr Surg. 1995 Feb;30(2):289-94; discussion 295. [PMID: 7738753]

Handgretinger R, Baader P, Dopfer R, Klingebiel T, Reuland P, Treuner J, Reisfeld RA, Niethammer D. (1992) A phase I study of neuroblastoma with the anti-ganglioside GD2 antibody 14.G2a. Cancer Immunol Immunother. 1992;35(3):199-204. [PMID: 1638557]

Handgretinger R, Anderson K, Lang P, Dopfer R, Klingebiel T, Schrappe M, Reuland P, Gillies SD, Reisfeld RA, Neithammer D. (1995). A phase I study of human/mouse chimeric antiganglioside GD2 antibody ch14.18 in patients with neuroblastoma. Eur J Cancer. 1995;31A(2):261-7. [PMID: 7718335]

Hank JA, Robinson RR, Surfus J, Mueller BM, Reisfeld RA, Cheung NK, Sondel PM. (1990). Augmentation of antibody dependent cell mediated cytotoxicity following in vivo therapy with recombinant interleukin 2. Cancer Res. 1990 Sep 1;50(17):5234-9. [PMID: 2386933]

Hank JA, Surfus J, Gan J, Chew TL, Hong R, Tans K, Reisfeld R, Seeger RC, Reynolds CP, Bauer M, Wiersma S, Hammond D, Sondel PM. (1994). Treatment of neuroblastoma patients with antiganglioside GD2 antibody plus interleukin-2 induces antibody-dependent cellular cytotoxicity against neuroblastoma detected in vitro. J Immunother Emphasis Tumor Immunol. 1994 Jan;15(1):29-37. [PMID: 8110728]

Hank JA, Surfus JE, Gan J, Jaeger P, Gillies SD, Reisfeld RA, Sondel PM. (1996). Activation of human effector cells by a tumor reactive recombinant anti-ganglioside GD2 interleukin-2 fusion protein (ch14.18-IL2). Clin Cancer Res. 1996 Dec;2(12):1951-9. [PMID: 9816154]

Hank JA, Albertini MR, Sondel PM. (1999). Monoclonal antibodies, cytokines and fusion proteins in the treatment of malignant disease. In Cancer Chemotherapy and Biological Response Modifiers Annual 18 (Pinedo, H.M., Longo, D.L. and Chabner, B.A., eds), pp. 210-222, Elsevier Science.

Hodi FS, O'Day SJ, McDermott DF, Weber RW, Sosman JA, Haanen JB, Gonzalez R, Robert C, Schadendorf D, Hassel JC, Akerley W, van den Eertwegh AJ, Lutzky J, Lorigan P, Vaubel JM, Linette GP, Hogg D, Ottensmeier CH, Lebbé C, Peschel C, Quirt I, Clark JI, Wolchok JD, Weber JS, Tian J, Yellin MJ, Nichol GM, Hoos A, Urba WJ. (2010). Improved survival with ipilimumab in patients with metastatic melanoma. N Engl J Med. 2010 Aug 19;363(8):711-23. [PMID: 20525992]

Horne ZD, Jack R, Gray ZT, Siegfried JM, Wilson DO, Yousem SA, Nason KS, Landreneau RJ, Luketich JD, Schuchert MJ. (2011). Increased levels of tumor-infiltrating lymphocytes are associated with improved recurrence-free survival in stage 1A non-small-cell lung cancer. J Surg Res. 2011 Nov;171(1):1-5. [PMID: 21571304]

Hsueh EC, Essner R, Foshag LJ, Ollila DW, Gammon G, O'Day SJ, Boasberg PD, Stern SL, Ye X, Morton DL. (2002). Prolonged Survival After Complete Resection of Disseminated Melanoma and Active Immunotherapy with a Therapeutic Cancer Vaccine. J Clin Oncol, 2002 Dec, 20(23):4549-4554. [PMID: 12454111]

Hwang WT, Adams SF, Tahirovic E, Hagemann IS, Coukos G. (2012). Prognostic significance of tumor-infiltrating T cells in ovarian cancer: a meta-analysis. Gynecol Oncol. 2012 Feb;124(2):192-8. [PMID: 22040834]

Ishola TA and Chung DH. Neuroblastoma. Surg Oncol. (2007). Nov;16(3):149-56. Epub 2007 Oct 31. Review. [PMID: 17976976]

Jemal A, Siegel R, Ward E, Murray T, Xu J, Thun MJ. Cancer statistics, (2007). CA Cancer J Clin. 2007 Jan-Feb;57(1):43-66. [PMID: 17237035]

Johnson E, Dean SM, Sondel PM. (2007). Antibody-based immunotherapy in high-risk neuroblastoma. Expert Rev Mol Med. 2007 Dec 17;9(34):1-21. [PMID: 18081947]

Johnson EE, Lum HD, Rakhmilevich AL, Schmidt BE, Furlong M, Buhtoiarov IN, Hank JA, Raubitschek A, Colcher D, Reisfeld RA, Gillies SD, Sondel PM. (2008) Intratumoral immunocytokine treatment results in enhanced antitumor effects. Cancer Immunol Immunother. 2008 Dec;57(12):1891-902. [PMID:18438664]

Jurcic JG, Scheinberg DA, Houghton AN. (1997). Monoclonal antibody therapy of cancer. Cancer Chemother Biol Response Modif. 1997;17:195-216. Review. [PMID: 9551215]

Karimi M, Cao TM, Baker JA, Verneris MR, Soares L, Negrin RS. (2005). Silencing human NKG2D, DAP10, and DAP12 reduces cytotoxicity of activated CD8+ T cells and NK cells. J Immunol. 2005 Dec 15;175(12):7819-28. [PMID: 16339517]

Kendra K, Gan J, Ricci M, Surfus J, Shaker A, Super M, Frost JD, Rakhmilevich A, Hank JA, Gillies SD, Sondel PM. (1999). Pharmacokinetics and stability of the ch14.18-interleukin-2 fusion protein in mice. Cancer Immunol Immunother. 1999 Aug;48(5):219-29. [PMID: 10478638]

King DM, Albertini MR, Schalch H, Hank JA, Gan J, Surfus J, Mahvi D, Schiller JH, Warner T, Kim K, Eickhoff J, Kendra K, Reisfeld R, Gillies SD, Sondel P. (2004). Phase I clinical trial of the immunocytokine EMD 273063 in melanoma patients. J Clin Oncol. 2004 Nov 15;22(22):4463-73. Epub 2004 Oct 13. [PMID:15483010]

Kirkwood JM, Ibrahim JG, Sosman JA, Sondak VK, Agarwala SS, Ernstoff MS, Rao U. (2001). High-dose interferon alfa-2b significantly prolongs relapse-free and overall survival compared with the GM2-KLH/QS-21 vaccine in patients with resected stage IIB-III melanoma: results of intergroup trial E1694/S9512/C509801. J Clin Oncol, 2001;19:2370-80 [PMID: 11331315]

Kramer K, Gerald WL, Kushner BH, Larson SM, Hameed M, Cheung NK. (1998). Disialoganglioside G(D2) loss following monoclonal antibody therapy is rare in neuroblastoma. Clin Cancer Res. 1998 Sep;4(9):2135-9. [PMID: 9748131]

Kushner BH and Cheung NK. (1989). GM-CSF enhances 3F8 monoclonal antibody-dependent cellular cytotoxicity against human melanoma and neuroblastoma. Blood. 1989 May 15;73(7):1936-41. [PMID: 2653466]

Kushner BH, LaQuaglia MP, Bonilla MA, Lindsley K, Rosenfield N, Yeh S, Eddy J, Gerald WL, Heller G, Cheung NK. (1994). Highly effective induction therapy for stage 4 neuroblastoma in children over 1 year of age. J Clin Oncol. 1994 Dec;12(12):2607-13. [PMID: 7527454]

Lammie GA, Cheung NKV, Gerald W, Rosenblum M, Cordoncardo C. (1993). Ganglioside gd(2) expression in the human nervous system and in neuroblastomas - an immunohistochemical study. International Journal of Oncology. 1993 Nov;3(5):909-15. [PMID: 21573452]

Liu Y, Zhang W, Cheung LH, Niu T, Wu Q, Li C, Van Pelt CS, Rosenblum MG. (2006). The antimelanoma immunocytokine scFvMEL/TNF shows reduced toxicity and potent antitumor activity against human tumor xenografts. Neoplasia. 2006 May;8(5):384-393. [PMID:16790087]

Lode HN, Xiang R, Varki NM, Dolman CS, Gillies SD, Reisfeld RA. (1997). Targeted interleukin-2 therapy for spontaneous neuroblastoma metastases to bone marrow. J Natl Cancer Inst. 1997 Nov 5;89(21):1586-1594. [PMID: 9362156]

Lode HN, Xiang R, Dreier T, Varki NM, Gillies SD, Reisfeld RA. (1998). Natural killer cell-mediated eradication of neuroblastoma metastases to bone marrow by targeted interleukin-2 therapy. Blood 1998;91(5):1706-1715. [PMID: 9473237]

Matthay KK, Villablanca JG, Seeger RC, Stram DO, Harris RE, Ramsay NK, Swift P, Shimada H, Black CT, Brodeur GM, Gerbing RB, Reynolds CP. (1999). Treatment of high-risk neuroblastoma with intensive chemotherapy, radiotherapy, autologous bone marrow transplantation, and 13-cis-retinoic acid. Children's Cancer Group. N Engl J Med. 1999 Oct 14;341(16):1165-73. [PMID: 10519894]

McMahon CW, Zajac AJ, Jamieson AM, Corral L, Hammer GE, Ahmed R, Raulet DH. (2002). Viral and bacterial infections induce expression of multiple NK cell receptors in responding CD8(+) T cells. J Immunol. 2002 Aug 1;169(3):1444-1452. [PMID: 12133970]

Moss TJ, Reynolds CP, Sather HN, Romansky SG, Hammond GD, Seeger RC. (1991). Prognostic value of immunocytologic detection of bone marrow metastases in neuroblastoma. N Engl J Med. 1991 Jan 24;324(4):219-26. [PMID: 1985243]

Mujoo K, Cheresh DA, Yang HM, Reisfeld RA. (1987). Disialoganglioside GD2 on human neuroblastoma cells: target antigen for monoclonal antibody-mediated cytolysis and suppression of tumor growth. Cancer Res. 1987 Feb 15;47(4):1098-104. [PMID: 3100030]

Mulé JJ, Yang JC, Afreniere RL, Shu SY, Rosenberg SA. (1987). Identification of cellular mechanisms operational in vivo during the regression of established pulmonary metastases by the systemic administration of high-dose recombinant interleukin 2. J Immunol. 1987 Jul 1;139(1):285-94. [PMID: 3108401]

Murray JL, Cunningham JE, Brewer H, Mujoo K, Zukiwski AA, Podoloff DA, Kasi LP, Bhadkamkar V, Fritsche HA, Benjamin RS, et al. (1994). Phase I trial of murine monoclonal antibody 14G2a administered by prolonged intravenous infusion in patients with neuroectodermal tumors. J Clin Oncol. 1994 Jan;12(1):184-93. [PMID: 8270976]

Neal ZC, Yang JC, Rakhmilevich AL, Buhtoiarov IN, Lum HE, Imboden M, Hank JA, Lode HN, Reisfeld RA, Gillies SD, Sondel PM. (2004). Enhanced activity of hu14.18-IL2 immunocytokine against murine NXS2 neuroblastoma when combined with interleukin 2 therapy. Clin Cancer Res. 2004 Jul 15;10(14):4839-47. [PMID:15269160]

Osenga KL, Hank JA, Albertini MR, Gan J, Sternberg AG, Eickhoff J, Seeger RC, Matthay KK, Reynolds CP, Twist C, Krailo M, Adamson PC, Reisfeld RA, Gillies SD, Sondel PM. (2006). Children's Oncology Group. A phase I clinical trial of the hu14.18-IL2 (EMD 273063) as a treatment for children with refractory or recurrent neuroblastoma and melanoma: a study of the Children's Oncology Group. Clin Cancer Res. 2006 Mar 15;12(6):1750-9. [PMID: 16551859]

Ozkaynak MF, Sondel PM, Krailo MD, Gan J, Javorsky B, Reisfeld RA, Matthay KK, Reaman GH, Seeger RC. (2000). Phase I study of chimeric human/murine anti-ganglioside G(D2) monoclonal antibody (ch14.18) with granulocyte-macrophage colony-stimulating factor in children with neuroblastoma immediately after hematopoietic stem-cell transplantation: a Children's Cancer Group Study. J Clin Oncol. 2000 Dec 15;18(24):4077-85. [PMID: 11118469]

Park JR, Eggert A, Caron H. (2008). Neuroblastoma: biology, prognosis, and treatment. Pediatr Clin North Am. 2008 Feb;55(1):97-120, x. Review. [PMID: 18242317]

Patel PR, Mansfield PF, Crane CH, Wu TT, Lee JH, Lynch PM, Morris J, Pisters PW, Feig B, Sunder PK, Izzo JG, Ajani JA. (2007). Clinical stage after preoperative chemoradiation is a better predictor of patient outcome than the baseline stage for localized gastric cancer. Cancer. 2007 Sep 1;110(5):989-95. [PMID: 17636525]

Ribas A, Kirkwood JM, Atkins MB, Whiteside TL, Gooding W, Kovar A, Gillies SD, Kashala O, Morse MA. (2009). Phase I/II open-label study of the biologic effects of the interleukin-2 immunocytokine EMD 273063 (hu14.18-IL2) in patients with metastatic malignant melanoma. J Transl Med; 7:68, 2009. [PMID: 19640287]

Ries LAG, Melbert D, Krapcho M, Mariotto A, Miller BA, Feuer EJ, Clegg L, Horner MJ, Howlader N, Eisner MP, Reichman M, Edwards BK (eds). (2007). SEER Cancer Statistics Review, 1975-2004, National Cancer Institute. Bethesda, MD, http://seer.cancer.gov/csr/1975_2004/, based on November 2006 SEER data submission, posted to the SEER web site, 2007.

Rosenberg SA, Yang JC, Topalian SL, Schwartzentruber DJ, Weber JS, Parkinson DR, Seipp CA, Einhorn JH, White DE. (1994). Treatment of 283 consecutive patients with metastatic melanoma or renal cell cancer using high-dose bolus interleukin 2. JAMA. 1994 Mar 23-30;271(12):907-13. [PMID: 8120958]

Saleh MN, Khazaeli MB, Wheeler RH, Dropcho E, Liu T, Urist M, Miller DM, Lawson S, Dixon P, Russell CH, et al. (1992a). Phase I trial of the murine monoclonal anti-GD2 antibody 14G2a in metastatic melanoma. Cancer Res. 1992 Aug 15;52(16):4342-7. [PMID: 1643631]

Saleh MN, Khazaeli MB, Wheeler RH, Allen L, Tilden AB, Grizzle W, Reisfeld RA, Yu AL, Gillies SD, LoBuglio AF. (1992b). Phase I trial of the chimeric anti-GD2 monoclonal antibody ch14.18 in patients with malignant melanoma. Hum Antibodies Hybridomas. 1992 Jan;3(1):19-24. [PMID: 1576319]

Schmidt ML, Lukens JN, Seeger RC, Brodeur GM, Shimada H, Gerbing RB, Stram DO, Perez C, Haase GM, Matthay KK. (2000). Biologic factors determine prognosis in infants with stage IV neuroblastoma: A prospective Children's Cancer Group study. J Clin Oncol. 2000 Mar;18(6):1260-8. [PMID: 10715296]

Schulz G, Cheresh DA, Varki NM, Yu A, Staffileno LK, Reisfeld RA. (1984). Detection of ganglioside GD2 in tumor tissues and sera of neuroblastoma patients. Cancer Res. 1984 Dec;44(12 Pt 1):5914-20. [PMID: 6498849]

Seeger RC, Reynolds CP, Gallego R, Stram DO, Gerbing RB, Matthay KK. (2000). Quantitative tumor cell content of bone marrow and blood as a predictor of outcome in stage IV neuroblastoma: a Children's Cancer Group Study. J Clin Oncol. 2000 Dec 15;18(24):4067-76. [PMID: 11118468]

Shusterman S, London, Gilles S, Hank JA, Voss S, Seeger RC, Hecht T, Reisfeld R, Maris JM, Sondel PM. (2008). Anti-neuroblastoma activity of hu14.18-IL2 against minimal residual disease in a Children's Oncology Group (COG) phase II study. (abstract 3002) J. Clin. Oncol. 26, 15s, p. 132s, 2008.

Shusterman S, London WB, Gillies SD, Hank JA, Voss S, Seeger RC, Reynolds CP, Kimball J, Albertini MA, Wagner B, Gan J, Eickhoff J, DeSantes KD, Cohn SL, Hecht T, Gadbaw B, Reisfeld RA, Maris JM, Sondel PM. (2010). Anti-tumor activity of hu14.18-IL2 in relapsed/refractory neuroblastoma patients: a Children's Oncology Group (COG) phase II study. J Clin Oncol. 2010 Nov 20;28(33):4969-75. [PMID: 20921469]

Simon T, Hero B, Faldum A, Handgretinger R, Schrappe M, Niethammer D, Berthold F. (2004). Consolidation treatment with chimeric anti-GD2-antibody ch14.18 in children older than 1 year with metastatic neuroblastoma. J Clin Oncol. 2004 Sep 1;22(17):3549-57. [PMID: 15337804]

Simon T, Hero B, Faldum A, Handgretinger R, Schrappe M, Niethammer D, Berthold F. (2005). Infants with stage 4 neuroblastoma: the impact of the chimeric anti-GD2-antibody ch14.18 consolidation therapy. Klin Padiatr. 2005 May-Jun;217(3):147-52. [PMID: 15858706]

Smith FO, Downey SG, Klapper JA, Yang JC, Sherry RM, Royal RE, Kammula US, Hughes MS, Restifo NP, Levy CL, White DE, Steinberg SM, Rosenberg SA. (2008). Treatment of metastatic melanoma using interleukin-2 alone or in conjunction with vaccines. Clin Cancer Res. 2008 Sep 1;14(17):5610-8. [PMID: 18765555]

Sondel PM, Kohler PC, Hank JA, Moore KH, Rosenthal NS, Sosman JA, Bechhofer R, Storer B. (1988). Clinical and immunological effects of recombinant interleukin 2 given by repetitive weekly cycles to patients with cancer. Cancer Res. 1988 May 1;48(9):2561-7. [PMID: 3258545]

Sondel PM and Hank JA. (1997). Combination therapy with interleukin-2 and antitumor monoclonal antibodies. Cancer J Sci Am. 1997 Dec;3 Suppl 1:S121-7. Review. [PMID: 9457407]

Sondel PM and Hank JA. (2001). Antibody-directed, effector cell-mediated tumor destruction. Hematol Oncol Clin North Am. 2001 Aug;15(4):703-21. [PMID: 11676280]

Sondel PM, Hank JA, Gan J, Neal Z, Albertini MR. (2003). Preclinical and clinical development of immunocytokines. Curr Opin Investig Drugs. 2003 Jun;4(6):696-700. [PMID: 12901228]

Sondel PM, Hank JA, Albertini MR, Gillies SD. (2008). Novel strategies for cytokine administration via targetting. In: Caligiuri MA, Lotze MT, editors, Cancer Drug Discovery and Development, Cytokines in the Genesis and Treatment of Cancer. Totowa, NJ: Humana Press Inc; 2008.

Sosman JA, Kim KB, Schuchter L, Gonzalez R, Pavlick AC, Weber JS, McArthur GA, Hutson TE, Moschos SJ, Flaherty KT, Hersey P, Kefford R, Lawrence D, Puzanov I, Lewis KD, Amaravadi RK, Chmielowski B, Lawrence HJ, Shyr Y, Ye F, Li J, Nolop KB, Lee RJ, Joe AK, Ribas A. (2012). Survival in BRAF V600-mutant advanced melanoma treated with vemurafenib. N Engl J Med. 2012 Feb 23;366(8):707-14. [PMID: 22356324]

Stephenson J. (1995). Reengineered monoclonal antibodies step up to the plate in cancer studies. JAMA. 1995 Dec 20;274(23):1821-2. [PMID: 7500516]

Svennerholm L, Boström K, Fredman P, Jungbjer B, Lekman A, Månsson JE, Rynmark BM. (1994). Gangliosides and allied glycosphingolipids in human peripheral nerve and spinal cord. Biochim Biophys Acta. 1994 Sep 15;1214(2):115-23. [PMID: 7918590]

Taylor RC, Patel A, Panageas KS, Busam KJ, Brady MS. (2007). Tumor-infiltrating lymphocytes predict sentinel lymph node positivity in patients with cutaneous melanoma. J Clin Oncol. 2007 Mar 1;25(7):869-75. [PMID: 17327608]

Vance RE, Kraft JR, Altman JD, Jensen PE, Raulet DH. (1998). Mouse CD94/NKG2A is a natural killer cell receptor for the nonclassical major histocompatibility complex (MHC) class I molecule Qa-1(b). J Exp Med. 1998 Nov 16;188(10):1841-1848. [PMID: 9815261]

Vance RE, Jamieson AM, Cado D, Raulet DH. (2002). Implications of CD94 deficiency and monoallelic NKG2A expression for natural killer cell development and repertoire formation. Proc Natl Acad Sci U S A. 2002. 99:868-73. [PMID: 11782535]

Verneris MR, Karami M, Baker J, Jayaswal A, Negrin RS. (2004). Role of NKG2D signaling in the cytotoxicity of activated and expanded CD8+ T cells. Blood. 2004 Apr 15;103(8):3065-72. [PMID: 15070686]

Voss SD, Robb RJ, Weil-Hillman G, Hank JA, Sugamura K, Tsudo M, Sondel PM. (1990). Increased expression of the interleukin 2 (IL-2) receptor beta chain (p70) on CD56+ natural killer cells after in vivo IL-2 therapy: p70 expression does not alone predict the level of intermediate affinity IL-2 binding. J Exp Med. 1990 Oct 1;172(4):1101-14. [PMID: 1698909]

Weide B, Derhovanessian E, Pflugfelder A, Eigentler TK, Radny P, Zelba H, Pföhler C, Pawelec G, Garbe C. (2010). High response rate after intratumoral treatment with interleukin-2: results from a phase 2 study in 51 patients with metastasized melanoma. Cancer. 2010 Sep 1;116(17):4139-46. [PMID:20564107]

Weide B, Eigentler TK, Pflugfelder A, Leiter U, Meier F, Bauer J, Schmidt D, Radny P, Pföhler C, Garbe C. (2011). Survival after intratumoral interleukin-2 treatment of 72 melanoma patients and response upon the first chemotherapy during follow-up. Cancer Immunol Immunother. 2011 Apr;60(4):487-93. Epub 2010 Dec 21. [PMID:21174093]

Weil-Hillman G, Fisch P, Prieve AF, Sosman JA, Hank JA, Sondel PM. (1989). Lymphokine-activated killer activity induced by in vivo interleukin 2 therapy: predominant role for lymphocytes with increased expression of CD2 and leu19 antigens but negative expression of CD16 antigens. Cancer Res. 1989 Jul 1;49(13):3680-8. [PMID: 2471587]

Weng WK and Levy R. (2003). Two immunoglobulin G fragment C receptor polymorphisms independently predict response to rituximab in patients with follicular lymphoma. J Clin Oncol. 2003 Nov 1;21(21):3940-7. Epub 2003 Sep 15. [PMID: 12975461]

Xiang R, Lode HN, Dolman CS, Dreier T, Varki NM, Qian X, Lo KM, Lan Y, Super M, Gillies SD, Reisfeld RA. (1997). Elimination of established murine colon carcinoma metastases by antibody-interleukin 2 fusion protein therapy. Cancer Res. 1997 Nov 1;57(21):4948-4955. [PMID: 9354462]

Xiao WH, Yu AL, Sorkin LS. (1997). Electrophysiological characteristics of primary afferent fibers after systemic administration of anti-GD2 ganglioside antibody. Pain. 1997 Jan;69(1-2):145-51. [PMID: 9060025]

Yu AL, Uttenreuther MM, Kamps A, Batova A, Reisfeld RA. (1995). Combined use of a human-mouse chimeric anti-GD2 (ch14.18) and GM-CSF in the treatment of refractory neuroblastoma. Antibody Immunoconjugates Radiopharmaceuticals. 1995;8:12.

Yu AL, Batova A, Alvarado C, Rao VJ, Castelberry RP. (1997). Usefulness of a chimeric anti-GD2 (ch14.18) and GM-CSF for refractory neuroblastoma: a POG phase II study. Proc. Am. Soc. Clin. Oncol. 1997;16:1846.

Yu AL, Uttenreuther-Fischer MM, Huang CS, Tsui CC, Gillies SD, Reisfeld RA, Kung FH. (1998). Phase I trial of a human-mouse chimeric anti-disialoganglioside monoclonal antibody ch14.18 in patients with refractory neuroblastoma and osteosarcoma. J Clin Oncol. 1998 Jun;16(6):2169-80. [PMID: 9626218]

Yu A, Gilman A, Ozkaynak F, Kletzel M, Castleberry R, Kretschmar C, Cohn S, Shimada H, Hoh CK, Sondel PM, Wiernikowski S, Bickert P, Seeger R, Reynolds CP, Matthay KK, Lalonde D, Shulkin B, London W, Frierdich S, Maloney A. (2001). COG ANBL0032. A Phase III trial of ch14.18 mAb plus IL2 plus GMCSF for children with high risk neuroblastoma following ASCT. COG protocol, open Dec. 2001. Available on COG website, and NCI-PDQ.

Yu AL, Gilman AL, Ozkaynak MF, London WB, Kreissman SG, Chen HX, Smith M, Anderson B, Villablanca JG, Matthay KK, Shimada H, Grupp SA, Seeger R, Reynolds CP, Buxton A, Reisfeld RA, Gillies SD, Cohn SL, Maris JM, Sondel PM. (2010). Children's Oncology Group. Anti-GD2 antibody with GM-CSF, interleukin-2, and isotretinoin for neuroblastoma. N Engl J Med. 2010 Sep 30;363(14):1324-34. [PMID: 20879881]

Yuki N, Yamada M, Tagawa Y, Takahashi H, Handa S. (1997). Pathogenesis of the neurotoxicity caused by anti-GD2 antibody therapy. J Neurol Sci. 1997 Aug;149(2):127-30. [PMID: 9171318]

Zar, Jerrold H. (1984). Chapter 18: Comparing Simple Linear Regression Equations. Biostatistical Analysis. (2^{nd} edition), pgs. 363-378. Prentice-Hall, Englewood Cliffs, New Jersey, 1984.

Appendix

Related Publications

A.1 Anti-GD2 Strategy in the Treatment of Neuroblastoma

Published in final edited form as:
Drugs Future. 2010 ; 35(8): 665–.

Anti-GD2 Strategy in the Treatment of Neuroblastoma

Richard K. Yang and **Paul M. Sondel**

Abstract

The prognosis for advanced neuroblastoma remains poor with high risk of recurrence after consolidation. Therapies based on monoclonal antibodies that specifically target disialoganglioside GD2 on tumor cells are improving treatment results for high-risk neuroblastoma. This article reviews the use of anti-GD2 antibodies either as monotherapy or as part of a larger and more complex treatment approach for advanced neuroblastoma. We review how anti-GD2 antibodies can be combined with other treatments or strategies to enhance their clinical effects. Tumor resistance and other problems that decrease the efficacy of anti-GD2 antibodies are discussed. Future developments in the area of anti-GD2 immunotherapies for neuroblastoma are also addressed.

A. Neuroblastoma

1. Significance, Standard of Care, Clinical Strategies

Neuroblastoma is the most common malignancy in infants, the most common extracranial solid tumor of childhood, and the third most common cancer in children (1–5). The average age at diagnosis is 17 months with 50–60% of patients having metastatic disease when diagnosed (6–8). Overall treatment has improved in children under 15 years of age with 5-year overall survival rates for newly diagnosed patients increasing from 52% in the 1970s to 69% in the last decade (9,10).

Despite advances in the treatment of low- to intermediate-risk neuroblastoma, outcomes for patients with advanced disease remain poor. Standard treatment for high-risk patients includes surgery, radiation, and/or myeloablative chemotherapy with autologous stem cell transplantation, followed by cis-retinoic acid (CRA). CRA, an anti-proliferative agent, when given following completion of chemotherapy has been shown to have an increased survival effect in patients with stage 4 disease (4,11–12). With current standard therapy, most high risk patients achieve remission with no clinically evident disease (NED) status. However, complete eradication of tumor cells has remained elusive. Microscopic residual tumor cells (minimal residual disease) survive treatment and cause recurrent refractory disease. The 3-year event-free survival of these high risk patients remains as low as ~30% (4,6,13–14). Fortunately, a recent COG randomized trial has shown that a combination of anti-GD2 antibody and cytokines in this setting can help prevent recurrence (15,16).

In this review, we examine several current strategies using monoclonal antibodies (mAbs) against the disialoganglioside GD2, and their derivatives, for the treatment of high risk neuroblastoma, either as primary therapy or as part of a multifaceted treatment approach, in clinical trials. We review the pitfalls of this treatment approach, including tumor resistance and the development of blocking antibodies that may interfere with mAb therapy. Finally, we look ahead at potential future therapies.

2. GD2-Importance, Rationale

Surface antigens expressed on neuroblastoma that have been used as targets for mAbs include the gangliosides GD2, GD3 and GM3, and the glycoproteins CD56 (NCAM), L1-CAM, GP58 and GP95 (17). GD2 is a disialoganglioside antigen that is expressed on tumors of

neuroectodermal origin including neuroblastoma and melanoma (18–19). These tumors express GD2 with relatively little heterogeneity between cells (20–21). Patients with neuroblastoma were found to have significantly elevated free GD2 levels in serum compared with normal children and children with other tumors (20). Also, GD2 expression is not lost from the cell surface of neuroblastoma cells even when bound to antibody, unlike other tumor antigens described previously (21).

In normal tissues, GD2 expression on is largely limited to neurons, skin melanocytes, and peripheral pain fibers (22), making it well suited for targeted antitumor therapy. Recently, GD2 has been "ranked" 12th in priority of all clinical cancer antigens by an NCI workshop (23). In addition to neuroblastoma and melanoma, GD2 is expressed on some soft tissue sarcomas, osteosarcomas, and small cell lung cancers (24,18). In all, GD2+ diseases account for ~8% of all cancer deaths in the US (25).

GD2 has been used extensively as a target in mAb therapy and has been the primary target of antibody recognition in neuroblastoma. In 1984, a murine mAb (mAB126) was produced against cultured human neuroblastoma cells (LAN1). The original murine anti-GD2 mAbs described were 3F8, 14.18 and 14.G2a (18–19). Clinical testing has been performed with 3F8, 14.G2a, and ch14.18 (the human-mouse chimeric variant of 14.18) in neuroblastoma and melanoma (26–33).

B. Single Agent Antibodies

1. ADCC and CDC

An ideal anticancer agent would specifically target tumor cells and minimize injury to healthy cells (24). Monoclonal antibody (mAb) therapy creates specificity to tumor cells through its recognition of cell surface antigens found exclusively on tumor cells or that are found in much greater amounts on tumor cells compared to normal cells (34–35). Currently, mAbs are in use in the detection, diagnosis, and treatment of neuroblastoma (14,36–38). Antibodies can mediate destruction of tumor cells through several mechanisms including antibody-dependent cell-mediated cytotoxicity (ADCC). After the variable region of the antibody binds to antigen on the tumor cell, the Fc portion of the antibody can bind to the Fc receptor on monocytes, macrophages, neutrophils and/or natural killer (NK) cells and stimulate tumor cell lysis via ADCC (39–40).

In addition, complement-dependent cytotoxicity (CDC) may be induced after an antibody binds to the tumor cell surface (24). However, dose limiting toxicities (DLT) caused by anti-GD2 mAb do occur and include fever, chills, anaphylactoid reactions most likely from cytokine and complement activation, and transient neuropathic pain, which are controllable with analgesics. These toxicities are mostly likely the result of mAb recognition of GD2 on peripheral pain fibers and complement deposition (40–42,22,29).

2. 3F8 Clinical Testing

The first mAb tested in clinical trials was the anti-GD2 mAb 3F8 (26,43–46). In the initial Phase I and II trials using 3F8 in patients with stage 4 neuroblastoma, there was no significant antitumor effect on bulky disease but some response in microscopic bone marrow disease (17,47–50). Side effects included pain most commonly, hypertension, hypotension, fever, vomiting, diarrhea, and urticaria. Pain can be dose limiting and has been attributed to antibody recognition of peripheral pain fibers expressing GD2 (40–42). Also, human antimouse antibodies (HAMA) can develop in patients treated with 3F8. As these neutralize the function of 3F8, development of HAMA has resulted in termination of therapy (51). 3F8 has been shown to activate tumor cell destruction by both CDC and ADCC *in vitro* (52–53).

3. 14.G2a

The 14.18 antibody is a separate IgG3 murine mAb targeted to the GD2 antigen (18). In an effort to enhance ADCC, a class switch variant called 14.G2a has also been prepared (54). The 14.G2a antibody activates complement and mediates ADCC with monocytes, neutrophils, NK cells, and lymphokine-activated killer (LAK) cells (55–56). The 14.G2a antibody has undergone clinical testing both as single-agent therapy and in combination approaches. Its toxicities and induction of HAMA responses were similar to that seen with 3F8.

4. Ch14.18 Clinical Testing

A human-mouse chimeric form of the 14.18 murine anti-GD2 mab, designated ch14.18, was subsequently created to reduce the immunogenicity associated with the murine antibody (Fig. 1). The chimeric antibody is less immunogenic and is more effective than 14.G2a in mediating lysis of neuroblastoma cells with NK cells (57). The ch14.18 antibody has undergone clinical testing as a single-agent therapy. Simon et al. have published their results using standard induction treatment (chemotherapy with autologous stem cell rescue) for children and infants with stage 4 neuroblastoma followed by consolidation with chimeric 14.18 antibody for 5 days every 2 months, versus 12 months of oral maintenance chemotherapy or no further therapy (58). In patients <1 year old, there was no significant difference in event-free survival or overall survival in the three consolidation groups, with an overall survival of >90%. In patients >1 year old, the 3-year overall survival of ch14.18 treatment was superior to maintenance therapy or no additional therapy (P = 0.018) (59), although there was no difference in event free survival.

5. Hu14.18K322A Clinical Testing

A Phase I clinical trial is now underway at St. Jude Hospital using a novel hu14.18K322A anti-GD2 mAb, which was made using the same variable region as the ch14.18 mAb. However, this mAb has 3 major differences from the ch14.18 mAb. First, it is a humanized, not chimeric, mAb and thus could be less immunogenic with less allergic toxicity than ch14.18. Second, there is a single amino acid switch, from K to A at position 322 in the Fc region, which nearly abrogates complement activation, hopefully resulting in less neuropathic toxicity than ch14.18. Third, this mAb is produced in the YB2/O cell line, rather than CHO or NS/O lines, eliminating the normal fucosylation of the Fc region, and hopefully augmenting interaction with FcRs to increase ADCC (60). Thus, this novel hu14.18K322A is designed to cause less allergic reactions, less complement dependent toxicity, and more ADCC-mediated antitumor effects than ch14.18.

C. Antibodies Combined with other Agents

1. Antibody plus ADCC-Augmenting Cytokines

As the mechanisms of mAb-based tumor cell lysis were discovered, it was evident that the antibody must accomplish three separate jobs to kill a tumor cell. First, the antibody must recognize and bind to the tumor cell. Second, it must bind long enough and avoid internalization to adequately signal immune effector mechanisms. Third, the activated immune effector cells or effector proteins must be able to create a destructive signal (24). Since mAb-mediated tumor cell destruction relies on ADCC and/or CDC to kill tumor cells, strong effector functions are required. However, effector function, particularly ADCC, is often compromised in cancer patients due to immune suppression from metastatic cancer and/or chemotherapy (17,53,61). It is thought that the addition of cytokines that activate cells to mediate enhanced ADCC to mAb therapy will augment effector cell function and improve the overall antibody therapy efficacy (24).

a. 14.G2a + IL-2 Trial—Interleukin 2 (IL-2) is a strong pro-inflammatory cytokine with effects on both innate immunity, increasing the number and activation state of NK cells, and adaptive immunity, stimulating antigen-specific T cells (62–63). A Phase I trial through the Children's Cancer Group involved 33 patients. IL-2 was administered by three 96 hr infusions on days 1, 8, and 15 over consecutive weeks and 14.G2a was given as a daily 2 h infusion between days 9–13 (64). The treatment timing sought to take advantage of IL-2 induced lymphocytosis and maximal NK cell cytotoxic activity seen in several previously conducted *in vitro* analyses (65). One patient had a partial response with a 70% size decrease in an abdominal tumor facilitating complete resection. Three additional patients had a transient reduction in microscopic bone marrow disease but no overall reduction in tumor burden. Serum samples from these patients were found to have sufficient levels of 14.G2a to result in ADCC of GD2-positive tumor cells in *in vitro* assays (66). HAMA responses were also noted.

b. Ch14.18 + GM-CSF + IL-2 + CRA Pilot Trial—Testing of ch14.18 in refractory neuroblastoma included co-administration of GM-CSF in studies done by the Pediatric Oncology Group (67,68). Also, the Children's Cancer Group conducted a Phase I clinical trial of ch14.18 with GM-CSF in children with neuroblastoma immediately after hematopoietic stem cell transplant (69). Results of this trial determined the MTD of ch14.18 in combination with GM-CSF to be 40 mg/m^2/day for 4 days in the early post-transplant period. A subsequent Phase I study found the MTD of ch14.18 to be 25 mg/m^2/d for 4 days given concurrently with 4.5×10^6 U/m^2/d of IL-2 for 4 days with alternating cycles of IL-2 and GM-CSF. Though two patients experienced DLTs from ch14.18 and IL-2, this combination was deemed tolerable in the early post-transplant period. This study also found that cis-RA can be safely administered between courses of ch14.18 and cytokines (70).

c. Phase III Neuroblastoma Ch14.18 + GM-CSF + IL-2 + CRA Trial—Preliminary data led to the design of the Children's Oncology Group (COG) Phase III trial, ANBL0032, which prospectively examined this ch14.18 + GM-CSF + IL-2 + CRA combination therapy in patients after myeloablative chemotherapy and autologous stem cell rescue. CRA was added to the regimen because it was shown previously in a Phase III clinical trial to improve overall survival in patients with stage 4 neuroblastoma (4). Following autologous transplant, patients were randomized to receive CRA alone or CRA in combination with ch14.18 and GM-CSF (in courses 1, 3 and 5) and IL-2 (in courses 2 and 4) (16).

From 226 patients with high-risk neuroblastoma, the results showed a two-year event-free survival of 66% in the immunotherapy group versus 46% in the standard treatment group (p=0.0115). Overall survival at two years was 86% for the immunotherapy group versus 75% for the standard treatment group (p= 0.016). The results from this phase III trial have been recently reported (16).

This study shows a substantive increase in survival for high risk neuroblastoma. It is the first clinical trial to document that a combination of an anti-cancer mAb with ADCC-augmenting cytokines is an effective anticancer therapy. Also, it is the first time an antibody targeting a non-protein antigen (as GD2 is a glycolipid) has proven to be effective for immunotherapy of cancer. The 20% improvement in 2-year prevention of relapse for children with neuroblastoma receiving the experimental immunotherapy represents an advance in treatment that is being regarded now as the treatment of choice for high risk patients that achieve remission, in order to decrease the chance of relapse (16).

This study also shows the use of a monoclonal antibody combined with cytokines (GM-CSF and IL-2) to enhance antibody dependent cell-mediated cytotoxicity (ADCC) having made an impact on increasing survival in neuroblastoma in a minimal residual disease setting. Other monoclonal antibodies also mediate ADCC (Rituxan, Erbitux, Herceptin), but have yet to be

tested with cytokines in a minimal residual disease setting. This trial may portend future clinical trials testing cytokine combinations in more common malignancies that are currently treated with monoclonal antibodies (16).

d. 3F8 plus β-glucan—3F8 therapy is enhanced in mice when used in combination with the glucose polymer β-glucan (71). β-glucan sugars act as strong signals to the innate immune system, are well tolerated, and have been shown to stimulate TNF-α secretion and ADCC mediated by NK cells, monocytes, and neutrophils (72–76). 3F8 mAb binds to a tumor cell and coats tumor cells with iC3b. Soluble β-glucans can be used to prime CR3, the iC3b receptor, on the leukocytes, and cause dual ligation of the CR3 receptor on leukocytes to both iC3b and soluble β-glucan, which enhances tumor cytotoxicity (71,72). *In vivo*, oral or intraperitoneal β-glucan has been shown to be effective against neuroblastoma in mice. In nude mice bearing human neuroblastoma tumors, β-glucan and 3F8 mAb therapy resulted in near-complete tumor resolution while either agent alone had less effect. Survival was also increased compared with control animals and this effect was lost when tested on GD2-negative tumors (44,77). The use of β-glucan in conjunction with 3F8 is currently in clinical investigation.

D. Conjugated Antibodies

1. Antibodies Linked to Toxic Agents (Toxins, Chemotherapeutics, Radionuclides)

Antibodies are fairly easy to manufacture and can be linked to toxic agents. Conjugating mAbs to agents for selective delivery to tumor cells has included toxins, chemotherapeutic agents, radioactive isotopes, and immunological agents. Preclinical and some clinical work have been performed with these agents.

2. Radioimmunoconjugates

Radiolabeled mAbs have been used for both disease detection and targeted treatment of a variety of adult cancers but very few childhood tumors. However, radioimmunotherapy is attractive in neuroblastoma because of extensive studies on GD2 directed mAbs and because its tendency to be radiosensitive (78). The only widely studied radio-labeled mAb for treatment of neuroblastoma is ^{131}I-labelled 3F8. A Phase I dose-escalation study performed at Memorial Sloan-Kettering Cancer Center (MSKCC, New York) enrolled 23 patients with refractory stage 4 neuroblastoma. Out of ten patients evaluable, two had complete response (CR) of bone marrow disease and two had a partial response (PR) of soft-tissue disease (78). Based on these results, ^{131}I-labelled 3F8 was added to a multimodal treatment regimen under study at MSKCC for children with high-risk neuroblastoma (79).

3. Immunocytokines (ICs) - Antibodies Linked to Cytokines

a. ch14.18-IL2—The ch14.18-IL2 is an immunocytokine (IC) formed by linking IL-2 to the carboxyl end of the constant region of the chimeric mouse–human IgG1 ch14.18 mAb (80–82). Preclinical data in mice show that treatment with ch14.18-IL2 is far superior to comparable doses of ch14.18 mAb combined with IL-2 in mediating antitumor effects. In general, ADCC depends on the number and function of Fc receptors (FcR) on effector cells including activated NK cells (83,24,61,84). However, activated NK cells also have augmented IL-2 receptor (IL-2R) expression (85) leading to a dramatic *in vitro* response to IL-2 (86). In mouse models, the IL-2 component of this IC can activate NK cells without FcR, through their IL-2R (87). Thus, it is thought that effector cell binding to tumor is mediated in T-cells via IL-2Rs and in NK cells via FcRs and IL-2Rs (82,88). Data suggest that ch14.18-IL-2 could function as both a T-cell inducing vaccine as well as an activator of NK mediated ADCC. These data provided the basis for initiating clinical testing of this 14.18 based IC molecule as therapy for neuroblastoma (83) using an immunocytokine based on the humanized, rather than chimeric, form of the mAb; this IC is hu14.18-IL2.

b. hu14.18-IL2

i. Preclinical Development: When murine (14.G2a) or chimeric (ch14.18) anti-GD2 IgG mAbs are injected intravenously (IV) in mice, half-life is 2–5 days (29,62). In contrast, the half-life of the ch14.18-IL-2 and hu14.18-IL2 is only ~4hrs (89) when injected intravenously into mice. These data led to hu14.18-IL2 being given frequently (daily) to maintain both IL-2 and hu14.18 *in vivo* activity (83).

ii. Phase I Testing in Neuroblastoma: The Children's Oncology Group has completed a Phase I trial using hu14.18-IL2 in 27 pediatric patients with recurrent neuroblastoma using four courses of hu14.18-IL2 for patients with stable disease (90). The MTD was 12 mg/m2/day with dose limiting toxicities (DLTs) of hypotension, allergic reaction, blurred vision, neutropenia, thrombocytopenia, and leukopenia. No CR or PR was noted, but three patients had clinical changes suggestive of antitumor activity with radiographic and bone marrow response. Immune activation was noted with elevated sIL-2Rα and lymphocytosis. All toxicities were reversible, and there were no treatment-related deaths.

iii. Phase II Study: A Phase II study (COG-ANBL0322) of hu14.18-IL2 in children with recurrent or refractory neuroblastoma was designed to evaluate the clinical antitumor activity and *in vivo* immunological effects of hu14.18-IL2. Also, this study sought to differentiate between patients with bulky disease and patients with minimal evaluable neuroblastoma. Patients received 3 daily IV doses of 12.0 mg/M^2/d hu14.18-IL2 in each of 4 monthly courses (91). Fifteen patients had disease measurable by standard radiographical criteria (stratum-1) and 24 patients had disease evaluable only by meta-iodobenzylguanidine (MIBG) scanning and/or bone marrow (BM) histology (stratum-2). Responses were confirmed by independent radiological review and immunocytochemical (ICC) evaluation of the bone marrow.

No responses were seen in the 15 stratum-1 patients. In the 24 stratum-2 patients, 5 showed CR (MIBG and BM/ICC resolution). These response data support the conclusion that this agent and regimen have clinical activity in stratum-2 but not in stratum-1 patients (92). As all patients in this study had recurrent/refractory disease to prior multi-modality therapy, these responses are of interest to pediatric oncologists (91).

E. Anti-Idiotypic Antibodies

1. Mechanism of Tumor Resistance to Anti-GD2 Ab (HAMA, HACA, HAHA)

A problem with mouse mAb therapy has been the development of blocking antibodies to the mAb itself, called a HAMA (human anti-mouse antibody) response (80,57). The development of a HAMA response has been detected within 7 days of treatment and can neutralize any further treatments with the mouse anti-GD2 antibody (83,80). This led to the development of increasingly humanized versions of these mAbs. Chimeric antibodies have linked the GD2 specific variable ends of the immunoglobulin light and heavy chains from the mouse antibody to the human constanst regions of the immunoglobulin light and heavy chains from the human antibody to create a less immunogenic mAb. Unfortunately, human "antichimeric" antibody (HACA) responses can still be detected (80,69).

The current humanized mAb, hu14.18, was developed retaining only the complementarity-determining regions (CDRs) of the original mouse antibody. It is ~98% human amino acid sequence (Fig. 1) (83,80,65). This humanized form of IC, hu14.18-IL2, was made with hopes of reducing immunogenicity of the IC in patients and has been studied in recently completed Phase I and II trials (80,90). The humanized mAb making the hu14.18-IL2 less immunogenic typically does not stimulate a neutralizing HACA or human antihumanized antibody (HAHA) response (24).

2. Anti–IC Antibodies and Antibody-Response Networks

Normally, the HAMA response inhibits antitumor effect. However, a HAMA response has been associated with increased antitumor effect that was also associated with enhanced survival (12). Current thinking suggests that an antibody-response network mechanism may be responsible for providing antitumor benefit. The antigen binding component of an anti-GD2 mAb (Ab-1) serves as an antigen for another antibody (Ab-2) generated in response to Ab-1 treatment. This binding region of Ab-2 may be "immunologically similar" to the GD2 antigen itself (as both bind to the antigen binding portion of the anti-GD2 mAb) and may serve as an additional antigen source for induction of a third antibody (Ab-3). Ab-3 in certain cases can bind to GD2 as well as Ab-2 and can generate antitumor responses similar to those elicited by Ab-1 (24,93,94).

In patients receiving 3F8 antibody, presence of Ab-3 was a predictor of overall survival (6, 94). Ab-3 is not seen in all patients. Anti-idiotypic antibodies (Ab-2) have been used as an antigen source in clinical trials (6,95–97). Also, similar to Ab-2, peptide mimics that bind to the therapeutic Ab-1 have been used in place of GD2 or Ab-2 molecule in an effort to induce an active antitumor response following vaccination (98,99). Currently, efforts at inducing ADCC are focused on patients entering remission, which typically requires intense immunosuppressive treatment to achieve. Therefore, as of now, the paradigm of immunotherapy is to avoid the HACA/HAMA (Ab-2) response.

F. T-cell Engineering in the Treatment of Neuroblastoma

T-cell activation and tumor-specific memory responses have been shown in response to mAbs in animal models and clinical settings (100). T-cell cytotoxicity can be enhanced through manipulation of the T-cell receptor (TCR) to redirect its specificity toward tumor antigens (101). T cells have been genetically altered to express chimeric TCRs consisting of a variable domain of an anti-GD2 antibody linked to a cytoplasmic signaling domain. Engagement of the TCR complex initiates cytotoxic effector function and release of pro-inflammatory cytokines including GM-CSF and IFN-γ upon incubation with GD2-positive tumor cells. These modified T cells mediate antitumor killing with minimal effects on GD2-negative targets (102).

Isolation of CD8+ T cells with altered TCR specificity from plasmids encoding engineered antigen receptors has been shown in human patients (103,104). Incorporation of DNA encoding the novel antigen receptors has been achieved via uptake of naked plasmid DNA by electroporation and retrovirus transfection (102,105). Typically, infusions of autologous tumor-specific T cells had half-lives of 1–42 days with minimal toxicity. Although this approach has been used more extensively for leukemia and lymphoma, human clinical trials targeting neuroblastoma are also under way (104–108). Patients who undergo stem cell transplantation require months to regenerate a functional immune system. Thus, the infusion of large numbers of tumor-specific effector T cells is an attractive alternative to waiting for an autologous immune response, especially in a minimal residual disease setting.

G. Summary

Current conventional therapy of high-risk neuroblastoma (surgery, radiation therapy and multi-agent chemotherapy) can put most children into remission. However, the majority of these patients eventually succumb to recurrent or refractory disease. The current strategy for treatment development is to utilize separate therapeutic approaches for patients in remission but harboring minimal residual disease. The use of anti-GD2 mAbs in this setting has been a promising approach under investigation. Preclinical data using these mAbs show strong anti-tumor effects in the minimal residual disease setting, and antitumor efficacy preclinically can be enhanced by using cytokines that stimulate ADCC. This has potential clinical implications

for patients, who have already undergone conventional surgery, radiation and/or chemotherapy, and who are in remission but suspected to carry minimal residual disease. A recent Phase III trial of this approach by the Children's Oncology Group has shown a 20% increase in event-free survival after two years. Novel approaches, using genetically engineered mAb derivatives, alone or combined with other agents, are even more effective in preclinical testing. Clinical trials of these concepts are underway to determine how best to integrate these approaches into an overall multi-modality treatment that can provide improved long-term disease free survival.

Acknowledgments

This work was supported by NIH-NCI grants CA87025 and CA32685, a grant from the Midwest Athletes Against Childhood Cancer (MACC) Fund, and support from The Crawdaddy Foundation.

References

1. Park JR, Eggert A, Caron H. Neuroblastoma: biology, prognosis, and treatment. Pediatr Clin North Am 2008 Feb;55(1):97–120. x. Review. [PMID: 18242317]. [PubMed: 18242317]
2. Ishola TA, Chung DH. Neuroblastoma. Surg Oncol 2007 Nov;16(3):149–156. Epub 2007 Oct 31. Review. [PMID: 17976976]. [PubMed: 17976976]
3. Brodeur, GM.; Maris, JM. Neuroblastoma. In: Pizzo, PA.; Poplack, DG., editors. Principles and practice of pediatric Oncology. Philadelphia: Lippincott; 2002. p. 895-938.
4. Matthay KK, Villablanca JG, Seeger RC, Stram DO, Harris RE, Ramsay NK, Swift P, Shimada H, Black CT, Brodeur GM, Gerbing RB, Reynolds CP. Children's Cancer Group. Treatment of high-risk neuroblastoma with intensive chemotherapy, radiotherapy, autologous bone marrow transplantation, and 13-cis-retinoic acid. N Engl J Med 1999 Oct 14;341(16):1165–1173. [PMID: 10519894]. [PubMed: 10519894]
5. Brodeur GM. Significance of intratumoral genetic heterogeneity in neuroblastomas. Med Pediatr Oncol 2002 Feb;38(2):112–113. [PMID: 11813176]. [PubMed: 11813176]
6. Cheung NK, Kushner BH, Kramer K. Monoclonal antibody-based therapy of neuroblastoma. Hematol Oncol Clin North Am 2001 Oct;15(5):853–866. Review. [PMID: 11765377]. [PubMed: 11765377]
7. Cheung, NK., et al. Treatment of advanced stage neuroblastoma. In: Reghavan, D., editor. Principles and Practice of Genitourinary Oncology. Lippincott, Williams, and Wilkins; 1997. p. 1101-1111.
8. Ater, JL. Neuroblastoma. In: Behrman, RE.; Kliegman, RM.; Jenson, HA., editors. Behrman: Nelson Textbook of Pediatrics. 17th edn. Saunders; 2004. p. 1709-1711.
9. Jemal A, Siegel R, Ward E, Murray T, Xu J, Thun MJ. Cancer statistics, 2007. CA Cancer J Clin 2007 Jan–Feb;57(1):43–66. [PMID: 17237035]. [PubMed: 17237035]
10. Ries, LAG., et al. SEER Cancer Statistics Review, 1975–2004. Bethesda, MD: National Cancer Institute; 2007. http://seer.cancer.gov/csr/1975_2004/, based on November 2006 SEER data submission, posted to the SEER Web site, 2007
11. Schmidt ML, Lukens JN, Seeger RC, Brodeur GM, Shimada H, Gerbing RB, Stram DO, Perez C, Haase GM, Matthay KK. Children's Cancer Group study. Biologic factors determine prognosis in infants with stage IV neuroblastoma: A prospective. J Clin Oncol 2000 Mar;18(6):1260–1268. [PMID: 10715296]. [PubMed: 10715296]
12. Kushner BH, LaQuaglia MP, Bonilla MA, Lindsley K, Rosenfield N, Yeh S, Eddy J, Gerald WL, Heller G, Cheung NK. Highly effective induction therapy for stage 4 neuroblastoma in children over 1 year of age. J Clin Oncol 1994 Dec;12(12):2607–2613. [PMID: 7527454]. [PubMed: 7527454]
13. Berthold F, Boos J, Burdach S, Erttmann R, Henze G, Hermann J, Klingebiel T, Kremens B, Schilling FH, Schrappe M, Simon T, Hero B. Myeloablative megatherapy with autologous stem-cell rescue versus oral maintenance chemotherapy as consolidation treatment in patients with high-risk neuroblastoma: a randomised controlled trial. Lancet Oncol 2005 Sep;6(9):649–658. [PMID: 16129365]. [PubMed: 16129365]

14. Franks LM, Bollen A, Seeger RC, Stram DO, Matthay KK. Neuroblastoma in adults and adolescents: an indolent course with poor survival. Cancer 1997 May 15;79(10):2028–2035. [PMID: 9149032]. [PubMed: 9149032]

15. Yu A, Gilman A, Ozkaynak F, Kletzel M, Castleberry R, Kretschmar C, Cohn S, Shimada H, Hoh CK, Sondel PM, Wiernikowski S, Bickert P, Seeger R, Reynolds CP, Matthay KK, Lalonde D, Shulkin B, London W, Frierdich S, Maloney A. COG ANBL0032. A Phase III trial of ch14.18 mAb plus IL2 plus GMCSF for children with high risk neuroblastoma following ASCT. COG protocol, open. 2001 Dec.; Available on COG website, and NCI-PDQ.

16. Yu AL, Gilman AL, Ozkaynak MF, London WB, Kreissman S, Chen H, Smith M, Anderson B, Villablanca J, Matthay KK, Shimada H, Grupp SA, Seeger R, Reynolds CP, Buxton A, Reisfeld RA, Gillies SD, Cohn SL, Maris JM, Sondel PM. Chimeric Anti-GD2 Antibody with GM-CSF, IL2 and 13-cis Retinoic Acid for High-risk Neuroblastoma: A Children's Oncology Group (COG) Phase 3 Study. NEJM. In press.

17. Cheung, NK.; Sondel, PM. Neuroblastoma immunology and immunotherapy. In: Cohn, S.; Cheung, NK., editors. Neuroblastoma. Springer Press; 2005. p. 223-242.

18. Mujoo K, Cheresh DA, Yang HM, Reisfeld RA. Disialoganglioside GD2 on human neuroblastoma cells: target antigen for monoclonal antibody-mediated cytolysis and suppression of tumor growth. Cancer Res 1987 Feb 15;47(4):1098–1104. [PMID: 3100030]. [PubMed: 3100030]

19. Cheung NK, Saarinen UM, Neely JE, Landmeier B, Donovan D, Coccia PF. Monoclonal antibodies to a glycolipid antigen on human neuroblastoma cells. Cancer Res 1985 Jun;45(6):2642–2649. [PMID: 2580625]. [PubMed: 2580625]

20. Schulz G, Cheresh DA, Varki NM, Yu A, Staffileno LK, Reisfeld RA. Detection of ganglioside GD2 in tumor tissues and sera of neuroblastoma patients. Cancer Res 1984 Dec;44(12 Pt 1):5914–5920. [PMID: 6498849]. [PubMed: 6498849]

21. Kramer K, Gerald WL, Kushner BH, Larson SM, Hameed M, Cheung NK. Disialoganglioside G(D2) loss following monoclonal antibody therapy is rare in neuroblastoma. Clin Cancer Res 1998 Sep;4 (9):2135–2139. [PMID: 9748131]. [PubMed: 9748131]

22. Svennerholm L, Boström K, Fredman P, Jungbjer B, Lekman A, Månsson JE, Rynmark BM. Gangliosides and allied glycosphingolipids in human peripheral nerve and spinal cord. Biochim Biophys Acta 1994 Sep 15;1214(2):115–123. [PMID: 7918590]. [PubMed: 7918590]

23. Cheever MA, Allison JP, Ferris AS, Finn OJ, Hastings BM, Hecht TT, Mellman I, Prindiville SA, Viner JL, Weiner LM, Matrisian LM. The prioritization of cancer antigens: a national cancer institute pilot project for the acceleration of translational research. Clin Cancer Res 2009 Sep 1;15(17):5323–5337. [PMID: 19723653]. [PubMed: 19723653]

24. Sondel PM, Hank JA. Antibody-directed, effector cell-mediated tumor destruction. Hematol Oncol Clin North Am 2001 Aug;15(4):703–721. [PMID: 11676280]. [PubMed: 11676280]

25. American Cancer Society. Cancer Facts and Figures. Atlanta, GA: ACS publications; 2004.

26. Cheung NK, Lazarus H, Miraldi FD, Abramowsky CR, Kallick S, Saarinen UM, Spitzer T, Strandjord SE, Coccia PF, Berger NA. Ganglioside GD2 specific monoclonal antibody 3F8: a phase I study in patients with neuroblastoma and malignant melanoma. J Clin Oncol 1987 Sep;5(9):1430–1440. [PMID: 3625258]. [PubMed: 3625258]

27. Cheung NK, Kushner BH, Cheung IY, Kramer K, Canete A, Gerald W, Bonilla MA, Finn R, Yeh SJ, Larson SM. Anti-G(D2) antibody treatment of minimal residual stage 4 neuroblastoma diagnosed at more than 1 year of age. J Clin Oncol 1998 Sep;16(9):3053–3060. [PMID: 9738575]. [PubMed: 9738575]

28. Handgretinger R, Baader P, Dopfer R, Klingebiel T, Reuland P, Treuner J, Reisfeld RA, Niethammer D. A phase I study of neuroblastoma with the anti-ganglioside GD2 antibody 14.G2a. Cancer Immunol Immunother 1992;35(3):199–204. [PMID: 1638557]. [PubMed: 1638557]

29. Yu AL, Uttenreuther-Fischer MM, Huang CS, Tsui CC, Gillies SD, Reisfeld RA, Kung FH. Phase I trial of a human-mouse chimeric anti-disialoganglioside monoclonal antibody ch14.18 in patients with refractory neuroblastoma and osteosarcoma. J Clin Oncol 1998 Jun;16(6):2169–2180. [PMID: 9626218]. [PubMed: 9626218]

30. Handgretinger R, Anderson K, Lang P, Dopfer R, Klingebiel T, Schrappe M, Reuland P, Gillies SD, Reisfeld RA, Neithammer D. A phase I study of human/mouse chimeric antiganglioside GD2

antibody ch14.18 in patients with neuroblastoma. Eur J Cancer 1995;31A(2):261–267. [PMID: 7718335]. [PubMed: 7718335]

31. Murray JL, Cunningham JE, Brewer H, Mujoo K, Zukiwski AA, Podoloff DA, Kasi LP, Bhadkamkar V, Fritsche HA, Benjamin RS, et al. Phase I trial of murine monoclonal antibody 14G2a administered by prolonged intravenous infusion in patients with neuroectodermal tumors. J Clin Oncol 1994 Jan; 12(1):184–193. [PMID: 8270976]. [PubMed: 8270976]
32. Saleh MN, Khazaeli MB, Wheeler RH, Dropcho E, Liu T, Urist M, Miller DM, Lawson S, Dixon P, Russell CH, et al. Phase I trial of the murine monoclonal anti-GD2 antibody 14G2a in metastatic melanoma. Cancer Res 1992 Aug 15;52(16):4342–4347. [PMID: 1643631]. [PubMed: 1643631]
33. Saleh MN, Khazaeli MB, Wheeler RH, Allen L, Tilden AB, Grizzle W, Reisfeld RA, Yu AL, Gillies SD, LoBuglio AF. Phase I trial of the chimeric anti-GD2 monoclonal antibody ch14.18 in patients with malignant melanoma. Hum Antibodies Hybridomas 1992 Jan;3(1):19–24. [PMID: 1576319]. [PubMed: 1576319]
34. Stephenson J. Reengineered monoclonal antibodies step up to the plate in cancer studies. JAMA 1995 Dec 20;274(23):1821–1822. [PMID: 7500516]. [PubMed: 7500516]
35. Sondel PM, Hank JA, Gan J, Neal Z, Albertini MR. Preclinical and clinical development of immunocytokines. Curr Opin Investig Drugs 2003 Jun;4(6):696–700. [PMID: 12901228].
36. Jurcic JG, Scheinberg DA, Houghton AN. Monoclonal antibody therapy of cancer. Cancer Chemother Biol Response Modif 1997;17:195–216. Review. No abstract available. [PMID: 9551215]. [PubMed: 9551215]
37. Moss TJ, Reynolds CP, Sather HN, Romansky SG, Hammond GD, Seeger RC. Prognostic value of immunocytologic detection of bone marrow metastases in neuroblastoma. N Engl J Med 1991 Jan 24;324(4):219–226. [PMID: 1985243]. [PubMed: 1985243]
38. Seeger RC, Reynolds CP, Gallego R, Stram DO, Gerbing RB, Matthay KK. Quantitative tumor cell content of bone marrow and blood as a predictor of outcome in stage IV neuroblastoma: a Children's Cancer Group Study. J Clin Oncol 2000 Dec 15;18(24):4067–4076. [PMID: 11118468]. [PubMed: 11118468]
39. Colucci F, Caligiuri MA, Di Santo JP. What does it take to make a natural killer? Nat Rev Immunol 2003 May;3(5):413–425. [PMID: 12766763]. [PubMed: 12766763]
40. Lammie GA, Cheung NKV, Gerald W, et al. Ganglioside GD2 expression in the human nervous system and in neuroblastomas - an immunohistochemical study. International Journal of Oncology 1993;3:909–915.
41. Xiao WH, Yu AL, Sorkin LS. Electrophysiological characteristics of primary afferent fibers after systemic administration of anti-GD2 ganglioside antibody. Pain 1997 Jan;69(1–2):145–151. [PMID: 9060025]. [PubMed: 9060025]
42. Yuki N, Yamada M, Tagawa Y, Takahashi H, Handa S. Pathogenesis of the neurotoxicity caused by anti-GD2 antibody therapy. J Neurol Sci 1997 Aug;149(2):127–130. [PMID: 9171318]. [PubMed: 9171318]
43. Kushner BH, Kramer K, LaQuaglia MP, Cheung NK. Curability of recurrent disseminated disease after surgery alone for local-regional neuroblastoma using intensive chemotherapy and anti-G(D2) immunotherapy. J Pediatr Hematol Oncol 2003 Jul;25(7):515–519. [PMID: 12847316]. [PubMed: 12847316]
44. Cheung NK, Modak S. Oral (1-->3),(1-->4)-beta-D-glucan synergizes with antiganglioside GD2 monoclonal antibody 3F8 in the therapy of neuroblastoma. Clin Cancer Res 2002 May;8(5):1217–1223. [PMID: 12006541]. [PubMed: 12006541]
45. Sondel, PM.; Gillies, SD. Immunocytokines for Cancer Immunotherapy. In: Morse, MA.; Clay, TM.; Lyerly, HK., editors. Handbook of Cancer Vaccines. Humana Press; 2002. p. 341-358.
46. Yeh SD, Larson SM, Burch L, Kushner BH, Laquaglia M, Finn R, Cheung NK. Radioimmunodetection of neuroblastoma with iodine-131-3F8: correlation with biopsy, iodine-131-metaiodobenzylguanidine and standard diagnostic modalities. J Nucl Med 1991 May;32(5):769–776. [PMID: 1902508]. [PubMed: 1902508]
47. Cheung NK, Kushner BH, Yeh SD, Larson SM. 3F8 monoclonal antibody treatment of patients with stage 4 neuroblastoma: a phase II study. Int J Oncol 1998 Jun;12(6):1299–1306. [PMID: 9592190]. [PubMed: 9592190]

48. Cheung NK. Monoclonal antibody-based therapy for neuroblastoma. Curr Oncol Rep 2000 Nov;2 (6):547–553. [PMID: 11122891]. [PubMed: 11122891]
49. Cheung IY, Lo Piccolo MS, Kushner BH, Cheung NK. Early molecular response of marrow disease to biologic therapy is highly prognostic in neuroblastoma. J Clin Oncol 2003 Oct 15;21(20):3853–3858. [PMID: 14551304]. [PubMed: 14551304]
50. Cheung IY, Lo Piccolo MS, Kushner BH, Kramer K, Cheung NK. Quantitation of GD2 synthase mRNA by real-time reverse transcriptase polymerase chain reaction: clinical utility in evaluating adjuvant therapy in neuroblastoma. J Clin Oncol 2003 Mar 15;21(6):1087–1093. [PMID: 12637475]. [PubMed: 12637475]
51. Kushner BH, Kramer K, Cheung NK. Phase II trial of the anti-G(D2) monoclonal antibody 3F8 and granulocyte-macrophage colony-stimulating factor for neuroblastoma. J Clin Oncol 2001 Nov 15;19 (22):4189–4194. [PMID: 11709561]. [PubMed: 11709561]
52. Cheung NK, Walter EI, Smith-Mensah WH, Ratnoff WD, Tykocinski ML, Medof ME. Decay-accelerating factor protects human tumor cells from complement-mediated cytotoxicity in vitro. J Clin Invest 1988 Apr;81(4):1122–1128. [PMID: 2450893]. [PubMed: 2450893]
53. Kushner BH, Cheung NK. GM-CSF enhances 3F8 monoclonal antibody-dependent cellular cytotoxicity against human melanoma and neuroblastoma. Blood 1989 May 15;73(7):1936–1941. [PMID: 2653466]. [PubMed: 2653466]
54. Mujoo K, Kipps TJ, Yang HM, Cheresh DA, Wargalla U, Sander DJ, Reisfeld RA. Functional properties and effect on growth suppression of human neuroblastoma tumors by isotype switch variants of monoclonal antiganglioside GD2 antibody 14.18. Cancer Res 1989 Jun 1;49(11):2857–2861. [PMID: 2720646]. [PubMed: 2720646]
55. Saarinen UM, Coccia PF, Gerson SL, Pelley R, Cheung NK. Eradication of neuroblastoma cells in vitro by monoclonal antibody and human complement: method for purging autologous bone marrow. Cancer Res 1985 Nov;45(11 Pt 2):5969–5975. [PMID: 2414004]. [PubMed: 2414004]
56. Munn DH, Cheung NK. Interleukin-2 enhancement of monoclonal antibody-mediated cellular cytotoxicity against human melanoma. Cancer Res 1987 Dec 15;47(24 Pt 1):6600–6605. [PMID: 3499978]. [PubMed: 3499978]
57. Barker E, Mueller BM, Handgretinger R, Herter M, Yu AL, Reisfeld RA. Effect of a chimeric anti-ganglioside GD2 antibody on cell-mediated lysis of human neuroblastoma cells. Cancer Res 1991 Jan 1;51(1):144–149. [PMID: 1988079]. [PubMed: 1988079]
58. Simon T, Hero B, Faldum A, Handgretinger R, Schrappe M, Niethammer D, Berthold F. Consolidation treatment with chimeric anti-GD2-antibody ch14.18 in children older than 1 year with metastatic neuroblastoma. J Clin Oncol 2004 Sep 1;22(17):3549–3557. [PMID: 15337804]. [PubMed: 15337804]
59. Simon T, Hero B, Faldum A, Handgretinger R, Schrappe M, Niethammer D, Berthold F. Infants with stage 4 neuroblastoma: the impact of the chimeric anti-GD2-antibody ch14.18 consolidation therapy. Klin Padiatr 2005 May–Jun;217(3):147–152. [PMID: 15858706]. [PubMed: 15858706]
60. Ito A, Ishida T, Yano H, Inagaki A, Suzuki S, Sato F, Takino H, Mori F, Ri M, Kusumoto S, Komatsu H, Iida S, Inagaki H, Ueda R. Defucosylated anti-CCR4 monoclonal antibody exercises potent ADCC-mediated antitumor effect in the novel tumor-bearing humanized NOD/Shi-scid, IL-2Rgamma(null) mouse model. Cancer Immunol Immunother 2009 Aug;58(8):1195–1206. Epub 2008 Dec 2. [PMID: 19048251]. [PubMed: 19048251]
61. Hank JA, Robinson RR, Surfus J, Mueller BM, Reisfeld RA, Cheung NK, Sondel PM. Augmentation of antibody dependent cell mediated cytotoxicity following in vivo therapy with recombinant interleukin 2. Cancer Res 1990 Sep 1;50(17):5234–5239. [PMID: 2386933]. [PubMed: 2386933]
62. Mulé JJ, Yang JC, Afreniere RL, Shu SY, Rosenberg SA. Identification of cellular mechanisms operational in vivo during the regression of established pulmonary metastases by the systemic administration of high-dose recombinant interleukin 2. J Immunol 1987 Jul 1;139(1):285–294. [PMID: 3108401]. [PubMed: 3108401]
63. Sondel PM, Hank JA. Combination therapy with interleukin-2 and antitumor monoclonal antibodies. Cancer J Sci Am 1997 Dec;3 Suppl 1:S121–S127. Review. [PMID: 9457407]. [PubMed: 9457407]
64. Frost JD, Hank JA, Reaman GH, Frierdich S, Seeger RC, Gan J, Anderson PM, Ettinger LJ, Cairo MS, Blazar BR, Krailo MD, Matthay KK, Reisfeld RA, Sondel PM. A phase I/IB trial of murine

monoclonal anti-GD2 antibody 14.G2a plus interleukin-2 in children with refractory neuroblastoma: a report of the Children's Cancer Group. Cancer 1997 Jul 15;80(2):317–333. [PMID: 9217046]. [PubMed: 9217046]

65. Hank, JA.; Albertini, MR.; Sondel, PM. Monoclonal antibodies, cytokines and fusion proteins in the treatment of malignant disease. In: Pinedo, HM.; Longo, DL.; Chabner, BA., editors. Cancer Chemotherapy and Biological Response Modifiers Annual 18. Elsevier Science; 1999. p. 210-222.
66. Hank JA, Surfus J, Gan J, Chew TL, Hong R, Tans K, Reisfeld R, Seeger RC, Reynolds CP, Bauer M, et al. Treatment of neuroblastoma patients with antiganglioside GD2 antibody plus interleukin-2 induces antibody-dependent cellular cytotoxicity against neuroblastoma detected in vitro. J Immunother Emphasis Tumor Immunol 1994 Jan;15(1):29–37. [PMID: 8110728]. [PubMed: 8110728]
67. Yu AL, Batova A, Alvarado C, Rao VJ, Castelberry RP. Usefulness of a chimeric anti-GD2 (ch14.18) and GM-CSF for refractory neuroblastoma: a POG phase II study. Proc. Am. Soc. Clin. Oncol 1997;16:1846.
68. Yu AL, Uttenreuther MM, Kamps A, Batova A, Reisfeld RA. Combined use of a human-mouse chimeric anti-GD2 (ch14.18) and GM-CSF in the treatment of refractory neuroblastoma. Antibody Immunoconjugates Radiopharmaceuticals 1995;8:12.
69. Ozkaynak MF, Sondel PM, Krailo MD, Gan J, Javorsky B, Reisfeld RA, Matthay KK, Reaman GH, Seeger RC. Phase I study of chimeric human/murine anti-ganglioside G(D2) monoclonal antibody (ch14.18) with granulocyte-macrophage colony-stimulating factor in children with neuroblastoma immediately after hematopoietic stem-cell transplantation: a Children's Cancer Group Study. J Clin Oncol 2000 Dec 15;18(24):4077–4085. [PMID: 11118469]. [PubMed: 11118469]
70. Gilman AL, Ozkaynak MF, Matthay KK, Krailo M, Yu AL, Gan J, Sternberg A, Hank JA, Seeger R, Reaman GH, Sondel PM. Phase I study of ch14.18 with granulocyte-macrophage colony-stimulating factor and interleukin-2 in children with neuroblastoma after autologous bone marrow transplantation or stem-cell rescue: a report from the Children's Oncology Group. J Clin Oncol 2009 Jan 1;27(1):85. Epub 2008 Dec 1. [PMID: 19047298]. [PubMed: 19047298]
71. Xia Y, Vetvicka V, Yan J, Hanikýrová M, Mayadas T, Ross GD. The beta-glucan-binding lectin site of mouse CR3 (CD11b/CD18) and its function in generating a primed state of the receptor that mediates cytotoxic activation in response to iC3b-opsonized target cells. J Immunol 1999 Feb 15;162 (4):2281–2290. [PMID: 9973505]. [PubMed: 9973505]
72. Vetvicka V, Thornton BP, Wieman TJ, Ross GD. Targeting of natural killer cells to mammary carcinoma via naturally occurring tumor cell-bound iC3b and beta-glucan-primed CR3 (CD11b/CD18). J Immunol 1997 Jul 15;159(2):599–605. [PMID: 9218574]. [PubMed: 9218574]
73. Di Renzo L, Yefenof E, Klein E. The function of human NK cells is enhanced by beta-glucan, a ligand of CR3 (CD11b/CD18). Eur J Immunol 1991 Jul;21(7):1755–1758. [PMID: 2060581]. [PubMed: 2060581]
74. Vetvicka V, Thornton BP, Ross GD. Soluble beta-glucan polysaccharide binding to the lectin site of neutrophil or natural killer cell complement receptor type 3 (CD11b/CD18) generates a primed state of the receptor capable of mediating cytotoxicity of iC3b-opsonized target cells. J Clin Invest 1996 Jul 1;98(1):50–61. [PMID: 8690804]. [PubMed: 8690804]
75. Czop JK, Austen KF. Properties of glycans that activate the human alternative complement pathway and interact with the human monocyte beta-glucan receptor. J Immunol 1985 Nov;135(5):3388–3393. [PMID: 4045195]. [PubMed: 4045195]
76. Thornton BP, Větvicka V, Pitman M, Goldman RC, Ross GD. Analysis of the sugar specificity and molecular location of the beta-glucan-binding lectin site of complement receptor type 3 (CD11b/CD18). J Immunol 1996 Feb 1;156(3):1235–1246. [PMID: 8558003]. [PubMed: 8558003]
77. Hong F, Yan J, Baran JT, Allendorf DJ, Hansen RD, Ostroff GR, Xing PX, Cheung NK, Ross GD. Mechanism by which orally administered beta-1,3-glucans enhance the tumoricidal activity of antitumor monoclonal antibodies in murine tumor models. J Immunol 2004 Jul 15;173(2):797–806. [PMID: 15240666]. [PubMed: 15240666]
78. Modak S, Cheung NK. Antibody-based targeted radiation to pediatric tumors. J Nucl Med 2005 Jan; 46 Suppl 1:157S–163S. [PMID: 15653664]. [PubMed: 15653664]
79. Cheung NK, Kushner BH, LaQuaglia M, Kramer K, Gollamudi S, Heller G, Gerald W, Yeh S, Finn R, Larson SM, Wuest D, Byrnes M, Dantis E, Mora J, Cheung IY, Rosenfield N, Abramson S,

O'Reilly RJ. N7: a novel multi-modality therapy of high risk neuroblastoma (NB) in children diagnosed over 1 year of age. Med Pediatr Oncol 2001 Jan;36(1):227–230. [PMID: 11464891]. [PubMed: 11464891]

80. Johnson E, Dean SM, Sondel PM. Antibody-based immunotherapy in high-risk neuroblastoma. Expert Rev Mol Med 2007 Dec 17;9(34):1–21. [PMID: 18081947]. [PubMed: 18081947]
81. Gillies SD, Young D, Lo KM, Roberts S. Biological activity and in vivo clearance of antitumor antibody/cytokine fusion proteins. Bioconjug Chem 1993 May–Jun;4(3):230–235. [PMID: 8324014]. [PubMed: 8324014]
82. Gillies SD, Reilly EB, Lo KM, Reisfeld RA. Antibody-targeted interleukin 2 stimulates T-cell killing of autologous tumor cells. Proc Natl Acad Sci U S A 1992 Feb 15;89(4):1428–1432. [PMID: 1741398]. [PubMed: 1741398]
83. Sondel, PM.; Hank, JA.; Albertini, MR.; Gillies, SD. Novel strategies for cytokine administration via targetting. In: Caligiuri, MA.; Lotze, MT., editors. Cancer Drug Discovery and Development, Cytokines in the Genesis and Treatment of Cancer. Totowa, NJ: Humana Press Inc; 2008.
84. Weng WK, Levy R. Two immunoglobulin G fragment C receptor polymorphisms independently predict response to rituximab in patients with follicular lymphoma. J Clin Oncol 2003 Nov 1;21(21): 3940–3947. Epub 2003 Sep 15. [PMID: 12975461]. [PubMed: 12975461]
85. Voss SD, Robb RJ, Weil-Hillman G, Hank JA, Sugamura K, Tsudo M, Sondel PM. Increased expression of the interleukin 2 (IL-2) receptor beta chain (p70) on CD56+ natural killer cells after in vivo IL-2 therapy: p70 expression does not alone predict the level of intermediate affinity IL-2 binding. J Exp Med 1990 Oct 1;172(4):1101–1114. [PMID: 1698909]. [PubMed: 1698909]
86. Sondel PM, Kohler PC, Hank JA, Moore KH, Rosenthal NS, Sosman JA, Bechhofer R, Storer B. Clinical and immunological effects of recombinant interleukin 2 given by repetitive weekly cycles to patients with cancer. Cancer Res 1988 May 1;48(9):2561–2567. [PMID: 3258545]. [PubMed: 3258545]
87. Weil-Hillman G, Fisch P, Prieve AF, Sosman JA, Hank JA, Sondel PM. Lymphokine-activated killer activity induced by in vivo interleukin 2 therapy: predominant role for lymphocytes with increased expression of CD2 and leu19 antigens but negative expression of CD16 antigens. Cancer Res 1989 Jul 1;49(13):3680–3688. [PMID: 2471587]. [PubMed: 2471587]
88. Hank JA, Surfus JE, Gan J, Jaeger P, Gillies SD, Reisfeld RA, Sondel PM. Activation of human effector cells by a tumor reactive recombinant anti-ganglioside GD2 interleukin-2 fusion protein (ch14.18-IL2). Clin Cancer Res 1996 Dec;2(12):1951–1959. [PMID: 9816154]. [PubMed: 9816154]
89. Kendra K, Gan J, Ricci M, Surfus J, Shaker A, Super M, Frost JD, Rakhmilevich A, Hank JA, Gillies SD, Sondel PM. Pharmacokinetics and stability of the ch14.18-interleukin-2 fusion protein in mice. Cancer Immunol Immunother 1999 Aug;48(5):219–229. [PMID: 10478638]. [PubMed: 10478638]
90. Osenga KL, Hank JA, Albertini MR, Gan J, Sternberg AG, Eickhoff J, Seeger RC, Matthay KK, Reynolds CP, Twist C, Krailo M, Adamson PC, Reisfeld RA, Gillies SD, Sondel PM. Children's Oncology Group. A phase I clinical trial of the hu14.18-IL2 (EMD 273063) as a treatment for children with refractory or recurrent neuroblastoma and melanoma: a study of the Children's Oncology Group. Clin Cancer Res 2006 Mar 15;12(6):1750–1759. [PMID: 16551859]. [PubMed: 16551859]
91. Shusterman S, London, Gilles S, Hank JA, Voss S, Seeger RC, Hecht T, Reisfeld R, Maris JM, Sondel PM. Anti-neuroblastoma activity of hu14.18-IL2 against minimal residual disease in a Children's Oncology Group (COG) phase II study. J. Clin. Oncol 2008;26(15s):132s. (abstract 3002).
92. Shusterman S, London WB, Gillies SD, Hank JA, Voss S, Seeger RC, Reynolds CP, Kimball J, Albertini MA, Wagner B, Gan J, Eickhoff J, DeSantes KD, Cohn SL, Hecht T, Gadbaw B, Reisfeld RA, Maris JM, Sondel PM, et al. Anti-tumor activity of hu14.18-IL2 in relapsed/refractory neuroblastoma patients: a Children's Oncology Group (COG) phase II study. 2010 To be Submitted.
93. Wang X, Luo W, Foon KA, Ferrone S. Tumor associated antigen (TAA) mimicry and immunotherapy of malignant diseases from anti-idiotypic antibodies to peptide mimics. Cancer Chemother Biol Response Modif 2001;19:309–326. [PMID: 11686020]. [PubMed: 11686020]
94. Cheung NK, Guo HF, Heller G, Cheung IY. Induction of Ab3 and Ab3' antibody was associated with long-term survival after anti-G(D2) antibody therapy of stage 4 neuroblastoma. Clin Cancer Res 2000 Jul;6(7):2653–2660. [PMID: 10914706]. [PubMed: 10914706]

95. Chatterjee MB, Foon KA, Köhler H. Idiotypic antibody immunotherapy of cancer. Cancer Immunol Immunother 1994 Feb;38(2):75–82. Review. [PMID: 8306369]. [PubMed: 8306369]

96. Chatterjee M, Mrozek E, Vaickus L, Oseroff A, Stoll H, Russell D, Kohler H, Foon KA. Antiidiotype (Ab2) vaccine therapy for cutaneous T-cell lymphoma. Ann N Y Acad Sci 1993 Aug 12;690:376–377. [PMID: 8368761]. [PubMed: 8368761]

97. Chatterjee M, Barcos M, Han T, Liu XL, Bernstein Z, Foon KA. Shared idiotype expression by chronic lymphocytic leukemia and B-cell lymphoma. Blood 1990 Nov 1;76(9):1825–1829. [PMID: 2224130]. [PubMed: 2224130]

98. Luo W, Ko E, Hsu JC, Wang X, Ferrone S. Targeting melanoma cells with human high molecular weight-melanoma associated antigen-specific antibodies elicited by a peptide mimotope: functional effects. J Immunol 2006 May 15;176(10):6046–6054. [PMID: 16670313]. [PubMed: 16670313]

99. Fest S, Huebener N, Weixler S, Bleeke M, Zeng Y, Strandsby A, Volkmer-Engert R, Landgraf C, Gaedicke G, Riemer AB, Michalsky E, Jaeger IS, Preissner R, Förster-Wald E, Jensen-Jarolim E, Lode HN. Characterization of GD2 peptide mimotope DNA vaccines effective against spontaneous neuroblastoma metastases. Cancer Res 2006 Nov 1;66(21):10567–10575. [PMID: 17079481]. [PubMed: 17079481]

100. Coughlin CM, Vance BA, Grupp SA, Vonderheide RH. RNA-transfected CD40-activated B cells induce functional T-cell responses against viral and tumor antigen targets: implications for pediatric immunotherapy. Blood 2004 Mar 15;103(6):2046–2054. Epub 2003 Nov 20. [PMID: 14630810]. [PubMed: 14630810]

101. Rossig C, Brenner MK. Genetic modification of T lymphocytes for adoptive immunotherapy. Mol Ther 2004 Jul;10(1):5–18. [PMID: 15233937]. [PubMed: 15233937]

102. Rossig C, Bollard CM, Nuchtern JG, Merchant DA, Brenner MK. Targeting of G(D2)-positive tumor cells by human T lymphocytes engineered to express chimeric T-cell receptor genes. Int J Cancer 2001 Oct 15;94(2):228–236. [PMID: 11668503]. [PubMed: 11668503]

103. Gonzalez S, Naranjo A, Serrano LM, Chang WC, Wright CL, Jensen MC. Genetic engineering of cytolytic T lymphocytes for adoptive T-cell therapy of neuroblastoma. J Gene Med 2004 Jun;6(6):704–711. [PMID: 15170741]. [PubMed: 15170741]

104. Park JR, Digiusto DL, Slovak M, Wright C, Naranjo A, Wagner J, Meechoovet HB, Bautista C, Chang WC, Ostberg JR, Jensen MC. Adoptive transfer of chimeric antigen receptor re-directed cytolytic T lymphocyte clones in patients with neuroblastoma. Mol Ther 2007 Apr;15(4):825–833. Epub 2007 Feb 13. [PMID: 17299405]. [PubMed: 17299405]

105. Jensen MC, Clarke P, Tan G, Wright C, Chung-Chang W, Clark TN, Zhang F, Slovak ML, Wu AM, Forman SJ, Raubitschek A. Human T lymphocyte genetic modification with naked DNA. Mol Ther 2000 Jan;1(1):49–55. [PMID: 10933911]. [PubMed: 10933911]

106. Serrano LM, Pfeiffer T, Olivares S, Numbenjapon T, Bennitt J, Kim D, Smith D, McNamara G, Al-Kadhimi Z, Rosenthal J, Forman SJ, Jensen MC, Cooper LJ. Differentiation of naive cord-blood T cells into CD19-specific cytolytic effectors for posttransplantation adoptive immunotherapy. Blood 2006 Apr 1;107(7):2643–2652. Epub 2005 Dec 13. [PMID: 16352804]. [PubMed: 16352804]

107. Cooper LJ, Ausubel L, Gutierrez M, Stephan S, Shakeley R, Olivares S, Serrano LM, Burton L, Jensen MC, Forman SJ, DiGiusto DL. Manufacturing of gene-modified cytotoxic T lymphocytes for autologous cellular therapy for lymphoma. Cytotherapy 2006;8(2):105–117. [PMID: 16698684]. [PubMed: 16698684]

108. Savoldo B, Rooney CM, Di Stasi A, Abken H, Hombach A, Foster AE, Zhang L, Heslop HE, Brenner MK, Dotti G. Epstein Barr virus specific cytotoxic T lymphocytes expressing the anti-CD30zeta artificial chimeric T-cell receptor for immunotherapy of Hodgkin disease. Blood 2007 Oct 1;110(7):2620–2630. Epub 2007 May 16. [PMID: 17507664]. [PubMed: 17507664]

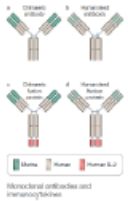

Figure 1.

Monoclonal Antibodies and Immunocytokines. (a) A chimeric monoclonal antibody (mAb) combines the constant region of a human antibody with the variable domain of a murine antibody. The antigen specificity is conferred by the murine variable domain. (b) In the humanised mAb, the murine framework determinants of both the heavy and light chains are replaced with human framework determinants, but the antigen specificity of the original murine mAb is retained. (c,d) Fusion proteins or immunocytokines combine the mAb with covalently linked cytokines, such as molecules of interleukin 2 (IL-2), to the end of each of the heavy chains at the C-terminus.

A.2 Genotypes of NK cell KIR Receptors, Their Ligands, and Fcγ Receptors in the Response of Neuroblastoma Patients to Hu14.18-IL2 Immunotherapy

Published OnlineFirst October 8, 2010; DOI:10.1158/0008-5472.CAN-10-2211

Clinical Studies

Cancer Research

Genotypes of NK Cell KIR Receptors, Their Ligands, and Fcγ Receptors in the Response of Neuroblastoma Patients to Hu14.18-IL2 Immunotherapy

David C. Delgado[1], Jacquelyn A. Hank[2], Jill Kolesar[5], David Lorentzen[3], Jacek Gan[2], Songwon Seo[4], KyungMann Kim[4], Suzanne Shusterman[6], Stephen D. Gillies[7], Ralph A. Reisfeld[8], Richard Yang[2], Brian Gadbaw[2], Kenneth B. DeSantes[1], Wendy B. London[6,9], Robert C. Seeger[10], John M. Maris[11], and Paul M. Sondel[1,2]

Abstract

Response to immunocytokine (IC) therapy is dependent on natural killer cells in murine neuroblastoma (NBL) models. Furthermore, killer immunoglobulin-like receptor (KIR)/KIR-ligand mismatch is associated with improved outcome to autologous stem cell transplant for NBL. Additionally, clinical antitumor response to monoclonal antibodies has been associated with specific polymorphic-FcγR alleles. Relapsed/refractory NBL patients received the hu14.18-IL2 IC (humanized anti-GD2 monoclonal antibody linked to human IL2) in a Children's Oncology Group phase II trial. In this report, these patients were genotyped for KIR, HLA, and FcR alleles to determine whether KIR receptor–ligand mismatch or specific FcγR alleles were associated with antitumor response. DNA samples were available for 38 of 39 patients enrolled: 24 were found to have autologous KIR/KIR-ligand mismatch; 14 were matched. Of the 24 mismatched patients, 7 experienced either complete response or improvement of their disease after IC therapy. There was no response or comparable improvement of disease in patients who were matched. Thus KIR/KIR-ligand mismatch was associated with response/improvement to IC ($P = 0.03$). There was a trend toward patients with the FcγR2A 131-H/H genotype showing a higher response rate than other FcγR2A genotypes ($P = 0.06$). These analyses indicate that response or improvement of relapsed/refractory NBL patients after IC treatment is associated with autologous KIR/KIR-ligand mismatch, consistent with a role for natural killer cells in this clinical response. *Cancer Res; 70(23); 9554–61. ©2010 AACR*

Introduction

The therapeutic role of natural killer (NK) cells in allogeneic hematopoietic stem cell transplant (HSCT) has been well described. Ruggeri et al. (1) first reported on the phenomenon of killer immunoglobulin-like receptor (KIR)/KIR-ligand incompatibility and response to HLA-haploidentical HSCT, primarily in adult patients with acute myeloid leukemia (AML). According to this analysis, a difference in HLA between the donor and recipient such that the donor KIR receptors lack their cognate ligand in the recipient results in improved leukemia control. Leung et al. defined the principle of missing KIR ligand (designated here as KIR/KIR-ligand mismatch), in which the HSCT recipient lacks 1 or more HLA class-I ligands for the HSCT donor's inhibitory KIRs (2). The KIR/KIR-ligand mismatch principle posits that a difference in HLA between the donor and recipient is not necessary for the benefit of KIR-HLA mismatching. They found that response of pediatric patients with AML and acute lymphoid leukemia (ALL) to haploidentical HSCT could be predicted by the presence of this KIR/KIR-ligand mismatch. An analysis of results of HLA-identical T cell–depleted sibling HSCT also revealed a benefit of KIR/KIR-ligand mismatch (3). KIR/KIR-ligand mismatch also extends to the autologous transplant setting. Because the genes encoding for KIR and HLA class I KIR ligands are inherited independently, it is possible for an individual to be KIR/KIR-ligand mismatched with himself. This scenario has been implicated as a favorable prognostic factor in pediatric solid tumor patients following autologous HSCT (ASCT) (4, 5). To date, there have been no reports relating KIR/KIR-ligand mismatch and response of cancer

Authors' Affiliations: Departments of [1]Pediatrics, [2]Human Oncology, [3]Pathology and Laboratory Medicine, and [4]Biostatistics and Medical Informatics, and [5]School of Pharmacy, Carbone Cancer Center, University of Wisconsin, Madison, Wisconsin; [6]The Dana Farber Cancer Institute and Children's Hospital, Boston, Massachusetts; [7]Provenance Biopharmaceuticals Corp., Waltham, Massachusetts; [8]The Scripps Research Institute, La Jolla, California; [9]Children's Oncology Group (COG) Statistics and Data Center, Gainesville, Florida; [10]Division of Hematology/Oncology, Children's Hospital of Los Angeles, Los Angeles, California; and [11]Division of Oncology and Center for Childhood Cancer Research, Children's Hospital of Philadelphia and the University of Pennsylvania, Philadelphia, Pennsylvania

Note: This study has not been previously published, but was presented at the 2010 American Society of Pediatric Hematology and Oncology (ASPHO) meeting in Montreal, Quebec, Canada, on April 9, 2010.This is manuscript no. 9982 of the Children's Oncology Group (COG).

Corresponding Author: Paul M. Sondel, Departments of Pediatrics and Human Oncology, University of Wisconsin, 1159 WIMR, 1111 Highland Ave, Madison, WI 53705. Phone: 608-263-9069; Fax: 608-263-4226; E-mail: pmsondel@humonc.wisc.edu.

doi: 10.1158/0008-5472.CAN-10-2211

Published OnlineFirst October 8, 2010; DOI:10.1158/0008-5472.CAN-10-2211

patients to immunotherapy or other treatments outside of the HSCT or allogeneic NK cell infusion settings (6).

Several groups have investigated the role of fragment c gamma receptor (FcγR) polymorphisms in the response of cancer patients to rituximab, the chimeric anti-CD20 immunoglobulin G1 (IgG1) monoclonal antibody (mAb). Some have found an association between FcγR genotypes for higher-affinity FcγR alleles (FcγR2A-131 H/H and FcγR3A-158 V/V genotypes) and response to rituximab-based therapy (7–9). Association between FcγR genotype and response, for both FcγR2A (found largely on neutrophils and monocytes/macrophages) and FcγR3A (found predominantly on NK cells) genotypes, has now been observed in cancer patients receiving other mAbs (i.e., cetuximab and trastuzumab) as well (10, 11). Cheung et al. (12) reported a correlation between FcγR2A polymorphism and response of neuroblastoma (NBL) patients to the anti-GD2 murine IgG3 mAb, 3F8, plus granulocyte macrophage colony-stimulating factor (GM-CSF). In that study, progression-free survival was associated with the FcγR2A 131-R/R alleles with the highest affinity for the 3F8 murine mAb.

GD2 is a disialoganglioside that is expressed on human melanoma and NBL cells. Our recent Children's Oncology Group (COG) phase III study has shown a significant improvement in overall survival and event-free survival for children receiving an immunotherapy regimen of a chimeric anti-GD2 mAb (ch14.18-IL2) in combination with interleukin 2 (IL2) and GM-CSF (13). The hu14.18-IL2 immunocytokine (IC) is a fusion protein linking a molecule of IL2 to the carboxyl terminus of each of the IgG1 heavy chains of the humanized anti-GD2 mAb hu14.18. Tumor response to this IC in mice is superior to the antitumor effects of comparable amounts of anti-GD2 mAb infused together with comparable amounts of IL2 (14). Antitumor effects in mice are primarily dependent on NK cells in a murine model of NBL (15), with better responses seen in the face of less-established disease (16). Furthermore, augmented major histocompatibility complex (MHC) class I expression on murine NBL was associated with escape from IC-mediated immunotherapy, implying a role for MHC-induced inhibition of NK cell function (17). Our recent phase II COG trial has demonstrated antitumor activity for hu14.18-IL2 in children with relapsed or refractory NBL (18).

In this study we evaluated the role of genotypes for KIR, KIR ligands (HLA class I), and FcγR polymorphisms, in the response of relapsed/refractory NBL patients to hu14.18-IL2 from our phase II trial (18).

Materials and Methods

Patients

Patients included in this analysis were eligible for and enrolled on a COG phase II trial of hu14.18-IL2 (ANBL0322); the clinical findings from that study have been reported separately (18). In brief, children (ages 1–21 years) with refractory or recurrent NBL who met all study criteria were enrolled in 1 of 2 strata. Stratum 1 included 15 patients with measurable disease (using standard radiographic criteria). Stratum 2 included 24 patients with disease that was not measurable by standard imaging, but was evaluable by ^{123}I-metaiodobenzylguanidine (MIBG) scan and/or bone marrow histology. DNA samples were available for 38 of the 39 enrolled patients. Informed consent was obtained from Institutional Review Board–approved clinical protocols for all patients and/or their families.

Hu14.18-IL2

The clinical grade hu14.18-IL2 IC (EMD 273063) was generously provided by Merck Serono (Darmstadt, Germany) via Dr. Toby Hecht, and the NCI-Biological Resources Branch (Frederick, MD).

KIR/KIR-ligand genotyping

KIR genotyping was performed on patient DNA samples by PCR sequence-specific primer technique (SSP Unitray assay; Invitrogen Corporation, Carlsbad, CA). KIR-ligand typing was performed at low resolution on the same samples for HLA-B and -C loci by reverse PCR-SSO methodology (LifeMatch assay; Gen-Probe, Inc., Stamford, CT) and for high-resolution HLA-C alleles by direct sequencing (AlleleSEQR assay; Abbott Labs, Des Plaines, IL).

FcγR genotyping

Genotyping of FcgR2A 131-H/R (rs1801274) and FcgR3A 158-F/V (rs396991) polymorphisms were detected using pyrosequencing and TaqMan (19). Forward and reverse primers are given in Table 1. PCR was performed in 25 μL reactions using 2X PCR Master Mix (Promega, Madison, WI) with 5 pmole forward, 0.5 pmole reverse, and 4.5 pmole of universal biotin primer. The biotinylated PCR products were isolated with Streptavidin-Sepharose HP (GE Healthcare, Piscataway, NJ) and Sepharose beads. Allele quantification was performed using a Pyrogold reagent kit (dATP, dCTP, dGTP, dTTP, enzyme, and substrate mixtures) on the PSQ HS96A system (Biotage AB, Uppsala, Sweden). Negative controls were included on each plate. Plates were read on a PSQ HS pyrosequencer using PSQ HS 96A SNP analysis software version 2.1 in AQ mode.

To account for variation in the accuracy of FcγR3A 158-V/F allele frequency determination, standard curves were generated by using synthesized biotin-labeled DNA oligonucleotides. Two oligonucleotides with either a "T" or "G" in the mutation position (representing F and V alleles, respectively) were combined in ratios (10:0, 9:1, . . .1:9, 0:10) and underwent pyrosequencing. The expected and observed allele frequencies were plotted. Backwards fitting was used to find the most parsimonious fit.

Genotyping of FcγR3A 158-V/F mutation polymorphisms was confirmed using TaqMan SNP genotyping assay (C_25815666–10, Chr-1, DIS484) in accordance with the manufacturer's instructions on a 7300 Real-Time PCR system (Applied Biosystems, Foster City, CA). This TaqMan Assay uses primers and probes that are predesigned and validated by the company. The probes are conjugated with VIC-MGB or FAM-MGB dyes, 1 to each allele. The amount of volume required for each 25 μL reaction was TaqMan Genotyping PCR Master Mix 12.5 μL and TaqMan SNP Genotyping Assay 1 μL. The reaction conditions were as follows: 95°C for 10 minutes, and 50 cycles of 92°C for 15 seconds and 60°C

Published OnlineFirst October 8, 2010; DOI:10.1158/0008-5472.CAN-10-2211

Table 1. Forward and reverse primer sequences for FcγR2A 131-H/R & FcγR3A 158-V/F polymorphism genotyping

Primers	Sequences
FcγR2A 131-H/R: Forward	TTT TGC TGC TAT GGG CTT TC
FcγR2A 131-H/R: Reverse	/5Biosg/CCA GAA TGG AAA ATC CCA GAA A
FcγR2A 131-H/R: Sequencing	AAG GTG GGA TCC AAA
FcγR3A 158-V/F: Forward	/5Biosg/CAC TCA AAG ACA GCG GCT CCT
FcγR3A 158-V/F: Reverse	ATT CCA GGG TGG CAC ATG TC
FcγR3A 158-V/F: Sequencing	AGT CTC TGA AGA CAC ATT TTT

for 1 minute. Plates were read by the 7300 Real-Time PCR system according to manufacturer protocols.

Statistical methods

Fisher's exact test was used to examine the association between 2 categorical variables (i.e., KIR mismatch versus response/improvement, genotype versus response/improvement, and KIR mismatch versus stratum). Chi-square test of homogeneity was used to determine whether there was a difference in distributions of KIR mismatch/match and FcγR genotypes between our study population and others' (5, 12). For the analysis of the association between genotype and response/improvement, FcγR2A were dichotomized into H/H versus H/R or R/R, and FcγR3A into V/V versus V/F or F/F. Statistical significance was defined as a 2-tailed $P < 0.05$, and a P value from 0.05 to 0.1 was regarded as marginally statistically significant. Because of the exploratory nature of this study, no multiplicity adjustment was made for significance tests.

Results

KIR/KIR-ligand genotyping

The 4 inhibitory KIR genes (KIR2DL1, KIR2DL2, KIR2DL3, KIR3DL1) evaluated in this study and their corresponding KIR-ligands (HLA-C1, HLA-C2, or HLA-Bw4) are listed in Table 2. KIR/KIR-ligand mismatch was defined as absence of 1 or more HLA alleles known to be ligands for the inhibitory KIR genes present, using previously published criteria (2). The specific KIR and KIR-ligand genotypes for all 38 patients (with DNA available) are shown in Table 3. Two patients showed evidence for only 2 of the 3 inhibitory KIR gene specificities evaluated in this study; the other 36 patients had all 3 inhibitory KIR gene specificities present. KIR/KIR-ligand mismatch was observed in 24 of 38 patients whereas in 14 of 38 patients these were matched (Table 4). This ratio of matched to mismatched genotypes, when using this set of KIR genes and KIR ligand genes, is not significantly different ($P = 0.93$) from that reported for the set of NBL patients undergoing ASCT reported by Venstrom et al. (5).

FcγR genotyping

FcγR genotyping data for all patients tested are also included in Table 3, and is summarized in Table 4. The genotype distributions for both FcγR2A and FcγR3A were in Hardy–Weinberg Equilibrium (HWE). The FcγR2A 131-H/R genotype was more prevalent (16 of 38 patients) than the H/H genotype (10 of 38) and R/R genotype (12 of 38) (P value of HWE is 0.34). Two of 38 patients (patients 8 and 35) were excluded from the analysis of FcγR3A genotyping (and relevant analyses of associations) due to discrepant results of pyrosequencing and TaqMan; both patients were F/V by pyrosequencing and F/F by TaqMan. If patients 8 and 35 are included in the analyses as either F/F or F/V the relevant statistical analyses, as do their conclusions, remain virtually unchanged. The FcγR3A 158-F/F and F/V genotypes were equally prevalent (both present in 17 of 36 patients) in this patient population, whereas the V/V genotype was present in only 2 patients (P of HWE = 0.39). These distributions of the FcγR2A ($P = 0.5$) and FcγR3A ($P = 0.92$) genotypes were not significantly different from those reported for the population of NBL patients reported by Cheung et al. (12).

Clinical response to hu14.18-IL2

The clinical details for this phase II trial have been reported separately (18). Individual response and stratum data are included in Table 3. For the purposes of the associations examined in this report, 5 patients (2, 10, 22, 27, and 29) showed a complete response (CR). These CRs lasted 13, 9, 20, 30, and >35 months, respectively. Two additional patients (3 and 22) were scored as showing stable disease, but showed clear clinical signs of improvement (clearing of all marrow disease and MIBG improvement not quite meeting partial response criteria for patient 3, and resolution of all MIBG-detectable disease with near clearing of marrow disease for patient 22). All 5 patients with CR and the 2 with "improved" status were in stratum 2.

Table 2. KIR receptors and their MHC class I ligands that were determined by genotyping

Receptor	Ligand
KIR2DL1 (CD158a)	HLA-C2 (Cw2, Cw4, Cw5, Cw6, Cw15, Cw1602, Cw17, Cw18)
KIR2DL2/KIR2DL3 (CD158b)	HLA-C1 (Cw1, Cw3, Cw7, Cw8, Cw12, Cw13, Cw14, Cw1601)
KIR3DL1 (CD158e)	HLA-Bw4

Published OnlineFirst October 8, 2010; DOI:10.1158/0008-5472.CAN-10-2211

Table 3. KIR, KIR ligand, FcγR, and response data for each patient

Patient no.	Stratum	KIR genotype	KIR ligand	Match vs mismatch	FcγR2A-131	FcγR3A -158	Response
1	1	2DL1, 2DL2/2DL3, 3DL1	Cw1, Cw5, Bw4	M	R/R	F/V	PD
2	2	2DL1, 2DL2/2DL3, 3DL1	Cw1, Cw3, Bw4	MM	R/R	F/V	CR
3	2	2DL1, 2DL3, 3DL1	Cw4, Cw15	MM	H/H	F/V	I
4	2	2DL1, 2DL2/2DL3, 3DL1	Cw2, Cw8, Bw4	M	R/R	F/V	SD
5	2	2DL1, 2DL2/2DL3, 3DL1	Cw7, Cw16, Bw4	MM	R/R	F/V	PD
6	2	2DL1, 2DL3, 3DL1	Cw6, Cw7	MM	H/H	F/V	PD
7	2	2DL1, 2DL2/2DL3, 3DL1	Cw7	MM	H/H	F/V	PD
8	2	2DL1, 2DL3, 3DL1	Cw12, Bw4	MM	R/R	[b]	PD
9	2	2DL1, 2DL2/2DL3, 3DL1	Cw6, Cw7, Bw4	M	R/R	F/V	PD
10	2	2DL1, 2DL3, 3DL1	Cw4, Cw7	MM	H/H	F/F	CR
11	1	2DL1, 2DL3, 3DL1	Cw5, Bw4	MM	R/R	F/F	PD
12[a]							
13	1	2DL1, 2DL3, 3DL1	Cw2, Cw7, Bw4	M	H/R	F/V	NE
14	2	2DL1, 2DL2/2DL3, 3DL1	Cw3, Cw6, Bw4	M	H/R	F/F	PD
15	2	2DL1, 2DL3, 3DL1	Cw7	MM	H/H	F/F	PD
16	2	2DL1, 2DL3, 3DL1	Cw12, Cw16, Bw4	MM	R/R	F/V	PD
17	1	2DL1, 2DL2/2DL3, 3DL1	Cw2, Cw16	MM	H/R	V/V	SD
18	1	2DL1, 2DL3,	Cw4, Bw4	MM	H/R	F/F	PD
19	1	2DL1, 2DL2/2DL3, 3DL1	Cw2, Cw7, Bw4	M	H/H	F/V	SD
20	1	2DL1, 2DL2/2DL3, 3DL1	Cw7, Bw4	MM	R/R	V/V	PD
21	2	2DL1, 2DL2/2DL3, 3DL1	Cw4, Cw6, Bw4	MM	H/R	F/V	I
22	2	2DL1, 2DL2/2DL3, 3DL1	Cw5, Bw4	MM	H/H	F/F	CR
23	2	2DL1, 2DL3, 3DL1	Cw8, Cw15	MM	H/R	F/F	PD
24	1	2DL1, 2DL2/2DL3, 3DL1	Cw2, Cw3, Bw4	M	H/R	F/F	NR
25	2	2DL1, 2DL3, 3DL1	Cw5, Bw4	MM	R/R	F/F	SD
26	2	2DL1, 2DL2/2DL3, 3DL1	Cw2, Cw6, Bw4	MM	H/R	F/V	PD
27	2	2DL1, 2DL3, 3DL1	Cw12, Cw16, Bw4	MM	H/H	F/V	CR
28	1	2DL1, 2DL2/2DL3, 3DL1	Cw6, Cw8, Bw4	M	H/R	F/V	PD
29	2	2DL1, 2DL3, 3DL1	Cw5, Cw7	MM	R/R	F/V	CR
30	1	2DL1, 2DL2/2DL3, 3DL1	Cw12, Cw15, Bw4	M	H/H	F/F	PD
31	1	2DL1, 2DL3, 3DL1	Cw4, Cw7	MM	H/R	F/F	PD
32	2	2DL1, 2DL3, 3DL1	Cw6, Cw7, Bw4	M	H/R	F/V	PD
33	2	2DL1, 2DL3, 3DL1	Cw6, Cw7, Bw4	M	R/R	F/F	PD
34	2	2DL2, 3DL1	Cw12, Cw17	MM	H/R	F/F	PD
35	2	2DL1, 2DL2, 3DL1	Cw6, Cw7	MM	H/R	[b]	PD
36	2	2DL1, 2DL2/2DL3, 3DL1	Cw3, Cw7, Bw4	M	H/H	F/F	PD
37	1	2DL1, 2DL3, 3DL1	Cw3, Cw14, Bw4	MM	H/R	F/F	PD
38	1	2DL1, 2DL3, 3DL1	Cw4, Cw7, Bw4	M	H/R	F/F	PD
39	1	2DL1, 2DL2/2DL3, 3DL1	Cw6, Cw7, Bw4	M	H/R	F/F	PD

[a]Patient 12 not included, DNA was not available.

[b]FcγR3A genotyping results from patients 8 and 35 excluded from analysis due to discrepancy in results of pyrosequencing and TaqMan.

Abbreviations: CR, complete response; I, (clinically) improved; M, match; MM, mismatch; PD, progressive disease; SD, stable disease.

Associations between clinical response and genotype data

KIR. The analyses of KIR/KIR-ligand mismatch and FcγR genotyping data for clinical associations are summarized in Tables 5–7. All 7 patients who responded (5 of 38) or showed improvement (2 of 38) following IC therapy were mismatched for their KIR/KIR-ligand genotypes (i.e., lacked HLA ligand for at least 1 of their KIR genes; Table 5, Mismatch versus response/improvement of all patients). In contrast, none of the 14 KIR/KIR-ligand matched patients demonstrated any response or improvement. Thus, KIR/KIR-ligand mismatch was associated with clinical response/improvement following

Published OnlineFirst October 8, 2010; DOI:10.1158/0008-5472.CAN-10-2211

Table 4. Distribution of genotypes for KIR mismatch/match and FcγR genotypes among the 38 patients evaluated

KIR Mismatch: 24/38 (63%)	KIR Match: 14/38 (37%)		$P = 0.93$[a*]
FcγR2A 131-H/H: 10/38 (26%)	FcγR2A 131-H/R: 16/38 (42%)	FcγR2A 131-R/R: 12/38 (32%)	$P = 0.5$[b]
FcγR3A 158-F/F: 17/36 (47%)	FcγR3A 158-F/V: 17/36 (47%)	FcγR3A 158-V/V: 2/36 (6%)	P[c] $= 0.92$[b]

[a]*P* value for the difference in distribution of KIR match/mismatch for this population versus comparable population of NBL patients evaluated for KIR match/mismatch by Venstrom et al. (5).
[b]*P* value for the difference in distribution of FcγR genotypes for this population versus that of comparable NBL patients described by Cheung et al. (12).
[c]*P* value remains 0.79 to 1.0 regardless of whether patients 8 and 35 are FF or FV and included.

IC treatment ($P = 0.03$). When this same analysis was done for the 24 stratum 2 patients, there was a trend (that did not meet criteria for statistical significance) toward a similar association of mismatch and response/improvement (7 of 7) versus nonimprovement (11 of 17) ($P = 0.13$, Table 5, Mismatch versus response/improvement for patients in stratum 2 only). In addition, there appeared to be a greater fraction of KIR/KIR-ligand mismatched patients enrolled in stratum 2 (18 of 24, 75%) than in stratum 1 (6 of 14, 43%) with marginal statistical significance ($P = 0.08$, Table 5, Mismatch versus both strata 1 and 2).

FcγR. The FcγR2A genotype data analysis for association with response suggests, with marginal statistical significance, that patients with the H/H genotype showed a higher likelihood of response/improvement (Table 6, $P = 0.06$). In contrast, there was no suggestion of association between FcγR3A genotype and response/improvement to IC ($P = 1.0$, Table 7).

Discussion

NK-mediated lysis of NBL cell lines *in vitro* is augmented by the addition of IL2 (20), especially when using NK cells from patients receiving IL2 (21). Furthermore, NK-mediated antibody dependent cell-mediated cytotoxicity (ADCC) is augmented when the NK cells are obtained following *in vivo* administration of IL2 (22). Initial studies with chimeric anti-GD2 antibody, ch14.18, fused with human IL-2 (ch14.18-IL2), demonstrated NK-mediated regression of local and disseminated murine NBL (15). Similar results were later seen in murine NBL models with administration of hu14.18-IL2 (16). As escape from this NK-mediated response to

Table 5. Tests of association of mismatch versus response/improvement of all patients, response/improvement for patients in stratum 2 only, and both stratum 1 and stratum 2

	KIR-mismatch	KIR-match	Total
Mismatch vs response/improvement (strata 1 and 2)[a]			
Response/improvement	7 (29%)	0 (0%)	7
No response/no improvement	17 (71%)	14 (100%)	31
Total	24	14	38
Mismatch vs response (stratum 2 only)[b]			
Response/improvement	7 (39%)	0 (0%)	7
No response/no improvement	11 (61%)	6 (100%)	17
Total	18	6	24
	Stratum 1	**Stratum 2**	**Total**
Mismatch vs stratum (strata 1 and 2)[c]			
KIR-mismatch	6 (43%)	18 (75%)	24
KIR-match	8 (57%)	6 (25%)	14
Total	14	24	38

[a]$P = 0.03$.
[b]$P = 0.13$.
[c]$P = 0.08$.

Published OnlineFirst October 8, 2010; DOI:10.1158/0008-5472.CAN-10-2211

Table 6. Response/Improvement for patients with higher-affinity receptor genotype (H/H) for FcγR2A-131 versus other 2 genotypes (H/R and R/R)

FcγR2A	HH	HR + RR	Total
Response/improvement	4 (40%)	3 (11%)	7
Nonresponse/nonimprovement	6 (60%)	25 (89%)	31
Total	10	28	38

$P = 0.06$.

hu14.18-IL2 was associated with upregulation of MHC class I on NBL cells (known to induce inhibitory responses via Ly-49 receptors on murine NK cells) (17), we hypothesized that similar relationships may influence the clinical response to hu14.18-IL2. To test this hypothesis, it was first necessary to identify a population that shows some clinical response to hu14.18-IL2.

Our recently reported phase II study of hu14.18-IL2 in patients with relapsed or refractory NBL demonstrated CR or improved disease in 7 of 38 treated patients (18). All 7 of these responding/improved patients were in stratum 2 (evaluable but not radiographically measurable disease), consistent with our preclinical data showing greater detection of antitumor activity in animals with less tumor burden (16). Although the role of KIRs has been evaluated in the setting of autologous and allogeneic stem cell transplantation and infusions of allogeneic NK cells following lymphodepletive chemotherapy (1–6), it has not been studied for association with antitumor response in patients receiving only cytokines or mAbs for immunotherapy. We hypothesized that children with recurrent/refractory NBL, who received the hu14.18-IL2 in our phase II COG study, would demonstrate greater response to IC in the presence of KIR/KIR-ligand mismatch. When the data were analyzed for all 38 patients who had provided DNA samples, 24 of them were found to be KIR/KIR-ligand mismatched, and all 7 of the responding or improved patients were found in this group ($P = 0.03$, Table 5, Mismatch versus response/improvement of all patients). Because the KIR/KIR-ligand interaction is primarily a mechanism controlling NK cell activity, this result is consistent with the murine data showing that the anti-NBL effect of ch14.18-IL2 and hu14.18-IL2 is primarily mediated by NK cells (15–17). Even prior to the administration of hu14.18-IL2, there is a trend toward greater KIR/KIR-ligand mismatch in the patients who enter stratum 2 than in stratum 1 ($P = 0.08$, Table 5, Mismatch versus both strata 1 and 2). If additional data validate this trend, it would suggest that a child's endogenous KIR/KIR-ligand status might play a role in the clinical pattern of relapse; namely, the patients who are KIR-mismatched may be less likely to relapse with "bulky" (measurable/stratum 1) disease. Similarly, if additional data validate the trend ($P = 0.13$) that KIR/KIR-ligand mismatch is associated with response within Stratum 2 patients (Table 5, Mismatch versus response/improvement for patients in stratum 2 only); the presence of Stratum 2 status and KIR/KIR-ligand mismatch might be considered as eligibility criteria for future treatment with hu14.18-IL2 for children with relapsed or refractory NBL.

The roles of the activating Fc receptors involved in ADCC, FcγR2A ,and FcγR3A, have been demonstrated in response to rituximab, cetuximab, and trastuzumab (7–11). Cheung et al. (12) have found an association between FcγR2A polymorphism and outcome of NBL patients receiving the murine anti-GD2 IgG3 antibody, 3F8, but only when given in combination with GM-CSF. This result suggests that when neutrophils or monocytes/macrophages are activated with GM-CSF, they facilitate clinically meaningful ADCC via the high-affinity alleles of FcγR2A for 3F8 (12). This response was unlikely to be NK-mediated, as FcγR2A is not present on NK cells. As preclinical data and our current results (Table 5, Mismatch versus response/improvement of all patients) suggest that NK cells are playing a role in the clinical response to hu14.18-IL2 in NBL patients, we initially hypothesized that the response/improvement of NBL patients to the IgG1-containing IC might be associated with the presence of the high-affinity FcγR3A 158-V/V genotype (influencing NK function), and not the high-affinity FcγR2A 131-H/H genotype reflecting neutrophil and macrophage ADCC. However, we found that patients with the H/H genotype for FcγR2A did show a trend toward higher

Table 7. Response/Improvement for patients with higher-affinity receptor genotype (V/V) for FcγR3A-158 veersus other 2 genotypes (V/F and F/F)

FcγR3A	VV	VF + FF	Total
Response/improvement	0 (0%)	7 (21%)	7
Non-Response/Non-improvement	2 (100%)	27 (79%)	29
Total	2	34[a]	36

$P = 1.0$.

[a]*P* value remains 1.0 regardless of whether patients 8 and 35 (both FF or FV) are included.

Published OnlineFirst October 8, 2010; DOI:10.1158/0008-5472.CAN-10-2211

response rate, which was of marginal statistical significance ($P = 0.06$). Clearly these comparisons are underpowered. Even so, the near significant association of improvement with the FcγR2A 131-H/H genotype would be consistent with the activation of some neutrophil or macrophage-mediated ADCC. IL2 treatment is known to induce release of GM-CSF by IL2 responsive cells (23), and it is possible that activation of ADCC by these FcγR2A-bearing cells is resulting from GM-CSF production stimulated by the IL2 component of the IC.

Given the infrequency of the FcγR3A 158-V/V genotype in the general population, with only 2 of our 36 genotyped patients identified with this genotype, it is no surprise that a statistically significant association was not seen between this genotype and response. However, this lack of statistical significance cannot be equated with the lack of proof in this study due to inadequate sample size with a highly unbalanced design. Even so, it may be surprising that none of the 7 patients who showed response or improvement had this V/V genotype. This very preliminary result would suggest that there may not be an association between the V/V genotype and improvement in this population when treated with hu14.18-IL2. The lack of an association with FcγR3A alleles and response (even if confirmed in a larger sample) does not necessarily indicate that NK cells are uninvolved in mediating ADCC. Rather, it could suggest that there is no advantage for high versus lower affinity FcγR3A alleles in this setting of IC-mediated ADCC. We have recently shown that some NK cells can use their IL2 receptors to recognize the membrane-bound IL2 on tumor cells coated with tumor-reactive IC (Gubbels et al., submitted manuscript). This results in NK adhesion to the IC-coated tumor cells, activation of an immune synapse, and subsequent tumor cell destruction, apparently without requiring Fc receptors (Buhtoiarov et al., submitted manuscript). In the face of this IL2 receptor–facilitated IC-mediated killing, high-affinity FcγRs on the NK cells might not be needed. In other words, although high-affinity FcγRs play an important role in the clinical effects of FcR-mediated ADCC using conventional mAbs, they might not be as important for NK mediated antitumor effects of ICs. This might enable NK cells with the F/V or F/F FcγR3A alleles to mediate comparable *in vivo* destruction to that mediated by cells with V/V alleles. Clearly, these are speculative hypotheses as the results were obtained from a limited number of subjects and must be extended to a larger population to draw firmer conclusions.

The COG plans to perform a follow-up study of hu14.18-IL2 in stratum 2 patients, to further characterize these responses. That follow-up study should provide additional data to better test the associations analyzed in this report. Furthermore, the KIR/KIR-ligand mismatch might also be further tested by genotyping of subjects participating in larger trials of clinically effective mAbs that mediate ADCC, such as ch14.18, rituximab, cetuximab, and trastuzumab (7–11).

In summary, we conclude that response or improvement of relapsed or refractory NBL patients following treatment with hu14.18-IL2 is associated with KIR receptor–ligand mismatch, consistent with a role for NK cells in this clinical response. Although there appears to be no statistical significance of FcγR genotype in response of NBL patients to IC in this COG trial, further clinical and *in vitro* data are needed to better clarify the potential roles of FcγR2A and FcγR3A in these clinical responses.

Disclosure of Potential Conflicts of Interest

No potential conflict of interest was disclosed.

Acknowledgments

We thank Dr. Toby Hecht and the NCI Biological Resources Branch for their provision, through a MCRADA with Merck Serono KGAa of Darmstadt, Germany, of the clinical grade hu14.18-IL2 used for this clinical trial, Bill Clements, Stuart McMillan, and Drs. Claudia Herrman, Jens Oliver Funk, and Jean Henslee Downey of Merck Serono/EMD Serono for their input and help in this clinical study, the physicians and researchers from the COG institutions that entered patients into this trial, the participating patients and their families, and Dr. Bartosz Grzywacz for helpful discussion and editing.

Grant Support

This work was supported by U10CA98543 COG Group Chair Grant, U10 CA98413 COG Statistics and Data Center, R01-CA-32685–25, P30-CA14520, CA87025, CA81403, RR03186, K12 CA087718, and grants from the Midwest Athletes for Childhood Cancer Fund, The Crawdaddy Foundation, The St. Baldrick's Foundation, The Evan Dunbar Foundation, and Abbie's Fund.

Received 07/01/2010; revised 09/03/2010; accepted 09/21/2010; published OnlineFirst 10/08/2010.

References

1. Ruggeri L, Capanni M, Casucci M, Volpi I, Tosti A, Perruccio K, et al. Role of natural killer cell alloreactivity in HLA-mismatched hematopoietic stem cell transplantation. Blood 1999;94:333–9.
2. Leung W, Iyengar R, Turner V, Lang P, Bader P, Conn P, et al. Determinants of antileukemia effects of allogeneic NK cells. J Immunol 2004;172:644–50.
3. Hsu KC, Keever-Taylor CA, Wilton A, Pinto C, Heller G, Arkun K, et al. Improved outcome in HLA-identical sibling hematopoietic stem-cell transplantation for acute myelogenous leukemia predicted by KIR and HLA genotypes. Blood 2005;105:4878–84.
4. Leung W, Handgretinger R, Iyengar R, Turner V, Holladay MS, Hale GA. Inhibitory KIR-HLA receptor-ligand mismatch in autologous haematopoietic stem cell transplantation for solid tumour and lymphoma. Br J Cancer 2007;97:539–42.
5. Venstrom JM, Zheng J, Noor N, Danis KE, Yeh AW, Cheung IY, et al. KIR and HLA genotypes are associated with disease progression and survival following autologous hematopoietic stem cell transplantation for high-risk neuroblastoma. Clin Cancer Res. 2009;15:7330–4.
6. Miller JS, Soignier Y, Panoskaltsis-Mortari A, McNearney SA, Yun GH, Fautsch SK, et al. Successful adoptive transfer and in vivo expansion of human haploidentical NK cells in patients with cancer. Blood 2005;105:3051–7.
7. Cartron G, Dacheux L, Salles G, Solal-Celigny P, Bardos P, Colombat P, et al. Therapeutic activity of humanized anti-CD20 monoclonal antibody and polymorphism in IgG Fc receptor FcgammaRIIIa gene. Blood 2002;99:754–8.
8. Weng WK, Levy R. Two immunoglobulin G fragment C receptor polymorphisms independently predict response to rituximab

Published OnlineFirst October 8, 2010; DOI:10.1158/0008-5472.CAN-10-2211

in patients with follicular lymphoma. J Clin Oncol 2003;21: 3940–7.
9. Paiva M, Marques H, Martins A, Ferreira P, Catarino R, Medeiros R. FcgammaRIIa polymorphism and clinical response to rituximab in non-Hodgkin lymphoma patients. Cancer Genet Cytogenet 2008;183:35–40.
10. Zhang W, Gordon M, Schultheis AM, Yang DY, Nagashima F, Azuma M, et al. FCGR2A and FCGR3A polymorphisms associated with clinical outcome of epidermal growth factor receptor expressing metastatic colorectal cancer patients treated with single-agent cetuximab. J Clin Oncol 2007;25:3712–8.
11. Musolino A, Naldi N, Bortesi B, Pezzuolo D, Capelletti M, Missale G, et al. Immunoglobulin G fragment C receptor polymorphisms and clinical efficacy of trastuzumab-based therapy in patients with HER-2/neu-positive metastatic breast cancer. J Clin Oncol 2008;26:1789–96.
12. Cheung NK, Sowers R, Vickers AJ, Cheung IY, Kushner BH, Gorlick R. FCGR2A polymorphism is correlated with clinical outcome after immunotherapy of neuroblastoma with anti-GD2 antibody and granulocyte macrophage colony-stimulating factor. J Clin Oncol 2006;24:2885–90.
13. Yu AL, Gilman AL, Ozkaynak MF, London WB, Kreissman S, Chen H, et al. Chimeric anti-GD2 antibody with GM-CSF, IL2 and 13-cis retinoic acid for high-risk neuroblastoma: a Children's Oncology Group (COG) phase 3 study. New Engl J Med 2010;363:1324–34.
14. Lode HN, Xiang R, Varki NM, Dolman CS, Gillies SD, Reisfeld RA. Targeted interleukin-2 therapy for spontaneous neuroblastoma metastases to bone marrow. J Natl Cancer Inst 1997;89:1586–94.
15. Lode HN, Xiang R, Dreier T, Varki NM, Gillies SD, Reisfeld RA. Natural killer cell-mediated eradication of neuroblastoma metastases to bone marrow by targeted interleukin-2 therapy. Blood 1998;91:1706–15.
16. Neal ZC, Yang JC, Rakhmilevich AL, Buhtoiarov IN, Lum HE, Imboden M, et al. Enhanced activity of hu14.18-IL2 immunocytokine against murine NXS2 neuroblastoma when combined with interleukin 2 therapy. Clin Cancer Res 2004;10:4839–47.
17. Neal ZC, Imboden M, Rakhmilevich AL, Kim KM, Hank JA, Surfus J, et al. NXS2 murine neuroblastomas express increased levels of MHC class I antigens upon recurrence following NK-dependent immunotherapy. Cancer Immunol Immunother 2004;53:41–52.
18. Shusterman S, London WB, Gillies SD, Hank JA, Voss S, Seeger RC, et al.. Anti-tumor activity of hu14.18-IL2 in relapsed/refractory neuroblastoma patients: a Children's Oncology Group (COG) phase II study. J Clin Oncology. Epub 2010 Oct 4.
19. Ronaghi M, Elahi E. Discovery of single nucleotide polymorphisms and mutations by pyrosequencing. Comp Funct Genomics 2002; 3:51–6.
20. Rossi AR, Peridle F, Rashleigh S, Janiec J, Djeu JY. Lysis of neuroblastoma cell lines by human natural killer cells activated by interleukin-2 and interleukin-12. Blood 1994;83:1323–8.
21. Hank JA, Weil-Hillman G, Surfus JE, Sosman JA, Sondel PM. Addition of interleukin-2 in vitro augments detection of lymphokine-activated killer activity generated in vivo. Cancer Immunol Immunother 1990; 31:53–9.
22. Hank JA, Robinson RR, Surfus J, Mueller BM, Reisfeld RA, Cheung NK, et al. Augmentation of antibody dependent cell mediated cytotoxicity following in vivo therapy with recombinant interleukin 2. Cancer Res 1990;50:5234–9.
23. Heslop HE, Duncombe AS, Reittie JE, Bello-Fernandez C, Gottlieb DJ, Prentice HG, et al. Interleukin 2 infusion induces haemopoietic growth factors and modifies marrow regeneration after chemotherapy or autologous marrow transplantation. Br J Haematol 1991; 77:237–44.

A.3 The Anti-tumor Effect of Resveratrol Alone or in Combination with Immunotherapy in a Neuroblastoma Model

Published in final edited form as:
Cancer Immunol Immunother. 2011 May ; 60(5): 731–738. doi:10.1007/s00262-011-0971-0.

The anti-tumor effect of resveratrol alone or in combination with immunotherapy in a neuroblastoma model

Brenda L. Soto[1], **Jacquelyn A. Hank**[1,5], **Tyler J. Van De Voort**[1], **Lalita Subramanian**[3], **Arthur S. Polans**[3], **Alexander L. Rakhmilevich**[1,5], **Richard K. Yang**[1], **Songwong Seo**[5], **KyungMann Kim**[4,5], **Ralph A. Reisfeld**[6], **Stephen D. Gillies**[7], and **Paul M. Sondel**[1,2,5]

[1]Department of Human Oncology, University of Wisconsin, Madison, WI 53792

[2]Department of Pediatrics, University of Wisconsin, Madison, WI 53792

[3]Ophthalmology Department, University of Wisconsin, Madison, WI 53792

[4]Department of Biostatistics and Medical Informatics, University of Wisconsin, Madison, WI 53792

[5]Paul Carbone Comprehensive Cancer Center, University of Wisconsin, Madison, WI 53792

[6]Scripps Research Institute, La Jolla, CA 92037

[7]Provenance Biopharmaceuticals Corp. Waltham MA

Abstract

We investigated the anti-tumor effect of peritumoral resveratrol in combination with immunotherapy *in vivo* in neuroblastoma-bearing mice. Subcutaneous NXS2 tumors were induced in A/J mice. On day 10 some mice received 15mcg of intravenous immunocytokine for 5 days, mice received of 20mg of peritumoral resveratrol twice a week (starting on day 12) for a total of 5 injections, and a separate group received a combination of both regimens. Tumor progression and survival were assessed every 3–4 days. Blood and primary tumor tissue samples were collected on day 20 for Complete Blood Count and CD45 immunohistochemistry and histology, respectively. The primary tumor regressed in all mice receiving peritumoral resveratrol. Most of these mice receiving peritumoral resveratrol alone developed metastatic tumors and recurrence of the primary tumor after cessation of therapy. When resveratrol and immunocytokine regimens were combined, 61% of the mice receiving this combination therapy resolved their primary tumors and survived without developing metastatic tumors, compared to 15% and 13% receiving resveratrol or immunocytokine alone, respectively. None of the therapeutic regimes prevented lymphocyte infiltration or affected the Complete Blood Count. Greater necrosis was observed microscopically in tumors from mice receiving the combination therapy. These results demonstrate that the combination therapy of peritumoral resveratrol plus intravenous immunocytokine provides better anti-tumor effects in this model than either therapy alone.

Keywords

Resveratrol; Immunocytokine; anti-GD2 antibody; Neuroblastoma; hu14.18-IL2

Address correspondence to: Paul M. Sondel MD, PhD, Wisconsin Institute for Medical Research-Room 4159, 1111 Highland Avenue, Madison WI, 53705-2275, pmsondel@humonc.wisc.edu.

Information of the graphics programs used to create the figures
Figure #1 was created using Excel Chart Wizard based on SAS 9.1 software outpout.
Figure #2 was created using Kaplan-Meier plot using R 2.5.0 software
Figure #5 was created using Excel Chart Wizard

Introduction

Resveratrol (RV), a natural compound found in red wine, some fruits and nuts, has shown anti-tumor activity in concentrations and regimens that appear to show minimal toxicity to normal cells [1]. RV slows tumor growth and, depending on the dose and route of administration, can also lead to the regression of local tumors [1–2]. The anti-tumor action of RV has been tested in mice bearing different types of malignant tumors such as breast, lung, liver, melanoma and neuroblastoma [3–6]. This study on the anti-tumor activity of RV combined with immunotherapy is focused on neuroblastoma because $GD2^+$ mouse NXS2 neuroblastoma has been a useful model of cancer immunotherapy with hu14.18-IL2 immunicytokine (IC) in our preclinical studies [7–8].

Neuroblastoma (NB) is the most common pediatric extra cranial solid tumor. Current therapies against NB are able to induce remissions or significant responses in most patients but unfortunately they do not prevent recurrence of the disease in the majority of patients with high risk factors [9]. Also the ability to add additional chemotherapy agents is limited due to the cumulative toxicity to normal cells [10–11]. Our group is involved in the development of a novel immunotherapy based on a fusion protein composed of a humanized IgG mAb linked to interleukin-2 (IL-2), known as the hu14.18-IL2 immunocytokine (IC) [8]. The mAb component of this IC recognizes GD2, a disialoganglioside expressed with relatively little heterogeneity and at high density on the cell surface of tumors of neuroectodermal origin such as melanoma and NB. The proposed mechanisms of action of this IC involve recruitment of IL-2 receptor- and Fc receptor- positive immune cells to the tumor microenvironment where it facilitates tumor-specific cell destruction mainly via antibody dependent cell-mediated cytotoxicity (ADCC) executed by NK cells [12]. When this IC is injected i.v. in tumor-bearing mice it has anti-tumor activity against small subcutaneous tumors [13–14] and is able to prevent or reduce the development of metastatic tumors induced experimentally or arising spontaneously [7].

Studies on combinations of RV with chemotherapeutic agents, suggest that RV, in addition to being a tumor growth inhibitor, may also enhance the antitumor effect of other agents [15–18]. RV improved the anti-tumor activity of 5-FU when given to mice carrying lung tumors [18]. The strategy of using RV in combination with other cancer therapeutics may hold a clinical promise. In this study, we aimed to determine whether RV can act synergistically with IC to result in enhanced anti-tumor effects, than observed with either agent alone.

The antitumor response induced by the hu14.18-IL2 IC is dependent on functional NK cells. RV can cause concentration-dependent immunosuppression *in vitro* to certain components of the immune system; while systemic *in vivo* immunosuppression has not been reproducibly observed after RV treatment in certain mouse models [19–22]. This discrepancy may be due to the different doses used *in vitro* and the level of RV achieved *in vivo* following systemic administration. The concentrations exerting anti-tumor and immunosuppressive activity *in vitro* are about 25 to 50 fold higher than the peak plasma levels of RV [~1 micromolar (mcM)] after systemic administration [1]. In separate *in vitro studies*, concentrations of RV ≥ 25 mcM inhibited cell proliferation, blocked DNA synthesis and induced G1 phase arrest in tumor and immune cells. In addition, RV at 12–50 mcM inhibits antibody dependent cell mediated cytotoxicity (ADCC) of tumor cells facilitated by the IC. In contrast, 1–10 mcM RV had no inhibitory effects in these proliferative and ADCC assays [1] (see footnote at end of discussion). *In vivo* studies using systemic RV regimens as anti-tumor therapy showed that RV can slow tumor growth but does not induce tumor regression [1–2]. The *in vivo* activity of RV may be limited by amount or dose of RV actually reaching the tumor. One way of increasing the RV content in the tumor

environment is by directly injecting RV into the tissues surrounding the tumor. van Ginkel *et al*. previously used this approach by injecting 5mg RV peritumorally (p.t.) to xenografts models of human neuroblastoma [1]. This route of RV administration was able to provide a robust anti-tumor effect, achieving tumor regression without causing toxicity to the mice. In this report we confirm and extend these findings by demonstrating temporal regression of subcutaneous NXS2 murine neuroblastoma in syngeneic mice after local RV treatment. Moreover, we show that a combination of RV with IC immunotherapy prevents tumor recurrence and metastases in the majority of the treated mice.

Here we report on: 1) the action of RV administered by direct injection locally into the tissues surrounding a subcutaneous NXS2 murine neuroblastoma tumor (RV was given as single agent therapy and in combination with systemic IC; 2) the effect of local RV on circulating leukocytes as well as the infiltration of $CD45^+$ cells to these tumors; 3) the level of RV in the serum of mice receiving local RV; and 4) the influence of RV *in vitro* on GD2 expression.

Materials and Methods

Cells, media and reagents

NXS2, a GD2-positive murine neuroblastoma cell line was provided by Dr. R. Reisfeld (Scripps Research Institute, La Jolla, CA). Cells were cultured in high glucose Dulbecco's Modified Eagle Medium (DMEM) media supplemented with 10% fetal calf serum, 100 units/ml of penicillin, 100ug/ml streptomycin and 2nM L-glutamine. Media and supplements were purchased from Fisher scientific, Pittsburgh, PA. Cultures were maintained at 37 °C, 5% CO_2. Resveratrol was obtained from Cayman laboratories, Dallas, TX (provided by Dr. A. Polans). The IC was obtained from EMD-Lexigen-Research Center (Billerica, MA). As the concentrations of RV used in this study are not soluble in aqueous solvents, the organic solvent Dimethyl sulfoxide (DMSO) was used. RV diluted in DMSO has been used in *in vivo* studies by others without any reported toxicity to rodents [1].

Mice

Six to eight week-old female A/J mice, were obtained from Jackson Laboratories (Bar Harbor, Maine). All animals were housed in the University of WI AAALAC–approved facilities and handled according to the NIH and UW-Madison Research Animal Resource Center guidelines.

Resveratrol plus IC combination in vivo study

NXS2 tumors were induced in A/J mice (n=86) by injecting 2×10^6 cells in 100mcL PBS subcutaneously (s.c) on the left flank proximal to the spleen. This is designated as the "primary" tumor. On day 10 the average tumor size was between 60–70mm^3 and mice were randomized into 4 groups. One group of mice (n=23) received 15mcg of IC intravenously (i.v.) in 100mcL on days 10 through 14. Two other groups of mice (n=20 each) received a total of 5 p.t. injections of vehicle DMSO or 20mg of resveratrol/injection in 100mcL. These injections were given on days 12, 16, 19, 22 and 26. The 20mg dose was chosen because it showed the best anti-tumor activity on NXS2 upon initial *in vivo* screening compared to other doses (data not shown). The remaining group (n=23) received combination treatment of IC and RV by the same schedule. Tumors were measured every 3–4 days. Tumor volume was determined using the formula: V = (width × length × width/2)= mm^3. Mice were

[8]Brenda L. Soto, Jacquelyn A. Hank, Soesiawati R. Darjatmoko, Arthur S. Polans, Eric M. Yanke, Alexander L. Rakhmilevich, Songwong Seo, KyungMann Kim, Ralph A. Reisfeld, Stephen D. Gillies, and Paul M. Sondel. Anti-tumor and immunomodulatory activity of resveratrol *in vitro* and its potential for future combination cancer immunotherapy. Submitted manuscript, 2010.

observed for survival for 100 days or their primary tumor reached the size required by our animal facility for euthanasia (15mm in any dimension). In this experiment, 2 mice were randomly selected from each treatment group, sacrificed after the third RV injection and blood and tumor were collected, as previously described [1]. Blood was sent to a commercial lab (Marshfield's laboratories, Marshfield WI) for Complete Blood Count (CBC) and differential count. Tumor tissue was used for immunohistochemistry (see below).

Metastasis assessment

Metastatic disease was assessed by mouse necropsy and visual inspection of lymph nodes, lungs and organs in the peritoneum at the time of sacrifice due to progressive disease or when a mouse was found dead. The comparison of metastatic tumor development between groups was not performed, because mice presenting exponential tumor progression (eg. DMSO-treated mice) had to be sacrificed due to their tumor reaching the allowed maximum size before gross metastases were evident

Immunohistochemistry

On day 20 (24-hrs after the third injection of RV), tumors were excised and placed in disposable base molds (Fisher Scientific, Pittsburgh, PA) containing tissue freezing medium (O.C.T.). Tumors were processed and stained by the Experimental Pathology Shared Services of the Carbone Cancer Center at the University of Wisconsin- (Madison, WI). O.C.T. embedded tissue sections were cut at 5 μm on the cryostat, mounted on slides, fixed in acetone for 10 minutes at 4° C, then air dried. Slides were washed three times with PBS. Nonspecific binding was blocked with 10% goat serum in PBS for one hour and endogenous peroxidase was blocked with 0.3% hydrogen peroxide in methanol for 10 minutes. Endogenous biotin was blocked with 0.001% avidin in PBS for ten minutes and the avidin quenched with 0.001% biotin in PBS for ten minutes, both at 25° C. The slides were then incubated with CD45 (Ly-5) rat monoclonal primary antibody (eBioscience, San Diego, CA, 14-0451-85,clone 30F11) at a 1:160 dilution in PBS with 1% goat serum for one hour at 37° C. After washing with PBS, the sections were incubated with biotinylated goat anti-rat (Vector Laboratories, Burlingame, CA) at 1:200 in PBS for one hour at room temperature. Slides were washed in PBS and then incubated 30 minutes at room temperature with Vectastain ABC Elite (Vector Laboratories, Burlingame CA). Following three washes in PBS, slides were developed with DAB (3,3-diaminobenzidine) (Vector Laboratories, Burlingame CA), counterstained with Mayer's hematoxylin, dehydrated and cover slipped with permount. For Hematoxylin and Eosin (H&E) staining a modified version of the routine Mayer's staining protocol [23] was used. Slides containing dried frozen sections were fixed in 100% EtOH for 2 minutes followed by a rinse in tap H_2O for 2 minutes. Sections were stained with Mayer's Hematoxylin, for 15 minutes, then the excess of stain was washed off under running tap H_2O for 20 minutes. Eighty % EtOH was applied for 1 minute and sections were counterstained with Eosin (Surgipath, Richmond, IL) for 30 seconds. The slides were then dipped 3 times in 95% EtOH and once in 100% EtOH for 15 seconds each. Then 100% EtOH was applied to sections for 2 minutes. Xylene was applied 3 times over sections for 2 minutes each. Finally, coverslips were placed over slides with Micromount (Surgipath, Richmond, IL). All reagents and chemicals were obtained from Sigma, St. Louis, MO unless otherwise noted. Slides were blindly photographed by one of the authors using an AxioPhot microscope (Zeiss, Thornwood, New York).

RV concentration in mouse serum

A/J mice (n=4) with subcutaneous NXS2 tumors received a peritumoral injection of 20mg RV. Blood was collected 20 minutes (n=2) or 24 hours (n=2) post-injection. The concentration of RV in the serum was determined as previously described [1].

Detection of GD2 levels by flow cytometry

NXS2 cells (1×10^6) were seeded in 12 well plates (n=4), in duplicate wells, and incubated at 37°C and 5% CO_2 for 3 days with DMSO, 50, 10 or 1mcM RV. At the end of the incubation period cells were washed with PBS and 0.5×10^6 cells were incubated with 1.4mcg of hu14.18-IL2-FITC for 1hr at 4°C. Cells were then washed with PBS and stained with propidium iodine. Twenty thousand viable events were collected using a BD FACSCalibur (San Diego, CA). Data were analyzed using FlowJo (Ashland, OR). MFI ratio was calculated by dividing the geometric mean of the sample by the geometric mean of the isotype control immunocytokine.

Statistical analyses

In order to avoid underestimation of tumor volume due to sacrificed mice, tumor volume among treatment groups was analyzed when ≥ 75% of mice remain alive in each group. These were compared using nonparametric Wilcoxon rank sum test. The survival function of time to death or euthanasia was estimated using the Kaplan-Meier method and compared among treatment groups using logrank test. Bonferonni multiple adjustments were applied when significance was obtained with the above mentioned tests. GD2 level in MFI ratio was compared using one-way analysis of variance (ANOVA). When ANOVA yielded significance, pairwise comparisons using two-tailed t-test were conducted between two groups with no adjustments were made for multiple comparisons.

Results

Combination of RV and IC enhanced anti-tumor activity and improved tumor-free survival

The anti-tumor effects of RV or IC alone and the combination of the two were assessed. Mice were treated with the control vehicle, DMSO, or with 20mg RV given p.t. or with IC given i.v. The combined treatment was IC with RV. The tumors in the mice treated with vehicle-DMSO progressed and grew in an exponential fashion (Fig. 1). The majority of the tumors in mice receiving IC i.v. alone stabilized and did not progress during the time of treatment; however following completion of the i.v. IC treatment, 20 out of 23 tumors progressed. Conversely, all tumors treated with RV regressed. However, 14 of 20 primary tumors recurred approximately one week after cessation of RV treatment. In addition, in 11 of these 20 mice, grossly evident metastatic tumors developed in one or more of the following organs: lymph nodes, liver or kidney (Fig. 2b). Mice also developed metastatic tumors in the lungs and ovaries. For the group receiving the combined IC/RV treatment, the primary tumors all regressed as in the RV alone group (Fig.2a); however, unlike the RV alone group, only 5 of 23 mice receiving the IC/RV combination showed primary tumor recurrence following cessation of treatment and only one of these 5 mice developed grossly evident metastases.

Survival of mice was assessed for 100 days after initial tumor induction (Fig. 3). Sixty-one % of the mice in the combination therapy were alive with no detectable tumor on day 100, compared to 15% and 13% in both RV and IC alone groups, respectively. Overall, the group treated with the combination therapy showed a statistically greater survival (survival with no tumor requiring euthanasia) than that of all other therapy groups. The results from Figures 1 and 3 indicate that RV in combination with IC provides an enhanced anti-tumor activity above that seen by treating with either agent alone. These data are combined from 3 independent experiments which showed similar results.

Influence of RV on leukocyte counts and tumor infiltration

Next we asked if RV treatment affected immune cells. The 20mg p.t. RV regimen was not found to markedly affect the circulating leukocyte population in treated mice; as comparable

white blood cell numbers were obtained from all animals using 2 representative mice from each treatment group on day 20 just after the third RV injection (data not shown). Peritumoral treatment with RV alone did not reduce, but seemed to increase the infiltration of leukocytes into the tumor microenvironment. This was seen in the CD45 staining for infiltrating leukocytes (Fig. 4a and b). The H&E staining revealed that tumors obtained from mice treated with RV alone or in combination with IC, showed areas of significant tumor necrosis(Figures 4f and h) when compared to tissue from tumors treated with DMSO or IC alone (Fig. 4e and g). The tumor tissue destruction was more prominent in tumors from mice receiving combination therapy (Fig. 4h) than RV alone (Fig. 4f). These combined results of the blood counts and histology suggest that the peritumoral injections of RV caused tumor tissue damage without interfering with leukocyte infiltration into the tumor or changing the leukocytes in the circulation. Furthermore the combination of RV and IC appeared to induce more tumor damage than RV alone.

Concentration of RV in mouse serum after peritumoral administration

The concentration of free or un-metabolized RV in the serum of mice receiving 20mg RV by peritumoral injection was determined in the serum obtained following a single injection. At 20 minutes, the serum RV level was 24mcM and at 24 hours the RV level had fallen to 2.8mcM. The RV level in serum 20 minutes after administration is in the range of concentrations known to be immunosuppressive *in vitro*[1] (see footnote at end of discussion) [22], however, in our *in vivo* studies this concentration did not affect the number of circulating lymphocytes and $CD45^+$ cell infiltration to the tumor. These results show that the amount of RV available after local administration is higher than after systemic administration (~1mcM), resulting in tumor cell death at higher concentrations [1].

RV induces increased levels of GD2 in tumor cells in vitro

To determine a possible mechanism of the increased anti-tumor effect of RV with IC (Fig. 1), we asked if RV would upregulate the density of GD2 in tumor cells. To test this, NXS2 tumor cells were incubated with 50mcM and 10mcM RV for 3 days. On day 3 the GD2 content on the cells was assessed by flow cytometry using the IC directly conjugated with FITC.

After incubation of the NXS2 tumor cells with 50mcM RV the GD2 density was significantly higher than the GD2 density seen on cells incubated with the DMSO control (Fig. 5). Cells incubated with RV at 10mcM RV also showed an increase in GD2 when compared with the GD2 expression on cells cultured with the DMSO control. In a separate experiment, media alone and 1mcM RV did not modulate GD2 levels (data not shown). These results indicate that RV induces a concentration-dependent GD2 increase and this increase is seen at 50mcM RV, a concentration previously shown to stop proliferation of NXS2 cells *in vitro*[1] (see footnote at end of discussion).

Discussion

Treatment of mice bearing NXS2 tumors with peritumoral injections of 20mg RV induced tumor regression; however, the animals developed late local recurrence at the primary tumor site as well as metastatic tumors after cessation of RV treatment. We sought to identify an agent to be used in combination with RV that would prevent the development of these recurrent and metastatic tumors. IC therapy, given i.v., lowers the metastatic tumor incidence in mice bearing NXS2 tumors and can be effective against small local tumors [7]. This study was designed to determine if the addition of IC to p.t. treatment with RV could improve survival in NXS2 tumor-bearing animals. NXS2 tumor-bearing mice received RV alone or in combination with IC. The combination of IC plus RV resulted in long term

survival of 61% of the mice. van Ginkel *et al*. demonstrated in a previous study [1], that p.t. RV-treated tumors have significant tumor destruction when examined histologically and compared to tumors treated with DMSO, the RV vehicle. DMSO-treated tumors appeared histologically similar to untreated tumors [1]. We obtained similar results in our NXS2 tumor model, as tumors treated with RV alone or in combination appeared to have marked tumor necrosis. These results indicate that RV causes significant tumor tissue damage *in vivo* and that there is an additional benefit in using the p.t. RV in combination with i.v. IC. As DMSO is not an optimal solvent for clinical administration, other vehicles are being pursued as a vehicle for p.t. RV for subsequent preclinical studies (Polans A. Unpublished).

Resveratrol as a local p.t. treatment induced a robust anti-tumor effect over a period of two weeks. However, during this period of time some tumor cells may have spread and established undetectable or micro-metastatic disease in different tissues, accounting for local and distant recurrences in these mice. Thus, this tumor debulking regimen of local RV provides a scenario for combining with systemic IC immunotherapy. Thus, our results with leukocyte blood counts and histological evaluation of $CD45^+$ cells in s.c. tumors suggest that RV treatment has no effect on systemic leukocyte numbers, but induces local leukocyte infiltration. The IC consists of a tumor specific anti-GD2 antibody linked to two molecules of IL-2. The IL-2 component of the IC induces the activation of lymphocytes through their IL-2 receptors. These may include antigen-specific T cells and NK cells. One of the anti-tumor mechanisms of the IC is ADCC performed mainly by NK cells [7, 12]. Initiating systemic treatment with the IC prior to giving RV may initiate priming of the lymphocytes so that tumor cells that spread systemically before or during local RV treatment are controlled by the activated lymphocytes via ADCC. These disseminated tumor cells are thereby destroyed and unable to establish metastatic sites of tumor. In addition, our *in vitro* data suggest that RV treatment may increase the level of GD2 on the surface of the tumor cells (Fig. 5). RV was shown to induce ceramide accumulation on tumor cell lines [24–26]. Ceramide is a sphingolipid metabolized to gangliosides including GD2. The modulation of GD2 in our cell line by RV may be via ceramide accumulation *in vitro* and this may be one pathway whereby RV causes tumor death as ceramide has been previously implicated in cell death [27–28]. *In vivo* p.t. RV (20mg) treatment may induce accumulation of ceramide in NXS2 tumors and consequently increase the levels of GD2 on the surface of the tumor cells. Thus peritumoral RV in addition to causing direct tumor cell death mightalso render the tumor cell more susceptible to recognition by the anti-GD2 IC and subsequent ADCC due to increased GD2 expression. However, the potential for RV to induce augmented *in vivo* GD2 expression has not yet been studied.

In summary, RV in combination with IC provided an enhanced anti-tumor treatment in this preclinical model as it lowered the tumor burden and increased survival.

Acknowledgments

We would like to acknowledge Ruth Sullivan, Joseph Hardin, and Jane Weeks for their help with histology and immunohistochemistry. This work was supported by R01-CA-32685-25, CA87025, GM67386, UL1RR025011, P30-CA14520 and grants from the Midwest Athletes for Childhood Cancer Fund, the Crawdaddy Foundation, The Evan Dunbar Foundation, Abbie's Fund, the Super Jake Foundation and Matthews Retina Research Foundation.

References

1. van Ginkel PR, Sareen D, Subramanian L, et al. Resveratrol inhibits tumor growth of human neuroblastoma and mediates apoptosis by directly targeting mitochondria. Clin Cancer Res. 2007; 13:5162–5169. [PubMed: 17785572]

2. Chen Y, Tseng SH, Lai HS, Chen WJ. Resveratrol-induced cellular apoptosis and cell cycle arrest in neuroblastoma cells and antitumor effects on neuroblastoma in mice. Surgery. 2004; 136:57–66. [PubMed: 15232540]
3. Busquets S, Ametller E, Fuster G, et al. Resveratrol, a natural diphenol, reduces metastatic growth in an experimental cancer model. Cancer Lett. 2007; 245:144–148. [PubMed: 16466851]
4. Garvin S, Ollinger K, Dabrosin C. Resveratrol induces apoptosis and inhibits angiogenesis in human breast cancer xenografts *in vivo*. Cancer Lett. 2006; 23:113–122. [PubMed: 16356836]
5. Kimura Y, Okuda H. Resveratrol isolated from Polygonum cuspidatum root prevents tumor growth and metastasis to lung and tumor-induced neovascularization in Lewis lung carcinoma-bearing mice. J Nutr. 2001; 131:1844–1849. [PubMed: 11385077]
6. Liu HS, Pan CE, Yang W, Liu XM. Antitumor and immunomodulatory activity of resveratrol on experimentally implanted tumor of H22 in Balb/c mice. World J Gastroenterol. 2003; 9:1474–1476. [PubMed: 12854144]
7. Neal ZC, Yang JC, Rakhmilevich AL, et al. Enhanced activity of hu14.18-IL2 immunocytokine against murine NXS2 neuroblastoma when combined with interleukin 2 therapy. Clin Cancer Res. 2004; 10:4839–4847. [PubMed: 15269160]
8. Yamane BH, Hank JA, Albertini MR, Sondel PM. The development of antibody-IL-2 based immunotherapy with hu14.18-IL2 (EMD-273063) in melanoma and neuroblastoma. Expert Opin Investig Drugs. 2009; 18:991–1000.
9. Laverdière C, Liu Q, Yasui Y, et al. Long-term outcomes in survivors of neuroblastoma: a report from the Childhood Cancer Survivor Study. J Natl Cancer Inst. 2009; 101:1131–1140. [PubMed: 19648511]
10. Peters GJ, van der Vijgh WJ. Protection of normal tissues from the cytotoxic effects of chemotherapy and radiation by amifostine (WR-2721): preclinical aspects. Eur J Cancer. 1995; 31A Suppl 1:S1–S7. [PubMed: 7577093]
11. Siebler T, Shalet SM, Robson H. Effects of chemotherapy on bone metabolism and skeletal growth. Horm Res. 2002; 58 Suppl 1:80–85. [PubMed: 12373019]
12. Hank JA, Robinson RR, Surfus J, et al. Augmentation of antibody dependent cell mediated cytotoxicity following *in vivo* therapy with recombinant Interleukin-2. Cancer Res. 1990; 50:5234–5239. [PubMed: 2386933]
13. Johnson EE, Lum HD, Rakhmilevich AL, et al. Intratumoral immunocytokine treatment results in enhanced antitumor effects. Cancer Immunol Immunother. 2008; 57:1891–1902. [PubMed: 18438664]
14. Neal ZC, Sondel PM, Bates MK, Gillies SD, Herweijer H. Flt3-L gene therapy enhances immunocytokine-mediated antitumor effects and induces long-term memory. Cancer Immunol Immunother. 2007; 56:1765–1774. [PubMed: 17426968]
15. Fuggetta MP, D'Atri S, Lanzilli G, et al. *In vitro* antitumour activity of resveratrol in human melanoma cells sensitive or resistant to temozolomide. Melanoma Res. 2004; 14:189–196. [PubMed: 15179187]
16. Kubota T, Uemura Y, Kobayashi M, Taguchi H. Combined effects of resveratrol and paclitaxel on lung cancer cells. Anticancer Res. 2003; 23:4039–4046. [PubMed: 14666716]
17. Nicolini G, Rigolio R, Miloso M, Bertelli AA, Tredici G. Anti-apoptotic effect of *trans*-resveratrol on paclitaxel-induced apoptosis in the human neuroblastoma SH-SY5Y cell line. Neurosci Lett. 2001; 302:41–44. [PubMed: 11278107]
18. Wu SL, Sun ZJ, Yu L, Meng KW, Qin XL, Pan CE. Effect of resveratrol in combination with 5-FU on murine liver cancer. Pharmacol Res. 2004; 10:3048–3052.
19. Boscolo P, del Signore A, Sabbioni E, et al. Effects of resveratrol on lymphocyte proliferation and cytokine release. Annals of Clinical and Laboratory Science. 2003; 33:226–231. [PubMed: 12817628]
20. Falchetti R, Fuggetta MP, Lanzilli G, Tricarico M, Ravagnan G. Effects of resveratrol on human immune cell function. Life Sciences. 2001; 70:81–96. [PubMed: 11764009]
21. Feng YH, Zhou WL, Wu QL, Li XY, Zhao WM, Zou JP. Low dose of resveratrol enhanced immune response of mice. Acta Pharmacol Sin. 2002; 23:893–897. [PubMed: 12370094]

22. Gao X, Deeb D, Media J, et al. Immunomodulatory activity of resveratrol: discrepant *in vitro* and *in vivo* immunological effects. Biochemical Pharamacology. 2003; 66:2427–2435.

23. Prophet, EB.; Mills, B.; Arrington, JB.; Sobin, LH. Laboratory Methods in Histotechnology. Washington, D.C.: Armed Froces Intitutes of Pathology; p. 53-55.

24. Dolfini E, Roncoroni L, Dogliotti E, et al. Resveratrol impairs the formation of MDA-MB-231 multicellular tumor spheroids concomitant with ceramide accumulation. Cancer Lett. 2007; 249:143–147. [PubMed: 16996206]

25. Signorelli P, Munoz-Olaya JM, Gagliostro V, Casas J, Ghidoni R, Fabriàs G. Dihydroceramide intracellular increase in response to resveratrol treatment mediates autophagy in gastric cancer cells. Cancer Lett. 2009; 282:238–243. [PubMed: 19394759]

26. Ulrich S, Huwiler A, Loitsch S, Schmidt H, Stein JM. De novo ceramide biosynthesis is associated with resveratrol-induced inhibition of ornithine decarboxylase activity. Biochem Pharmacol. 2007; 74:281–289. [PubMed: 17521618]

27. Minutolo F, Sala G, Bagnacani A, et al. Synthesis of a resveratrol analogue with high ceramide-mediated proapoptotic activity on human breast cancer cells. J Med Chem. 2005; 48:6783–6786. [PubMed: 16250636]

28. Scarlatti F, Sala G, Ricci C, et al. Resveratrol sensitization of DU145 prostate cancer cells to ionizing radiation is associated to ceramide increase. Cancer Lett. 2007; 253:124–130. [PubMed: 17321671]

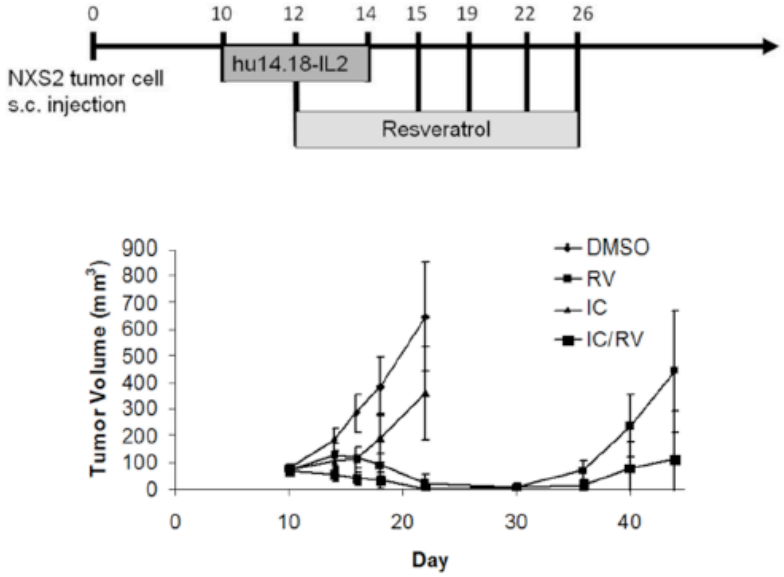

Fig. 1. NXS2 tumor growth in mice receiving IC/RV combination therapy

Mice carrying $GD2^+$ NXS2 tumors were treated with DMSO p.t. (n=20), 20mg RV p.t. (n=20), IC i.v. (n=23) or IC/RV in combination (n=23). Tumors treated with DMSO grew in an exponential fashion. In contrast, tumors treated with RV regressed, but animals developed metastatic tumors and in some animals the primary tumor recurred after cessation of therapy. IC induced anti-tumor activity initially, but eventually tumors progressed. Data shown are tumor volume measurements of the primary tumors at the indicated times. Bars represent the standard deviation. The distribution of tumor volume for the RV group differs from the IC/RV group (p=0.004 on day 44).

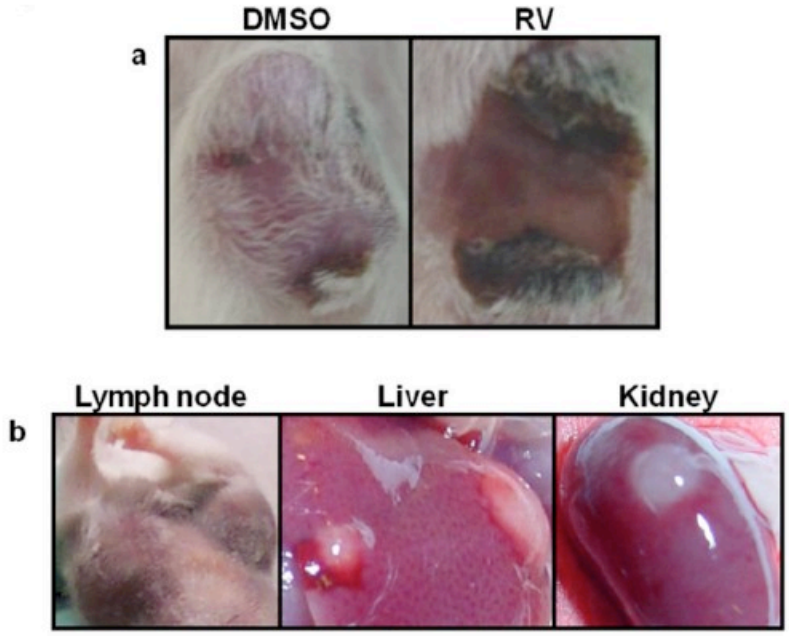

Fig. 2. Representative pictures of primary and metastatic tumors after treatment

Representative pictures of an NXS2 primary tumor from a DMSO-treated and RV-treated mouse (a), and of organs where metastatic tumors were observed after microscopic examination (b), after treatment completion.

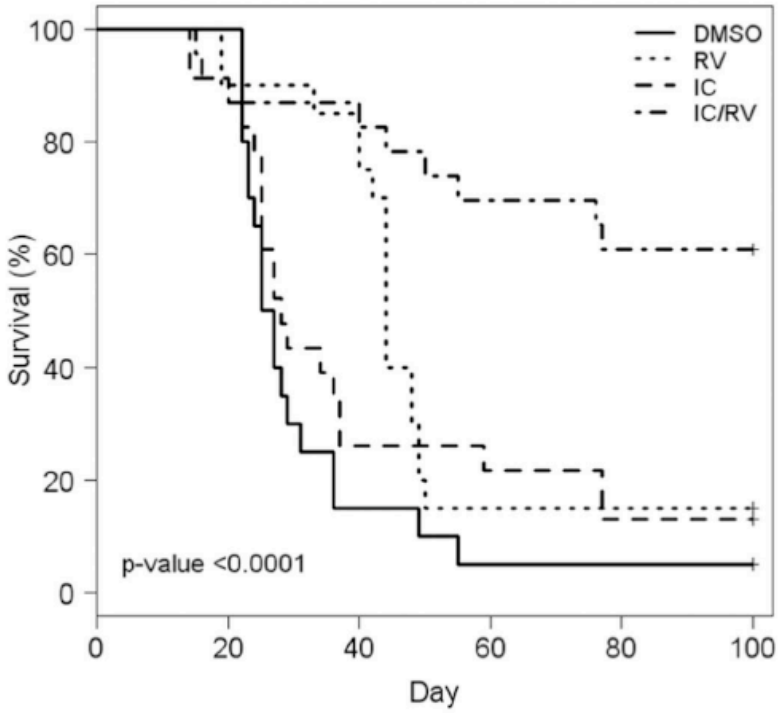

Fig. 3. Survival of mice receiving IC/RV combination therapy

NXS2 tumor-bearing mice were treated with DMSO p.t. (n=20), 20mg RV p.t.(n=20), IC i.v. (n=23) or IC/RV in combination (n=23). Mice were observed for survival for 100 days or until their primary tumor reached the size limit (15mm in any dimension) requiring euthanasia. Sixty-one % of the mice receiving IC/RV combination survived to day 100 with no detectable tumors compared to 15% and 13% of the mice in the RV-alone or the IC-alone group, respectively. There was a significant difference in overall survival among the four treatment groups ($p<0.0001$). Pair-wise comparisons of survival distribution over time: DMSO vs. RV: p=0.005, DMSO vs. IC: p=0.19, DMSO vs. IC/RV: $p<0.0001$, IC/RV vs. IC: p=0.0003, IC/RV vs. RV: p=0.001, RV vs. IC: p=0.16

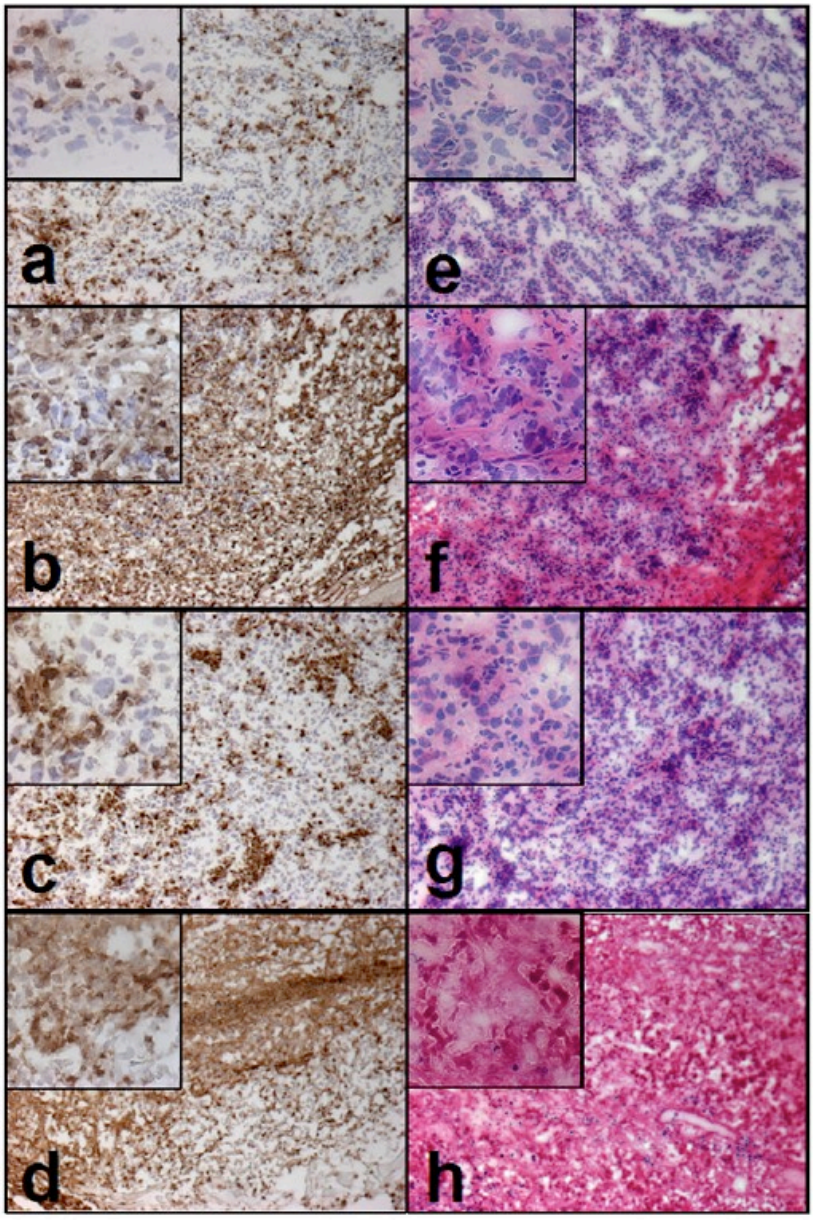

Fig. 4. Immunohistochemistry of tumors from the IC/RV combination study

Tumor tissue was obtained on day 20 from mice treated with p.t. DMSO (a,e), p.t. 20mg RV (b,f), IC i.v. (c,g) or IC/RV in combination (d,h). Tissue was stained with anti-CD45 (a–d) and, H & E (e–f). Pictures were taken on a bright field at 10X, the inserts on each picture are at 40X. Representative fields are show.

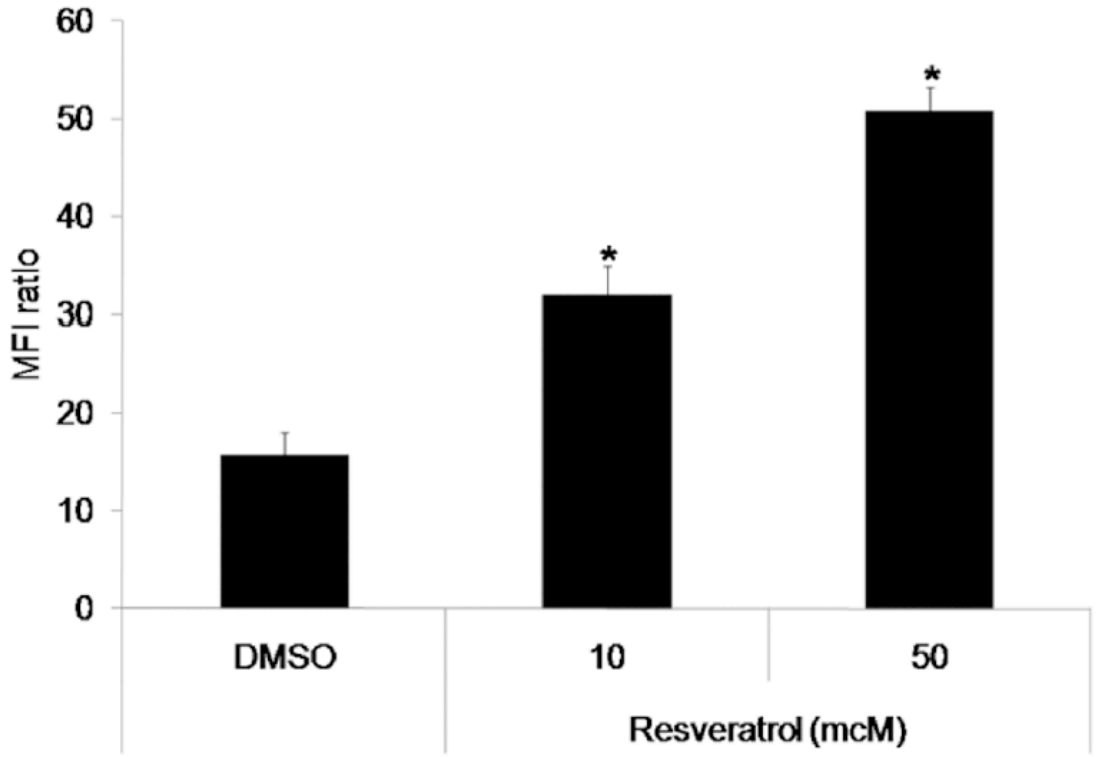

Fig. 5. GD2 levels in tumor cells incubated with RV

NXS2 cells were incubated with DMSO, 50mcM or 10mcM RV for 3 days. On day 3 cells were harvested and analyzed by flow cytometry for GD2 expression. Cells incubated with RV for 3 days showed an increase in GD2 compared to DMSO in a concentration-dependent manner. Bars represent the standard deviation. *p<0.001 vs. DMSO.

A.4 Soluble interleukin-2 receptor α Activation in a Children's Oncology Group Randomized Trial of Interleukin-2 Therapy for Pediatric Acute Myeloid Leukemia

Pediatr Blood Cancer

Soluble Interleukin-2 Receptor α Activation in a Children's Oncology Group Randomized Trial of Interleukin-2 Therapy for Pediatric Acute Myeloid Leukemia

Beverly J. Lange, MD,[1]* Richard K. Yang, BS,[2] Jacek Gan, PhD,[2] Jaquelyn A. Hank, PhD,[2] Eric L. Sievers, MD,[3] Todd A. Alonzo, PhD,[4,5] Robert B. Gerbing, MA,[5] and Paul M. Sondel, MD, PhD[2]

Purpose. To assess associations of soluble IL-2 receptor alpha (sIL-2rα) concentration with outcomes in pediatric acute myeloid leukemia (AML) in a phase 3 trial of IL-2 therapy. ***Procedures.*** We randomized 289 children with AML in first remission after intensive chemotherapy to receive IL-2 infused on days 0–3 and 8–17 (IL-2 group) or no further therapy (AML control group). We measured sequential serum sIL-2rα concentrations in both groups before, during and after therapy in both groups and in reference controls without AML. ***Results.*** Before treatment, mean sIL-2rα concentrations were similar in the IL-2 group and AML controls, but significantly higher than in reference controls. Both AML groups experienced reduction in sIL-2rα concentration after chemotherapy. Thereafter in the IL-2 group, mean sIL-2rα concentration increased from 2,669 pg/ml before IL-2 to 15,534 pg/ml on day 4 ($P < 0.001$) and 10,585 pg/ml on day 18 ($P < 0.001$). In the control group sIL-2rα concentration did not change after 28 days of follow-up. Five-year disease-free survival (DFS) was 51% in the IL-2 group and 58% in the controls ($P = 0.489$) and overall survival was 70% and 73%, respectively ($P = 0.727$). ***Conclusion.*** SIL-2rα concentration was elevated in AML at diagnosis and tended to normalize after chemotherapy. IL-2 infusion significantly increased sIL-2rα concentration, but did not improve DFS or survival in pediatric AML. Furthermore, sIL-2rα concentration was not predictive of outcome before, during or after treatment for AML. Pediatr Blood Cancer

Key words: acute myeloid leukemia; interleukin-2; soluble interleukin-2 receptor alpha

INTRODUCTION

The graft versus leukemia effect of allogeneic hematopoietic stem cell transplantation in acute myeloid leukemia (AML) is mediated by the immune system [1–3]. IL-2 has substantial anti-tumor activity in several cancers in which the immune system contributes to disease control [4–8]. In AML, IL-2 can stimulate proliferation of antigen-specific T cells, can enhance cytolytic activity of natural killer cells against AML targets, and induces activated lymphocytes to release interferon gamma and tumor necrosis factor alpha [4]. Responses to IL-2 are associated with release of the α chain of the tri-molecular αβγ high-affinity IL-2 receptor from the surface of responding lymphocytes [9–12]. The serum concentration of soluble α-chain reflects the extent of in vivo lymphocyte activation by IL-2 and in most cases elevated sIL-2rα is associated with poor prognosis [9,10].

These biologic activities of IL-2 led to many clinical trials of IL-2 therapy in AML and other cancers. Uncontrolled trials of single agent IL-2 with or without autologous stem cell transplantation (ASCT) sometimes reduced tumor burden, occasionally induced remissions and rarely achieved long-term survival [13–15]. While contribution of IL-2 in these uncontrolled studies was not clear, historically controlled studies of IL-2 therapy in adults with AML in remission after chemotherapy or ASCT suggested improvements in outcomes [16–21]. More recent randomized trials in adults with AML have not found any clinical benefits [22,23]. However, none of these trials systematically documented the in vivo immunological activation resulting from IL-2 administration.

The Children's Cancer Group (CCG) conducted a pilot study that demonstrated feasibility of IL-2 infusion following completion of chemotherapy in children in first remission AML and showed correlative increases in soluble IL-2 receptor alpha (sIL-2rα) concentration and NK cell numbers [24]. The subsequent phase 3 trial for newly diagnosed AML patients (CCG-2961) [24], randomized patients in remission after 3 courses of chemotherapy to IL-2 therapy or observation. Serial sIL-2rα concentrations were measured from before treatment, after chemotherapy and after IL-2 or follow-up.

DOI 10.1002/pbc.22966
Published online in Wiley Online Library (wileyonlinelibrary.com).

METHODS

Subjects

CCG-2961 (ClinicalTrials.gov NCT0002798, Combination Chemotherapy With or Without Bone Marrow Transplantation

Additional supporting information may be found in the online version of this article.

[1]The Children's Hospital of Philadelphia, Philadelphia, PA; [2]University of Wisconsin School of Medicine and Public Health, Madison Wisconsin; [3]Fred Hutchison Cancer Center and currently Seattle Genetics, Inc., Seattle, Washington; [4]University of Southern California, Arcadia, California; [5]The Children's Oncology Group, Arcadia, California

Conflicts of Interest: Dr. Sievers' is employed by Seattle Genetics, which has a product that could compete with IL-2. There are not other conflicts.

Author contributions: Beverly Lange, designed and oversaw CCG-2961 and wrote first draft of manuscript; Richard Yang, Jacek Gan, and Jaquelyn A. Hank performed and analyzed laboratory studies on IL-2 receptor and wrote methods section; Eric L. Sievers designed IL-2 clinical trial; Todd A. Alonzo PhD and Robert B. Gerbing MA performed and distributed data analyses and wrote statistical section; Paul M. Sondel designed B-972 correlative trial, oversaw specimen processing and reporting, and wrote background. All authors reviewed data and edited the manuscript.

Grant sponsor: National Institutes of Health; Grant numbers: CA 13539, CA 98543, CA 032685, CA 087025.

*Correspondence to: Beverly J. Lange, MD, Yetta Dietch Novotny Professor in Clinical Oncology, Medical Director of Pediatric Oncology, Children's Hospital of Philadelphia, 4308 Wood Building, Philadelphia, PA 19003. E-mail: lange@email.chop.edu

Received 16 September 2010; Accepted 15 November 2010

in Treating Children With Acute Myelogenous Leukemia or Myelodysplastic Syndrome) was a phase 3 trial for previously untreated AML [25]. Eligible patients were age 1 day to less than 21 years with French-American and -British (FAB) AML subtypes M0-M2 and M4-M7 [26]. CCG-2961 opened in August 1996 and closed in December 2002. Institutional Review Boards approved the study. Written informed consent was required. CCG-B972 was a correlative biology study that provided for acquisition and banking of serum specimens for sIL-2rα assessment from these same patients. Participation in CCG-B972 was not required for participation in the CCG-2961 study.

Four groups served as non-AML reference controls for the sIL-2rα assay: 55 healthy adults described in the manufacturer's brochure of the DuoSet ELISA Development Kit; R&D Systems (Minneapolis, MN); 15 healthy adult volunteers; 14 adult patients with malignant melanoma prior to receiving immunotherapy; and 36 children with neuroblastoma 56–100 days following autologous HSCT.

IL-2 Treatment and sIL-2rα Specimen Processing

Figure 1 shows the treatment schema, and Supplementary Figure 1 is the Consort diagram showing enrolled patients. After completion of chemotherapy, patients in remission were invited to participate in randomization to IL-2 therapy or observation. IL-2 randomization was performed centrally using fixed block allocation. The IL-2 group received IL-2 at 9×10^6 IU/m^2/day by continuous infusion (CI) on days 0–3 and 1.6×10^6 IU/m^2/day CI on days 8–17 as previously described (Inset, Fig. 1) [15,23]. Chiron, Inc. provided IL-2 to the National Cancer Institute, which distributed it to institutions. Serum samples were obtained at study entry and following completion of all chemotherapy and in the IL-2 group on days 4 and 18 of IL-2 of infusion therapy and in the control group, on days 0 and 28 of follow-up.

Figure 1 inset shows the timing of sIL-2rα specimen acquisition in relation to IL-2 administration. Specimens stripped of identifiers were shipped overnight to the COG Immunology Reference Laboratory at the University of Wisconsin. Clinical data were sent to the COG Operations office. Samples were frozen at −20°C. For analysis, all samples were thawed and spun down. One milliliter of supernatant was preserved with 1 μl 1% thimerosal at 4°C. Samples designated as "on study," "pre IL-2 day 0," "no IL-2 day 0", and "no IL-2 day 28" were diluted 1/5; samples labeled "IL-2 day 4," and "IL-2 day 18" were diluted 1/20 to fit in the optimal assay range (0–2,000 pg/ml) according to manufacturer's specifications for the sIL-2rα enzyme-linked immunosorbent assay (ELISA; DuoSet ELISA Development Kit; R&D Systems). Standards and serum samples diluted in PBS/BSA and 100 μL aliquots were added in duplicates to micro wells coated with mouse anti-human IL-2rα antibody in PBS overnight at room temperature, washed with PBS, blocked with PBS + 1% BSA for 3 hr at room temperature, rewashed with PBS + 0.05% Tween-20, incubated overnight at 4°C and rewashed with PBS/Tween. Biotinylated-goat anti-human IL-2Rα antibody was added. Wells were incubated for 3 hr at room temperature on an orbital shaker. After washing, streptavidin-peroxidase (HRP) was added for 20 min. Wells were washed, and tetramethylbenzidine (TMB) substrate was added to initiate the enzymatic reaction. Color development was stopped after 10 min with 2 N H_2SO_4. Microplates were evaluated at 450 nm (with a 570 nm reference) using a Spectra microelisa reader (TECAN, Männedorf, Austria). Soluble IL-2rα values were calculated against a standard curve based on a NS0-expressed recombinant human IL-2rα protein provided in the kit and with WinSelect data processing software. Results were sent to the COG statistician.

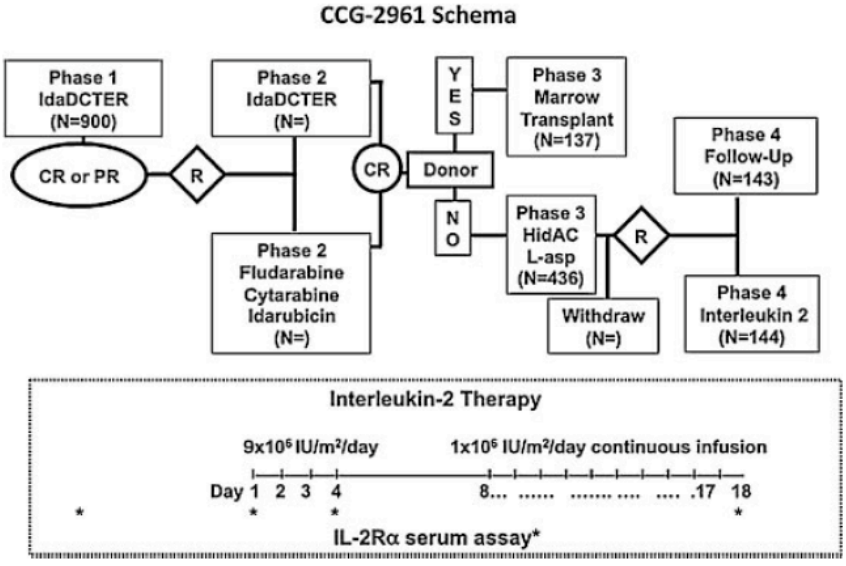

Fig. 1. Treatment schema for CCG-2961 and schedule of interleukin-2 (IL-2) infusions (inset) and sampling for serum IL-2 receptor (block arrows). IdaCTER, idarubicin, cytarabine, thioguanaine, etoposide, and rubidomycin (daunorubicin); HidAC, high dose Ara-C; L-asp, L-asparaginase; R, randomization.

TABLE I. Clinical Characteristics and Outcomes of Patients Eligible for Phase 4 Randomization

Time	Phase 4 randomization				None		*P*-value	
	Group A (IL-2)		Group B (No IL-2)		Group C (withdrawal)			
	N	%	N	%	N	%	A vs. B	AB vs. C
	144	37	145	38	96	25		
Variable								
Age (years)								
Median (range)	6.9 (0.04–17.9)		7.6 (0.01–19)		11 (0.11–19.8)		0.729	0.008
Male	89	62	67	46	45	47	0.011	0.276
Ethnicity								
White	92	67	96	66	59	61	0.965	0.447
Black	10	7	16	11	16	17	0.37	0.067
Asian	24	17	24	17	15	16	0.976	0.885
Hispanic	7	5	0	0	2	2	0.006	0.864
Other	5	4	9	6	4	4	0.467	0.974
Unknown	6	4	0	0	0	0	0.015	0.343
WBC $\times$ 10^9/L								
Median (range)	22.5 (1.0–860)		17.6 (0.8–378)		20 (0.7–269)		0.126	0.686
Karyotype								
Favorable	26	29	26	28	16	29	0.945	0.924
Standard	64	70	61	69	41	70	0.921	0.876
Unfavorable	1	1	2	2	2	1	0.619	0.599
Unknown	53	37	56	39	37	39	0.750	0.885
DFS $\pm$ 2SD	53 $\pm$ 9%		58 $\pm$ 8%		48 $\pm$ 11%		0.489	0.230
OS $\pm$ 2SD	70 $\pm$ 8%		73 $\pm$ 8%		56 $\pm$ 11%		0.727	0.021

Favorable karyotypes are t(8;21), inv(16) or t(16;16); unfavorable, del(7), 7q-, del (5), 5q-and complex ($\geq$3 abnormalities); and standard, all others. *P* values compare the two randomized groups (A vs. B) and both randomized groups to the withdrawal group (AB vs. C).

Statistical Analysis

Demographic and clinical variables were collected age, gender, ethnicity, white blood cell count at diagnosis, cytogenetic subset, day 14 marrow response, availability of a matched familial marrow donor, and randomized regimen in phases 2 and 4 (Fig. 1). Outcome measures include disease-free survival (DFS) and overall survival (OS) defined as follows: DFS, time from the end of phase 3 to relapse or death; and OS, time from study entry to death. The study was powered to show a 10% difference in DFS between IL-2 and control groups. The Kaplan–Meier method [27] was used to calculate the estimates of OS and DFS. Differences between groups of patients were tested for significance using the log-rank statistic [28]. Toxicities from primary toxicity categories are reported from phase 4 (IL-2 phase) as rates.

Children lost to follow-up were censored at date of last known contact or at a cutoff 6 months before October 2006. Patients who withdrew were followed for events and survival. This report analyzes data collected up to October 30, 2006 with a median follow-up of 56 months. All analyses are based on intention-to-treat. A *P*-value of <0.05 was set as a threshold for significance.

On-study AML sIL-2rα values were compared with single specimens from non-AML reference controls. AML patients provided specimens for sIL-2rα analyses at one or more time points. Correlations of on-study sIL-2rα concentration with outcome and correlations of the serial post-treatment specimens with outcome for randomized patients were analyzed. Mean values of sIL-2rα concentration were compared using an unpaired *t*-test; median values, using the Mann–Whitney test [29]. All authors had access to the complete data sets for phase 4 of the CCG-2961 and for the B972 studies.

RESULTS

Outcomes of IL-2 Randomization

Table I shows demographic and clinical characteristics and outcomes of the eligible patients. At the end of phase 3, of 385 eligible patients, 96 (25%) withdrew from the study, 144 were randomized to the IL-2 group and 145 to the control group. Those who withdrew were significantly older and experienced significantly inferior OS (Table I). There was a significantly higher proportion of males randomized to the IL-2 group. At 5 years, DFS is 51 + 9% in the IL-2 group and 58 + 8% in the control group (*P*-value = 0.489; Fig. 2). OS is also not different for the

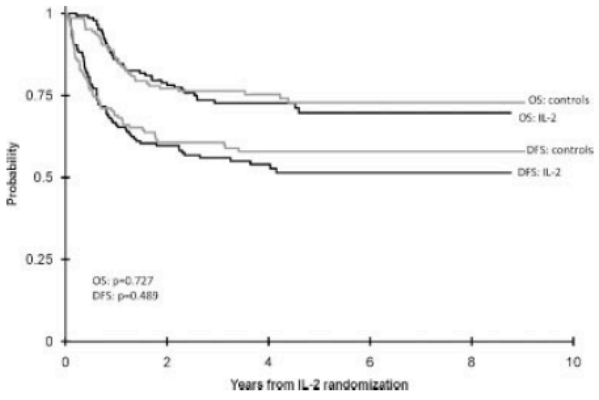

Fig. 2. Actuarial 5-year disease-free survival and overall survival of randomized patients.

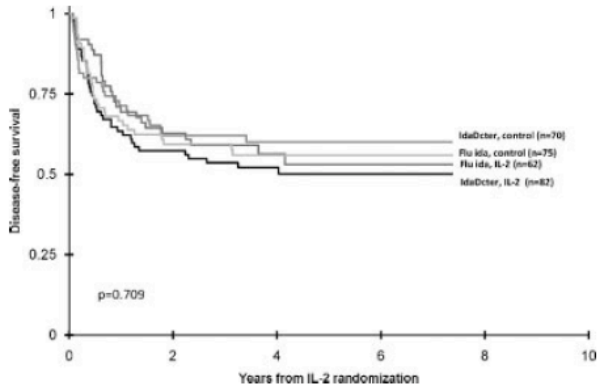

Fig. 3. Actuarial disease-free survival of interleukin-2 and control groups according to phase 2 randomization to IDADCTER (idarubicin, cytarabine, thioguanine, etoposide, and daunorubicin) and FLU IDA (fludarabine monophosphate, cytarabine, and idarubicin).

IL-2 and control groups, 70 ± 8% and 73 ± 8%, respectively (Fig. 2; *P*-value = 0.727). There is no trend for better or worse outcomes among those who received fludarabine/ara-C/idarubicin or the 5-drug IDA-DCTER regimens in phase 2 in either the IL-2 or control arms of the study (Fig. 3; *P*-value = 0.709).

Among the 144 patients in the IL-2 group, 28% experienced grade 3 toxicity and 14% grade 4 toxicity. The most common toxicity was blood pressure changes that were not otherwise classified. Fifteen percent had hepatic toxicity, most often enzyme elevation. In contrast to the CCG-2941 pilot study [21], fever and rash were not noted in this study which did not capture grade 1 or 2 toxicity. One patient discontinued therapy after the high-dose IL-2 infusion. ICU admissions were rare.

Sequential Changes in sIL-2rα Concentration

Table II compares the on-study sIL-2rα concentrations for 134 AML patients on CCG-2961 who contributed on-study specimens to those of four non-AML reference control groups. Mean

TABLE II. Comparison of Serum sIL-2Rrα Concentration of Children With AML With Those of Healthy Adults and Children and Adults With Other Cancers

Group	AML patients (on-study)	Non-AML controls	*P*-value
		Reference	AML vs. reference
N	134	55	
Mean sIL-2Rα[2]	3,668	1,055	[a]
Median	2,732	na	[a]
Range	239–1,1279	458–1,997	
SD	2,736	na	
SE	236	na	
		Volunteers	AML vs. volunteers
N		15	
Mean sIL-2Rα	826	<0.001	
Median		739	<0.001
Range		294–1,712	
SD		395	
SE		102	
		Melanoma	AML vs. melanoma
N		14	
Mean sIL-2Rα	941	<0.001	
Median		884	<0.001
Range		628–2,173	
SD		379	
SE		101	
		Neuroblastoma	AML vs. neuroblastoma
N		36	
Mean sIL-2Rα	1,772	<0.001	
Median		1,660	<0.001
Range		759–3,415	
SD		727	
SE		121	
		ALL non-AML	AML vs. non-AML
N		65	
Mean sIL-2Rα	1,376	<0.001	
Median		1,133	<0.001
Range		294–3,415	
SD		744	
SE		92	

On-study sIL-2rα concentration in pg/ml were obtained for 134 AML patients in this CCG2961 study. These are compared to values for the 4 indicated non-AML control groups. [a]Because the manufacturer did not provide median, SD, or SE, comparisons do not include the 55 healthy controls.

TABLE III. Sequential sIL-2rα Values for AML Patients Randomized to IL-2 Group or Control Group

	N	Mean sIL-2Rα	Median sIL-2Rα	Range	*P*-value (test of means)
On-study					
Time 1					
IL-2	34	3,342	2,447	475–8,691	0.439
Control	30	3,891	2,221	524–11,279	
Post-chemotherapy					
Time 2					
IL-2: day 0 F/U	39	2,669	1,353	364–30,567	0.276
Control: Pre-IL-2	30	1,594	1,440	547–3,630	
Time 3					
IL-2: Day 4	39	15,534	13,659	4,125–40,253	—
Time 4					
IL-2: Day 18	38	10,585	8,368	773–32,310	<0.001
Control: Day 28	31	1,713	1,586	699–3,966	

Figure 1 shows the sequential time points, Figure 3 shows the median values. *P* values compare the sIL-2rα values for the patients randomized to IL-2 versus control at times 1, 2, and 4.

on-study sIL-2Rα concentrations of the AML patients were notably higher than the reported range of values from the healthy volunteers provided by the manufacturer and significantly higher than the values obtained in the reference laboratory from healthy adults, melanoma patients prior to immunotherapy, and neuroblastoma patients 56–100 days following AHSCT.

Table III shows the serial changes in the sIL-2rα concentration in AML patients following chemotherapy and before, during and after IL-2 in the IL-2 group or at comparable times in the control group. Of the 289 patients randomized to IL-2 or control, 64 provided pre-chemotherapy serum samples, and 80 provided samples at the later time points. There were no differences in mean on-study sIL-2Rα concentrations between the 64 AML patients who provided on-study serum that participated in the phase 4 randomization and the 70 AML patients that provided on-study serum samples who did not participate ($P = 0.784$). Of the 64 randomized patients with on-study specimens, the 34 patients randomized to IL-2 showed no difference in on-study sIL-2Rα concentrations compared to the 30 randomized to observation (Table III, time 1). There was also no significant difference in mean sIL-2Rα concentration between the two groups after three courses of chemotherapy (Table III, time 2). However, comparison of pre- and post-chemotherapy samples within each group showed significant reduction in median sIL-2Rα concentration (Fig. 4, time 1 vs. time 2; $P = 0.001$): the elevated sIL-2Rα before treatment (time 1) was attenuated by three courses of chemotherapy (time 2). Of note, sIL-2Rα concentration of the AML patients after chemotherapy are similar to those of the treated neuroblastoma patients (Tables II and III).

In the IL-2 group during phase 4, the mean sIL-2Rα concentration increased from 2,669 pg/ml on day 0 to 15,534 pg/ml on day 4 ($P < 0.001$) and 10,585 pg/ml on day 18 ($P < 0.001$), whereas in the control group sIL-2Rα did not change between days 0 and 28 ($P = 0.521$). These data confirm that administration of IL-2 caused significant induction of lymphocyte activity. The higher sIL-2Rα concentration on day 4 than day 18 in the IL-2 group is consistent with this dose-dependent activation. Furthermore, the striking differences seen at time 4 between these two groups (Fig. 4, *P*-value < 0.001) confirms that the IL-2 group of patients did receive the IL-2, and that despite their prior aggressive multi-agent chemotherapy, their lymphocytes were able to respond to the IL-2.

Within the group of 134 patients with on-study sIL-2Rα data, four quartiles were defined based on sIL-2Rα concentration. No significant differences in 5-year OS or DFS were seen between the four quartiles. A similar quartile analysis was done based on sIL-2Rα data from each time point for both the IL-2 and control groups (Table IV). We saw no significant correlation between OS and the higher or lower quartiles of sIL-2α concentration for either IL-2 treatment or control groups, at any time. Given the fact that these analyses were not corrected for multiple comparisons, we saw no suggestion of any trend (despite occasional *P* values < 0.05) for correlation between DFS and the higher or lower quartiles of sIL-2α concentration for either IL-2 treatment or control groups at any time.

DISCUSSION

The CCG-2961 is the first study to evaluate serial concentrations of SIL-2Rα in the context of a large randomized controlled clinical trial of IL-2 in a relatively homogeneous population. The trial shows sIL-2Rα concentrations are elevated

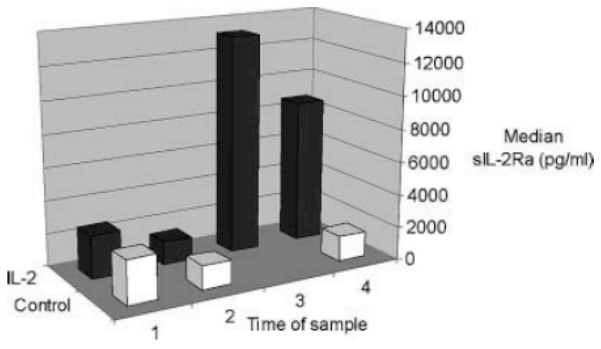

Fig. 4. Comparison of sequential changes in median concentration of serum soluble IL-2 receptor alpha over time in the IL-2 and control groups. Time 1 is on-study; time 2 is post-chemotherapy (pre-IL-2 for IL-2 group and day 0 for control); time 3 = day 4 of IL-2 for IL-2 group; Time 4 is day 18 of IL-2 for IL-2 group and day 28 follow-up for controls.

TABLE IV. Phase 4 Outcomes According to Quartile of sIL-2rα Values for the IL-2 and Control Groups

			5-year disease-free survival			5-year overall survival		
				P-value			*P*-value	
	N	%	% ± 2 SE %	Within IL-2	IL-2 vs. control	% ± 2 SE %	Within IL-2	IL-2 vs. control
Group IL-2								
Pre IL-2								
All	39	27	57 ± 17		ns	84 ± 12		ns
Quartile 1	10	26	40 ± 39	ns	ns	79 ± 27	ns	ns
Quartile 2	10	26	70 ± 29	ns	ns	90 ± 19	ns	ns
Quartile 3	10	26	60 ± 31	ns	ns	78 ± 28	ns	ns
Quartile 4	9	23	56 ± 33	ns	ns	89 ± 21	ns	ns
Day 4								
All	39	27	50 ± 17	—	ns	81 ± 13	—	ns
Quartile 1	10	26	53 ± 29	ns	ns	79 ± 27	ns	ns
Quartile 2	10	26	40 ± 31	ns	ns	89 ± 21	ns	ns
Quartile 3	10	26	50 ± 32	ns	ns	70 ± 29	ns	ns
Quartile 4	9	23	56 ± 33	ns	ns	89 ± 21	ns	ns
Day 18								
All	38	26	55 ± 16	—	—	78 ± 14	—	—
Quartile 1	9	24	67 ± 35	ns	—	67 ± 31	ns	—
Quartile 2	10	6	20 ± 25	0.006	—	76 ± 30	ns	—
Quartile 3	10	26	60 ± 31	ns	—	80 ± 25	ns	—
Quartile 4	9	24	78 ± 28	ns	—	89 ± 31	ns	—

	N	%	% ± 2 SE %	Within controls	IL-2 vs. control	% ± 2 SE %	Within Controls	IL-2 vs. control
Control								
End of chemotherapy								
All	30	21	65 ± 19	—	—	81 ± 16	—	—
Quartile 1	7	23	86 ± 26	ns	—	86 ± 26	ns	—
Quartile 2	8	27	50 ± 35	ns	—	75 ± 31	ns	—
Quartile 3	8	27	70 ± 36	ns	—	80 ± 36	ns	—
Quartile 4	7	23	57 ± 37	ns	—	86 ± 26	ns	—
Day 28								
All	31	21	68 ± 18	—	—	84 ± 15	na	—
Quartile 1	8	23	86 ± 23	ns	—	88 ± 23	ns	—
Quartile 2	8	27	56 ± 40	ns	—	83 ± 30	ns	—
Quartile 3	8	27	100 ± 0	0.047	—	100 ± 0	ns	—
Quartile 4	7	23	29 ± 34	0.001	—	71 ± 34	ns	—

Serum sIL-2rα values of patients randomized to IL-2 or Control groups were divided into quartiles at the indicated time points. Quartiles were evaluated for associations with DFS or OS; ns refers to non-significant *P*-value, and "—" indicates that there are no applicable comparisons.

in untreated pediatric AML patients compared to those of healthy controls and some other cancer patients. SIL-2Rα concentrations decline during chemotherapy and show consistent and significant dose-dependent increases in during IL-2 treatment but not during observation in control patients. These findings provide clear evidence of biologic activity of IL-2. Although sIL-2Rα has been reported as elevated at diagnosis in AML and in other cancers and as predictive of response to therapy, typically showing elevated sIL-2Rα as associated with inferior outcome [9,10], our study provides evidence that sIL-2Rα concentration is not a predictor of treatment outcome in pediatric AML when administered as per the CCG-2961 protocol.

The CCG-2961 study confirmed that IL-2 given in the dose and schedule used in this trial is tolerable, but is without clinical benefit in children with AML in remission after intensive chemotherapy. These findings are consistent with one study in which IL-2 was given at the same dose and schedule as in CCG-2961 after ASCT for refractory leukemia [30] and with two recent randomized trials in adults with AML where post-remission IL-2 given more intensively than in CCG-2961 had no impact on DFS or OS and was poorly tolerated [22,23]. Some of the differences between the apparent benefits in earlier trials [13–21] and the absence of benefit of more recent randomized trials [22–24] can be attributed to the larger sample sizes and randomized designs of the latter. Additionally, the IL-2 itself is a variable; compared to the Chiron product used in CCG-2961, the Amgen product may effect greater immunological stimulation and greater toxicity [31].

One limitation of this study is that the 25% of eligible patients withdrew. Withdrawal was a mixture of patient/parent refusal or physician recommendation. A 25% rate of withdrawal is typical for late randomization where the randomization is something versus nothing. For example, in CCG-213, the rate of refusal to randomize to continue on AML therapy or stop treatment was 38% [32]. Patients who withdrew in our study were significantly older than the randomized patients and had significantly inferior outcomes. In CCG-2961, older age was significantly associated with inferior outcome [22]. However, omission of these patients is unlikely to have affected the clinical or biological response to IL-2 among the randomized patients. A second limitation is that not all patients submitted specimens at each of the requested time points and the comparisons within and between groups over time are not limited to matched pairs. We did not have specimens to compare the sIL-2Rα concentration of untreated AML patients to newly diagnosed children with other malignancies or to age-matched healthy children.

Since conception of these studies, understanding of the role of the immune system in controlling cancer has advanced. IL-2 stimulates immune cells and their production of cytokines, some of which stimulate and others of which inhibit leukemic cell growth. Moreover, a population of immunosuppressive T cells (T regulatory cells [T_{regs}]) is both reactive to IL-2 through high affinity receptors and release sIL-2Rα. In some settings, IL-2 infusions may preferentially enhance proliferation and activity of T_{regs} [33]. More specific targeting of AML reactive immune cells may possibly be more effective. Other approaches to AML immunotherapy in development include myeloid-specific antibodies, donor lymphocyte infusions following allogeneic transplant, and redirected autologous effector cells, using genetically engineered chimeric antigen receptors or haploidentical natural killer cells expanded in vitro [34]. In these settings, addition of IL-2 appears to be potentially advantageous. Recent data from a COG trial have shown substantial improvement in both DFS and OS when IL-2 and GM-CSF are used in combination with a tumor reactive (anti-GD2) monoclonal antibody, if applied soon after autologous HSCT for children with high-risk neuroblastoma in remission [35]. Nevertheless, based on the results of the CCG-2961 trial and other recent trials, there appears to be no role for single agent IL-2 to prevent relapse of AML in remission.

ACKNOWLEDGMENT

The authors acknowledge the assistance of the COG Publications and Operations offices. The work was supported by grants CA 13539, CA 98543, CA 032685 and CA 087025 from the National Institutes of Health. A complete listing of grant support for research conducted by CCG before 2003 is available online at http://www. childrensoncologygroup.org/admin/grantinfo.htm. NCI provided Chiron Interleukin-2 to the CCG institutions. The National Child-hood Cancer Foundation, the MACC Fund, and the Crawdaddy Foundation also supported the laboratory work of Dr. Sondel. The Yetta Dietch Novotny Chair in Clinical Oncology supported Dr. Lange's contributions.

REFERENCES

1. Mackall CL, Gress RE. Pathways of T-cell regeneration in mice and humans: Implications for bone marrow transplantation and immunotherapy. Immunol Rev 1997;157:61–721.
2. Ruggeri L, Capanni M, Mancusi A, et al. The impact of donor natural killer cell alloreactivity on allogeneic hematopoietic transplantation. Transpl Immunol 2005; 203–206.
3. Kolb HJ. Graft-versus-leukemia effects of transplantation and donor lymphocytes. Blood 2008;11:24371–24383.
4. Waldman TA. The biology of interleukin-2 and interleukin-15: Implications for cancer therapy and vaccine design. Nat Rev Immunol 2006;6:595–601.
5. McDermott DF. Immunotherapy of metastatic renal cell carcinoma. Cancer 2009;115:2298–2305.
6. Bhatia S, Tykodi SS, Thompson JA. Treatment of metastatic melanoma: An overview. Oncology 2009;23:488–496.
7. Ringdén O, Karlsson H, Olsson R, et al. The allogeneic graft-versus-cancer effect. Br J Haematol 2009;147:614–633.
8. Toren A, Ackerstein A, Slavin S, et al. Role of interleukin-2 in human hematological malignancies. Med Oncol 1995;12:177–186.
9. Kuhn DJ, Dou QP. The role of interleukin-2 receptor alpha in cancer. Front Biosci 2005;10:1462–1474.
10. Murakami S. Soluble interleukin-2 receptor in cancer. Front Biosci 2004;9:3085–3090.
11. Bogner MP, Voss SD, Bechhofer R, et al. Serum CD25 levels during interleukin-2 therapy: Dose dependence and correlations with clinical toxicity and lymphocyte surface sCD25 expression. J Immunother 1992;11:111–118.
12. Bien E, Balcerska A. Serum soluble interleukin 2 receptor alpha in human cancer of adults and children: A review. Biomarkers 2008;13:1–26.
13. Higuchi CM, Thompson JA, Petersen FB, et al. Toxicity and immunomodulatory effects of interleukin-2 after autologous bone marrow transplantation for hematologic malignancies. Blood 1991;71: 2561–2568.
14. Foa R, Meloni G, Guarini A, et al. Interleukin 2 (IL-2) in the management of acute myeloid leukemia: Clinical and biological findings. Leukemia 1992;6:115S–116S.
15. Meloni G, Foà R, Tosti S, et al. Autologous bone marrow transplantation followed by interleukin-2 in children with advanced leukemia: A pilot study. Leukemia 1993;6:780–785.
16. Benyunes MC, Massumoto C, York A, et al. Interleukin-2 with or without lymphokine-activated killer cells as consolidative immunotherapy after autologous bone marrow transplantation for acute myelogenous leukemia. Bone Marrow Transplant 1993;12:159–163.
17. Fefer A, Benyunes MC, Massumoto C, et al. Interleukin-2 therapy after autologous bone marrow transplantation for hematologic malignancies. Semin Oncol 1993; 2041–2045.
18. Bergmann L, Heil G, Kolbe K, et al. Interleukin-2 bolus infusion as late consolidation therapy in 2nd remission of acute myeloblastic leukemia. Leuk Lymphoma 1995;16:271–279.
19. Meloni G, Trisolini SM, Capria S, et al. How long can we give interleukin-2? Clinical and immunological evaluation of AML patients after 10 or more years of IL2 administration. Leukemia 2002;16:2016–2018.
20. Stein AS, O'Donnell MR, Slovak ML, et al. Interleukin-2 after autologous stem-cell transplantation for adult patients with acute myeloid leukemia in first complete remission. J Clin Oncol 2003; 21:615–623.
21. Stone RM, DeAngelo DJ, Janosova A, et al. Low dose interleukin-2 following intensification therapy with high dose cytarabine for acute myelogenous leukemia in first complete remission. Am J Hematol 2008;83:1–17.
22. Baer MR, George SL, Caligiuri MA, et al. Low-dose interleukin-2 immunotherapy does not improve outcome of patients age

60 years and older with acute myeloid leukemia in first complete remission: Cancer and Leukemia Group B Study 9720. J Clin Oncol 2008; 26:4934–4939.
23. Pautas C, Merabet F, Thomas X, et al. Randomized study of intensified anthracycline doses for induction and recombinant interleukin-2 for maintenance in patients with acute myeloid leukemia age 50 to 70 years: Results of the ALFA-9801 study. J Clin Oncol 2010;28:8–14.
24. Sievers EL, Lange BJ, Sondel PM, et al. Feasibility, toxicity, and biologic response of interleukin-2 after consolidation chemotherapy for acute myelogenous leukemia: A report from the Children's Cancer Group. J Clin Oncol 1998;16:914–919.
25. Lange BJ, Smith FO, Feusner J, et al. Outcomes in CCG-2961, a children's oncology group phase 3 trial for untreated pediatric acute myeloid leukemia: A report from the children's oncology group. Blood 2008;111:1044–1053.
26. Bennett JM, Catovsky D, Daniel MT, et al. Proposed revised criteria for the classification of acute myeloid leukemia. A report of the French-American-British Cooperative Group. Ann Intern Med 1985;103:620–625.
27. Kaplan EL, Meier P. Nonparametric estimation from incomplete observations. J Am Stat Assoc 1958;53:457.
28. Peto R, Peto J. Asymptotically efficient rank in variant test procedures. J R Stat Soc A 1972;2:185–206.
29. Mann HB, Whitney DR. On a test of whether one or two random variables is stochastically larger than the other. Ann Math Stat 1947;18:50–60.
30. Robinson N, Sanders JE, Benyunes MC, et al. Phase I trial of interleukin-2 after unmodified HLA-matched sibling bone marrow transplantation for children with acute leukemia. Blood 1996;87: 1249–1254.
31. Hank JA, Surfus J, Gan J, et al. Distinct clinical and laboratory activity of two recombinant interleukin-2 preparations. Clin Cancer Res 1999;5:281–289.
32. Wells RJ, Woods WG, Buckley JD, et al. Treatment of newly diagnosed children and adolescents with acute myeloid leukemia: A Children's Cancer Group study. J Clin Oncol 1994;12: 2367–2377.
33. Zhang H, Chua KS, Guimond M, et al. Lymphopenia and interleukin-2 therapy alter homeostasis of CD4+CD25+ regulatory T cells. Nat Med 2005;11:1238–1243.
34. Rubnitz JE, Inaba H, Ribeiro RC, et al. NKAML: A pilot study to determine the safety and feasibility of haploidentical natural killer cell transplantation in childhood acute myeloid leukemia. J Clin Oncol 2010;28:955–959.
35. Yu AL, Gilman AL, Ozkaynak MF, et al. Chimeric anti-GD2 antibody with GM-CSF, IL2 and 13-cis retinoic acid for high-risk neuroblastoma: A Children's Oncology Group (COG) phase 3 study. N Engl J Med 2010;363:1324–1334.

A.5 Tumor-associated Myeloid Cells can be Activated in vitro and in vivo to Mediate Antitumor Effects

Cancer Immunol Immunother
DOI 10.1007/s00262-012-1236-2

ORIGINAL ARTICLE

Tumor-associated myeloid cells can be activated in vitro and in vivo to mediate antitumor effects

Alexander L. Rakhmilevich · Mark J. Baldeshwiler · Tyler J. Van De Voort · Mildred A. R. Felder · Richard K. Yang · Nicholas A. Kalogriopoulos · David S. Koslov · Nico Van Rooijen · Paul M. Sondel

Received: 9 November 2011 / Accepted: 22 February 2012

Abstract Tumor growth is often accompanied by the accumulation of myeloid cells in the tumors and lymphoid organs. These cells can suppress T cell immunity, thereby posing an obstacle to T cell-targeted cancer immunotherapy. In this study, we tested the possibility of activating tumor-associated myeloid cells to mediate antitumor effects. Using the peritoneal model of B16 melanoma, we show that peritoneal cells (PEC) in tumor-bearing mice (TBM) had reduced ability to secrete nitric oxide (NO) following in vitro stimulation with interferon gamma and lipopolysaccharide, as compared to PEC from control mice. This reduced function of PEC was accompanied by the influx of $CD11b^+$ $Gr\text{-}1^+$ myeloid cells to the peritoneal cavity. Nonadherent PEC were responsible for most of the NO production in TBM, whereas in naïve mice NO was mainly secreted by adherent $CD11b^+$ $F4/80^+$ macrophages. Sorted $CD11b^+$ $Gr\text{-}1^-$ monocytic and $CD11b^+$ $Gr\text{-}1^+$ granulocytic PEC from TBM had a reduced ability to secrete NO following in vitro stimulation (compared to naïve PEC), but effectively suppressed proliferation of tumor cells in vitro. In vivo, treatment of mice bearing established peritoneal B16 tumors with anti-CD40 and CpG resulted in activation of tumor-associated PEC, reduction in local tumor burden and prolongation of mouse survival. Inhibition of NO did not abrogate the antitumor effects of stimulated myeloid cells. Taken together, the results indicate that in tumor-bearing hosts, tumor-associated myeloid cells can be activated to mediate antitumor effects.

Keywords Myeloid cells · Anti-CD40 · CpG · Immunotherapy

Electronic supplementary material The online version of this article (doi:10.1007/s00262-012-1236-2) contains supplementary material, which is available to authorized users.

A. L. Rakhmilevich (✉) · M. J. Baldeshwiler · T. J. Van De Voort · R. K. Yang · N. A. Kalogriopoulos · D. S. Koslov · P. M. Sondel
Departments of Human Oncology, University of Wisconsin, 4136 WIMR, 1111 Highland Avenue, Madison, WI 53705, USA
e-mail: rakhmil@humonc.wisc.edu

A. L. Rakhmilevich · P. M. Sondel
Paul P. Carbone Comprehensive Cancer Center, University of Wisconsin, Madison, WI, USA

M. A. R. Felder
Department of Obstetrics and Gynecology, University of Wisconsin, Madison, WI, USA

N. Van Rooijen
Department of Molecular Cell Biology, Vrije Universiteit Medical Centre, Van der Boechorststraat, Amsterdam, The Netherlands

P. M. Sondel
Department of Pediatrics, University of Wisconsin, Madison, WI, USA

Abbreviations

IFN-γ	Interferon gamma
Mϕ	Macrophages
PEC	Peritoneal cells
TLR	Toll-like receptor
TAM	Tumor-associated macrophages
TNFα	Tumor necrosis factor alpha
TBM	Tumor-bearing mice

Introduction

Advanced cancer can induce immunosuppression (reviewed in [1]). This immunosuppression, especially of T cells, is considered to be one of the mechanisms by which

Published online: 06 March 2012

tumors evade immune-mediated destruction [2]. Several types of immune cells, including T cells, dendritic cells and macrophages (Mϕ), can be functionally suppressed by tumors. In particular, tumor-associated Mϕ (TAM) have been categorized as alternatively activated M2 Mϕ due to the influence of tumor-derived factors [3, 4]. Monocytes and Mϕ from tumor-bearing animals can suppress T cell function [5], and conversely, $CD4^+CD25^+$ T regulatory cells can exert direct suppressive effects on monocytes and Mϕ [6]. While Mϕ outside of the tumor compartment may remain unsuppressed [7], TAM are functionally inhibited, mediate immunosuppression and promote tumor growth [3, 8].

In addition to immunosuppressive TAM, immature myeloid cells accumulating in tumors and associated lymphoid organs in tumor-bearing hosts can also mediate suppression of T cell functions [9–11]. In mice, these myeloid-derived suppressor cells (MDSC) represent a heterogeneous population of myeloid cells that express both CD11b and Gr-1[11]. In addition, murine MDSC can express IL-4Rα and varying levels of F4/80, depending on the tumor model [8, 12, 13]. Immunosuppressive activities of MDSC are attributed, in part, to their production of nitric oxide (NO) or arginase in response to tumor-produced PGE_2 [14], which depletes arginine necessary for T cell functions [15]. In addition to suppressing T cell responses, MDSC have been found to inhibit Mϕ functions in TBM [16].

Although TAM have been reported to promote tumor growth, and the histological detection of abundant TAM has been associated with poor prognosis for patients with certain cancers [17, 18], Mϕ in TBM can also become antitumor effector cells following proper activation. Thus, disruption of the immunosuppressive IL-10 pathway in combination with the Mϕ-activating agents CpG and LEC/CCL16 influenced TAM to become potent antitumor effectors, presumably causing M2 inhibitory Mϕ to convert to M1 effector cells [19]. However, a potential role of TAM and other tumor-associated myeloid cells as antitumor effector cells has not been well characterized. We have previously shown that a combination of two distinct immunomodulators, anti-CD40 mAb (anti-CD40) and class B oligodeoxynucleotides containing unmethylated CpG motifs (CpG), induced a strong synergistic activation of Mϕ resulting in antitumor effects in mice [20–22]. These studies, for the most part, involved subcutaneous tumors, whereas functional and phenotypic analysis was performed on peritoneal Mϕ. In this study, we hypothesized that tumor-associated myeloid cells could induce antitumor effects following activation in vitro and in vivo. Specifically, using a peritoneal B16 model, we sought to determine whether anti-CD40 and CpG treatment can activate tumor-associated myeloid cells in TBM to mediate antitumor effects. The results presented here show that myeloid cells at, or near, sites of tumor growth are indeed capable of being activated in vitro and in vivo to mediate antitumor effects.

Materials and methods

Mice and cell lines

Female C57BL/6 mice, 8–12 weeks old, were obtained from Taconic, Germantown, NY. C57BL/6-Tg(CAG-EGFP)1Osb/J transgenic mice with an "enhanced" green fluorescent protein (EGFP) cDNA were obtained from Jackson Labs (Bar Harbor, ME) and bred at the UW-Madison animal facility. Mice were housed at the UW-Madison animal facility, and animal experiments were performed under protocols approved by the Animal Care and Use Committees of UW-Madison. The murine B16 melanoma tumor cell line was grown in RPMI 1640 complete medium supplemented with 10% FCS (Sigma Chemicals, St. Louis, MO), 2 mM L-glutamine, and 100 U/ml of penicillin/streptomycin (all from Life Technologies, Inc., Grand Island, NY) at 37°C in a humidified 5% CO_2 atmosphere.

Antibodies and reagents

Anti-CD40 was prepared from the FGK 45.5 hybridoma cell line as described previously [20]. Toll-like receptor 9 (TLR9) agonist CpG1826 was purchased from Coley Pharmaceuticals Group, Wellesley, MA. Bacterial LPS from *Salmonella enteritidis* was purchased from Sigma Chemical, St. Louis, MO. Mouse recombinant IFN-γ was purchased from eBioscience, San Diego, CA.

In vivo tumor models and therapy

C57BL/6 mice were injected subcutaneously (s.c.) or intraperitoneally (i.p.) with 1×10^5 B16 melanoma cells in 0.1 or 0.5 ml PBS, respectively (day 0). For tumor therapy, the mice with i.p. tumors were injected i.p. with 0.5-mg anti-CD40 on days 4, 11 and 18 after tumor implantation and 50-μg CpG on days 7 and 14. Antitumor effects were evaluated by extended survival of the mice and by the decrease in the number of $CD45^-$ B16 cells in PEC as detected by flow cytometry.

Activation of peritoneal cells (PEC)

PEC were obtained via a peritoneal cavity lavage with 5 ml of cold RPMI 1640 complete medium, supplemented with 1 IU/ml of heparin (American Pharmaceutical Partners, Inc., Schaumburg, IL) when collected from TBM.

Collected PEC were placed into 96-well flat-bottomed cell culture plates (Corning Inc, Corning, NY) at a concentration of 2–2.5 $\times$ 10^6 cells/ml (or 1 $\times$ 10^6 cells/ml for sorted cell populations), 0.1 ml/well. The peritoneal Mϕ population was enriched by allowing PEC to adhere to plastic for 1.5–2 h, followed by removal of nonadherent cells. For in vitro activation, total PEC, nonadherent cells, or adherent Mϕ were stimulated with 10 U/ml of IFN-γ and 1 ng/ml of LPS, unless stated otherwise, for 48 h. For in vivo activation, mice were injected i.p. with 0.5 mg of anti-CD40 in 0.5 ml PBS. On day 3, PEC were harvested, enriched as described above and incubated for 48 h either in medium alone or in the presence of LPS (10 ng/ml).

Mϕ: mediated tumoristasis in vitro

Tumoristatic activity of Mϕ was determined by the inhibition of DNA synthesis in tumor cells. Briefly, adherent Mϕ were stimulated in vitro as described above and simultaneously co-cultured with B16 tumor cells (1 $\times$ 10^4/well) for 48 h. To estimate DNA synthesis, cells were pulsed with ^{3}H-TdR (1 µCi/well) during the last 6 h of incubation. ^{3}H-TdR-incorporation was determined by β-scintillation of total cells harvested from the cell culture clusters onto glass fiber filters (Packard, Meriden, CT), using the Packard Matrix 9600 Direct β-counter (Packard, Meriden, CT). Results are presented as counts per 5 min for triplicate wells $\pm$ SE.

Nitric oxide production

Peritoneal Mϕ were prepared and co-cultured with B16 cells for 48 h, as described above in the Mϕ cytostatic assay. Supernatants were collected and nitrite accumulation was determined using Griess reagent (Sigma, St. Louis, MO). Equal volumes of supernatants and Griess reagent were mixed for 10 min, and the A_{570} was measured by a microplate reader and compared to a standard nitrite curve ranging from 0–125 µM.

Inhibition of cytotoxic factors

Inducible NO synthase inhibitor L-NAME (Sigma St. Louis, MO) was added to the cultures at a dose of 10 mM to neutralize the effect of NO. To neutralize arginase, N^{ω}-hydroxy-nor-L-arginine, diacetate salt (nor-NOHA, EMD Biosciences Inc., San Diego, CA) was used at a dose of 100 µM. To block TNFα, anti-TNFα mAb, clone MP6-XT3 (BD Biosciences, San Jose, CA) was used at a final concentration of 10 µg/ml. To neutralize NO in vivo, L-NAME was either injected i.p. at a dose of 50 mg/kg twice a day or given in the drinking water at a dose of 0.5 g/l for 4 days during anti-CD40/CpG treatment.

Flow cytometric analysis and sorting

PEC from treated and control C57BL/6 mice were harvested and stained with anti-F4/80 APC mAb, anti-F4/80 FITC mAb, anti-Gr-1 PE mAb, anti-CD11b APC mAb, anti-CD45 FITC mAb (all from eBioscience, San Diego, CA), anti-CD40 PE mAb, anti-CD80 PE mAb, or anti-CD86 PE mAb (all from BDPharmingen, San Diego, CA) for 40 min at 4°C. Isotype-matched irrelevant rat IgG FITC, IgG APC and IgG PE, purchased from eBioscience or BDPharmingen, were used as background controls. After washing the cells in ice-cold PBS supplemented with 0.5–2% FCS (flow buffer), the cell pellet was resuspended in 0.3-ml flow buffer and analyzed by flow cytometry using a FACSCalibur flow cytometer and FlowJo software (Ashland, OR). Data were collected for 10,000 live events per sample.

Immunohistochemistry

PEC (10^4–10^5 cells in 100 µl media with FCS) were centrifuged at 800 rpm for 3 min using a Shandon Cytospin 2. After air-drying for 5 min, slides were fixed in 100% methanol for 2 min, allowed to dry and stained horizontally with Wright-Giemsa Stain (Sigma) for 45 s. An equal volume of glass filtered water was immediately added to the Wright-Giemsa stain solution, and after staining in the dilute solution for 10 min, the slides were washed off with glass filtered water and destained horizontally with glass filtered water for 5 min. Slides were allowed to dry and mounted with glass coverslips using Cytoseal 60. Pictures of cells were taken at 40× magnification with an Optronics camera using the attached computer software (Magnafire 2.1).

In vivo depletion of Mϕ

Peritoneal Mϕ were depleted in vivo with clodronate liposomes as described [23]. Clodronate was a gift of Roche Diagnostics GmbH, Mannheim, Germany. Clodronate liposomes were prepared as described [23] and injected i.p. in TBM on day 9 post tumor cell implantation (0.3 ml) and on day 13 (0.2 ml). Depletion of Mϕ with clodronate liposomes was confirmed in naïve mice by elimination of more than 95% of PEC positively stained with both anti-CD11b APC and anti-F4/80 FITC.

Adoptive transfer of EGFP PEC

PEC were removed from EGFP mice and counted, and 4.8 $\times$ 10^6 cells were injected i.p. in wild-type C57BL/6 mice (day 0). To facilitate survival of adoptively transferred cells, the recipient mice were depleted of T cells by a

mixture of anti-CD4 and anti-CD8 given i.p. on days −1 and 4. On day 1, half of the mice were injected i.p. with 1×10^5 B16 cells. PEC were removed on day 8, stained with anti-CD11b APC mAb and anti-Gr-1 PE mAb, and analyzed by flow cytometry.

Statistical analysis

A two-tailed Student's t test was used to determine significance of differences between experimental and relevant control values. For survival studies, the Gehan–Breslow–Wilcoxon test was used.

Results

Functional and phenotypic changes in PEC from TBM

Our previous studies demonstrated that anti-CD40 and CpG induced antitumor effects which involved Mϕ [20]. In this study, we sought to determine how anti-CD40 and CpG treatment affects TAM and other myeloid cells in tumor-bearing mice. We hypothesized that CD40/TLR9 ligation of TAM in tumor-bearing mice can change them from being functionally suppressed to becoming antitumor effector cells.

We asked first whether B16 tumor growth in mice resulted in suppressed Mϕ function (as determined by decreased NO production in response to in vitro stimulation with IFN-γ and LPS) and altered Mϕ phenotype compared to Mϕ from naïve mice. We wanted to evaluate these Mϕ features for TAM and for Mϕ obtained from sites other than the tumor (non-TAM) in TBM. We used two tumor models to address these questions. Peritoneal cells (PEC) were obtained either from syngeneic C57BL/6 mice bearing advanced s.c. B16 tumors (a source of non-TAM) or from mice bearing advanced i.p. B16 tumors (a source of TAM). PEC from mice bearing i.p. B16 tumors, rather than the cells from s.c. tumors, were chosen as a source of TAM because of the better accessibility, viability and yield of these PEC for functional and phenotypic characterization, compared to TAM that can be recovered from s.c. B16 tumors. The results show that adherent PEC from mice with advanced s.c. B16 tumors, killed on day 18 post tumor cell injection (Mean tumor volume 514 ± 31 mm^3, $n = 4$), secreted a similar amount of NO (Fig. 1a) and displayed a similar ability to inhibit tumor cell proliferation in vitro (data not shown) compared to adherent PEC from naïve mice. There was a small increase in the percentage of CD11b$^+$ Gr-1$^+$ cells in the spleens, but not in the peritoneal cavities, of s.c. TBM (Fig. 1c). In contrast to the s.c. model, adherent PEC from mice bearing i.p. B16 tumors had reduced NO production (Fig. 1b) and displayed a different surface phenotype. Specifically, expression of the F4/80 marker was downregulated on PEC from TBM, and a new population of CD11b$^+$ Gr-1$^+$ cells emerged comprising 55% of PEC (Fig. 1d). CD11b$^+$ PEC from TBM expressed IL-4Rα, but did not express mannose receptor, CD206 (data not shown). These results suggest that PEC from TBM are suppressed and phenotypically altered when the mice bear peritoneal tumor, but when the tumor is s.c. at a distant site.

Next we looked at the kinetics of both functional and phenotypic changes in PEC obtained from mice injected i.p. 14–15 days earlier with 10^5 B16 cells. The results show that as tumor burden increases with time, adherent PEC from TBM gradually lose their ability to secrete NO upon stimulation with IFNγ and LPS (Fig. 2a). A similar, but less complete loss of NO secretory ability was also seen with the total PEC population from TBM (Fig. 2a). These changes in PEC were not observed on days 3 or 7, but were observed after day 11 post tumor cell injection and were more pronounced by day 14. The percentage of total PEC that co-expressed CD11b$^+$ and Gr-1$^+$ increased starting 1 week post tumor cell injection (Fig. 2b). The decreased ability of PEC from TBM to secrete NO (Fig. 2a) correlated with an increased number of CD11b$^+$ Gr-1$^+$ cells in the peritoneal cavities (Fig. 2b) of these mice (Pearson correlation coefficient -0.87, $p < 0.001$). In contrast to B16 tumor cell injection, daily i.p. injections of B16 supernatants for 14 days failed to induce both CD11b$^+$ Gr-1$^+$ PEC accumulation and NO production inhibition (data not shown). When mice were injected i.p. with 1.6×10^7 B16 tumor cells (rather than 10^5 cells, as in Fig. 2a) and adherent PEC were tested for NO production 4 days later, there was no suppression of NO production compared with control PEC (Supplemental Figure, A). This observation that a large number of tumor cells in the peritoneum for 4 days does not inhibit NO production suggests that the in vivo tumor-induced suppression of Mϕ function is more dependent on the duration of exposure to the peritoneal tumor than on the total number of peritoneal tumor cells.

Using flow cytometric analysis of PEC with anti-CD45 mAb to distinguish between CD45$^+$ host hematopoietic-derived cells and CD45$^-$ nonhematopoietic cells (primarily tumor cells), we found tumor cells in PEC from TBM. To determine whether these contaminating tumor cells may account for the suppressed activity of tumor-associated PEC, we tested the in vitro effect of different doses of B16 cells on NO production by adherent PEC from naïve mice. We found that B16 cells had a dose-dependent immunosuppressive effect on NO production, starting at a tumor cell: Mϕ ratio of 1:1 (Supplemental Figure, B). In contrast, in some of our experiments adherent PEC from day 14 TBM had markedly reduced NO production when the percentage of B16 cells in PEC was only 10%, suggesting

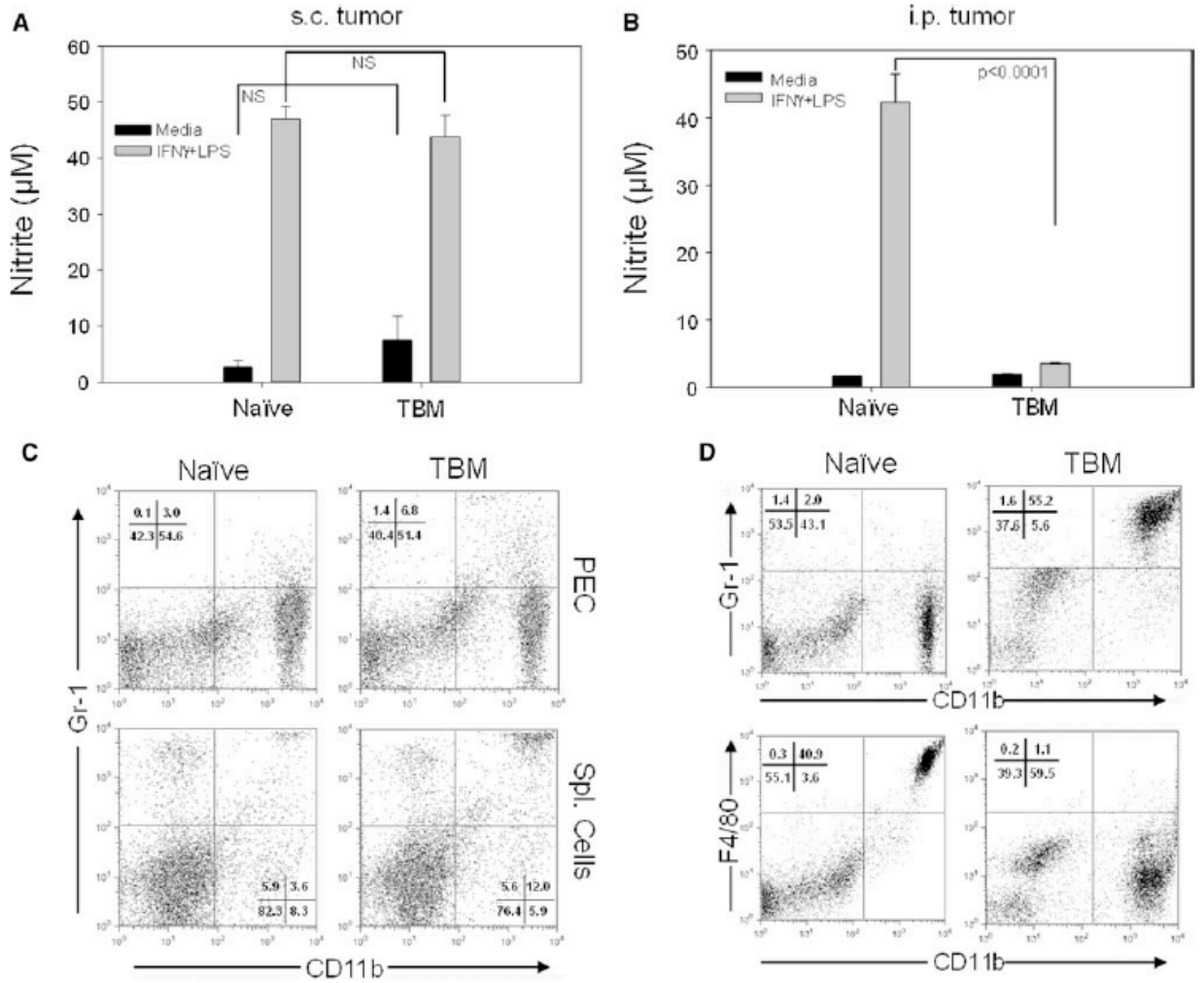

Fig. 1 Effect of s.c. and i.p. B16 tumor on function and phenotype of PEC. C57BL/6 mice were injected s.c. (**a**, **c**) or i.p. (**b**, **d**) with 10^5 B16 cells. Eighteen (**a**, **c**) or 14 (**b**, **d**) days later, PEC from TBM and naïve mice were removed and analyzed for NO production following stimulation with LPS or IFNγ and LPS (**a**, **b**) and phenotype using flow cytometry (**c**, **d**). In mice bearing s.c. tumors, spleen cells were analyzed for expression of CD11b and Gr-1 as well (**c**). NO activity is expressed as nitrite levels for 4 mice per group (mean ± SEM). Phenotypes of PEC and spleen cells are shown on representative dot plots. The experiments were repeated 2–3 times with similar results

that more than just the presence of tumor cells in PEC is responsible for the observed inhibition of NO production.

Ability of PEC from TBM to produce NO resides in nonadherent cells

Adherence to plastic is one of the main features of Mϕ that allows for their enrichment for functional studies. In our previous studies, we have found that the majority of adherent PEC from naïve mice were CD11b$^+$ F4/80$^+$ cells that produced NO upon in vitro stimulation [24]. To test whether nonadherent PEC rather than, or in addition to, adherent PEC in TBM are capable of producing NO upon in vitro stimulation, PEC from TBM were separated into nonadherent cells (removed from the plastic by gentle pipetting) and adherent cells (removed from the plastic with scraping in EDTA solution after removal of nonadherent cells). Nonadherent PEC in TBM were comprised mostly of F4/80$^{dim/-}$ Gr-1$^+$ (Ly6G$^+$ Ly6C$^+$) cells (Fig. 3a) and were the main source of NO production (Fig. 3b). In both naïve and TBM, cells producing NO were phagocytes, as shown by the reduction in NO levels in mice treated with clodronate liposomes (Fig. 3b). These results suggest that a majority of NO-producing phagocytic PEC from TBM, in contrast to PEC from naïve mice, do not adhere to plastic. Consistent with this suggestion, an MTT adherence test showed that adherence of PEC to plastic was reduced in TBM on day 14 (data not shown).

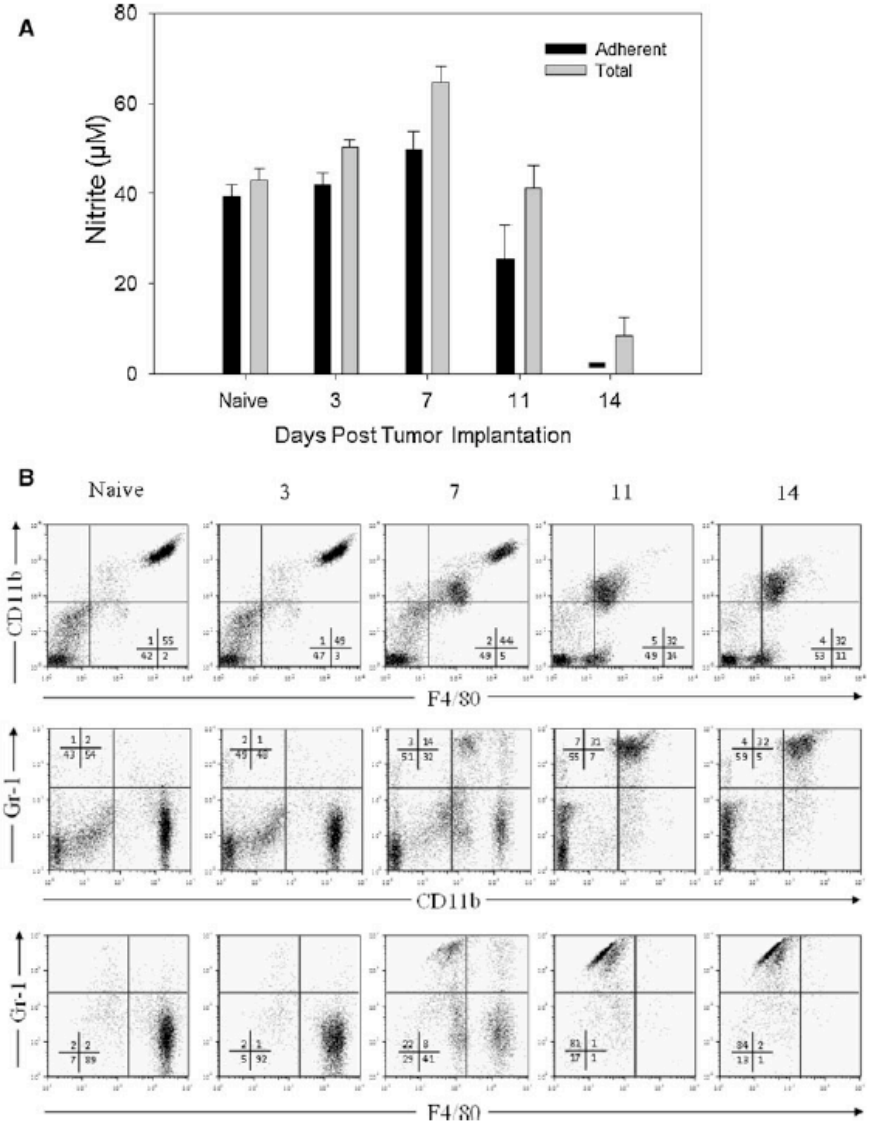

Fig. 2 Kinetics of functional and phenotypic changes in PEC during tumor growth. C57BL/6 mice were injected i.p. with 10^5 B16 cells (day 0). On days 3, 7, 11 and 14, mice were killed and PEC were removed. **a** PEC were placed in 96-well plate, and total (unseparated) or plastic-adherent cells were stimulated with IFN-γ (10 U/ml) and LPS (1 ng/ml). The supernatants were collected 48 h later, and NO activity was determined by nitrite levels. The results are presented as the mean ± SEM nitrite concentration from 4 mice per group. *Dash* signifies value below detection limit. **b** PEC were also analyzed by flow cytometry for CD11b, F4/80 and Gr-1 expression. The *numbers* indicate percentages of cells in each quadrant

Resident PEC do not acquire the Gr-1^+ phenotype during tumor growth

To determine whether resident peritoneal Mϕ acquire the Gr-1^+ phenotype during tumor growth, we performed adoptive transfer of PEC from naïve GFP transgenic mice before injecting the recipient mice with tumor cells. The results in Fig. 3c show that both control (i.e., non-TBM) and TBM contained CD11b^+ Gr1^- donor cells (GFP$^+$), and that the TBM also contained a population of Gr-1^+ PEC that were not seen in the control mice. Importantly, almost all of the CD11b^+ Gr-1^+ PEC in TBM were GFP negative and thus of recipient origin. In addition, host PEC (i.e., EGFP$^-$ cells) in TBM contained a population of F4/80^{dim} cells (both Gr-1^- and Gr-1^+), which was not observed in adoptively transferred EGFP PEC from TBM or in PEC from naïve mice (data not shown). Furthermore, a three-day culture of B16 cells with naïve peritoneal Mϕ or the Mϕ cell line RAW 264.7 did not result in the appearance of Gr-1^+ cells (Supplemental Figure, C). Together these results indicate that resident PEC do not change to the F4/80^{dim}Gr-1^+ phenotype when exposed to B16 (either in vitro or in the peritonea of mice bearing i.p. tumors). These results suggest that bone marrow-derived CD11b^+ F4/80^{dim} Gr-1^+ immature cells are attracted to the peritoneal cavity in response to the presence of peritoneal tumor cells.

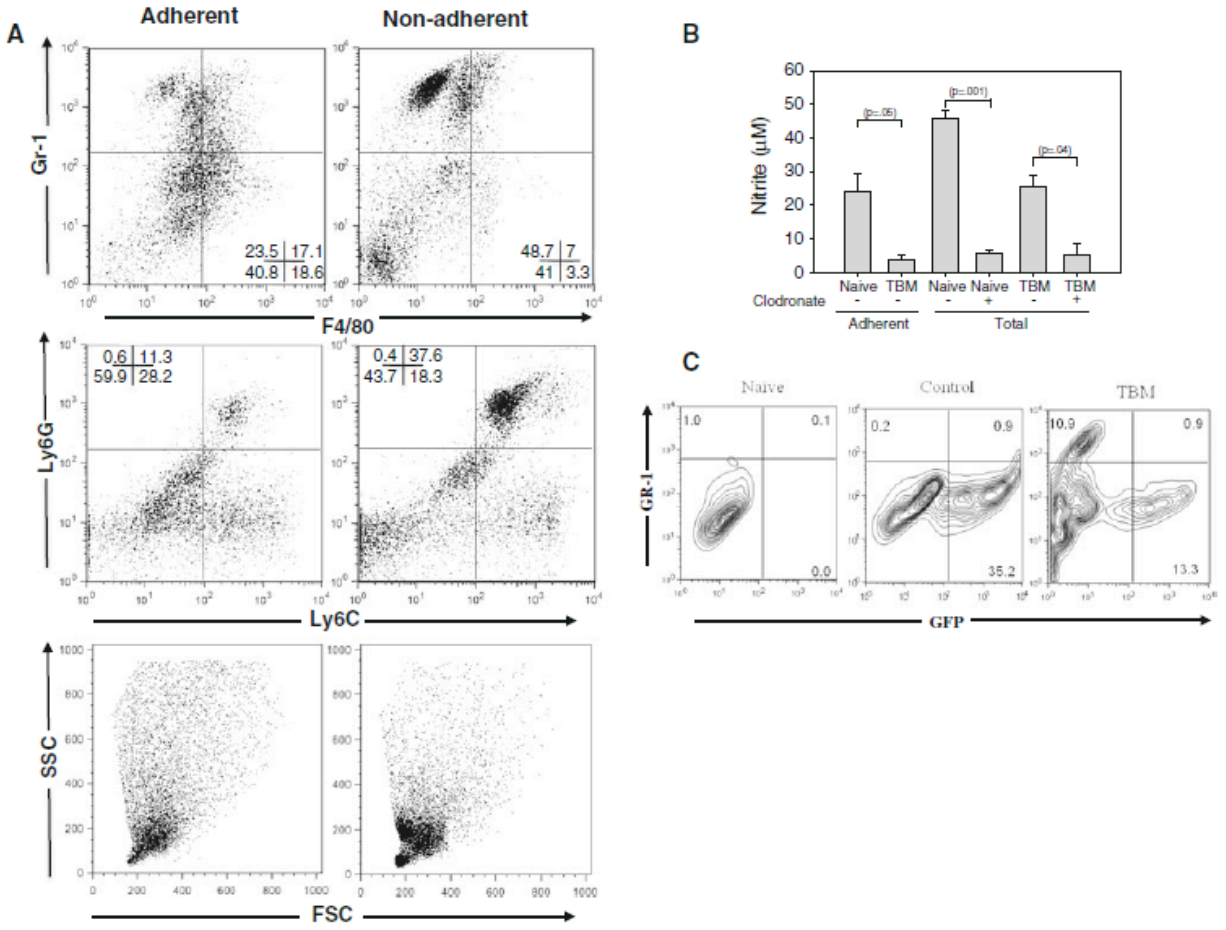

Fig. 3 Functional and phenotypic profile of PEC in tumor-bearing mice. C57BL/6 mice were injected i.p. with 10^5 B16 cells. Fourteen days later, PEC were collected from these mice and from naïve mice and allowed to adhere to plastic for 1.5–2 h. Nonadherent cells were removed by gentle pipetting, and adherent cells were detached from plastic by scraping after N/A cells were washed off. **a** Representative dot plots of PEC from naïve and tumor-bearing mice showing expression of Gr-1, F4/80, Ly6G and Ly6C. **b** NO production by adherent and total (unseparated) PEC from naïve and tumor-bearing mice. Phagocytic cells were depleted from the peritoneal cavity by injecting the mice i.p. with clodronate liposomes 2 days before collecting PEC on day 13 post tumor cell inoculation. Mean ± SEM of triplicate average values of PEC obtained individually from 2–3 mice per group. **c** To determine whether resident Mϕ acquire the Gr-1^+ phenotype during tumor growth, C57BL/6 mice were given a mixture of anti-CD4 and anti-CD8 (day 0, 5) and injected i.p. with 4.8×10^6 PEC from naïve EGFP transgenic mice (day 1).One day later, half of the recipient mice were injected i.p. with 10^5 B16 cells (TBM), while the other half did not receive B16 cells (control). Seven days later, PEC were removed and analyzed for expression of GFP and Gr-1 by flow cytometry after gating on $CD11b^+$ cells, and compared to naïve mice that had not received either B16 or $EGFP^+$ PEC. The results of one out of two representative experiments are shown. The *numbers* indicate percentages of cells in each quadrant

Characterization of sorted PEC from TBM

The change in adherence and presence of B16 tumor cells in PEC from TBM interfered with the accuracy of our culture assay systems to quantitatively compare NO production by identical numbers of PEC subpopulations from naïve and TBM, and interfered with our assay to evaluate the effect of PEC on tumor cell proliferation in vitro. To circumvent these technical problems, we used flow cytometry to sort PEC from tumor-bearing and naïve mice, and were then able to evaluate and directly compare the contribution of specific cell subsets in these functional assays.

In TBM, $CD11b^+Gr\text{-}1^+$ cells, independent of the level of Gr-1 expression (Fig. 4a), secreted less NO than $CD11b^+$ Mϕ from naïve mice (populations 2 and 3, vs. population 1 in Fig. 4c), but still suppressed B16 cell proliferation similarly to $CD11b^+$ cells from naïve mice (Fig. 4d). When mixed at the 1:1 ratio, $CD11b^+Gr\text{-}1^{high}$ cells did not suppress NO production or antitumor effect by naïve Mϕ in response to IFNγ and LPS (data not shown). Among $CD11b^+Gr\text{-}1^+$ cells from TBM, $F4/80^+$

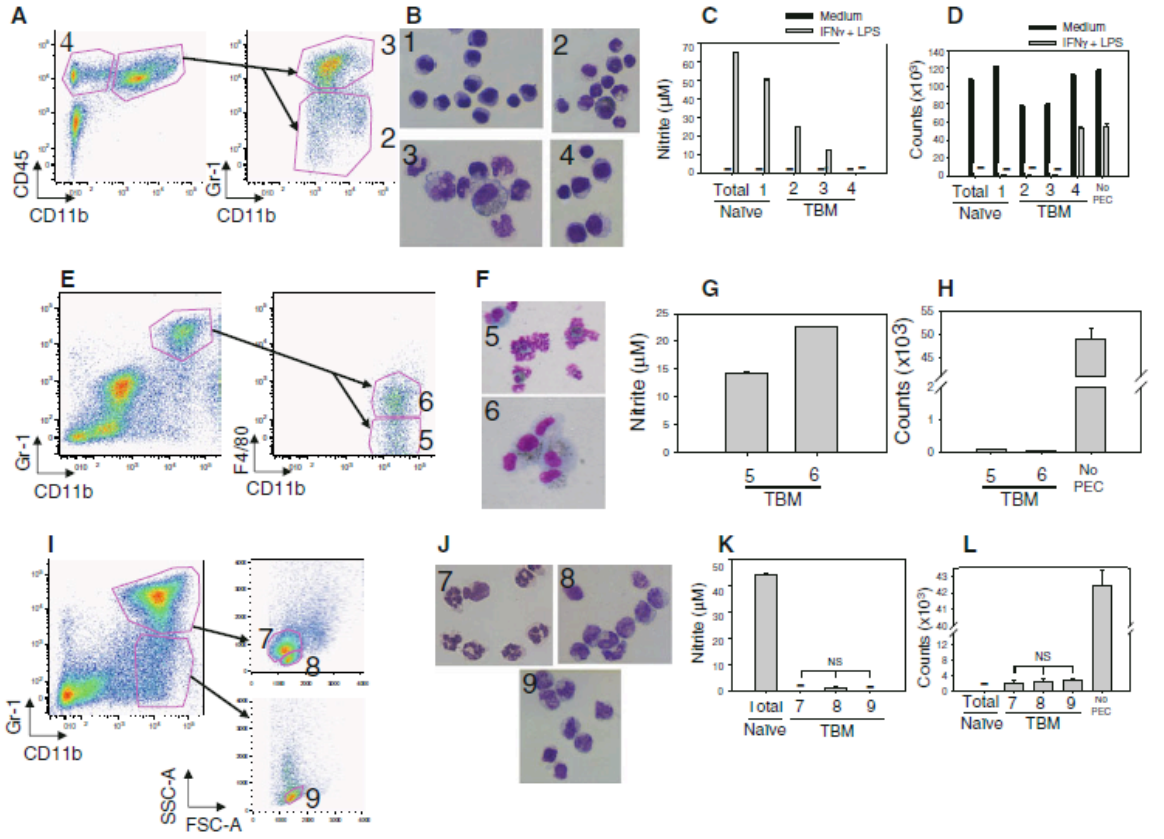

Fig. 4 Functional activity of sorted PEC from tumor-bearing mice. PEC were obtained 14–15 days after injecting C57BL/6 mice i.p. with 1×10^5 B16 cells. PEC were sorted based on their phenotype (**a**, **e**, **i**) and also forward-side scatter characteristics (**i**). The results of three such experiments are presented (**a**–**d**, **e**–**h** and **i**–**l**). The sorting strategy of PEC from TBM is depicted in **a**, **e** and **i**. The morphology of sorted cell fractions from naïve and TBM is presented in **b**, **f** and **j**. The functional data show nitrite levels produced by IFNγ + LPS-stimulated sorted cell fractions (**c**, **g**, **k**) and the ability of these activated sorted cells to inhibit the proliferation of B16 cells in vitro (**d**, **h**, **l**). The numbers designate the sorted cell fraction for that experiment; namely in **a**, the designations 2, 3 and 4 correspond to the populations shown in **b**, **c**, **d**, where "1" depicts sorted CD11b$^+$ PEC from naïve mice. Similarly, in **e**, the designations 5 and 6 correspond to those same designated populations in **f**, **g** and **h**. In **i**, the designations 7, 8 and 9 correspond to those designations in **j**, **k** and **l**. "Total" refers to unsorted PEC from naïve mice. *Dashes* signify values below nitrite detection limit (**c**, **k**) or below 500 cpm (**d**, **l**)

and F4/80$^-$ PEC (Fig. 4e) had a similar ability to both secrete NO and suppress tumor cell proliferation (Fig. 4g, h). Histological evaluation showed that CD11b$^+$Gr-1^{high} cells (population 3 in Fig. 4b) and CD11b$^+$Gr-1^{high}F4/80$^-$ cells (population 5 in Fig. 4f) consisted mostly of granulocytes with a smaller percentage of Mϕ/monocytic cells, while a reverse relationship (predominant Mϕ/monocytes with few granulocytes) was observed in CD11b$^+$Gr-1$^{int/-}$ cells (population 2 in Fig. 4b) and CD11b$^+$Gr-1^{high}F4/80$^+$ cells (population 6 in Fig. 4f). In an attempt to obtain more pure cell populations, CD11b$^+$ PEC were sorted according to their Gr-1 expression and side/forward scatter characteristics (using the gates for granulocytes and monocytes) as shown in Fig. 4i. As a result, relatively pure populations of granulocytes (population 7) and Mϕ/monocytes (populations 8 and 9), respectively, were obtained (Fig. 4j). When each of these populations was stimulated with IFNγ and LPS, each secreted no or minimal NO (Fig. 4k), but still suppressed, to a similar extent, B16 cell proliferation (Fig. 4l). An additional group of sorted cells, CD11b$^+$Gr-1^{high} PEC gated on large cells based on forward scatter and comprising Mϕ according to histological examination, showed similar responses (data not shown). Taken together, these sorting experiments show that following in vitro stimulation with IFNγ and LPS, granulocytic and monocytic CD11b$^+$ PEC from TBM produce less NO than PEC from naïve mice, confirming the results with unsorted PEC in

Fig. 2a, but still effectively suppress tumor cell proliferation in vitro.

Anti-CD40/CpG therapy enhances the antitumor efficacy of tumor-associated myeloid cells

The experiments with sorted PEC showed that tumor-associated myeloid cells can be activated in vitro with IFN-γ and LPS to suppress proliferation of tumor cells. We hypothesized that PEC in TBM can be similarly activated in vivo to mediate antitumor effects against peritoneal tumors. In our previous studies, we had shown that anti-CD40 activates Mϕ via an IFNγ-dependent mechanism [24], and CpG provides a triggering signal to anti-CD40-primed Mϕ in a manner similar to that of LPS, resulting in synergistic antitumor effects against subcutaneous tumors [20]. To determine whether anti-CD40 and CpG given i.p. induce antitumor effects against peritoneal B16 tumors, B16 tumor cells were injected i.p. (day 0) and mice were treated with anti-CD40 on days 4, 11 and 18, and with CpG on days 7 and 14. The combined results of two experiments (Fig. 5a) show that i.p. treatment of TBM with anti-CD40 and CpG resulted in the extended survival of mice compared with control-treated mice (21 vs. 15 median survival days, respectively, $p = 0.0111$ using Gehan–Breslow–Wilcoxon test). This extended survival corresponded to the grossly visible reduction in tumor load in the peritoneal cavity as shown on day 14 (Fig. 5b). Next, we characterized the phenotype and function of PEC following anti-CD40 and CpG therapy. Control-treated and anti-CD40/CpG-treated TBM had similarly increased levels of $CD11^+Gr\text{-}1^+$ PEC compared to non-TBM (Fig. 5c). However, anti-CD40/CpG-treated TBM had an increased percentage of $Ly6C^+$ cells (a marker of monocytic lineage [10, 11]), whereas the percentage of $Ly6G^+$ cells (a marker of granulocytic lineage [10, 11]) remained unchanged (Fig. 5c), suggesting that anti-CD40/CpG treatment leads to the prevalence of monocytic cells in the peritoneal cavity. Histological examination of PEC from anti-CD40/CpG-treated mice revealed tumor cells surrounded by monocytes and PMNs (data not shown). When anti-CD40 treatment was started at an early time point, day 4 post tumor cell implantation, tumor-associated PEC regained their ability to secrete NO in response to IFNγ and LPS in vitro (Fig. 5d). When anti-CD40 treatment was started at a later time point, day 11 post tumor cell implantation, NO production increased only marginally (Fig. 5e). Yet, a substantial antitumor effect in the peritoneal cavities of such treated mice was observed as revealed by the reduced number of $CD45^-$ PEC in anti-CD40/CpG-treated mice (Fig. 5f). Histological examination of sorted $CD45^-$ PEC from B16 tumor-bearing mice, gated to exclude red blood cells, showed that 94% of them were tumor cells (data not shown). Together, these results suggest that, in addition to their activation in vitro, tumor-associated myeloid PEC can be activated in vivo to mediate antitumor effects.

Role of NO, arginase and TNFα in the antitumor effects of stimulated myeloid cells

Our experiments have shown that NO production by PEC from naïve mice correlates with their antitumor effects (Fig. 3b, c); however, this correlation was not observed with sorted PEC from TBM (Fig. 4) or with the antitumor effect of anti-CD40/CpG in vivo (Fig. 5e, f). We therefore investigated the role of NO in antitumor responses in vitro and in vivo. In vitro, the iNOS inhibitor L-NAME substantially reduced nitrite levels (Fig. 6a, c), but did not reduce the antitumor activity of sorted polymorphonuclear neutrophils (PMN) or monocytes from TBM (Fig. 6b). Interestingly, when $CD11b^+$ $Gr\text{-}1^+$ myeloid cells were kept as a single population and not further separated into granulocyte and monocyte fractions, L-NAME significantly reduced, but did not abrogate, the in vitro antitumor effect (Fig. 6d). Inhibition of other cytotoxic molecules, such as arginase and TNF, did not reduce the in vitro antitumor activity of $CD11b^+$ $Gr\text{-}1^+$ cells stimulated with IFN-γ and LPS (Fig. 6d). Inhibition of both iNOS and TNFα in naïve PEC reduced the in vitro antitumor effect to a greater degree than iNOS inhibition alone, but did not have an additive effect in tumor-bearing PEC (Fig. 6d). In vivo, treatment of TBM with iNOS inhibitor L-NAME and anti-CD40/CpG did not reduce, but rather augmented the antitumor effect of anti-CD40/CpG in the mice that survived (Fig. 6e). Together, these results argue against NO playing a major role in the antitumor effects mediated by tumor-associated myeloid cells stimulated in vitro or in vivo.

Discussion

Tumor-induced suppression is one of the obstacles for successful immunotherapy. Most experimental attention has been devoted to investigating the mechanisms of T cell immunosuppression in tumor-bearing hosts, as T cells are considered to be the best effector candidate for immunotherapy due to their greater specificity. T cell suppression in TBM has been attributed to the action of T regulatory cells [25] and MDSC [9–11]. Among other mechanisms, MDSC can suppress T cells by producing NO [26–28]. Although NO inhibits T cell function, it also can kill tumor cells [29], and NO secretion by TAM can be an important mechanism of antitumor effects of cytotoxic T cells [30]. Therefore, activation of cells, such as Mϕ and MDSC, may be an alternative immunotherapy strategy, which may

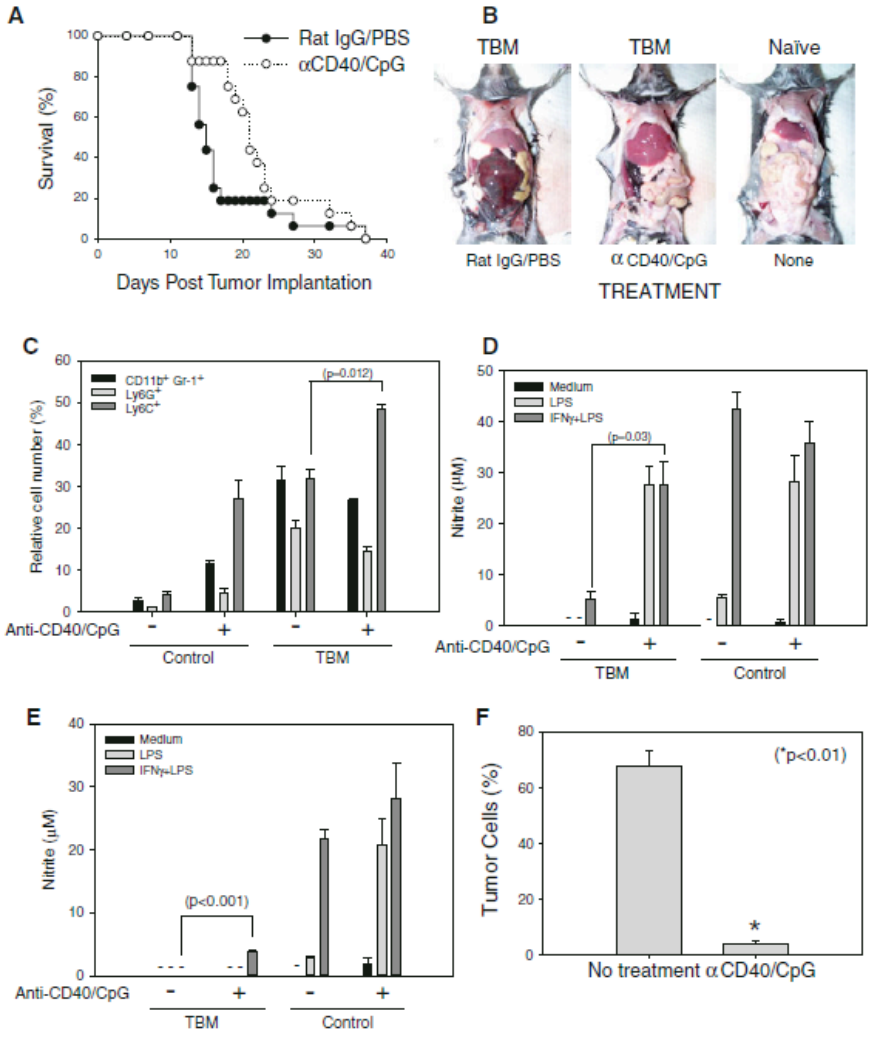

Fig. 5 Antitumor effects of anti-CD40/CpG therapy in vivo are accompanied by the activation of tumor-associated PEC. C57BL/6 mice were injected i.p. with 10^5 B16 cells. Anti-CD40/CpG treatments were administered on day 4/7, 11/14, and an additional injection of anti-CD40 was given in some experiments on day 18. Control mice received rat IgG and PBS, respectively. **a** The mice were followed for survival. The results of two combined experiments are shown ($n = 16$ mice per group). **b** Photographs of representative mice showing peritoneal tumor loads were taken on day 14 post B16 tumor cell injections; a naïve mouse is shown for comparison. The peritoneal tumor appears hemorrhagic. **c** Percentage of $CD11b^+Gr\text{-}1^+$ cells, as well as $Ly6G^+$ and $Ly6C^+$ cells, are shown (mean ± SEM, 3 mice per group). **d**–**f** Tumor-bearing mice were treated with anti-CD40/CpG on days 4/7 and 10 (**d**) or on days 11/14 (**e**, **f**) post tumor cell implantation. PEC were isolated on day 14 (**d**) or 15 (**e**, **f**), and adherent cells were tested for NO production (**d**, **e**). *Dashes* signify values below detection limit. The antitumor effect was determined by the percentage of B16 tumor cells ($CD45^-$ PEC) using flow cytometry (**f**). Mean ± SEM of 4 mice per group. * $p < 0.001$

involve NO and does not require T cells. In support of this hypothesis, we have previously shown that treatment of TBM with anti-CD40 caused T cell-independent tumor growth suppression which involved NO production by Mϕ [31]. The synergistic antitumor effects were achieved by the combination of anti-CD40 and CpG [20], even in mice whose T cell and NK functions were inhibited by chemotherapy [22, 32]. In this study, we show that both granulocytic and monocytic myeloid cells at the site of tumor growth are capable of being activated to mediate antitumor effects.

Our results show that peritoneal Mϕ in mice bearing advanced s.c. B16 tumors are not immunologically inert. In fact, they produced high levels of NO in response to IFNγ and LPS, similar to those produced by Mϕ in naïve mice. These findings are similar to those obtained with the

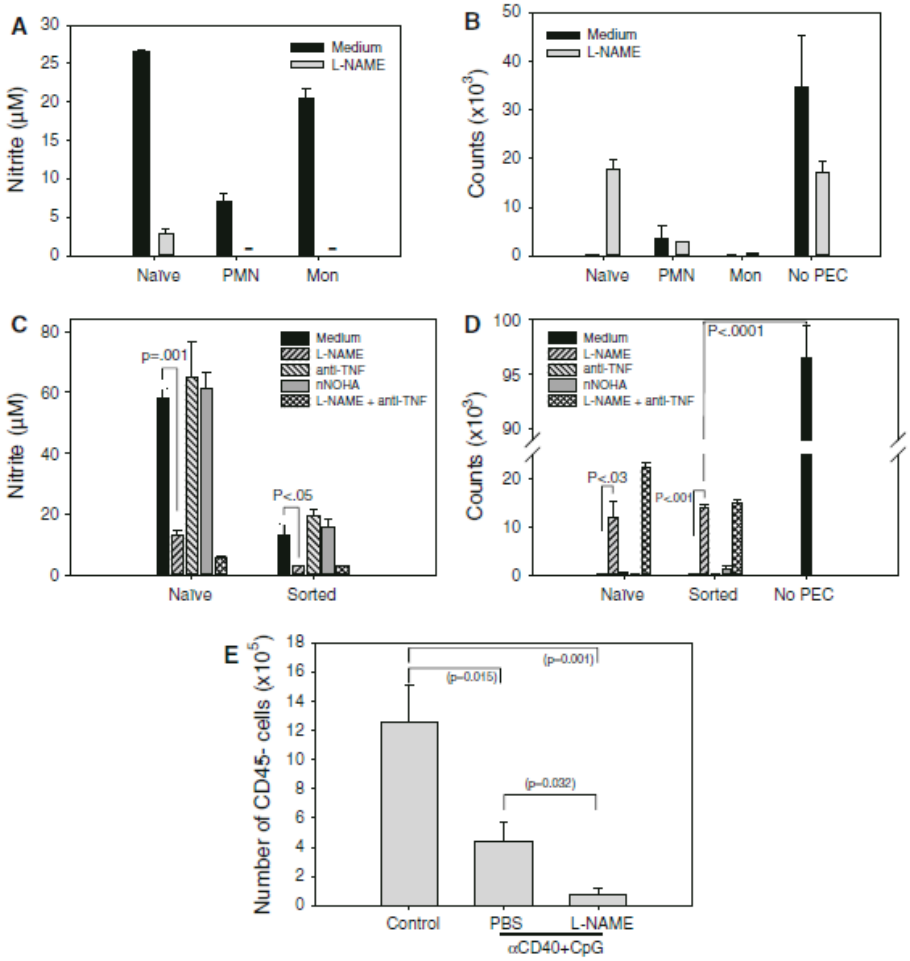

Fig. 6 Role of NO, arginase and TNFα in the antitumor effects mediated by myeloid cells. PEC were obtained 15 (**a**, **b**) or 14 (**c**, **d**) days following injecting C57BL/6 mice i.p. with 10^5 B16 cells. PEC were sorted based on their $CD11b^+Gr\text{-}1^+$ phenotype (**a**–**d**) and also forward-side scatter characteristics, resulting in populations enriched for polymorphonuclear cells (PMN) and monocytes (Mon) (**a**, **b**) as also was verified by histology (not shown). PEC from naïve mice were used as the control. The inhibitors of NO, arginase and TNFα were added as described in "Materials and methods." The functional data show mean ± SEM of nitrite levels produced by IFN-γ + LPS-stimulated sorted cell fractions (**a**, **c**) and the ability of the sorted cells to inhibit proliferation of B16 cells in vitro (**b**, **d**). *Dashes* signify values below detection limit (**a**). e Tumor-bearing mice were treated with anti-CD40 on day 11 and CpG on day 14 post tumor cell implantation. To neutralize NO in vivo, L-NAME was injected either i.p. at the dose of 50 mg/kg twice a day or given in the drinking water at the dose of 0.5 g/l on days 11–14. PEC were isolated on day 15, and the percentage of B16 tumor cells ($CD45^-$ PEC) was determined by flow cytometry. The combined data of two experiments are presented. Mean ± SEM of 10 mice per group or 7 mice for the last group (3 of 5 mice treated with anti-CD40/CpG/L-NAME died from toxicity following i.p. injections)

D1-DMBA-3 mammary tumor model [33] and are consistent with the results of Danna et al. [7], which show that the systemic function of Mϕ is not inhibited in mice bearing advanced s.c. 4T1 tumors. The reported inhibited ability of peritoneal Mϕ from mice bearing s.c. B16 melanoma to produce NO [34] may be due to the fact that these Mϕ were elicited, rather than resident, as in our experiments. Therefore, our results in the s.c. B16 melanoma model indicate that tumor growth does not induce systemic suppression of Mϕ functions.

To analyze the phenotype and function of tumor-associated cells, we chose the peritoneal model as it offers the possibility of locally determining the number and phenotype of both host and tumor cells while avoiding the loss of cell populations caused by enzymatic digestion of s.c. tumors. Our results using NO production as the readout confirm the studies showing reduced NO production by immunosuppressed TAM [33]. The ability of B16 tumor cells to suppress NO production by adherent PEC 2 weeks after i.p. injection of 10^5 B16 cells, but not 4 days after i.p.

injection of 1.6×10^7 B16 cells, suggests that prolonged interaction of tumor cells and Mϕ is required for Mϕ suppression. These functional findings suggest that TAM from peritoneal TBM may express the M2 phenotype, similar to data we reported for the s.c. B16 model in our previous study, where TAM expressed high surface levels of B7-H1 and intracellular levels of IL-10 and IL-4, but negligible levels of IFN-γ, TNF-α and IL-12 [32].

It has been shown that tumor growth leads to expansion of CD11b$^+$ Gr-1$^+$ cells in mice [9–11, 14]. In this study, we confirmed this observation in the peritoneal B16 model and found an inverse correlation of the percentage of CD11b$^+$ Gr-1$^+$ PEC and the NO levels they produced. The phenotypic change of Mϕ from Gr-1$^-$ to Gr-1$^+$ does not appear to be tumor-specific, as it was described in response to certain agents, such as dextrans [35], treatments with anti-CD40/CpG [22] or chemotherapy [32], or infections, such as toxoplasmosis [36]. We found that CD11b$^+$ F4/80^{bright} Gr-1$^-$ Mϕ present in naïve mice disappeared from the peritoneal cavity of TBM and were replaced with CD11b$^+$ F4/80$^{dim/-}$ Gr-1$^+$ cells. The results of in vivo experiments using adoptive transfer of PEC from EGFP transgenic mice (Fig. 3c) and short-term in vitro experiments show that resident PEC do not acquire the Gr-1$^+$ phenotype in response to the tumor's presence, suggesting that bone marrow-derived (potentially immature) cells with the CD11b$^+$ F4/80$^{dim/-}$ Gr-1$^+$ phenotype enter the peritoneal cavity in response to the tumor. In agreement with this suggestion, it has been recently shown that circulating monocytes in TBM reduce expression of F4/80 and acquire expression of Gr-1[37]. The experiments with sorted PEC from TBM (Fig. 4) revealed that these CD11b$^+$ Gr-1$^+$ myeloid cells can be activated to secrete NO and mediate antitumor effects. This finding is in agreement with recent results showing that CD11b$^+$ Gr-1$^+$ MDSC can be activated in vivo with IFN-γ and LPS to secrete NO and suppress T cells [38]. Similarly, it was shown that cyclophosphamide induces the expansion of early myeloid cells, inhibiting tumor cell growth by a mechanism that involves NO [39]. Although there are anecdotal reports on the antitumor effects of MDSC, we believe our data show, for the first time, that tumor-induced myeloid cells can be specifically targeted by immunotherapy to mediate antitumor effects in vitro and in vivo.

It is possible that sorted CD11b$^+$ PEC from TBM displayed antitumor activity in vitro because they were separated from B16 cells and therefore released from tumor-related suppression. However, the antitumor activity of the sorted CD11b$^+$ Gr-1$^+$ PEC from TBM was not inhibited by adding B16 cell supernatant to the assay (data not shown). Moreover, our results show that anti-CD40 and CpG treatment of mice with an advanced peritoneal B16 tumor (tumor cells injected i.p. 10 days earlier) resulted in significant reduction in local tumor load (Fig. 5). This in vivo result suggests that, even in the presence of growing tumor, myeloid PEC can be activated to mediate antitumor effects in vivo (Fig. 5).

TAM have been reported to facilitate tumor growth and serve as a negative prognostic factor for patients with certain cancers [17, 18]. The studies presented here show, in addition, that tumor-associated myeloid cells including TAM can be activated in vitro and in vivo to mediate antitumor effects. One of the mechanisms by which anti-CD40 and CpG affect tumor-associated cells can involve switching the Mϕ phenotype from M2 to M1. This assertion is supported by previous data in which anti-CD40 plus CpG immunotherapy in a s.c. B16 model downregulated the expression of B7-H1, IL-10 and IL-4 in TAM, and upregulated the expression of CD40, CD80, CD86, MHC class II, IFN-γ, TNF-α and IL-12 (32). These results are in agreement with the findings by Guiducci et al. [19] that demonstrated that CpG plus anti–interleukin-10 receptor antibody switched TAM from M2 to M1, resulting in antitumor activity. Our past [21, 24, 32] and present data are consistent with recent preclinical and clinical data showing that, in mice and in patients with pancreatic cancer, antitumor effects induced by agonistic anti-CD40 appear to involve M1 macrophages [40].

The nature of antitumor effector cells in the peritoneal cavity of TBM is not entirely clear. When flow cytometry was used to sort PEC based on their phenotype and size/granularity, tumor-associated PEC that become antitumor effector cells in vitro in response to IFN-γ and LPS consisted of two major groups of cells: CD11b$^+$Gr-1^{high} F4/80$^-$ granulocytes and CD11b$^+$Gr-1$^{+/-}$ F4/80^{dim} monocytes/Mϕ. These findings are in agreement with reports showing that MDSC consist of granulocytes and monocytes/Mϕ in mice [27, 41] and in people with cancer [41]. Each cell type was equally effective in suppressing B16 cell proliferation in vitro. We found that in TBM, NO-producing PEC capable of phagocytosing clodronate liposomes (as evidenced by the reduction in NO production) were mainly nonadherent to plastic. Together with the downregulation of the Mϕ marker F4/80, these results suggest that either Mϕ change their phenotype and properties in TBM, or that functional PEC are not mature Mϕ at all, but are rather MDSC or monocytes. In support of the second hypothesis, the results in Fig. 3a show that most nonadherent PEC in TBM have high expression of Ly6C, a marker that is highly expressed on precursor cells and downregulated when monocytes mature in the blood [42].

The mechanism of the antitumor effect mediated by activated myeloid cells is not completely understood. The main factors implicated in the antitumor mechanisms of activated Mϕ are NO [29–31, 43, 44], TNFα [31, 44, 45] or arginase [46]. Our in vitro results indicate that NO does not

play a major role in tumor cell suppression by sorted PEC from TBM. Our in vivo data using iNOS inhibitor L-NAME (Fig. 6e) suggest that NO can even suppress the antitumor effect of anti-C40 + CpG immunotherapy. This result (Fig. 6e) may be analogous to a recently published study in which L-NAME treatment in vivo augmented the antitumor effect of IL-12 [47]. The mechanism of the enhanced antitumor effect by iNOS inhibition is not clear. It is known that NO may have protumor and antitumor effects depending on the level and persistence of NO in the tissue, microenvironment and tumor cell sensitivity [48]. It has been shown that iNOS inhibitors reduced the growth of human gastric tumors [49] or melanomas [50] in immunodeficient mice, an effect that was associated with reduced angiogenesis. Whether inhibition of angiogenesis or another mechanism (e.g., increased lymphatic contraction suppressed by $CD11b^+$ $Gr\text{-}1^+$ cells via NO production [51]) is responsible for the increased antitumor effect of iNOS inhibitor L-NAME in our model warrants further investigation.

In addition to a limited role of NO, our in vitro results suggest no role of TNFα and arginase in tumor cell suppression (Fig. 6). It is possible that the mechanism of tumor killing by activated myeloid cells is similar to that of Mϕ activated by cyclophosphamide and IL-12 [52]. This mechanism was found to be NO-independent and contact-dependent. It cannot be excluded, however, that NO may play a role in suppressing tumor metastasis, while being ineffective against primary tumors, as was recently shown for IL-2/anti-CD40 immunotherapy [53]. It appears that anti-CD40/CpG immunotherapy can induce antitumor effects of myeloid cells at least by two mechanisms: by directly activating them to mediate antitumor effects, as found in this study, and indirectly by reducing their suppression of antitumor T cells, as was recently reported for CpG immunotherapy [54]. Given the expansion of myeloid cells in cancer patients [55], strategies for activating these cells against the tumor, as shown in this study, might be a novel approach for cancer immunotherapy that warrants further investigation.

Acknowledgments. We thank Songwon Seo for performing correlative statistical analysis and Jennifer Levenson for breeding EGFP transgenic mice. This work was supported by NIH-NCI grants CA87025 and CA32685, a grant from the Midwest Athletes Against Childhood Cancer (MACC) Fund and support from The Crawdaddy Foundation.

Conflict of interest The authors declare that they have no conflict of interest.

References

1. De Souza AP, Bonorino C (2009) Tumor immunosuppressive environment: effects on tumor-specific and nontumor antigen immune responses. Expert Rev Anticancer Ther 9:1317–1332 (Review)
2. Ostrand-Rosenberg S, Sinha P, Danna EA, Miller S, Davis C, Dissanayake SK (2004) Antagonists of tumor-specific immunity: tumor-induced immune suppression and host genes that co-opt the anti-tumor immune response. Breast Dis 20:127–135
3. Mantovani A, Allavena P, Sica A (2004) Tumour-associated macrophages as a prototypic type II polarized phagocyte population: role in tumour progression. Eur J Cancer 40:1660–1667
4. Mullins DW, Martins RS, Elgert KD (2003) Tumor-derived cytokines dysregulate macrophage interferon-gamma responsiveness and interferon regulatory factor-8 expression. Exp Biol Med (Maywood) 228:270–277
5. Jaffe ML, Arai H, Nabel GJ (1996) Mechanisms of tumor-induced immunosuppression: evidence for contact-dependent T cell suppression by monocytes. Mol Med 2:692–701
6. Taams LS, van Amelsfort JM, Tiemessen MM, Jacobs KM, de Jong EC, Akbar AN, Bijlsma JW, Lafeber FP (2005) Modulation of monocyte/macrophage function by human CD4+CD25+ regulatory T cells. Hum Immunol 66:222–230
7. Danna EA, Sinha P, Gilbert M, Clements VK, Pulaski BA, Ostrand-Rosenberg S (2004) Surgical removal of primary tumor reverses tumor-induced immunosuppression despite the presence of metastatic disease. Cancer Res 64:2205–2211
8. Sinha P, Clements VK, Ostrand-Rosenberg S (2005) Reduction of myeloid-derived suppressor cells and induction of M1 macrophages facilitate the rejection of established metastatic disease. J Immunol 174:636–645
9. Talmadge JE (2007) Pathways mediating the expansion and immunosuppressive activity of myeloid-derived suppressor cells and their relevance to cancer therapy. Clin Cancer Res 13:5243–5248
10. Gabrilovich DI, Nagaraj S (2009) Myeloid-derived suppressor cells as regulators of the immune system. Nat Rev Immunol 9:162–174 (Review)
11. Peranzoni E, Zilio S, Marigo I, Dolcetti L, Zanovello P, Mandruzzato S, Bronte V (2010) Myeloid-derived suppressor cell heterogeneity and subset definition. Curr Opin Immunol 22:238–244 (Review)
12. Apolloni E, Bronte V, Mazzoni A, Serafini P, Cabrelle A, Segal DM, Young HA, Zanovello P (2000) Immortalized myeloid suppressor cells trigger apoptosis in antigen-activated T lymphocytes. J Immunol 165:6723–6730
13. Huang B, Pan PY, Li Q, Sato AI, Levy DE, Bromberg J, Divino CM, Chen SH (2006) Gr-1+CD115+ immature myeloid suppressor cells mediate the development of tumor-induced T regulatory cells and T-cell anergy in tumor-bearing host. Cancer Res 66:1123–1131
14. Sinha P, Clements VK, Fulton AM, Ostrand-Rosenberg S (2007) Prostaglandin E2 promotes tumor progression by inducing myeloid-derived suppressor cells. Cancer Res 67:4507–4513
15. Popovic PJ, Zeh HJ III, Ochoa JB (2007) Arginine and immunity. J Nutr 137:1681S–1686S (Review)
16. Sinha P, Clements VK, Bunt SK, Albelda SM, Ostrand-Rosenberg S (2007) Cross-talk between myeloid-derived suppressor cells and macrophages subverts tumor immunity toward a type 2 response. J Immunol 179:977–983
17. Leek RD, Harris AL (2002) Tumor-associated macrophages in breast cancer. J Mammary Gland Biol Neoplasia 7:177–189
18. Knowles H, Leek R, Harris AL (2004) Macrophage infiltration and angiogenesis in human malignancy. Novartis Found Symp 256:189–200
19. Guiducci C, Vicari AP, Sangaletti S, Trinchieri G, Colombo MP (2005) Redirecting in vivo elicited tumor infiltrating macrophages and dendritic cells towards tumor rejection. Cancer Res 65:3437–3446
20. Buhtoiarov IN, Lum H, Berke G, Sondel PM, Rakhmilevich AL (2006) Synergistic activation of macrophages via CD40 and

TLR9 results in T cell independent antitumor effects. J Immunol 176:309–318
21. Wu Q, Buhtoiarov IN, Sondel PM, Rakhmilevich AL, Ranheim EA (2009) Tumoricidal effects of activated macrophages in a mouse model of chronic lymphocytic leukemia. J Immunol 182:6771–6778
22. Johnson EE, Buhtoiarov IN, Baldeshwiler MJ, Felder MAR, Van Rooijen N, Sondel PM, Rakhmilevich AL (2011) Enhanced T cell-independent antitumor effect of cyclophosphamide combined with anti-CD40 mAb and CpG in mice. J Immunother 34:76–84
23. Van Rooijen N, Sanders A (1994) Liposome mediated depletion of macrophages: mechanism of action, preparation of liposomes and applications. J Immunol Methods 174:83–93
24. Buhtoiarov IN, Lum H, Berke G, Paulnock D, Sondel PM, Rakhmilevich AL (2005) CD40 ligation induces antitumor reactivity of murine macrophages via an IFN gamma-dependent mechanism. J Immunol 174:6013–6022
25. Elkord E, Alcantar-Orozco EM, Dovedi SJ, Tran DQ, Hawkins RE, Gilham DE (2010) T regulatory cells in cancer: recent advances and therapeutic potential. Expert Opin Biol Ther 10:1573–1586
26. Hegardt P, Widegren B, Sjögren HO (2000) Nitric-oxide-dependent systemic immunosuppression in animals with progressively growing malignant gliomas. Cell Immunol 200:116–127
27. Youn JI, Nagaraj S, Collazo M, Gabrilovich DI (2008) Subsets of myeloid-derived suppressor cells in tumor-bearing mice. J Immunol 181:5791–5802
28. Jia W, Jackson-Cook C, Graf MR (2010) Tumor-infiltrating, myeloid-derived suppressor cells inhibit T cell activity by nitric oxide production in an intracranial rat glioma + vaccination model. J Neuroimmunol 223:20–30
29. Ortega A, Carretero J, Obrador E, Estrela JM (2008) Tumoricidal activity of endothelium-derived NO and the survival of metastatic cells with high GSH and Bcl-2 levels. Nitric Oxide 19:107–114
30. Vicetti Miguel RD, Cherpes TL, Watson LJ, McKenna KC (2010) CTL induction of tumoricidal nitric oxide production by intratumoral macrophages is critical for tumor elimination. J Immunol 185:6706–6718
31. Lum HD, Buhtoiarov IN, Schmidt BE, Berke G, Paulnock DM, Sondel PM, Rakhmilevich AL (2006) Tumoristatic effects of anti-CD40 mAb-activated macrophages involve nitric oxide and tumor-necrosis factor-α. Immunology 118:261–270
32. Buhtoiarov IN, Sondel PM, Wigginton JM, Buhtoiarova TN, Yanke EM, Mahvi DA, Rakhmilevich AL (2011) Antitumor synergy of cytotoxic chemotherapy and anti-CD40 plus CpG-ODN immunotherapy through repolarization of tumor associated macrophages. Immunology 132:226–239
33. Dinapoli MR, Calderon CL, Lopez DM (1996) The altered tumoricidal capacity of macrophages isolated from tumor-bearing mice is related to reduce expression of the inducible nitric oxide synthase gene. J Exp Med 183:1323–1329
34. Naama HA, McCarter MD, Mack VE, Evoy DA, Hill AD, Shou J, Daly JM (2001) Suppression of macrophage nitric oxide production by melanoma: mediation by a melanoma-derived product. Melanoma Res 11:229–238
35. Atochina O, Daly-Engel T, Piskorska D, McGuire E, Harn DA (2001) A schistosome-expressed immunomodulatory glycoconjugate expands peritoneal Gr1(+) macrophages that suppress naive CD4(+) T cell proliferation via an IFN-gamma and nitric oxide-dependent mechanism. J Immunol 167:4293–4302
36. Dunay IR, Damatta RA, Fux B, Presti R, Greco S, Colonna M, Sibley LD (2008) Gr1(+) inflammatory monocytes are required for mucosal resistance to the pathogen Toxoplasma gondii. Immunity 29:306–317
37. Caso R, Silvera R, Carrio R, Iragavarapu-Charyulu V, Gonzalez-Perez RR, Torroella-Kouri M (2010) Blood monocytes from mammary tumor-bearing mice: early targets of tumor-induced immune suppression? Int J Oncol 37:891–900
38. Greifenberg V, Ribechini E, Rössner S, Lutz MB (2009) Myeloid-derived suppressor cell activation by combined LPS and IFN-gamma treatment impairs DC development. Eur J Immunol 39:2865–2876
39. Pelaez B, Campillo JA, Lopez-Asenjo JA, Subiza JL (2001) Cyclophosphamide induces the development of early myeloid cells suppressing tumor cell growth by a nitric oxide-dependent mechanism. J Immunol 166:6608–6615
40. Beatty GL, Chiorean EG, Fishman MP, Saboury B, Teitelbaum UR, Sun W, Huhn RD, Song W, Li D, Sharp LL, Torigian DA, O'Dwyer PJ, Vonderheide RH (2011) CD40 agonists alter tumor stroma and show efficacy against pancreatic carcinoma in mice and humans. Science 331:1612–1616
41. Dolcetti L, Peranzoni E, Ugel S, Marigo I, Fernandez Gomez A, Mesa C, Geilich M, Winkels G, Traggiai E, Casati A, Grassi F, Bronte V (2010) Hierarchy of immunosuppressive strength among myeloid-derived suppressor cell subsets is determined by GM-CSF. Eur J Immunol 40:22–35
42. Sunderkötter C, Nikolic T, Dillon MJ, van Rooijen N, Stehling M, Drevets DA, Leenen PJM (2004) Subpopulations of mouse blood monocytes differ in maturation stage and inflammatory response. J Immunol 172:4410–4417
43. Cui SJ, Reichner JS, Mateo RB, Albina JE (1994) Activated murine macrophages induce apoptosis in tumor-cells through nitric-oxide-dependent or nitric-oxide-independent mechanisms. Cancer Res 54:2462–2467
44. Klostergaard J, Leroux ME, Hung MC (1991) Cellular-models of macrophage tumoricidal effector mechanisms in vitro: characterization of cytolytic responses to tumor-necrosis-factor and nitric-oxide pathways in vitro. J Immunol 147:2802–2808
45. Decker T, Lohmannmatthes ML, Gifford GE (1987) Cell-associated tumor-necrosis-factor (TNF) as a killing mechanism of activated cytotoxic macrophages. J Immunol 138:957–962
46. Ellyard JI, Quah BJ, Simson L, Parish CR (2010) Alternatively activated macrophage possess antitumor cytotoxicity that is induced by IL-4 and mediated by arginase-1. J Immunother 33:443–452
47. Egilmez NK, Harden JL, Virtuoso LP, Schwendener RA, Kilinc MO (2011) Nitric oxide short-circuits interleukin-12-mediated tumor regression. Cancer Immunol Immunother 60:839–845
48. Fukumura D, Kashiwagi S, Jain RK (2006) The role of nitric oxide in tumour progression. Nat Rev Cancer 6:521–534 (Review)
49. Wang GY, Ji B, Wang X, Gu JH (2005) Anti-cancer effect of iNOS inhibitor and its correlation with angiogenesis in gastric cancer. World J Gastroenterol 1:3830–3833
50. Sikora AG, Gelbard A, Davies MA, Sano D, Ekmekcioglu S, Kwon J, Hailemichael Y, Jayaraman P, Myers JN, Grimm EA, Overwijk WW (2010) Targeted inhibition of inducible nitric oxide synthase inhibits growth of human melanoma in vivo and synergizes with chemotherapy. Clin Cancer Res 16:1834–1844
51. Liao S, Cheng G, Conner DA, Huang Y, Kucherlapati RS, Munn LL, Ruddle NH, Jain RK, Fukumura D, Padera TP (2011) Impaired lymphatic contraction associated with immunosuppression. Proc Natl Acad Sci USA 108:18784–18789
52. Tsung K, Dolan JP, Tsung YL, Norton JA (2002) Macrophages as effector cells in interleukin 12-induced T cell-dependent tumor rejection. Cancer Res 62:5069–5075
53. Weiss JM, Ridnour LA, Back T, Hussain SP, He P, Maciag AE, Keefer LK, Murphy WJ, Harris CC, Wink DA, Wiltrout RH (2010) Macrophage-dependent nitric oxide expression regulates tumor cell detachment and metastasis after IL-2/anti-CD40 immunotherapy. J Exp Med 207:2455–2467

54. Zoglmeier C, Bauer H, Noerenberg D, Wedekind G, Bittner P, Sandholzer N, Rapp M, Anz D, Endres S, Bourquin C (2011) CpG blocks immune suppression by myeloid-derived suppressor cells in tumor-bearing mice. Clin Cancer Res 17:1765–1775

55. Mandruzzato S, Solito S, Falisi E, Francescato S, Chiarion-Sileni V, Mocellin S, Zanon A, Rossi CR, Nitti D, Bronte V, Zanovello P (2009) IL4Ralpha+ myeloid-derived suppressor cell expansion in cancer patients. J Immunol 182:6562–6568

A.6 Intratumoral Delivery of Low Doses of anti-CD40 mAb Combined with Monophosphoryl Lipid A induces T cell-independent, Local and Systemic Antitumor Effects in Mice

Tyler J. Van De Voort[*], Mildred A.R. Felder[§], Richard K. Yang[*], Paul M. Sondel[*†‡], and Alexander L. Rakhmilevich[*‡]

[*]University of Wisconsin, Departments of Human Oncology, [†]Pediatrics, and [§]Obstetrics and Gynecology, [‡]Paul P. Carbone Comprehensive Cancer Center, Madison, WI USA

Running title: T cell-independent antitumor effects of anti-CD40 and MPL

Address correspondence and reprint requests to: Dr. Alexander L. Rakhmilevich, University of Wisconsin-Madison, Department of Human Oncology, 4136 WIMR, 1111 Highland Avenue, Madison, WI 53705. Phone: (608)263-5193; Fax: (608)263-4226; E-mail address: rakhmil@humonc.wisc.edu.

Conflicts of Interest and Source of Funding: The authors declare no existing conflicts of interest. This study was supported by NIH-NCI grants CA87025 and CA32685, a grant from the Midwest Athletes Against Childhood Cancer (MACC) Fund, support from The Crawdaddy Foundation, and a UW-Madison Hilldale Undergraduate Research Fellowship (to T.J.V.).

Key words: immunotherapy, anti-CD40, monophosphoryl lipid A, macrophages, intratumoral

Abbreviations used in this paper: MPL, monophosphoryl lipid A; Mϕ, macrophages; PEC, peritoneal exudate cells; i.t., intratumoral; [^{3}H]-TdR, tritiated thymidine

Abstract

In this study, an agonistic anti-CD40 monoclonal antibody (anti-CD40) was combined with monophosphoryl lipid A (MPL), a nontoxic derivative of LPS and agonist of toll-like receptor 4 (TLR4), to assess the immunomodulatory and antitumor synergy between the two agents in mice. Anti-CD40 was capable of priming macrophages to subsequent *ex vivo* activation by MPL in immunocompetent and T cell-deficient mice. Intraperitoneal injections of anti-CD40+MPL induced additive to synergistic suppression of poorly immunogenic B16-F10 melanoma growing subcutaneously in syngeneic mice. When anti-CD40+MPL were injected directly into the subcutaneous tumor, the combination treatment was more effective, even with a 25-fold reduction in dose. Low-dose intratumoral treatment also slowed the growth of a secondary tumor growing simultaneously at a distant, untreated site. These antitumor effects were reproduced in immunodeficient SCID mice and in T cell-depleted C57BL/6 mice. Taken together, our results show that the antitumor effects of anti-CD40 are enhanced by subsequent treatment with MPL, even in T cell-deficient hosts. These preclinical data suggest that an anti-CD40+MPL combined regimen is appropriate for clinical testing in human patients, including cancer patients that may be immunosuppressed from prior chemotherapy.

Introduction

The CD40 receptor protein is expressed on antigen-presenting cells and is an important co-stimulatory molecule for T cell, B cell, and macrophage (Mϕ) activation. Many experimental cancer immunotherapies are designed to activate the CD40 pathway in order to enhance the potency of tumor-specific cytotoxic T lymphocytes (1). Unfortunately, effective preclinical T cell-mediated therapies have been difficult to translate into clinical settings (2–7) because of immunosuppressive factors in the tumor microenvironment (6, 8) and immunosuppression caused by other factors, including conventional cancer treatments (9, 10). However, innate immune cells, including Mϕ have been shown to be more durable and recover from chemotherapy more quickly than B or T lymphocytes (3), suggesting that T cell-independent antitumor strategies based on the innate immune system may be of value as alternatives to T cell-dependent immunotherapies.

T cells are not the only type of cells that can be activated by CD40 ligation; our lab (11–14) and others (15) have shown that T cells may not be necessary for the antitumor effects observed when this pathway is activated. For instance, in a murine pancreatic tumor model, T cells seemed unable to infiltrate the tumor microenvironment upon anti-CD40 treatment, and instead migrated to the tumor periphery (15).

Our group has been using a murine B16-F10 melanoma model to explore T cell-independent antitumor mechanisms of CD40 ligation in combination with clinically relevant immunostimulants. Previous *in vitro* studies in our lab showed that anti-CD40 stimulated Mϕ to mediate antitumor effects in an IFNγ-dependent manner (12). Anti-CD40 was also found to initiate T cell-independent antitumor effects against intraperitoneal (i.p.) (13) and subcutaneous (s.c.) (14) B16 tumors in mice. When combined with a toll-like receptor (TLR) 9 agonist, CpG,

the antitumor effects of anti-CD40 were synergistically enhanced, retarding tumor growth and prolonging survival in C57BL/6 and SCID/beige mice bearing either B16 melanoma or NXS2 neuroblastoma tumors, respectively. The antitumor effects persisted in the absence of T cells, cytolytic NK cells, and neutrophils (14). CpG has been used as a T cell adjuvant preclinically (16) and clinically (17); while the ability of CpG to activate Mϕ and other cells of the mouse innate immune system has been documented by our group (14, 18) and others (19), CpG seems to be less effective in activating human Mϕ (20) .

As an activator of the TLR4 pathway, lipopolysaccharide (LPS) activates Mϕ (21, 22) and also synergizes with anti-CD40 to activate Mϕ *in vitro* (12). However, the therapeutic potential of LPS *in vivo* is limited because of its severe toxicity in mammals. Lipid A is the component of LPS that is primarily responsible for its immunologic effects; chemical modification of Lipid A produces monophosphoryl lipid A (MPL), a potent immunostimulant which is significantly less toxic than LPS (23, 24).

TLR agonists have potential as adjuvants for future cancer therapies, especially when combined with other agents (19). MPL has been effective as a vaccine adjuvant (5, 25–30), but its role in promoting the immune response against cancer has not been fully explored. The first goal of this study was to determine if MPL, in a manner similar to CpG or LPS, could be combined synergistically with anti-CD40 to prompt immune cells, specifically Mϕ, to inhibit tumor cell proliferation *in vitro*. Using the immunotherapy protocol that we established for anti-CD40+CpG, we then also assessed the *in vivo* antitumor effects of anti-CD40 combined with MPL. Two treatment approaches were explored: a high-dose, systemic treatment injected i.p.; and a local, low-dose treatment injected directly into a growing tumor. In addition, we tested

whether T cells were required for Mϕ activation and the resulting antitumor effects after treatment with anti-CD40+MPL.

Materials and Methods

Mice and cell lines

Female C57BL/6 and CB-17 SCID mice (6 to 8 weeks old), were obtained from Taconic Farms (Germantown, NY) or from The Jackson Laboratory (Bar Harbor, ME). Mice were housed in the University of Wisconsin-Madison animal facilities at the Wisconsin Institutes for Medical Research. All experimentation was performed in accordance to protocols approved by the National Institutes of Health and by the Animal Care and Use Committees of UW-Madison. The B16-F10 melanoma tumor cell line was used as a tumor model because it is weakly immunogenic and syngeneic to the C57BL/6 strain of mice. B16-F10 cells were grown in RPMI 1640 complete medium supplemented with 10% FCS (Sigma Chemicals, St. Louis, MO), 2 mM L-glutamine and 100 U/ml of penicillin/streptomycin (all from Life Technologies, Inc., Grand Island, NY) at 37°C in a humidified 5% CO_2 atmosphere.

Antibodies and reagents

FGK 45.5 hybridoma cells capable of producing the agonistic anti-CD40 Ab were a gift from Dr. F. Melchers (Basel Institute for Immunology, Basel, Switzerland). The mAb was obtained from ascites of nude mice injected previously with the hybridoma cells, and the ascites was then enriched for IgG by ammonium sulfate precipitation (12). MPL from *Salmonella enterica* serotype minnesota (#L6895) was purchased from Sigma-Aldrich (St. Louis, MO) and reconstituted as previously described (31). In brief, the lyophilized MPL was reconstituted to 1.0 mg/ml in distilled water containing 0.2% triethylamine, sonicated for 5 min, and stored at 4°C. MPL was sonicated for 5 min before each additional use. Rat IgG control Ab and bacterial LPS (from *Salmonella enteritidis*) were purchased from Sigma-Aldrich (St. Louis, MO).

Unmethylated CpG-1826 oligodeoxynucleotide (TCCATGACGTTCCTGACGTT) was purchased from TriLink Biotechnologies (San Diego CA).

Activation of Mϕ with anti-CD40 and MPL

Mice were injected i.p. with 0.5 mg of either anti-CD40 or Rat IgG in 0.5 ml calcium- and magnesium-free phosphate buffered saline (PBS). After 3 days, peritoneal exudate cells (PECs) were obtained by peritoneal cavity lavage with 5 ml of cold RPMI 1640 complete medium. Collected PECs were placed into 96 well flat-bottom cell culture plates (Corning Inc, Corning, NY) at a concentration of $2x10^5$ cells per well in 0.1 ml medium. The peritoneal Mϕ population was enriched by allowing PECs to adhere to the plastic wells for 1½ to 2 h, followed by careful aspiration and removal of non-adherent cells. In our previous studies, flow cytometry indicated that 95% of these adherent cells were Mϕ, based on their expression of the F4/80 Mϕ marker (12). Adherent Mϕ were then co-cultured with B16 melanoma cells (10^4 cells per well) for 48 h in complete RPMI 1640 medium, alone or in the presence of MPL (5 μg/ml), CpG (5 μg/ml), or LPS (10 ng/ml). Assay plates were incubated at 37°C in a humidified 5% CO_2 atmosphere.

Mϕ-induced tumor cytostasis assay

The antitumor effect of mouse Mϕ activated by anti-CD40 and MPL was determined by co-culturing Mϕ and B16 cells for 48 h and pulsing the wells with tritiated thymidine ([^{3}H]-TdR, PerkinElmer, Boston, MA, 1 μCi/well) for the last 6 h of incubation. [^{3}H]-TdR incorporation was determined by liquid β-scintillation counting of total cells after harvesting onto glass fiber filters (Packard, Meriden, CT), using the Packard Matrix 9600 Direct β-counter (Packard, Meriden,

CT). Mϕ incorporate negligible amounts of [^{3}H]-TdR compared to rapidly-dividing B16 cells (12, 32).

Nitric oxide (NO) production assay

Peritoneal Mϕ were prepared and co-cultured with B16 cells as described in the Mϕ cytostatic assay above. Supernatants were collected after 42 h, and nitrite accumulation was measured using Griess Reagent (Sigma, St. Louis, MO). Equal volumes of supernatants and Griess Reagent (50 μL each) were mixed for 10 min, and the absorbance at 570 nm was measured by a microplate reader and compared to a standard nitrite curve ranging in concentration from 0-125 μM.

Flow cytometric analysis of TLR expression

PECs from C57BL/6 mice injected on day -1, -3, or -5 with anti-CD40 or Rat IgG were collected on day 0. As TLR4 can only bind LPS or MPL when it is associated with MD-2 (lymphocyte antigen 96) (33), PECs were stained with anti-TLR4-MD-2-PE (clone MTS510, eBioscience, San Diego, CA), and also with anti-F4/80-APC (clone BM8), for 40 min at 4°C. After surface staining, cells were washed, fixed, and permeabilized as described previously (12). Cells were stained intracellularly with anti-TLR4-MD-2-PE and anti-TLR9-FITC (TLR9 expression data not shown) and resuspended in 0.3 ml flow buffer (PBS supplemented with 0.5% FCS). Propidium iodide was added to stain dead cells, which were excluded from subsequent analysis. Flow cytometry was performed on a FACSCalibur flow cytometer (BD, Franklin Lakes, NJ) and analyzed for TLR4 expression within the F4/80$^+$ cell population using FlowJo Software (Ashland, OR).

Fluorescence-activated cell sorting

PECs from anti-CD40-treated C57BL/6 mice were collected and stained for 40 min at 4°C with anti-CD11b-APC (clone M1/70, BioLegend, San Diego, CA), anti-Gr-1-PE (clone RB6-8C5), anti-F4/80-FITC (clone BM8), and anti-CD19-PECy7 fluorochromes (clone 1D3, eBioscience, San Diego, CA). Cells were then sorted into purified populations according to their immunophenotype or forward scatter and side scatter characteristics. FACS sorting was performed with a FACSAria cell sorter (BD, Franklin Lakes, NJ). The purity of the sorted populations was confirmed by standard flow cytometry. For functional assays involving sorted cells, $5x10^4$ sorted PECs and $1x10^4$ B16 tumor cells were plated in triplicate in 96-well flat-bottomed plates. The [^{3}H]-TdR incorporation and NO assays were performed as described in the sections above.

Immunohistochemistry.

The cytospin preparations of sorted PECs were stained with Wright-Giemsa Stain (Sigma) as described (34). Briefly, PECs were centrifuged at 800 rpm for 3 min, fixed in 100% methanol for 2 min, and stained horizontally with Wright-Giemsa Stain (Sigma) for 45 s. Cells were further stained with an equal volume mixture of Wright-Giemsa Stain and glass filtered water for 10 min, washed, and destained for 5 min. Pictures of cells were taken at 40x magnification using the Magnafire 2.1 computer software (Optronics, Goleta, California).

In vivo tumor model and therapy

C57BL/6 mice or CB-17 SCID mice were injected subcutaneously (s.c.) in the lower-right quadrant of the shaved abdomen with $1x10^5$ viable B16 melanoma cells in 0.1 ml PBS on day 0. In some experiments, a primary tumor was implanted s.c. in the right flank of the animal on day 0, followed by a secondary s.c. tumor injection in the left flank on day 3. Mice were randomized into treatment groups after tumors were injected. For mice receiving i.p. treatment, 0.5 mg anti-CD40 or 0.5 mg rat IgG was injected i.p. in 0.5 ml PBS on days 4 and 11, and 50 μg MPL in 0.5 ml or 0.5 ml PBS was injected i.p. on days 7 and 14. For mice receiving intratumoral (i.t.) therapy, 20 μg anti-CD40 or 20 μg rat IgG was injected i.t. into the primary tumor on days 5 and 12, and either 2 μg MPL or PBS was given i.t. on days 8 and 15. Intratumoral injections were administered in 0.1ml PBS. The perpendicular diameters of s.c. tumors were measured every 3 to 4 days using digital calipers. Tumor volumes were estimated according to the formula: $(1/2) \times \text{tumor length} \times \text{tumor width}^2$. Mice that had no visible or palpable tumors by day 8 post-tumor cell inoculation were excluded from experimental analysis.

In vivo T cell depletion

For certain experiments, C57BL/6 mice were depleted of T cells with a mixture of 250 μg anti-CD4 mAb and 250 μg anti-CD8 mAbs injected i.p. 2 days before the start of treatment. Injections of depleting Abs were repeated every 5 days for the remainder of the experiment. Non-depleted mice received 500 μg rat IgG as a control. The efficacy of T cell depletion was confirmed by flow cytometry showing an 83.4% reduction of $CD4^+$ lymphocytes and an 89.3% reduction of $CD8^+$ lymphocytes compared to $CD4^+$ and $CD8^+$ lymphocytes from IgG control mice.

Statistical analysis

A two-tailed Student's t-test was used to determine significant differences between experimental and relevant control means for *in vitro* experiments. Survival data were analyzed with the log-rank test. Differences in the mean tumor growth rate of treatment groups were determined by fitting the tumor growth curve of each mouse to an exponential curve using the equation for exponential growth ($V_t = V_0 e^{rt}$), where V_t is tumor volume, t is time, and the rate constant r is the parameter taken to describe the overall tumor growth rate for each mouse. The parameter V_0 was calculated to be the same for all mice within an experiment. The group mean r was compared between groups using Student's two-tailed t test. For all tests, $p<0.05$ was considered statistically significant. In all figures, p-values are represented with asterisks (*) as follows: $p<0.05$ (*), $p<0.01$ (**), $p<0.001$ (***). Graphs were generated and significance tests were performed using the GraphPad Prism 5.04 software.

Results

Anti-CD40 and MPL synergize to activate Mϕ.

Our first set of experiments tested whether an i.p. injection of 0.5 mg anti-CD40 into naïve C57BL/6 mice could prime Mϕ to further stimulation by MPL *ex vivo*. Our previous studies showed that CD40 ligation by anti-CD40 upregulated TLR9 expression in Mϕ in a time-dependent manner, peaking 3 days after anti-CD40 and correlating with anti-CD40/CpG-induced antitumor effects (14). Since the receptor for MPL is TLR4, we asked if there is a similar pattern of anti-CD40-mediated upregulation of TLR4. The level of MPL-responsive TLR4 was indeed enhanced in $F4/80^+$ cells (Mϕ) when analyzed by flow cytometry on days 1, 3, and 5 post-treatment with anti-CD40 (Fig 1*A*). A similar effect was seen for TLR9 expression (data not shown), in agreement with our previous data (14). Two mice were tested for each time point and gave consistent results. The baseline TLR4 expression from one representative naïve mouse had a mean fluorescence intensity (MFI) of 9.6, compared to MFIs of 25 on day 1, 33.2 on day 3, and 24.4 on day 5 following anti-CD40 (Fig. 1*A*).

Since TLR4 expression seemed to reach peak levels 3 days after *in vivo* treatment with anti-CD40, we hypothesized that Mϕ from anti-CD40-treated mice would show higher levels of antitumor activity upon exposure to MPL on day 3, compared to Mϕ from rat IgG-treated mice. Indeed, Mϕ from anti-CD40-treated mice were further activated by MPL *in vitro*, almost completely inhibiting B16 proliferation (Fig 1*B*) and secreting a significant amount of NO (Fig 1*C*). A comparable synergistic effect with anti-CD40 was also seen when the cells were stimulated by LPS or CpG, which were used as positive controls. In addition to their ability to suppress proliferation of B16 murine melanoma, Mϕ that were primed by anti-CD40 and activated by MPL also suppressed the proliferation of human tumor cell lines, including M21

melanoma, ECC-1 endometrial carcinoma, SKOV-3 ovarian carcinoma, and K562 myelogenous leukemia (data not shown).

$CD11b^+$ macrophages and monocytes are activated following anti-CD40 and MPL treatment.

In order to identify the specific subset of effector cells that can be activated by MPL on day 3 after anti-CD40 priming, PECs were collected from mice that had been injected with anti-CD40 3 days earlier, stained, gated on $CD11b^{high}$ cells, sorted into 4 sub-populations based on their expression of immunophenotypic surface markers (Fig. 2*A*), and were further characterized by histological staining (Fig. 2*B*) and functional analysis (Fig. 2*C* and 2*D*). Subpopulation 1 consisted of monocytes and naïve macrophages that did not suppress B16 proliferation (Fig. 2*C*) or secrete NO (Fig. 2*D*) following anti-CD40 treatment (black bars), but could be induced to do so by MPL (grey bars). Subpopulation 2 expressed slightly less F4/80 and slightly more Gr-1, and was shown by histological staining (Fig 2*B*) to be a distinct population from subpopulation 1. Subpopulation 2 consisted of a relatively pure population of activated macrophages that strongly inhibited B16 proliferation (Fig. 2*C*) and secreted large quantities of NO (Fig. 2*D*).

In a separate prior experiment (not shown), $CD11b^+$ $Gr\text{-}1^+$ cells were sorted as one population that consisted of a mixture of monocytes and polymorphonuclear cells, according to histology. These cells were capable of inhibiting B16 proliferation and secreting modest amounts of NO. In order to identify more precisely which cells were activated in the experiment shown in Fig. 2, this population of $CD11b^+$ $Gr\text{-}1^+$ cells was further purified by forward scatter and side scatter qualities into two distinct populations, one predominantly consisting of granulocytes (Fig. *2B,* 3) and the other, monocytes (Fig. 2*B,* 4). The granulocytes showed no antitumor activity (Fig *2C* and 2*D*). Monocytes were able to suppress B16 proliferation after stimulation by anti-CD40

(Fig. 2*C*), but these cells did not synergize with MPL to cause further suppression of B16 proliferation (Fig. 2*C*).

In a different experiment, $CD11b^-$ and $CD11b^{low}$ cells in anti-CD40-injected mice were found to be mostly $CD19^+$ naïve and activated B cells, respectively. Neither of these B cell populations mediated antitumor effect or produced NO following stimulation by MPL (data not shown).

Combining anti-CD40 and MPL in mice with intact immune systems slows s.c. B16 tumor growth and prolongs survival more effectively than treating with either agent individually.

The above experiments established synergy between anti-CD40 and MPL *in vitro*, indicating that the two immunostimulants could be therapeutically efficacious when used as a dual-agent cancer treatment. Since the route of administration for anti-cancer therapy may play a critical role in determining a treatment's outcome (5, 16, 35, 36), we looked at two methods of administering anti-CD40 and MPL, treating mice either intraperitoneally (i.p.) or intratumorally (i.t.). C57BL/6 mice were first engrafted with s.c. tumors on day 0 and then treated i.p. with anti-CD40 and MPL, either alone or in combination, as described in *Materials and Methods*. The mice that received both agents had a significantly reduced tumor burden compared to any other group, based on the rate at which the tumors grew after beginning treatment. The mice treated with the combination therapy also survived longer than the PBS+IgG and MPL+PBS groups, but not compared to the anti-CD40+PBS group (p=0.27) (Fig. 3*C*).

Next, we targeted immune cells in the tumor microenvironment by injecting anti-CD40 and MPL directly into the tumor. A dose titration pilot study was performed to determine suboptimal doses for i.t. anti-CD40 and i.t. MPL in order to reduce the ability of i.t. anti-CD40 or

i.t. MPL to overpower the tumor individually and mask a possible synergistic effect of the combination. Suboptimal doses of 20 μg anti-CD40 and 2 μg MPL were chosen (data not shown), each of which was 25 times less than the doses we used for i.p. therapy. These doses were used for all i.t. experiments. When injected locally into the growing tumor, the combination of anti-CD40 and MPL resulted in a significant reduction in tumor burden (Fig. 3*B*). The tumors treated with anti-CD40 or MPL alone were slightly smaller than the untreated tumors at the end of treatment on day 15, but the combination-treated tumors remained very small (1-4 mm^3) for several days after the cessation of treatment. Most combination-treated mice (6 / 8) eventually developed large tumors and died as a result, but some (2 / 8) rejected the tumor and remained tumor free, whereas none of the mice from other groups survived (Fig. 3*D*). Thus, anti-CD40 and MPL were synergistic *in vivo* in immunocompetent mice, and the antitumor effects of i.t. therapy with anti-CD40 and MPL were more pronounced than those of i.p. therapy.

MPL with and without anti-CD40 can activate Mϕ to in the absence of T cells

In the next series of experiments we tested whether T cells played a role in activating Mϕ or mediating the antitumor effects induced by anti-CD40 and MPL. Peritoneal Mϕ from immunocompetent C57BL/6 mice were primed with anti-CD40 for further activation by MPL, resulting in greatly augmented tumoristasis (Fig. 1*B*) and NO production (Fig. 1*C*). Because CD40 ligation may require additional T cell help to fully sensitize Mϕ to MPL, we depleted T cells in C57BL/6 mice with anti-CD8 and anti-CD4 depleting mAbs (250 μg each, injected i.p. in 0.5 ml) 2 days before giving a single dose of anti-CD40 or control rat IgG (0.5 mg, i.p.) on day 0. On day 3, PECs from these mice were collected and tested *in vitro* for their ability to suppress B16 proliferation (Fig 4*A*) and produce NO (Fig. 4*B*). Mϕ from T cell-depleted C57BL/6 mice

were activated by anti-CD40 and MPL, resulting in an almost complete inhibition of B16 proliferation (**p=0.009) (Fig. 4*A*). However, this anti-proliferative effect was equally strong in Mϕ obtained from T cell-depleted mice that received MPL and non-specific rat IgG instead of anti-CD40 (*p=0.035). Furthermore, in these CD4/CD8 depleted animals, the rat IgG treatment alone also induced some tumor inhibition, similar to that in anti-CD40-treated mice (Fig. 4*A*). As pretreatment of immunocompetent mice with the control rat IgG alone did not cause tumoristasis, NO production, or priming to MPL (Fig. 1*B* and Fig. 1*C*), we hypothesized that some systemic effect was induced by the CD4/CD8 depletion resulting in Mϕ priming similar to that induced by anti-CD40. In terms of NO levels, the combination of anti-CD40 and MPL was more effective than rat IgG and MPL in inducing NO production (*p=0.019) (Fig. 4*B*). Even without anti-CD40, Mϕ from IgG-treated mice secreted more NO when cultured in the presence of MPL than when cultured with media alone (*p=0.018).

In order to eliminate any potential stimulating effects of $CD4^+$ and $CD8^+$ T cell-depleting antibodies, we repeated these experiments using T and B cell-deficient CB-17 SCID mice. SCID mice were injected i.p. with either anti-CD40 or control rat IgG (0.5 mg in 0.5 ml PBS) and the PECs harvested 3 days later. Similar to the results observed with T cell-depleted C57BL/6 mice (Fig. 4*A*), anti-CD40-Mϕ and rat IgG- Mϕ from SCID mice showed an equally strong response to MPL (*p<0.05) (Fig. 4*C*). Anti-CD40, however, unlike its effects on NO production by Mϕ from T cell-depleted mice (Fig. 4*B*), was unable to induce SCID Mϕ to produce NO, with or without MPL, (Fig. 4*D*) for reasons that remain to be investigated.

Intratumoral MPL with or without anti-CD40 slows tumor growth in SCID mice

When combined into a single treatment regimen, anti-CD40 and MPL mediated potent antitumor effects in immunocompetent mice. Our previous studies showed that anti-CD40 could exert antitumor effects in the absence of T cells when given i.p. (11, 14, 32). In order to explore the role of T cells in i.t. treatment, anti-CD40 and MPL were given i.t. to CB-17 SCID mice bearing subcutaneous B16 tumors. The tumors were treated i.t. with anti-CD40 (20 μg/mouse) on day 5 and day 12 and with MPL (2 μg/mouse) on day 8 and day 15. Untreated mice received rat IgG in place of anti-CD40 and PBS in place of MPL. When CB-17 SCID mice were treated i.t. with a combination of anti-CD40 and MPL, there was a significant reduction in the growth of their tumor (Fig. 5*A*), but this antitumor benefit was no better than what was seen in mice given MPL without anti-CD40. Intratumoral MPL by itself seemed capable of slowing B16 tumor growth, consistent with our *in vitro* observations (Fig. 4*C*). In this setting, treatment with anti-CD40 + MPL, or MPL alone did not cause a significant prolongation of survival (Fig. 5B).

Intratumoral anti-CD40 and MPL can delay the growth of distant, untreated B16 tumors in immunodeficient hosts

Even though locally-administered MPL meditates T cell-independent antitumor effects in SCID mice, T cells may still be involved when immunocompetent mice receive this treatment. In order to determine whether T cells affect the growth of distant tumors, we injected primary s.c. tumors into C57BL/6 mice (Fig. 6*A-C*), anti-CD4/CD8-treated C57BL/6 mice (Fig. 6*D-F*), and, in a separate experiment, CB-17 SCID mice (Fig. 6*G-I*). Secondary tumors were injected s.c. into the opposite flanks of all mice on day 3. Primary tumors were treated i.t. with anti-CD40 on day 5 and with MPL on day 8, followed by a second round of anti-CD40 on day 12 and MPL on

day 15. In all 3 groups of mice (immunocompetent, T cell-depleted, and SCID), i.t. treatment resulted in a substantial retardation of the growth of the primary (Figs. 6*A, D, G)* and secondary tumors (Figs. 6 *B, E, H*), and significantly prolonged survival (Figs. 6*C, F, I*). In contrast with the results of single-tumor experiments, in which the low i.t. doses of anti-CD40+MPL occasionally resulted in complete tumor eradication and long-term survival (Fig. 3*D*), complete tumor rejection was not seen in these two-tumor experiments, with the exception of one treated SCID mouse. Collectively, these results suggest that the antitumor effects at the treated and distant secondary tumors appear, at least in this tumor model at the doses tested, to be mediated by cells other than T cells.

Discussion

Anti-CD40 (15, 37) and MPL (19, 38) have been used in clinical settings as individual therapies, but have not, to our knowledge, been combined into a single immunotherapy regimen for experimental or clinical cancer treatment. In this study, we show that anti-CD40 mAb and MPL can activate monocytes and Mϕ in both immunocompetent and T cell-deficient hosts, and induce suppression of tumor growth *in vitro* and *in vivo*. Moreover, the synergy between anti-CD40 and MPL was observed in immunocompetent mice.

This study is a clinically-relevant follow up to our lab's earlier work on the potential cellular effector mechanisms of CD40 ligation (11–14, 32, 37, 38). Most current therapies based on CD40 ligation are aimed toward the activation of T cells as the main effector cells (39), but we established that Mϕ and NK cells can also be activated by CD40 ligation to mediate antitumor effects that persist even when T cells are absent (13, 37). T cells were still unnecessary when we combined anti-CD40 *in vivo* with CpG (14), a TLR9 agonist, yielding results consistent with those presented here for TLR4 agonist MPL. Even though CpG is a powerful vaccine adjuvant in preclinical studies (16, 35) and activates mouse Mϕ (18), it seems to be less effective in activating human Mϕ (20). Alternatively, MPL is relatively non-toxic (24, 40), has a history of use in clinical trials as a single agent (41), and activates monocytes/ Mϕ in human patients (41). Because of these characteristics and our results, we believe that a combination of anti-CD40 and MPL may prove to be more clinically beneficial than a combination of anti-CD40 and CpG.

In this study we present evidence that anti-CD40+MPL treatment results in antitumor effects in which T cells are not the main effector cells, since Mϕ activation and antitumor effects against primary and distant tumors were observed in mice in the absence of T cells. In addition, our preliminary data indicate that subcutaneous injections of anti-CD40+MPL into healthy skin is similarly effective against a distant, untreated tumor as compared to i.t. injections of anti-

CD40+MPL, arguing against a necessary role of local T cell activation in the systemic antitumor effect of this combination against B16-F10 tumors. However, while not required for tumor suppression in this tumor model, T cells still may be activated. For instance, MPL has been reported to induce IFNγ release from T cells (42). MPL can also inhibit suppressor T cells, possibly leading to a strengthened immune response against the tumor (31). This activation of T cells by anti-CD40 and MPL may contribute to rejection of tumors that are more immunogenic than B16, as we have shown previously for anti-CD40 (32).

The T cell-independent, Mϕ-dependent mechanism of antitumor effects induced by anti-CD40 and MPL is in agreement with the recent clinical and preclinical results on anti-CD40 therapy of pancreatic cancer (14). A Phase I trial of the first fully-humanized anti-CD40 agonistic mAb (CP-870,893) (43) combined with gemcitabine chemotherapy resulted in tumor regression in 4 out of 21 pancreatic ductal adenocarcinoma (PDA) patients (15). Biopsies showed that regressing tumors had been infiltrated with Mϕ, but lacked signs of lymphocytes. In immunocompetent KPC mice that spontaneously developed PDA, anti-CD40 treatment resulted in Mϕ (but not lymphocyte) infiltration into tumors, failed to produce protective T cell immunity, and required Mϕ for anti-CD40-induced tumor regression (15), suggesting that the targets for the anti-CD40 mAb are immature Mϕ and monocytes.

During the course of our experiments, we observed that SCID and T cell-depleted C57BL/6 mice responded strongly to MPL, with or without initial priming by anti-CD40. SCID Mϕ might be primed as a compensatory defense mechanism in the absence of T- and B-cells. If SCID Mϕ are primed, then further priming by anti-CD40 may have no discernible effect. The results obtained from T cell-depleted C57BL/6 mice showing Mϕ activation (Fig. 4*C*) are potentially explained by the mechanism of T cell-depletion. The anti-CD8 and anti-CD4

depleting antibodies opsonize $CD8^+$ and $CD4^+$ T cells, leading to Mϕ-mediated antibody-dependent cellular cytotoxicity. Because Mϕ would be responsible for the depletion of T cells, they might still be in an activated or primed state upon removal from these T-cell depleted mice. This would explain why MPL by itself was a sufficient stimulus for Mϕ from T cell-depleted mice (Fig. 4*C*), but not from immunologically intact mice (Fig. 1*B*).

Compared to untreated controls, it appears that i.p. treatment with anti-CD40 alone was effective against tumors in immunocompetent mice (p=0.037), but i.p. treatment with MPL alone did not have an effect (p=0.49) (Fig. 3*A*). Conversely, when we injected these agents i.t. in lower doses, MPL slowed tumor growth (p=0.017), but anti-CD40 did not (p=0.42) (Fig. 3*B*). These observations may suggest a potential benefit of injecting anti-CD40 systemically in order to prime large numbers of monocytes or Mϕ that would then migrate to and infiltrate the tumor. If systemic anti-CD40 is followed by an i.t. injection of MPL, it might introduce a high local concentration of the activating signal in the tumor site for the newly-arrived primed Mϕ. By combining alternate routes of administrating anti-CD40 and MPL, it might be possible to further augment the therapeutic potential of this combination. However, the results of this present study demonstrate that injecting both agents intratumorally, even at very small doses, can still elicit a strong antitumor response. This suggests that local delivery is a potential strategy for reducing or eliminating the toxicity of anti-CD40 in the clinical setting.

Another promising use for anti-CD40 is combining it with other agents in addition to MPL (44). For example, the efficacy of anti-CD40 and CpG was enhanced in combination with cyclophosphamide (11) and other chemotherapeutic agents (45) which are normally immunosuppressive in high doses. Since anti-CD40 and MPL are effective at slowing tumor growth in immunocompromised CB-17 SCID mice and in C57BL/6 mice depleted of $CD4^+$ and

$CD8^+$ T cells, this combination immunotherapy may be appropriate for future testing in cancer patients that have become functionally immune suppressed by their chemotherapy regimens.

Acknowledgements

The authors would like to thank the UW Flow Cytometry staff for their assistance with sorting, Dr. Kory Alderson for helpful discussions and experimental advice, and Xiaoyi Qu and Nicholas Kalogriopoulos for technical help.

References

1. Tong, A. W., and M. J. Stone. 2003. Prospects for CD40-directed experimental therapy of human cancer. *Cancer Gene Ther.* 10: 1-13.

2. Weiner, L. M., R. Surana, and J. Murray. 2010. Vaccine prevention of cancer: Can endogenous antigens be targeted? *Cancer Prev. Res.* 3: 410-5.

3. Solomayer, E.-F., M. Feuerer, L. Bai, V. Umansky, P. Beckhove, G. C. Meyberg, G. Bastert, V. Schirrmacher, and I. J. Diel. 2003. Influence of adjuvant hormone therapy and chemotherapy on the immune system analysed in the bone marrow of patients with breast cancer. *Clin. Cancer Res.* 9: 174-180.

4. Speiser, D. E. 1997. Self antigens expressed by solid tumors do not efficiently stimulate naive or activated T cells: Implications for immunotherapy. *J. Exp. Med.* 186: 645-653.

5. Baldridge, J. R., and R. T. Crane. 1999. Monophosphoryl lipid A (MPL) formulations for the next generation of vaccines. *Methods* 19: 103-7.

6. Whiteside, T. L. 2006. Immune suppression in cancer: effects on immune cells, mechanisms and future therapeutic intervention. *Semin. Cancer Biol.* 16: 3-15.

7. Rosenberg, S. A., J. C. Yang, and N. P. Restifo. 2004. Cancer immunotherapy: moving beyond current vaccines. *Nat. Med.* 10: 909-15.

8. Stewart, T. J., and M. J. Smyth. 2011. Improving cancer immunotherapy by targeting tumor-induced immune suppression. *Cancer Metast. Rev.* 30: 125-40.

9. Harris, J., D. Sengar, T. Stewart, and D. Hyslop. 1976. The effect of immunosuppressive chemotherapy on immune function in patients with malignant disease. *Cancer* 37: 1058-69.

10. Nair, R. E., M. O. Kilinc, S. A. Jones, and N. K. Egilmez. 2006. Chronic immune therapy induces a progressive increase in intratumoral T suppressor activity and a concurrent loss of tumor-specific CD8+ T Effectors in her-2/neu transgenic mice bearing advanced spontaneous tumors. *J. Immunol.* 176: 7325-7334.

11. Johnson, E. E., I. N. Buhtoiarov, M. J. Baldeshwiler, M. A. R. Felder, N. Van Rooijen, P. M. Sondel, and A. L. Rakhmilevich. 2011. Enhanced T-cell-independent antitumor effect of cyclophosphamide combined with anti-CD40 mAb and CpG in mice. *J. Immunother.* 34: 76-84.

12. Buhtoiarov, I. N., H. Lum, G. Berke, D. M. Paulnock, P. M. Sondel, A. L. Rakhmilevich, I. N Buhtoiarov, D. M Paulnock, P. M Sondel, and A. L Rakhmilevich. 2005. CD40 Ligation Activates Murine Macrophages via an IFN-gamma-Dependent Mechanism Resulting in Tumor Cell Destruction In Vitro. *J. Immunol.* 174: 6013-6022.

13. Lum, H. D., I. N. Buhtoiarov, B. E. Schmidt, G. Berke, D. M. Paulnock, P. M. Sondel, and A. L. Rakhmilevich. 2006. In vivo CD40 ligation can induce T-cell-independent antitumor effects that involve macrophages. *J. Leukocyte Biol.* 79: 1181-92.

14. Buhtoiarov, I. N., H. D. Lum, G. Berke, M. Sondel, A. L. Rakhmilevich, and P. M. Sondel. 2006. Synergistic activation of macrophages via CD40 and TLR9 results in T Cell independent antitumor effects. *J. Immunol.* 176: 309-18.

15. Beatty, G. L., E. G. Chiorean, M. P. Fishman, B. Saboury, U. R. Teitelbaum, W. Sun, R. D. Huhn, W. Song, D. Li, L. L. Sharp, D. A. Torigian, P. J. O'Dwyer, and R. H. Vonderheide. 2011. CD40 agonists alter tumor stroma and show efficacy against pancreatic carcinoma in mice and humans. *Science* 331: 1612-6.

16. Nierkens, S., M. H. den Brok, T. Roelofsen, J. A. L. Wagenaars, C. G. Figdor, T. J. Ruers, and G. J. Adema. 2009. Route of administration of the TLR9 agonist CpG critically determines the efficacy of cancer immunotherapy in mice. *PloS One* 4: e8368.

17. Cooper, C. L., H. L. Davis, M. L. Morris, S. M. Efler, M. A. Adhami, A. M. Krieg, D. W. Cameron, and J. Heathcote. 2004. CPG 7909, an immunostimulatory TLR9 agonist oligodeoxynucleotide, as adjuvant to Engerix-B HBV vaccine in healthy adults: a double-blind phase I/II study. *J. Clin. Immunol.* 24: 693-701.

18. Buhtoiarov, I. N., P. M. Sondel, J. C. Eickhoff, and A. L. Rakhmilevich. 2007. Macrophages are essential for antitumour effects against weakly immunogenic murine tumours induced by class B CpG-oligodeoxynucleotides. *Immunology* 120: 412-23.

19. Ulevitch, R. J. 2004. Therapeutics targeting the innate immune system. *Nat. Rev. Immunol.* 4: 512-20.

20. Campbell, J. D., Y. Cho, M. L. Foster, H. Kanzler, M. A. Kachura, J. A. Lum, M. J. Ratcliffe, A. Sathe, A. J. Leishman, A. Bahl, M. McHale, R. L. Coffman, and E. M. Hessel. 2009. CpG-containing immunostimulatory DNA sequences elicit TNF-alpha-dependent toxicity in rodents but not in humans. *J. Clin. Invest.* 119: 2564-76.

21. Sweet, M. J., and D. A. Hume. 1996. Bacterial lipopolysaccharide confers resistance to G418, doxorubicin, and taxol in the murine macrophage cell line, RAW264. *J. Leukocyte Biol.* 59: 280-6.

22. Bode, J. G., C. Ehlting, and D. Häussinger. 2012. The macrophage response towards LPS and its control through the p38(MAPK)-STAT3 axis. *Cell. Signal.* 24: 1185-94.

23. Ribi, E., K. C. Milner, D. L. Granger, M. T. Kelly, K.-ichi Yamamoto, W. Brehmer, R. Parker, R. F. Smith, and S. M. Strain. 1976. Immunotherapy with nonviable microbial components. *Ann. NY Acad. Sci.* 277: 228-238.

24. Masihi, K. N., W. Lange, W. Brehmer, and E. Ribi. 1986. Immunobiological activities of nontoxic lipid A: enhancement of nonspecific resistance in combination with trehalose dimycolate against viral infection and adjuvant effects. *Int. Immunopharmacol.* 8: 339-45.

25. Baldridge, J. R., P. McGowan, J. T. Evans, C. Cluff, S. Mossman, D. Johnson, and D. Persing. 2004. Taking a Toll on human disease: Toll-like receptor 4 agonists as vaccine adjuvants and monotherapeutic agents. *Expert Opin. Biol. Th.* 4: 1129-38.

26. Vandepapelière, P., Y. Horsmans, P. Moris, M. Van Mechelen, M. Janssens, M. Koutsoukos, P. Van Belle, F. Clement, E. Hanon, M. Wettendorff, N. Garçon, and G. Leroux-Roels. 2008. Vaccine adjuvant systems containing monophosphoryl lipid A and QS21 induce strong and persistent humoral and T cell responses against hepatitis B surface antigen in healthy adult volunteers. *Vaccine* 26: 1375-86.

27. Persing, D. H., R. N. Coler, M. J. Lacy, D. A. Johnson, J. R. Baldridge, R. M. Hershberg, and S. G. Reed. 2002. Taking toll: lipid A mimetics as adjuvants and immunomodulators. *Trends Microbiol.* 10: s32–s37.

28. Garcon, N., and O. Leo. 2010. Innate Immunity and Vaccine Adjuvants: From Concepts to the Development of a Unique Adjuvant System AS04 Used for the Formulation of a Human Papillomavirus (HPV) Vaccine. *Curr. Cancer Ther. Rev.* 6: 126-137.

29. Evans, J. T., C. W. Cluff, D. A. Johnson, M. J. Lacy, D. H. Persing, and J. R. Baldridge. 2003. Enhancement of antigen-specific immunity via the TLR4 ligands MPL adjuvant and Ribi.529. *Expert Rev. Vaccines* 2: 219-29.

30. Didierlaurent, A. M., S. Morel, L. Lockman, S. L. Giannini, M. Bisteau, H. Carlsen, A. Kielland, O. Vosters, N. Vanderheyde, F. Schiavetti, D. Larocque, M. Van Mechelen, and N. Garçon. 2009. AS04, an aluminum salt- and TLR4 agonist-based adjuvant system, induces a transient localized innate immune response leading to enhanced adaptive immunity. *J. Immunol.* 183: 6186-97.

31. Baker, P. J., J. R. Hiernaux, M. B. Fauntleroy, B. Prescott, J. L. Cantrell, and J. a Rudbach. 1988. Inactivation of suppressor T-cell activity by nontoxic monophosphoryl lipid A. *Infect. Immun.* 56: 1076-83.

32. Rakhmilevich, A. L., I. N. Buhtoiarov, M. Malkovsky, and P. M. Sondel. 2008. CD40 ligation in vivo can induce T cell independent antitumor effects even against immunogenic tumors. *Cancer Immunol. Immunother.* 57: 1151-60.

33. Hyakushima, N., H. Mitsuzawa, C. Nishitani, H. Sano, K. Kuronuma, M. Konishi, T. Himi, K. Miyake, and Y. Kuroki. 2004. Interaction of soluble form of recombinant extracellular TLR4 domain with MD-2 enables lipopolysaccharide binding and attenuates TLR4-mediated signaling. *J. Immunol.* 173: 6949-54.

34. Rakhmilevich, A. L., M. J. Baldeshwiler, T. J. Van De Voort, M. A. R. Felder, R. K. Yang, N. A. Kalogriopoulos, D. S. Koslov, N. Van Rooijen, and P. M. Sondel. 2012. Tumor-associated myeloid cells can be activated in vitro and in vivo to mediate antitumor effects. *Cancer Immunol. Immunother.*

35. Lou, Y., C. Liu, G. Lize, W. Peng, C. Xu, Y. Ye, B. A. Rabinovich, Y. Hailemichael, A. Gelbard, D. Zhou, W. W. Overwijk, and P. Hwu. 2011. Antitumor Activity Mediated by CpG : The Route of Administration is Critical. *J. Immunother.* 34: 279-288.

36. Johnson, E. E., H. D. Lum, A. L. Rakhmilevich, B. E. Schmidt, M. Furlong, I. N. Buhtoiarov, J. A. Hank, A. Raubitschek, D. Colcher, R. A. Reisfeld, S. D. Gillies, and P. M. Sondel. 2008. Intratumoral immunocytokine treatment results in enhanced antitumor effects. *Cancer Immunol. Immunother.* 57: 1891-902.

37. Turner, J. G., A. L. Rakhmilevich, L. Burdelya, Z. Neal, M. Imboden, P. M. Sondel, and H. Yu. 2001. Anti-CD40 antibody induces antitumor and antimetastatic effects: the role of NK cells. *J. Immunol.* 166: 89-94.

38. Lum, H. D., I. N. Buhtoiarov, B. E. Schmidt, G. Berke, D. M. Paulnock, P. M. Sondel, and A. L. Rakhmilevich. 2006. Tumoristatic effects of anti-CD40 mAb-activated macrophages involve nitric oxide and tumour necrosis factor-alpha. *Immunology* 118: 261-70.

39. Fonsatti, E., M. Maio, M. Altomonte, and P. Hersey. 2010. Biology and clinical applications of CD40 in cancer treatment. *Semin. Oncol.* 37: 517-23.

40. Vosika, G. J., C. Barr, and D. Gilbertson. 1984. Phase-I study of intravenous modified lipid A. *Cancer Immunol. Immunother.* 18: 107-12.

41. Qureshi, N., K. Takayama, and E. Ribi. 1982. Purification and structural determination of nontoxic lipid A obtained from the lipopolysaccharide of Salmonella typhimurium. *J. Biol. Chem.* 257: 11808–11815.

42. Johnson, A. G. 1994. Molecular adjuvants and immunomodulators: new approaches to immunization. *Clin. Microbiol. Rev.* 7: 277-289.

43. Vonderheide, R. H., K. T. Flaherty, M. Khalil, M. S. Stumacher, D. L. Bajor, N. a Hutnick, P. Sullivan, J. J. Mahany, M. Gallagher, A. Kramer, S. J. Green, P. J. O'Dwyer, K. L. Running, R. D. Huhn, and S. J. Antonia. 2007. Clinical activity and immune modulation in cancer patients treated with CP-870,893, a novel CD40 agonist monoclonal antibody. *J. Clin. Oncol.* 25: 876-83.

44. Khalil, M., and R. H. Vonderheide. 2007. Anti-CD40 agonist antibodies: preclinical and clinical experience. *Update Cancer Ther.* 2: 61-65.

45. Buhtoiarov, I. N., P. M. Sondel, J. M. Wigginton, T. N. Buhtoiarova, E. M. Yanke, D. A. Mahvi, and A. L. Rakhmilevich. 2011. Anti-tumour synergy of cytotoxic chemotherapy and anti-CD40 plus CpG-ODN immunotherapy through repolarization of tumour-associated macrophages. *Immunology* 132: 226-39.

Figure Legends

FIGURE 1. Synergistic activation of Mϕ with anti-CD40 and MPL. **(A)** Expression of TLR4 on Mϕ from mice treated with anti-CD40. C57BL/6 mice were injected i.p. with anti-CD40 (0.5 mg/mouse in 0.5 ml PBS), and their PECs were collected 1, 3, or 5 days later and tested by flow cytometry for TLR4 expression. Results are presented as histograms of viable Mϕ (PI^- $F4/80^+$) from 1 representative mouse out of the 2 mice injected on each day. On histogram: black peak, baseline TLR4 expression from naïve mouse, MFI 9.6; open peaks, overlapping TLR4 expression 1 day or 5 days after anti-CD40, MFI 25 (1 d) and 24.4 (5 d); grey peak, TLR4 on Mϕ collected 3 days after anti-CD40, MFI: 33.2. **(B)** Tumoristatic synergy between anti-CD40 and MPL *in vitro*. C57BL/6 mice were injected with anti-CD40 (500 μg i.p.) or rat IgG (500 μg i.p.) on day 0. On day 3, PECs were collected and enriched for Mϕ by allowing cells ($2x10^5$ per well) to adhere to plastic wells for 2 hours, followed by gentle pipetting to remove non-adherent cells. Adherent cells were then co-cultured in triplicate wells for 48h with 10^4 B16 cells and stimulated with either MPL (5μg/ml), CpG (5 μg/ml), or LPS (10ng/ml). Wells were pulsed with [^{3}H] thymidine (1 μCi/well) for the last 6 h of incubation in order to measure proliferation of B16 cells. Results are presented as the mean total number of β counts over 5 min ± SE from 10 mice combined from 3 identical experiments. Cells from each mouse were tested in all 4 *in vitro* conditions. **(C)** Anti-CD40+MPL-Mϕ secrete NO in a synergistic manner. After 42 hr of stimulation IgG- or anti-CD40-Mϕ with medium alone, MPL (5 μg/ml), CpG (5 μg/ml), or LPS (10 ng/ml), supernatants were tested for nitrite concentration using the Griess test. Results from 2 identical experiments are presented. Each bar represents the mean nitrite concentration ± SE from 6 IgG-treated mice and 6 anti-CD40-treated mice. Cells from each mouse were tested in all

4 *in vitro* conditions. A two-tailed Student's t test was used to compare anti-CD40-Mϕ with rat IgG-Mϕ for each *in vitro* treatment (**p*<0.05; ***p*<0.01; ****p*<0.001).

FIGURE 2. $CD11b^{+}$ macrophages and monocytes are activated following anti-CD40 and MPL treatment. C57BL/6 mice were injected i.p. with 500 µg anti-CD40 on day 0. **(A)** On day 3, mice were euthanized and their PECs were collected, stained, gated on $CD11b^{high}$ cells and sorted into 4 sub-populations by a FACSAria cell sorter. The cells were divided as follows: (1) $CD11b^{+}$ $F4/80^{++}$ $Gr\text{-}1^{low}$ (monocytes), (2) $CD11b^{+}$ $F4/80^{+}$ $Gr\text{-}1^{dim}$ (activated macrophages). A separate group of cells showed a $CD11b^{+}$ $F4/80^{-}$ $Gr\text{-}1^{high}$ phenotype; these were further divided by forward and side scatter into populations (3) (granulocytes), and (4) (monocytes). **(B)** Each cell population was stained with a Wright-Giemsa stain to identify cell types based on morphology. The relative sizes of each sorted cell population have been maintained, and these 4 micrographs all show 40x magnification. **(C)** Each sorted population was tested in medium or 5 µg/ml MPL for the cells' ability to inhibit B16 proliferation ($[^{3}H]$ thymidine incorporation) and **(D)** produce NO. A two-tailed Student's T test was used to compare $[^{3}H]$ counts (*C*) or nitrite concentration (*D*) (**p*<0.05; ***p*<0.01; ****p*<0.001). This experiment was performed 3 times; data from 1 representative experiment is shown.

FIGURE 3. Anti-CD40 and MPL synergistically induce antitumor effects *in vivo*. **(A)** C57BL/6 mice (*n*=8-10, combined from two identical experiments) were injected s.c. with 10^{5} B16 melanoma cells on day 0 and treated i.p. with 0.5 mg anti-CD40 (or 0.5 mg rat IgG as control) on days 4 and 11. MPL (or PBS as control) was given on days 7 and 14. Graph shows the mean tumor volume ± SE. The tumor growth curve of each mouse was fit to an exponential curve, and

the mean specific growth constant from the combination-treated mice was compared to each of the 3 other groups individually using a two-tailed Student's T test. Asterisks indicate significant differences in growth rates (***p<0.001, Anti-CD40+MPL vs. IgG+PBS; *p<0.019, Anti-CD40+MPL vs. anti-CD40+PBS; ***p<0.001, Anti-CD40+MPL vs. MPL+IgG). **(B)** C57BL/6 mice (n=8-10, combined from two identical experiments) were implanted with a B16 tumor and treated i.t. with 20 μg anti-CD40 on days 5 and 12, and with 2 μg MPL on days 8 and 15. Control mice received 20 μg rat IgG or PBS, respectively, injected i.t. (***p<0.001, Anti-CD40+MPL vs. IgG+PBS; ***p<0.001, Anti-CD40+MPL vs. anti-CD40+PBS; **p=0.0099, Anti-CD40+MPL vs. MPL+IgG). **(C)** Overall survival of the mice shown in (A) (**p<0.0075, Anti-CD40+MPL vs. IgG+PBS; p=0.27, Anti-CD40+MPL vs. anti-CD40+PBS; **p=0.0048, Anti-CD40+MPL vs. IgG+MPL). **(D)** Overall survival of the mice shown in (B) (***p<0.001, Anti-CD40+MPL vs. IgG+PBS; ***p<0.001, Anti-CD40+MPL vs. anti-CD40+PBS; **p=0.0032, Anti-CD40+MPL vs. IgG+MPL).

FIGURE 4. PECs from T cell deficient mice treated with anti-CD40 *in vivo* cause tumoristatic effects and produce NO after *in vitro* culture with MPL. **(A)** C57BL/6 mice were injected i.p. with anti-CD4 (250 μg) and anti-CD8 (250 μg) mAbs on day -1. On day 0, mice were divided into two groups (n=4) and injected i.p. with either anti-CD40 or rat IgG (0.5 mg/mouse in 0.5 ml). Mice were euthanized on day 3. PECs were collected and enriched for adherent cells (Mϕ) by plating $2x10^5$ cells per mouse into each well of a 96-well plate. Non-adherent cells were removed after 1.5 – 2 h and adherent cells were co-cultured with 10^4 B16 cells per well and stimulated with MPL at a concentration of (5 μg/ml) for 48 hrs. Wells were pulsed with [^{3}H]-thymidine (1 μCi/well) for the last 6h of incubation in order to measure proliferation of B16

cells. Results are presented as the mean total number of β counts over 5 min ± SE from 4 mice per group. **(B)** T cells are not required for anti-CD40-induced NO production. After 42 h of stimulation, supernatants were taken from the wells described in (A) and tested for nitrite concentration using the Griess test. The experiments described in (A) and (B) were also repeated in SCID mice (C, D). **(C)** [^{3}H]-Thymidine incorporation into B16 cells in the presence of rat IgG- or anti-CD40-treated adherent SCID PEC. **(D)** Nitrite production of the same PEC as in (C). Mean ± SE of 9 mice from 3 separate experiments are included in (C) and (D). In all panels, groups were compared using a two-tailed Student's T test (*p<0.05; **p<0.01).

FIGURE 5. MPL with and without anti-CD40 slows tumor growth in SCID mice when injected i.t. **(A)** CB-17 SCID mice (n=5) were implanted with a B16 tumor and treated i.t. with 20 μg anti-CD40 on days 5 and 12, and with 2 μg MPL on days 8 and 13. Control mice received (20 μg rat IgG or PBS, respectively, injected i.t.) The graph shows the mean tumor volume ± SE. The tumor growth curve of each mouse was fit to an exponential curve, and the mean specific growth constants from the combination-treated group and the rat IgG+MPL group were compared to the rat IgG+PBS control group using a two-tailed Student's T test. Asterisks indicate significant differences in growth rates (*p<0.05). **(B)** Survival of the mice shown in (A). Although the combination-treated mice and the rat IgG+MPL had higher median survival times than the other two groups, the survival benefit was not statistically significant by the log-rank test.

FIGURE 6. I.t. anti-CD40 and MPL treatment is effective against local and distant tumors in immunocompentent C57BL/6 mice, T cell-depleted C57BL/6 mice, and CB-17 SCID mice.

Mice were implanted with 10^5 B16 melanoma cells on day 0 and with a second inoculum of 10^5 B16 into the opposite flank on day 3. Groups of mice received i.t. treatment with either the anti-CD40+MPL combination (triangles) or control rat IgG+PBS (circles) into the primary tumor for two rounds corresponding to days 5 and 12 for anti-CD40 and days 8 and 15 for MPL. **(A)** Primary tumor growth of immunologically intact C57BL/6 mice (injected i.p. with 500 μg rat IgG on days 3, 9, and 14 as control for T cell depletion) (**p=0.008). **(B)** Secondary tumor growth of the same mice as in (A) (*p=0.03). **(C)** Survival of the same mice as in (A) and (B) (**p=0.0054). **(D)** Primary tumor growth of C57BL/6 mice (injected i.p. with 250 μg of anti-CD4 and 250 μg anti-CD8 depleting mAbs on days 4, 9, and 14) (***p<0.001). **(E)** Secondary tumor growth of the same mice as in (D) (**p=0.004). **(F)** Survival of the same mice as in (D) and (E) (**p=0.0022). The experiments with C57BL/6 mice that are shown in (A) through (F) were performed in parallel using 5 – 7 mice per treatment group. **(G)** In a separate experiment, CB-17 SCID mice (n=4 for rat IgG+PBS; n=5 for anti-CD40+MPL) were injected s.c. with 10^5 B16 cells on day 0 and in the opposite flank on day 3, and treated i.t. with two rounds of treatment: anti-CD40 (20 μg) on day 5 and 12 and MPL (2 μg) on day 8 and 15 (*p<0.031). **(H)** Secondary tumor growth of the same mice as in (G) (*p=0.012). **(I)** Survival of the same mice as in (G) and (H) (**p=0.0054).

Figure 1

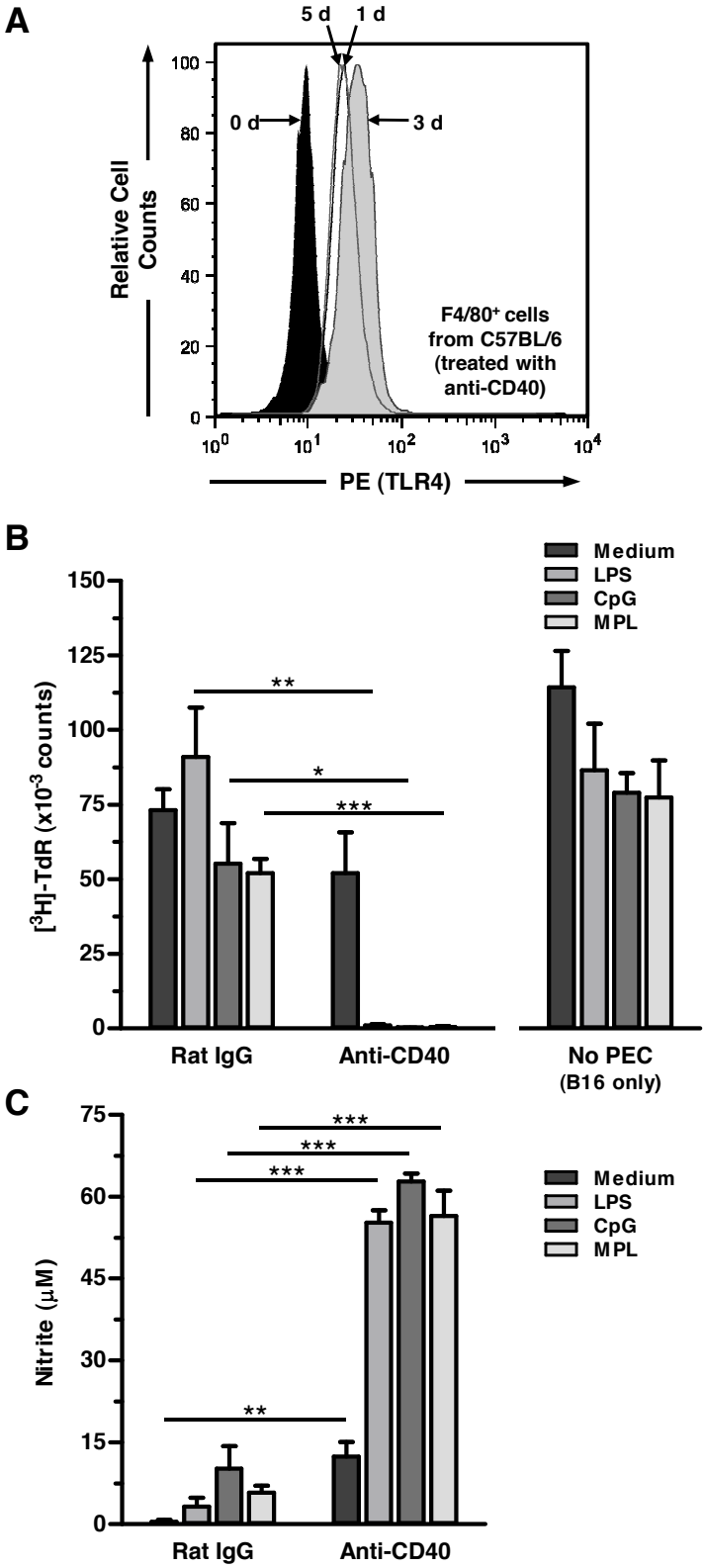
A
5 d
1 d
0 d
3 d
Relative Cell Counts
F4/80+ cells from C57BL/6 (treated with anti-CD40)
PE (TLR4)
B
Medium
LPS
CpG
MPL
[3H]-TdR (x10-3 counts)
Rat IgG
Anti-CD40
No PEC (B16 only)
C
Nitrite (μM)
Rat IgG
Anti-CD40

Figure 2

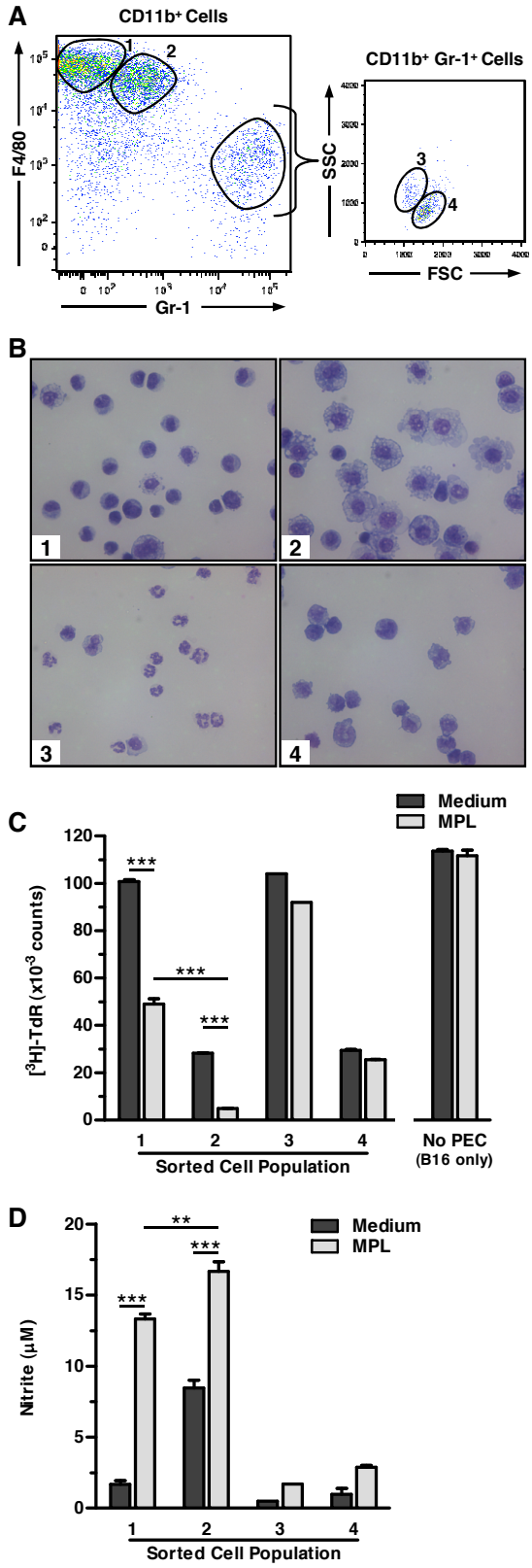
A
CD11b+ Cells
F4/80
Gr-1
1
2
CD11b+ Gr-1+ Cells
SSC
FSC
3
4
B
1
2
3
4
C
Medium
MPL
[3H]-TdR (x10-3 counts)
***
***
***
Sorted Cell Population
No PEC
(B16 only)
D
Medium
MPL
Nitrite (μM)
**
***
***
Sorted Cell Population

Figure 3

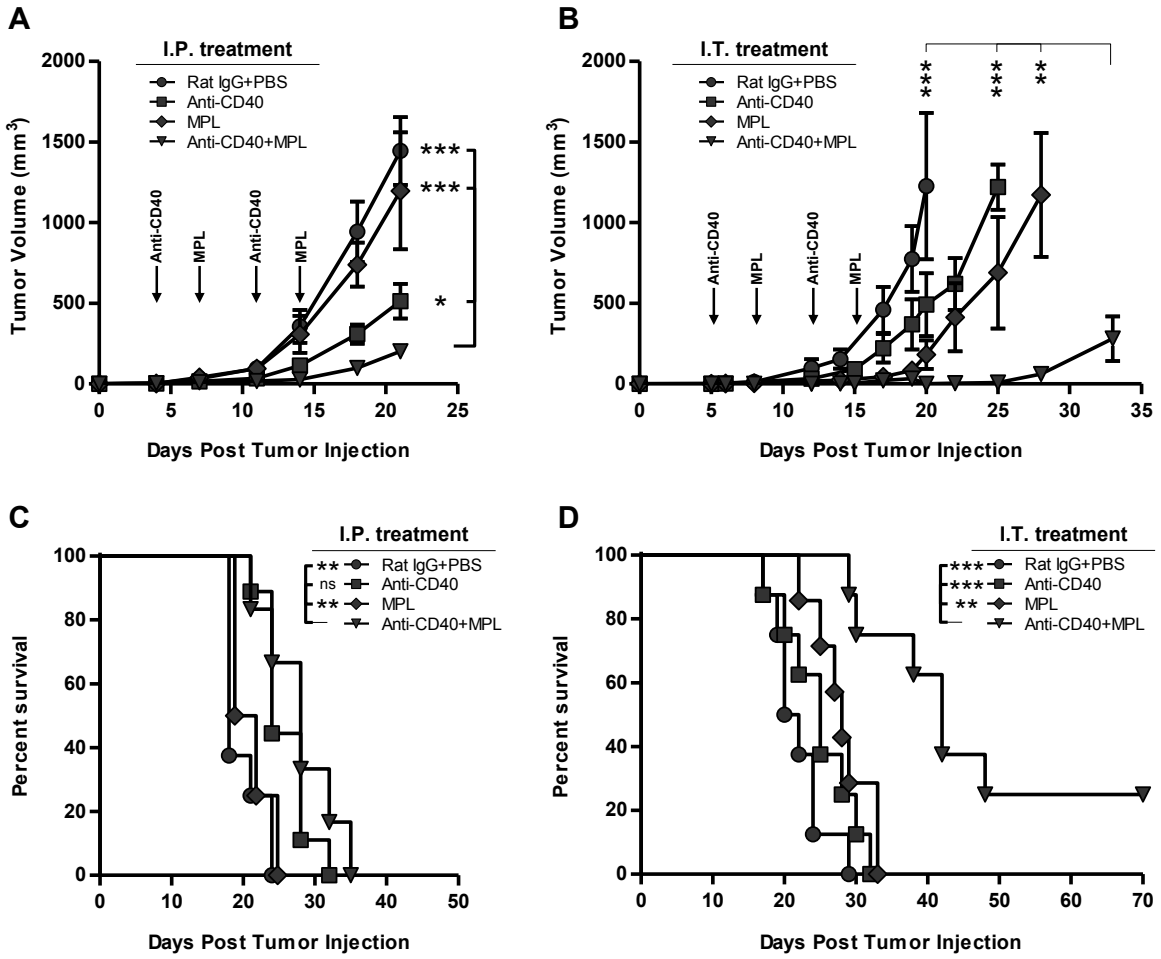
A
I.P. treatment
Rat IgG+PBS
Anti-CD40
MPL
Anti-CD40+MPL
Anti-CD40
MPL
Anti-CD40
MPL
***
***
*
Tumor Volume (mm3)
Days Post Tumor Injection
B
I.T. treatment
Rat IgG+PBS
Anti-CD40
MPL
Anti-CD40+MPL
Anti-CD40
MPL
Anti-CD40
MPL
Tumor Volume (mm3)
Days Post Tumor Injection
C
I.P. treatment
** Rat IgG+PBS
ns Anti-CD40
** MPL
Anti-CD40+MPL
Percent survival
Days Post Tumor Injection
D
I.T. treatment
*** Rat IgG+PBS
*** Anti-CD40
** MPL
Anti-CD40+MPL
Percent survival
Days Post Tumor Injection

Figure 4

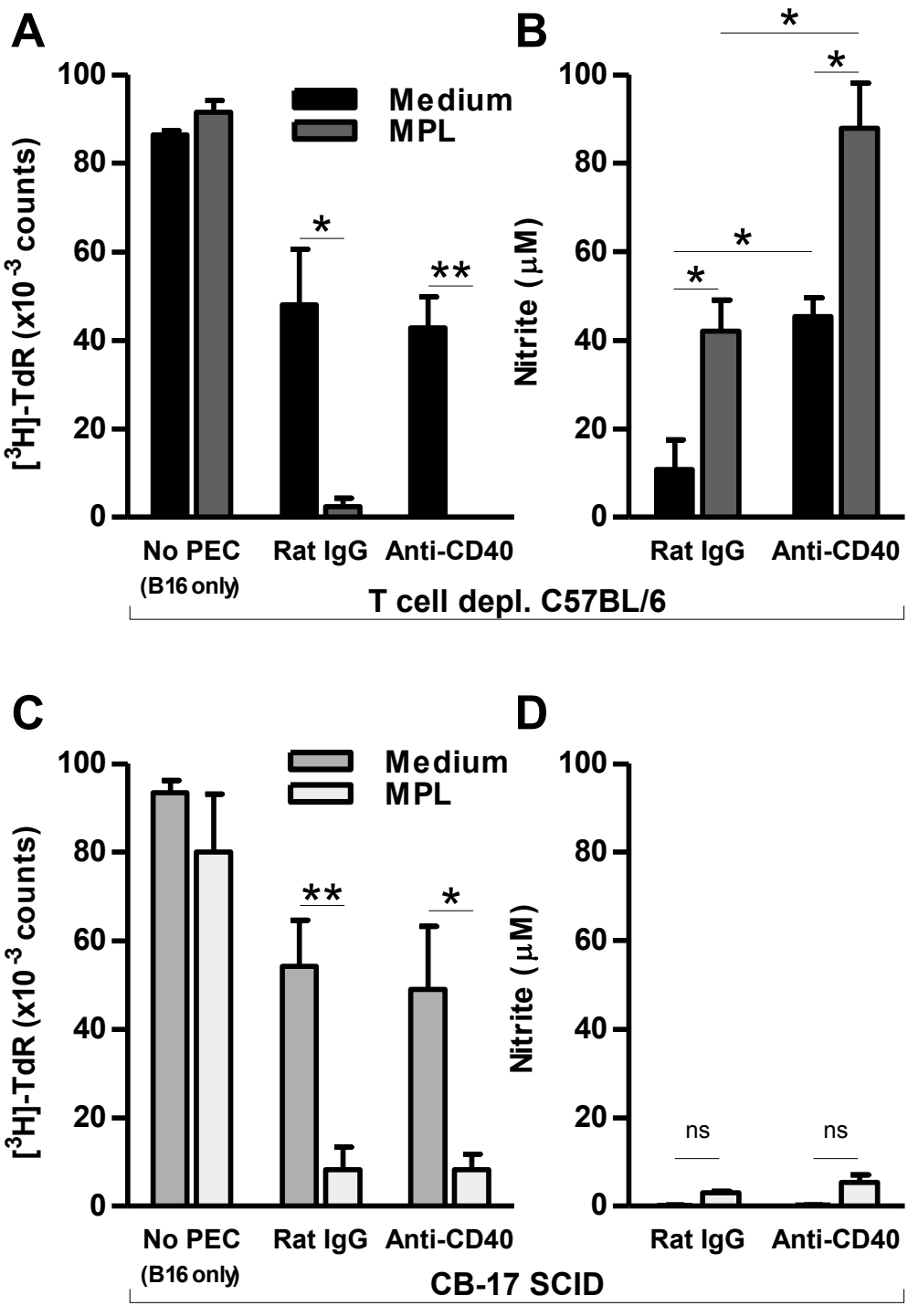
A
B
C
D
Medium
MPL
[3H]-TdR (x10-3 counts)
Nitrite (μM)
No PEC
(B16 only)
Rat IgG
Anti-CD40
T cell depl. C57BL/6
CB-17 SCID
ns

Figure 5

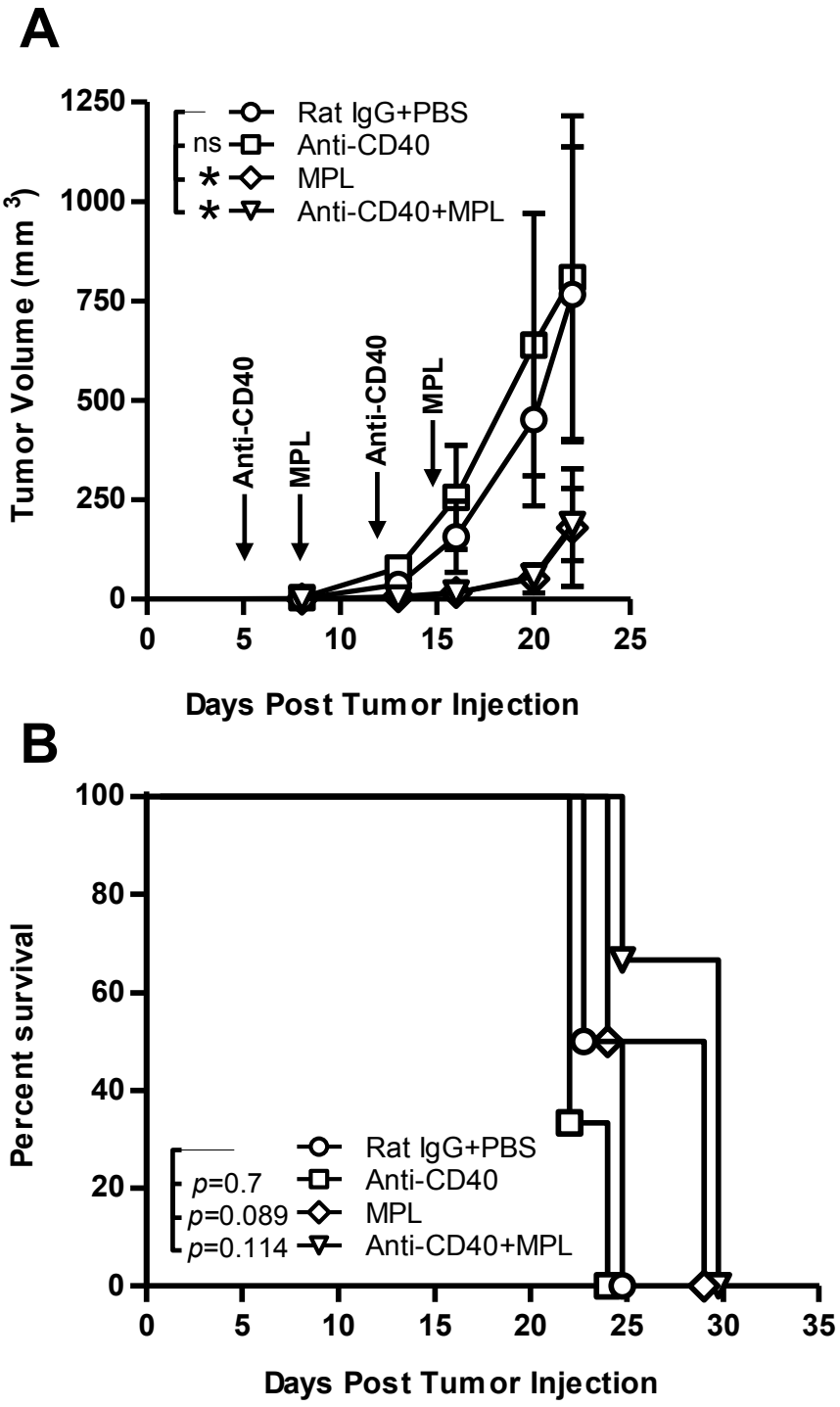
A
Tumor Volume (mm 3)
1250
1000
750
500
250
0
Rat IgG+PBS
ns Anti-CD40
* MPL
* Anti-CD40+MPL
Anti-CD40
MPL
Anti-CD40
MPL
0
5
10
15
20
25
Days Post Tumor Injection
B
Percent survival
100
80
60
40
20
0
p=0.7
p=0.089
p=0.114
Rat IgG+PBS
Anti-CD40
MPL
Anti-CD40+MPL
0
5
10
15
20
25
30
35
Days Post Tumor Injection

Figure 6

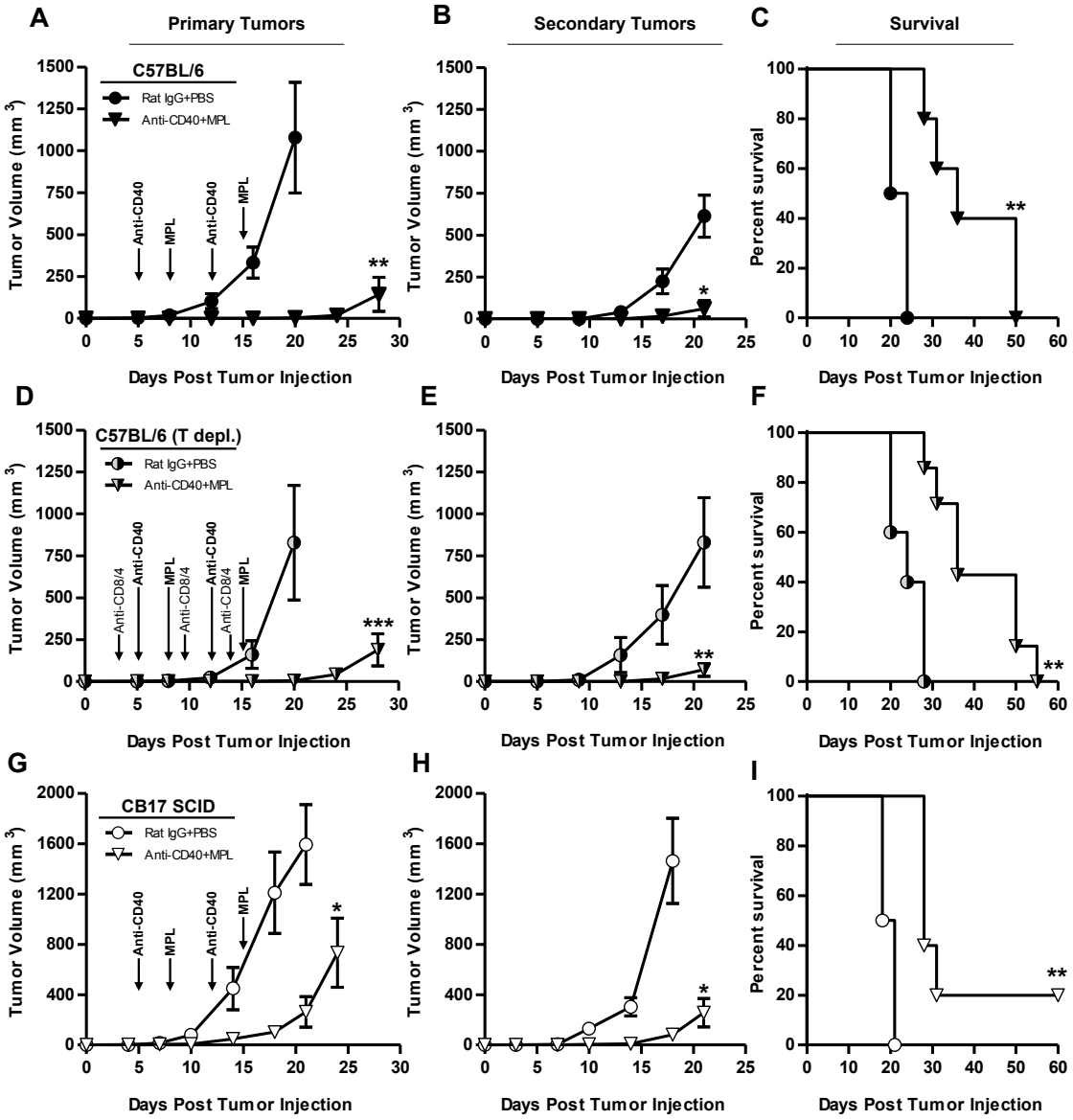
A
Primary Tumors
C57BL/6
Rat IgG+PBS
Anti-CD40+MPL
Anti-CD40
MPL
Anti-CD40
MPL
Tumor Volume (mm 3)
Days Post Tumor Injection
B
Secondary Tumors
C
Survival
Percent survival
D
C57BL/6 (T depl.)
Anti-CD8/4
E
F
G
CB17 SCID
H
I